4. Resultats

4. RESULTATS

4.1 Viabilitat de l'electrodeposició de cobalt-molibdè

4.1.1 Finalitat

Bo i tenint en compte els antecedents bibliogràfics, es va estimar convenient de fer, en primer lloc, un estudi bàsic del procés d'electrodeposició del sistema Co-Mo i avaluar, en segon lloc, la capacitat de l'electroquímica per obtenir dipòsits cobalt-molibdè amb perspectives de futur. Es van emprar dissolucions que contenien 0.2 mol dm^{-3} de citrat sòdic, 0.1 mol dm^{-3} $CoSO_4$ i una concentració variable de Na_2MoO_4 (0.001-0.015 mol dm^{-3}). Es va partir de concentracions baixes de molibdat per tenir, en principi, incorporacions discretes de molibdè a les capes de cobalt. El pH de preparació d'aquestes dissolucions és proper al neutre, de manera que es va decidir de treballar a pH=6.6. Tant en l'estudi electroquímic (voltametria, cronomètodes, *stripping* potenciodinàmic i *stripping* galvanostàtic) com en la preparació de dipòsits, es va emprar l'elèctrode de carboni vitri com a elèctrode de treball. Aquest elèctrode permet d'estudiar el procés d'electrodeposició en un ampli marge de potencials i densitats de corrent gràcies al fet que no dóna resposta pròpia. Per a l'anàlisi estructural i magnètica, però, es va usar l'elèctrode de grafit per poder disposar d'una àrea més gran i optimitzar la resolució de la resposta.

Es va fer una anàlisi in situ dels dipòsits formats amb l'objectiu d'avaluar la capacitat de les tècniques electroquímiques a l'hora de predir el tipus de dipòsit obtingut. És per això que es va intentar d'establir una correlació entre la forma de les corbes j-t i la qualitat dels dipòsits finals. Així mateix, es pretengué avaluar la idoneïtat de la tècnica de *stripping* a l'hora d'obtenir informació sobre el tipus i composició dels dipòsits.

Els dipòsits es van preparar en condicions d'agitació per evitar l'esgotament del molibdat a les proximitats de l'elèctrode. Es va fer una primera anàlisi de la morfologia, composició, estructura i propietats magnètiques dels dipòsits obtinguts. Les propietats exhibides pels dipòsits Co-Mo es van comparar amb les observades en dipòsits de Co pur obtinguts també a partir d'un bany sulfat-citrat. Aquesta anàlisi comparativa es va dur a terme amb l'objectiu d'esbrinar si les propietats magnètiques del cobalt canviaven en introduir molibdè.

Els resultats detallats d'aquest capítol s'inclouen en el següent article:

Electrodeposited cobalt-molibdenum magnetic materials
J. Electroanal. Chem. 517 (2001) 109

Electrodeposited cobalt-molybdenum magnetic materials

ELSEVIER

Journal of Electroanalytical Chemistry 517 (2001) 109–116

Journal of Electroanalytical Chemistry

www.elsevier.com/locate/jelechem

Electrodeposited cobalt–molybdenum magnetic materials

E. Gómez *, E. Pellicer, E. Vallés

Departament de Química Física, Div. Ciencies Expt.i Matemat., Laboratori de Ciència i Tecnologia Electroquímica dels Materials (LCTEM), Universitat de Barcelona, Martí i Franques 1, 08028 Barcelona, Spain

Received 4 June 2001; received in revised form 19 September 2001; accepted 21 September 2001

Abstract

Cobalt–molybdenum (Co–Mo) induced electrodeposition has been studied from a sulphate + citrate bath on carbon electrodes, under conditions near to neutral pH. Crack-free homogeneous deposits with a low percentage of molybdenum can be easily obtained from low molybdate concentrations applying low deposition potentials or current densities. The formation of this kind of deposit is related to Q_{ox}/Q_{red} around 1 in the voltammetric/stripping experiments. Moreover, percentages of molybdenum up to 60% can be obtained from high molybdate concentrations but, in this case, the deposits show cracks. The formation of these cracked deposits can be predicted from the observed distortions in the j–t and E–t deposition transients. Coatings with a partially amorphous structure, or with a crystalline structure of nanometric crystal size, are obtained. The magnetisation results show that the saturation magnetisation gradually decreases when the percentage of molybdenum increases in the deposit. Simultaneously, a clear decrease of the coercitivity is observed from the lowest percentage of molybdenum with respect to the value of pure cobalt coatings.

Keywords: Cobalt–molybdenum; Magnetic alloys; Electrodeposition; XRD; Stripping

1. Introduction

The electronic industry has gone through a very rapid evolution towards the use of thinner films, in which electrochemical techniques have often played an important role. Electrodeposition is a good technique to prepare highly functional magnetic recording materials [1–7]. Different alloys can be electrodeposited to attain useful soft magnetic films. In this field, Co–Ni can be used because of its magnetic properties [8–10] and this system presents advantageous properties because, depending on the cobalt percentage, the material shifts from soft magnetic to permanent magnetic with increasing cobalt percentage [11]. Nickel–cobalt soft magnetic alloy exhibits high permeability and low coercitivity, but in many applications for magnetic sensors lower coercitivity is required.

The magnetic properties of Co–Ni alloy can be modified by the introduction of low percentages of a third element in the alloy [12–19]. Thus, the introduction of some molybdenum in the cobalt–nickel alloy can be tested as a method of decreasing the coercitivity, maintaining high values of saturation magnetisation [5]. Such films are able to increase the efficiency of microactuators and to improve the sensibility of magnetic microsensors.

A previous study of the Co–Mo deposition process is suitable both as a test preparation method of alloys containing molybdenum and as a test of molybdenum influence in the magnetic properties of Co–Ni alloys. Moreover, the electrodeposition of molybdenum with iron-group metals has been gaining importance in recent years due to their magnetic properties.

The Co–Mo system is an example of induced codeposition. Molybdenum has not been deposited from aqueous solution by itself [20] but only in conjunction with the deposition of another metal. Induced molybdenum codeposition with iron-group metals takes place [21–31]. A knowledge of the induced discharge process is essential to correlate the properties of the coatings to the conditions of their deposition. In order to obtain molybdenum codeposited with iron-group metals, the

* Corresponding author. Tel.: +34-93-402-1234; fax: +34-93-402-1231.

E-mail address: e.gomez@qf.ub.es (E. Gómez).

0022-0728/01/$ - see front matter
PII: S0022-0728(01)00682-9

presence of a polycarboxylate is required [31]. In this case citrate was selected, in order to establish electrodeposition conditions leading to magnetic homogeneous Co–Mo deposits of variable composition. Citrate electrolytes can assure a stable pH value of the electrolyte during the deposition process.

2. Experimental

The electrochemical measurements were performed in a conventional three-electrode cell using a microcomputer-controlled potentiostat/galvanostat, model 273 from EG&G. Chemicals used were $CoSO_4 \cdot 7H_2O$, $Na_2MoO_4 \cdot 2H_2O$, $Na_3C_6H_5O_7 \cdot 2H_2O$, all of analytical grade. All solutions were freshly prepared with water, first doubly distilled and then treated with a Millipore Milli Q system. In all alloy deposition experiments 0.1 mol dm^{-3} $CoSO_4 + 0.2$ mol dm^{-3} $Na_3C_6H_5O_7$ solutions were used, and the Mo(VI) concentration was varied between 1×10^{-3} and 15×10^{-3} mol dm^{-3}. The pH was adjusted to 6.6. Before and during the experiments, solutions were de-aerated with argon. The temperature was maintained at 25 °C.

The morphology of the deposits was examined with a Hitachi S 2300 scanning electron microscope (SEM). The elemental composition was determined with an X-ray analyser incorporated in a Leica Cambridge Stereorcan S-360 SEM. X-ray diffraction (XRD) phase analysis was performed in a Philips MRD diffractometer with low resolution parallel beam optics. Cu–K_α radiation ($\lambda = 1.5418$ Å) was selected by means of a diffracted beam flat graphite monochromator. $2\theta/\theta$ diffractograms were obtained in the 24–100° 2θ range with a step range of 0.05° and a measuring time of 33 s per step. The magnetic measurements were performed with a Manics DSM8 pendulum-type magnetometer at room temperature. The instrument was calibrated by magnetisation measurement of standard ferrite.

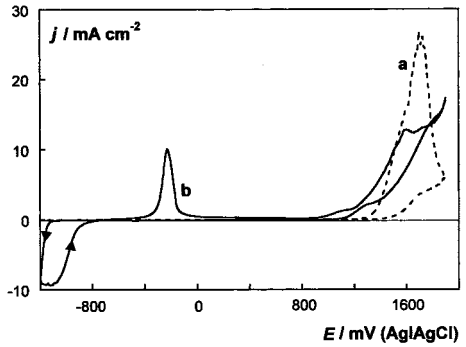

Fig. 1. Cyclic voltammograms of: (a) blank citrate solution: 0.2 mol dm^{-3} $Na_3C_6H_5O_7 + 0.2$ mol dm^{-3} Na_2SO_4 solution; (b) 0.1 mol dm^{-3} $CoSO_4 + 0.012$ mol dm^{-3} $Na_2MoO_4 + 0.2$ mol dm^{-3} $Na_3C_6H_5O_7$ solution. Stirred conditions.

Vitreous carbon (Metrohm, 0.0314 cm^2) and graphite (Alfa Aesar, 0.3117 cm^2) were used as working electrodes (WE). Graphite electrodes were used mainly for preparation of the deposits used in diffraction and magnetisation experiments. Both electrodes were polished to a mirror finish before each experiment using alumina of different grades (3.75 and 1.85 μm) and cleaned ultrasonically for 2 min in water. The reference electrode was Ag/AgCl/1 mol dm^{-3} NaCl mounted in a Luggin capillary containing 0.5 mol dm^{-3} Na_2SO_4 solution. All potentials are referred to this electrode. The counter electrode (CE) was a platinum spiral.

Voltammetric experiments were carried out at 50 mV s^{-1}, scanning initially towards negative potentials. Only one cycle was run in each voltammetric experiment. Stripping analyses were performed at a scan rate of 10 mV s^{-1} immediately after potentiostatic/galvanostatic deposition using an initial potential at which deposition did not occur. The oxidation was tested in different solutions: the same deposition solution without removing the electrode from the solution and in blank solutions.

For preparation of the deposits the solution was stirred moderately (using argon flow) to avoid the depletion of the minority element (molybdenum) to the electrode during the experiments and to maintain homogeneous composition of the deposits.

3. Results

3.1. Voltammetric results

The general trends of Co–Mo deposition were analysed from voltammetric experiments. Prior to the study of alloy deposition, the voltammetric response of a blank solution was recorded and no current between -1600 and $+1200$ mV was detected. Widening the scan to more positive potentials a net current related to citrate oxidation was observed (Fig. 1, curve a). The voltammetric response of cobalt(II) + molybdenum(VI) solution showed a typical nucleation loop in the reduction zone revealing that some deposition occurred (Fig. 1, curve b). During the positive scan and prior to citrate oxidation, only one peak around -200 mV was observed.

The comparison of the voltammograms, recorded from solutions containing different molybdate concentrations at fixed cobalt(II) concentration, revealed that the presence of molybdate in solution promoted and favoured the deposition process: small amounts of molybdate in solution clearly advanced the deposition with respect to the deposition from molybdate-free cobalt(II) solution (Fig. 2). However, this advancement attained a limit at very low molybdate concentration values (Fig. 2, curve e). Depending on the molybdate

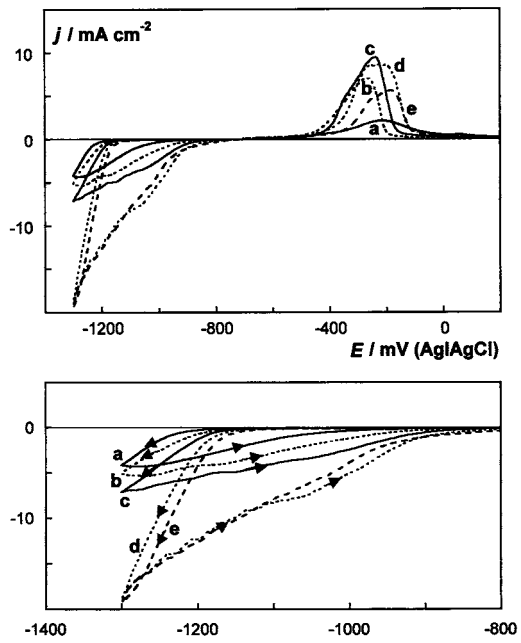

Fig. 2. Cyclic voltammogram and magnified detail of 0.1 mol dm^{-3} $CoSO_4 + x Na_2MoO_4 + 0.2$ mol dm^{-3} $Na_3C_6H_5O_7$ solution: (a) $x = 0$; (b) $x = 0.001$; (c) $x = 0.002$; (d) $x = 0.0048$; (e) $x = 0.011$. Stirred conditions.

concentration different features in the oxidation voltammetric response were observed. At a fixed moderate cathodic limit, for concentrations lower than 3×10^{-3} mol dm^{-3}, the peak appeared at more negative potentials than that obtained from molybdate-free solution (Fig. 2, curves a–c) but Q_{ox}/Q_{red} ratio remained the same. Upon increasing the molybdate concentration the peak became deformed and the Q_{ox}/Q_{red} ratio clearly decreased (Fig. 2, curves d, e).

3.2. Potentiostatic and galvanostatic transients

Fig. 3A shows a collection of potentiostatic curves obtained under stirred conditions for a fixed solution composition. An induction time was always observed prior to the appearance of the current, followed by a current increase that attained a quasi stationary value. For the higher Mo(VI) concentrations studied deformations in the j–t transients took place and simultaneous hydrogen evolution was easily detected. The induction time was greater than that observed under stationary conditions (Fig. 3B). The shape of the j–t transients for alloy deposition was clearly different from that corresponding to molybdenum-free cobalt deposition, for which, a monotonic current increase was observed until a stationary value was attained (Fig. 3C). Also, to attain similar deposition charges it was necessary to apply lower polarisation for the Mo–Co solution than for the cobalt one. Chronoamperometric experiments corroborated the voltammetric results: the deposition process was favoured when molybdenum was present in solution.

When the deposits were obtained by means of the chronopotentiostatic method at low current densities (Fig. 4A), a nucleation spike was observed followed by stabilisation of the potential. For the more negative applied current densities, deformations in the curve were detected after the nucleation spike and no clear stabilisation of the current was observed, probably due to simultaneous hydrogen evolution.

3.3. Electrochemical characterisation of deposits

In order to obtain in situ information of the prepared deposits, both potentiodynamic and galvanostatic strippings were performed, since these methods have been proved to be highly useful for the characterisation of electrodeposited alloys [32–36]. Both the deposition

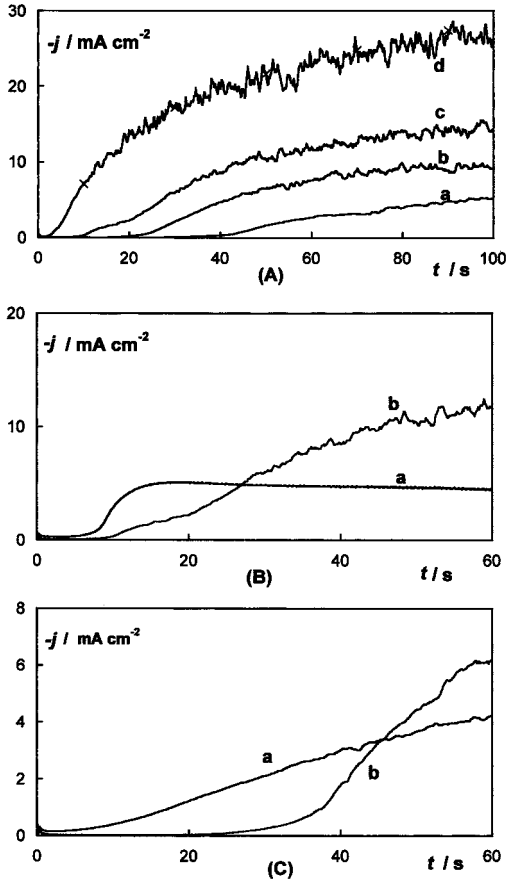

Fig. 3. (A) Potentiostatic transients of a 0.1 mol dm^{-3} $CoSO_4 +$ 0.005 mol dm^{-3} $Na_2MoO_4 + 0.2$ mol dm^{-3} $Na_3C_6H_5O_7$ solution at: (a) -990; (b) -1025; (c) -1075; (d) -1150 mV. Stirred conditions. (B) Potentiostatic transients of same solution, -1075 mV: (a) stationary conditions; (b) stirred conditions. (C) Potentiostatic transients of: (a) 0.1 mol dm^{-3} $CoSO_4 + 0.2$ mol dm^{-3} $Na_3C_6H_5O_7$ solution, -1130 mV; (b) 0.1 mol dm^{-3} $CoSO_4 + 0.005$ mol dm^{-3} $Na_2MoO_4 + 0.2$ mol dm^{-3} $Na_3C_6H_5O_7$ solution, -1000 mV. Stirred conditions.

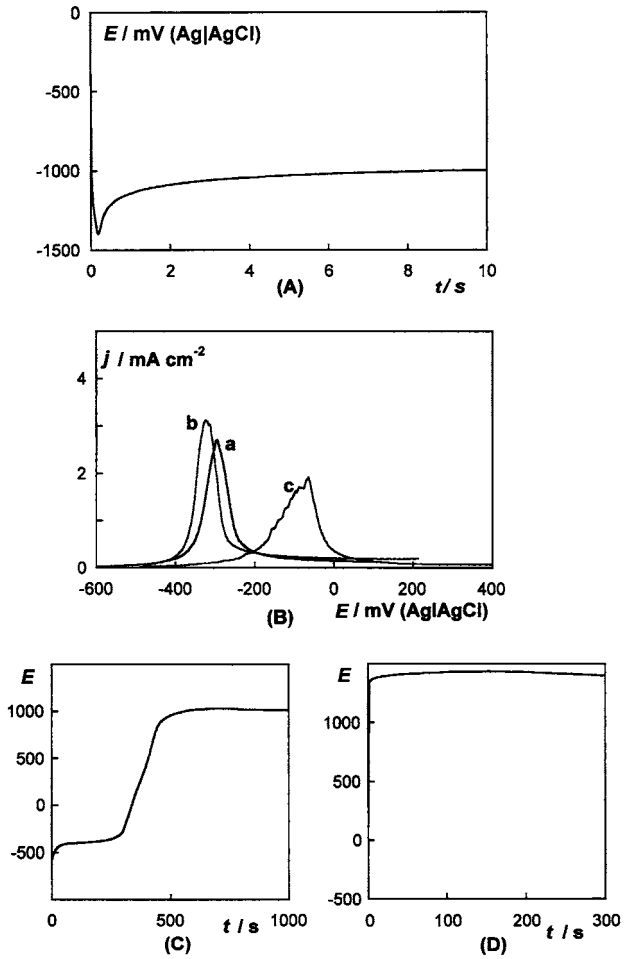

Fig. 4. (A) Galvanostatic transient of a 0.1 mol dm^{-3} $CoSO_4 + 0.012$ mol dm^{-3} $Na_2MoO_4 + 0.2$ mol dm^{-3} $Na_3C_6H_5O_7$ solution. Stirred conditions. (B) Stripping voltammograms of the deposit of Fig. 6A in: (a) the same deposition solution; (b) 0.2 mol dm^{-3} $Na_3C_6H_5O_7 +$ 0.2 mol dm^{-3} Na_2SO_4 solution; (c) 0.4 mol dm^{-3} Na_2SO_4, pH 4 solution. (C) Galvanostatic stripping, at 0.06 mA cm^{-2}, of the deposit of Fig. 6A. (D) Galvanostatic curve, at 0.64 mA cm^{-2} of a 0.2 mol dm^{-3} $Na_3C_6H_5O_7 + 0.2$ mol dm^{-3} Na_2SO_4 solution.

potentials and current densities were selected according to previous electrochemical results, and the solution was stirred during the electrodeposition in order to minimise the ion depletion around the electrode.

At first, deposits obtained from solutions containing the lowest Mo(VI) concentrations studied and/or obtained at low deposition potentials were analysed. Different solutions were tested to oxidise the deposits. Fig. 4B shows the stripping curves of different deposits obtained galvanostaticaly through the curve of Fig. 4A. When the stripping was made either in the same deposition solution or in a citrate blank solution (Fig. 4B, curves a, b), the recorded oxidation curves were similar. Only one oxidation peak was always obtained for moderate current densities and for all solution compositions analysed. With a wider voltammetric scan, citrate oxidation was recorded. Moreover, the stripping results obtained from a solution containing only sulphate salt were tested (Fig. 4B, curve c). Although in this medium the appearance of the oxidation current took place at more positive potentials, only one oxidation peak of a similar charge to that recorded in citrate media was obtained. Citrate medium clearly favoured deposit oxidation and, therefore, the same deposition solution was chosen as a good stripping medium since no replacement reaction took place during the oxidation scan. In all cases one oxidation peak centred around -300 mV was obtained and the calculated Q_{ox}/Q_{red} ratio was near 1.

When deposits were prepared either upon decreasing the applied current density or from solutions with a Mo(VI) concentration higher than 6×10^{-3} mol dm^{-3}, an important simultaneous hydrogen evolution occurred during the deposition. The stripping experiments of these deposits also showed one stripping peak, but a clear decrease of the Q_{ox}/Q_{red} ratio was observed, specially when the applied potentials were very negative. Some deposit remained on the electrode after the stripping experiments, revealing that complete oxidation was not attained. Therefore, for these deposits, little qualitative and no quantitative information was obtained by using in situ stripping characterisation.

For all types of deposits, parallel galvanostatic strippings were performed and two stabilisation plateaux were always observed (Fig. 4C). The first was related to oxidation of the deposit and the second was related to citrate oxidation. The galvanostatic oxidation curve of a just polished electrode corroborated the supposition that the plateau observed at positive potentials corresponded to citrate oxidation (Fig. 4D). This plateau was not observed in citrate-free sulphate solution.

3.4. Morphological, compositional and structural analysis of deposits

Morphological, structural and compositional analysis of the deposits obtained under different experimental conditions was carried out to detect the presence of molybdenum in the deposits and in order to correlate the type of deposit obtained to the electrochemical response.

Fig. 5 shows the SEM micrographs of a pure cobalt deposit (Fig. 5A) and of alloy deposits containing 17 and 45% w/w of molybdenum (Fig. 5B and C). All the deposits were obtained under the same deposition charge and under stirred conditions. Both Fig. 5A and B correspond to deposits of 0.2 μm thickness which were obtained with quite similar current efficiencies (around 93%). A thinner deposit was obtained when the molybdenum content was increased, due to the low current efficiency.

A clear modification in the morphology was observed for deposits containing molybdenum: they presented a

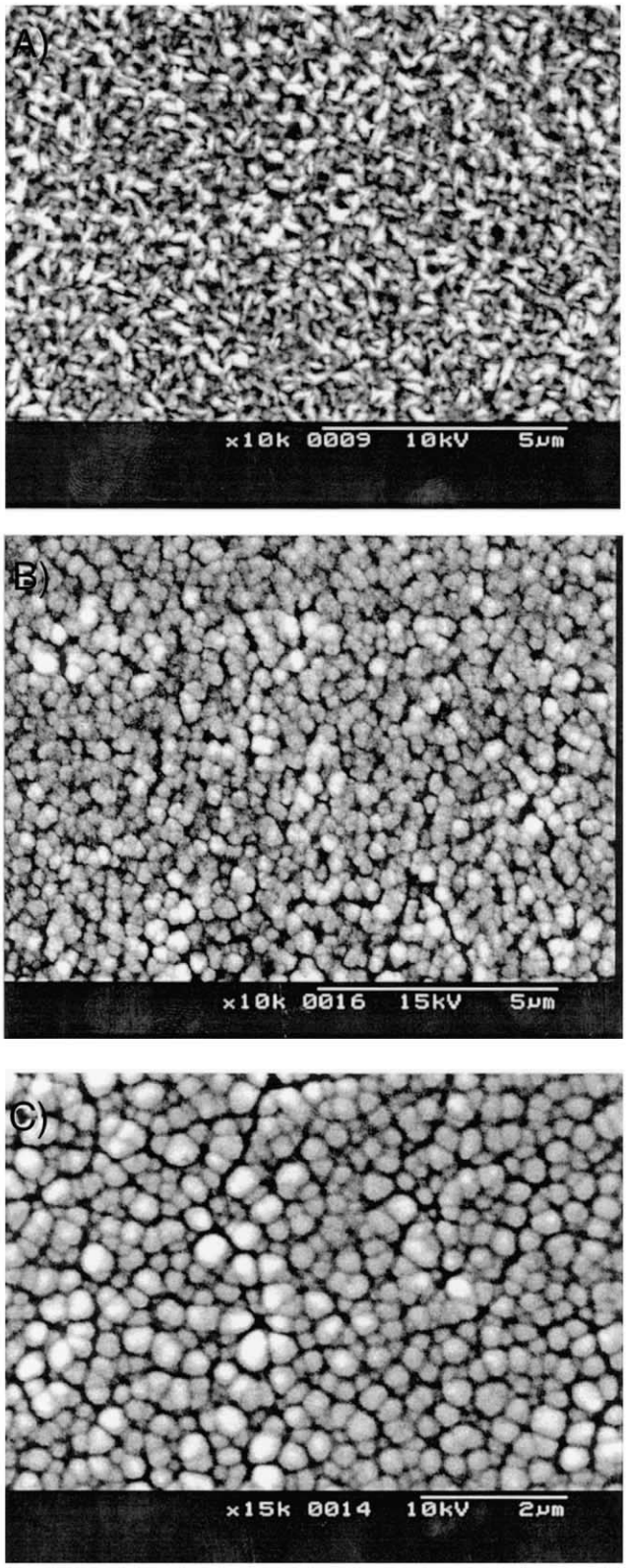

Fig. 5. SEM micrographs of deposits obtained potentiostatically under stirred conditions: (A) 0.1 mol dm^{-3} $CoSO_4$ + 0.2 mol dm^{-3} $Na_3C_6H_5O_7$ solution, 400 s at −1075 mV. (B) 0.1 mol dm^{-3} $CoSO_4$ + 0.005 mol dm^{-3} Na_2MoO_4 + 0.2 mol dm^{-3} $Na_3C_6H_5O_7$ solution, 400 s at −950 mV. 17% Mo. (C) 0.1 mol dm^{-3} $CoSO_4$ + 0.012 mol dm^{-3} Na_2MoO_4 + 0.2 mol dm^{-3} $Na_3C_6H_5O_7$ solution, 300 s at −1010 mV. 45% Mo.

nodular morphology whereas a needle like morphology was observed for the pure cobalt deposit. The analysis of nodular deposits revealed that they were composed of Co + Mo with a percentage of molybdenum that was a function of both the solution composition and the deposition potential or current density. Therefore, the nodular morphology reveals the existence of molybdenum in the deposit. Similar deposits were obtained using either vitreous carbon or graphite substrates.

The percentage of molybdenum in the deposits was increased by increasing the molybdate concentration in solution and by applying more negative deposition potentials or current densities in a moderate range of potentials. Very negative values of the deposition potentials implied a lower molybdenum incorporation in the deposit according to other authors [26–28] (Fig. 6). No oxygen was detected in the layers deposited under our conditions, revealing that Co–Mo metallic alloy is always obtained. Deposits of up to 60% molybdenum can be obtained from the highest molybdate concentrations studied, although these deposits with a large molybdenum content showed cracks. However, from the solutions with low molybdate concentration ($<$ 0.005 mol dm^{-3}), fine-grained and crack-free deposits were obtained with a percentage of molybdenum lower than 20%. Thus, only the lowest Mo(VI) concentrations are suitable to prepare homogeneous and crack-free deposits.

Structural analysis of the deposits was performed using XRD. Graphite substrates were used to increase the electrode area and to optimise the response resolution. The diffractograms of Co–Mo deposits ranging between 15 and 35% Mo and the diffractogram of a pure cobalt deposit, obtained from a molybdate-free bath, showed a very different profile. The diffractogram of the pure cobalt deposit showed narrow peaks (Fig. 7A) and a low signal corresponding to the graphite substrate. The main peaks correspond to a close-packed hexagonal structure (hcp), whereas a small peak around $2\theta = 51.5°$ is related to a deposited face-centred cubic (fcc) cobalt next to the main hcp structure.

Cobalt–molybdenum deposits showed one main broad peak around $2\theta = 44°$, next to the (111) line of fcc cobalt and a broad zone centred around $2\theta = 78°$ (Fig. 7B). These deposits seemed to correspond to a coating with a partially amorphous structure or with a crystalline structure of nanometric crystal size. The latter hypothesis was confirmed by an estimation of the crystallite size domain from the peak broadening, using Scherrer's equation.

In order to investigate the magnetic response of Co–Mo alloys containing different percentages of molybdenum, measurements of their magnetisation as a function of the applied magnetic field were performed and compared to the response of a pure cobalt deposit obtained under similar electrodeposition conditions.

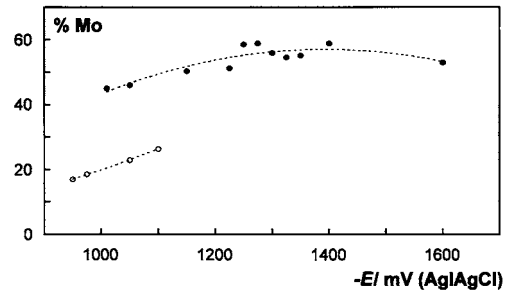

Fig. 6. Dependence of the percentage of molybdenum in the deposit as a function of deposition potential for two different solutions: 0.1 mol dm^{-3} $CoSO_4 + x$ mol dm^{-3} $Na_2MoO_4 + 0.2$ mol dm^{-3} $Na_3C_6H_5O_7$ solution (○) $x = 0.005$ mol dm^{-3} and (●) $x = 0.012$ mol dm^{-3}.

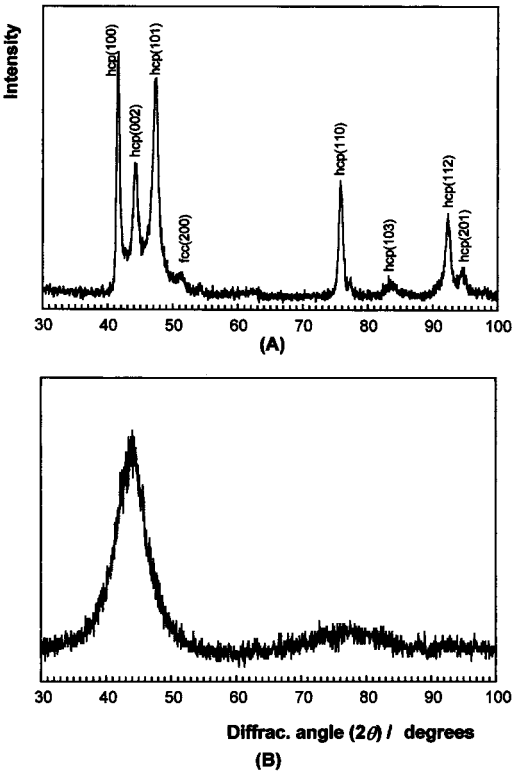

Fig. 7. (A) Diffraction peaks of cobalt deposit obtained at −1025 mV from a 0.1 mol dm^{-3} $CoSO_4 + 0.2$ mol dm^{-3} $Na_3C_6H_5O_7$ solution. (B) Diffraction peaks of a Co–Mo deposit of 35% Mo.

Two ranges of applied fields were used on each sample, in order to define both the saturation magnetisation and coercitivity of the material, because these are the main parameters of importance when characterising magnetic materials. For the cobalt electrodeposited from the citrate bath a high saturation magnetisation (145 emu g^{-1}) and a coercitivity value of around 140 Oe were observed (Fig. 8, curve a).

A clear modification was observed for Co–Mo coatings with respect to that obtained for a pure cobalt deposit. The saturation magnetisation gradually decreases when the percentage of molybdenum increases in the deposit. Simultaneously, an evident diminution in the coercitivity is observed when molybdenum is present (Fig. 8).

4. Discussion and conclusions

The sulphate–citrate bath, tested under conditions near to neutral pH, allows us to obtain Co–Mo alloys according to an induced codeposition. Under fixed electrodeposition conditions, the percentage of molybdenum in the final deposit is increased spectacularly by increasing the Mo(VI) concentration in solution.

Homogeneous deposits with a nodular morphology can be prepared from solutions containing a low molybdate concentration at a moderate applied deposition potential/current density. When the percentage of molybdenum in the deposits increases as a consequence of a high molybdate concentration in solution and/or more negative applied deposition potentials/current densities, stressed coatings are obtained with a cracked appearance. In all cases, amorphous deposits or deposits with a nanocrystalline structure that present soft magnetic properties are obtained. Therefore, the molybdate concentration in solution is critical in order to attain the desired kind of deposit.

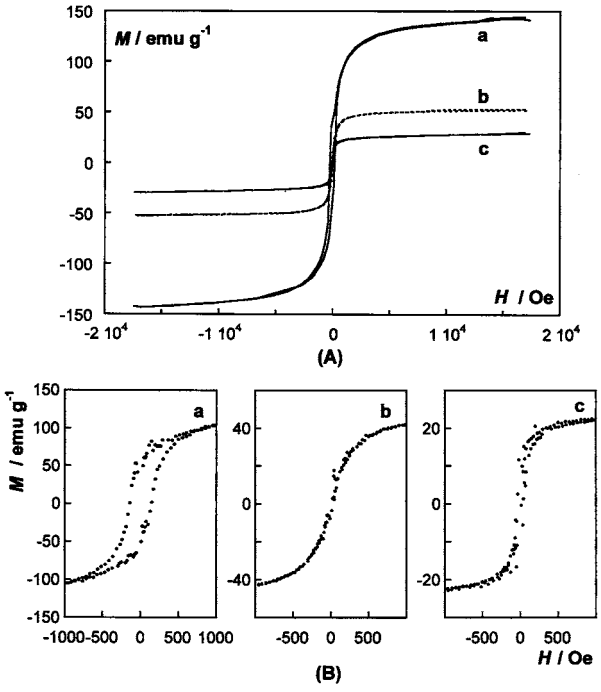

Fig. 8. Magnetic hysteresis curves (A) and magnified details (B) of deposits obtained in stirred conditions: (a) 0.1 mol dm^{-3} $CoSO_4 +$ 0.2 mol dm^{-3} $Na_3C_6H_5O_7$ solution, −1025 mV. 0.1 mol dm^{-3} $CoSO_4 + 0.005$ mol dm^{-3} $Na_2MoO_4 + 0.2$ mol dm^{-3} $Na_3C_6H_5O_7$ solution; (b) −950 mV, 15% Mo; (c) −1000 mV, 20% Mo.

Practical interest is always focused on obtaining homogeneous, crack-free films that allow their application by virtue of their soft magnetic properties. The magnetic results as well as the tendency toward the appearance of cracks when the percentage of molybdenum increases allows us to set the deposition conditions in a range leading to reasonably good deposits with a relatively low percentage of molybdenum ($< 20\%$) obtained at high current efficiency. Low percentages of molybdenum should be more suitable to attain small coercitivity values maintaining a high saturation magnetisation. According to the results obtained from the baths tested, low molybdate concentrations clearly lead to Co–Mo deposits with good mechanical properties, low coercitivity and high saturation magnetisation.

The level of molybdenum incorporation in the deposit could be followed by using the voltammetric technique. The advancement in the appearance of the reduction current reveals this molybdenum incorporation in the deposit. A very low molybdate concentration is sufficient to allow the observation that the appearance of the reduction current takes place at more positive potentials than that corresponding to molybdate-free cobalt solution. The formation of richer molybdenum deposits is detected from voltammetric experiments. From a certain applied negative limit value, deformations in the oxidation peak are observed with a clear fall of the Q_{ox}/Q_{red} ratio. Simultaneous hydrogen evolution favours hydroxide precipitation and the oxidation of the deposit is hindered. When little molybdenum is incorporated in the deposit, the ratio Q_{ox}/Q_{red} is near 1.

In the same way, when no distortions, in either the j–t or E–t deposition transients are observed, the probability of obtaining suitable final deposits with a low percentage of molybdenum increases. The Co–Mo alloy seems to be very catalytic to hydrogen evolution since deformations in the potentiostatic and galvanostatic transients, related to hydrogen evolution, are easily detected even at moderate deposition potentials or current densities.

In the voltammetric stripping response, one peak is recorded like that obtained in the voltammetric experiments. This peak is centred at more negative potentials than the oxidation peak corresponding to a pure cobalt deposit. When molybdenum is present, a more easily oxidizable structure is formed, and this is probably related to a poorly crystalline structure.

Therefore, the stripping results are not completely useful when deposits contain high percentages of molybdenum ($> 30\%$ w/w) because no total oxidation of deposit takes place, independent of the stripping solution used. These deposits, even at low thickness, are stressed and not adherent, a fact that probably hinders complete oxidation.

Nevertheless, for this Co–Mo system, the stripping technique could be a fast in situ test method to detect which kind of deposit has been obtained. The oxidation peak shape and the value of the Q_{ox}/Q_{red} ratio give information about the suitability of the final deposit.

Although a mechanism for Co–Mo deposition has not yet been completely elucidated, several proposals have been advanced in the literature to explain the mechanism of induced co-deposition between an iron-group metal and molybdenum, especially focused on the Ni–Mo system.

A quasi-unanimous proposal, mentioned as a first stage, is the reduction in several steps of the molybdic species present in solution leading to a low molybdenum oxide (the majority suggest MoO_2). The long induction time observed in the j–t transient, prior to the current increase, would correspond to the required time for this step. Different pathways are proposed to obtain the final M–Mo deposit (M being the iron-group metal). Some authors emphasise the hydrogen role in the mechanism, proposing that hydrogen previously adsorbed on the inducing metal (M) reduces the molybdenum oxide to molybdenum metal. Other authors postulate the formation of a complex between the nickel(II), citrate and the molybdenum oxide. This intermediate, adsorbed on the substrate, might promote further reduction of molybdenum.

Although our main interest was not focused on elucidating the mechanism of Co–Mo codeposition and although our results are insufficient to allow us to decide between the availability of the proposals mentioned above, our electrochemical results seem to permit us to discard some of the postulated assumptions/inputs. While for the Ni–Mo system it has been proposed that hydrogen included in the inducing metal promotes the reduction of molybdenum oxide [[24,25] and references therein], the existence of hydrogen in the Co–Mo system seems to be minimal. Hydrogen probably takes part in a side reaction and does not seem to be responsible for the molybdenum deposition. Moreover, this proposal does not take into account the essential presence of the citrate or a polycarboxylate anion in solution.

The fact that the deposition process is clearly favoured when molybdate is present in solution even at very low concentrations induce us to accept the assumptions proposed by Podhala and Landolt [26–28]: the formation of a complex that involves cobalt(II), citrate and molybdenum oxide absorbed on the surface promotes molybdenum reduction. This might justify the high percentage of molybdenum detected in the deposit with respect to the low molybdate concentration in solution.

Acknowledgements

The authors thank the Serveis Cientificotècnics (Universitat de Barcelona) for availability of equipment. This research was supported financially by contract MAT 2000-0986 of the Comisión Interministerial de Ciencia y Tecnología (CICYT) and by the Comissionat of the Generalitat de Catalunya under Research Project SGR 2000-017.

References

[1] T. Osaka, Electrochim. Acta 37 (1992) 989.
[2] J. Gobet, F. Cardot, J. Bergquist, F. Rudolf, in MME'93 Proceedings, Neuchatel (1993).
[3] P.L. Cavallotti, B. Bozzini, L. Nobili, G. Zangari, Electrochim. Acta 39 (1994) 1123.
[4] B. Löchel, A. Maciossek, J. Electrochem. Soc. 14 (1996) 3343.
[5] W.P. Taylor, M. Schneider, H. Baltes, M.G. Allen, in: Proceedings of the International Conference on Solid-State Sensors and Actuators, Transducers'97, Chicago, 1997.
[6] M. Takai, K. Hayashi, M. Aoyagi, T. Osaka, J. Electrochem. Soc. 144 (1997) 1209.
[7] O. Shinoura, T. Koyanagi, Electrochim. Acta 42 (1997) 3361.
[8] N. Fenineche, O. El Kedim, C. Coddet, Surf. Coat. Technol. 48 (1991) 205.
[9] J.S. Judge, J.R. Morrison, D.E. Speliotis, J. Appl. Phys. 36 (1965) 948.
[10] E. Gómez, E. Vallés, J. Appl. Electrochem. 29 (1999) 805.
[11] P.C. Andricacos, in: M. Paunovic (Ed.), Electrochemically Deposited Thin Films II, PV94-31, The Electrochemical Society Proceedings Series, Pennington, NJ, 1995, pp. 157.
[12] M.U. Sheleg, L.V. Nernstsevich, S.S. Grabchikov, T.A. Tochitskii, Phys. Stat. Sol. 126 (1991) 189.
[13] C. Byun, G.C. Ranch, D.J. Young, C.A. Klepper, J. Greggi Jr., J. Appl. Phys. 73 (1993) 5575.
[14] R. Chesnutt, J. Appl. Phys. 73 (1993) 6223.
[15] M. Onoda, K. Shinuzu, T. Tsuchiya, T. Watanabe, J. Magn. Magn. Mater. 126 (1993) 595.
[16] T. Homma, M. Suzuki, T. Osaka, J. Electrochem. Soc. 145 (1998) 134.
[17] T. Osaka, M. Takai, K. Hayashi, K. Ohashi, M. Saito, K. Yamada, Nature 392 (1998) 796.
[18] T. Osaka, T. Sawaguchi, F. Mizutani, T. Yokoshima, M. Takai, Y. Okinaka, J. Electrochem. Soc. 146 (1999) 3295.
[19] F.E. Rasmussen, J.T. Ravnkilde, P.T. Tang, O. Hansen, S. Bouwstra, Eurosensors XIV, The 14th European Conference on Solid-State Transducers, Copenhagen, 2000.
[20] A. Brenner, Electrodeposition of Alloys, vols. 1–2, Academic Press, New York, 1963.
[21] C.C. Nee, W. Kim, R. Weil, J. Electrochem. Soc. 135 (1988) 1100.
[22] E. Chassaing, K.V.u Quang, R. Wiart, J. Appl. Electrochem. 19 (1989) 839.
[23] E. Beltowska-Lehman, J. Appl. Electrochem. 20 (1990) 132.
[24] J. Crousier, M. Eyraud, J.-P. Crousier, J.-M. Roman, J. Appl. Electrochem. 22 (1992) 749.
[25] E. Chassaing, M.P. Roumegas, M.F. Trichet, J. Appl. Electrochem. 25 (1995) 667.
[26] E.J. Podhala, D. Landolt, J. Electrochem. Soc. 143 (1996) 885.
[27] E.J. Podhala, D. Landolt, J. Electrochem. Soc. 143 (1996) 893.
[28] E.J. Podhala, D. Landolt, J. Electrochem. Soc. 144 (1997) 1672.
[29] Z.J. Niu, S.B. Yao, S.M. Zhou, J. Electroanal. Chem. 455 (1998) 205.
[30] C.C. Hu, C.Y. Weng, J. Appl. Electrochem. 30 (2000) 499.
[31] K. Murase, H. Ando, E. Matsubara, T. Hirato, Y. Awakura, J. Electrochem. Soc. 147 (2000) 2210.
[32] V.D. Jovic, R.M. Zejnilovic, A.R. Despic, J.S. Stevanovic, J. Appl. Electrochem. 18 (1988) 511.
[33] M.L. Alcalá, E. Gómez, E. Vallés, J. Electroanal. Chem. 370 (1994) 73.
[34] E. Gómez, J. Ramírez, E. Vallés, J. Appl. Electrochem. 28 (1998) 71.
[35] E. Gómez, E. Peláez, E. Vallés, J. Electroanal. Chem. 469 (1999) 139.
[36] E. Gómez, X. Alcobé, E. Vallés, J. Electroanal. Chem. 475 (1999) 66.

4.1.3 Resum de resultats

L'obtenció de dipòsits homogenis cobalt-molibdè és factible a partir d'un bany sulfat-citrat a pH=6.6.

Els experiments voltamètrics mostren que concentracions molt baixes de molibdat en solució provoquen un avançament espectacular del procés de deposició respecte al del Co pur. Les corbes j-t presenten un *temps d'inducció* previ a l'increment sobtat del corrent que no s'observa en absència de molibdat. A mesura que s'apliquen potencials més negatius s'observen fluctuacions en les corbes j-t, relacionades amb la coevolució d'hidrogen. La tècnica de *stripping* potenciodinàmic ens revela que l'oxidació de dipòsits de Co pur o de Co-Mo té lloc a potencials semblants.

Les anàlisis d'EDS revelen que els dipòsits estan constituïts de Co+Mo. El percentatge de molibdè als dipòsits s'incrementa en augmentar la concentració de molibdat en el bany i/o aplicant potencials més negatius. La formació de dipòsits coherents és factible a partir d'un bany 0.2 mol dm^{-3} citrat + 0.1 mol dm^{-3} $CoSO_4$ + 0.005 mol dm^{-3} Na_2MoO_4, aplicant potencials/densitats de corrent moderats. En aquestes condicions, poden obtenir-se làmines amb percentatges de molibdè al voltant del 20% i amb una eficiència de corrent elevada. La formació d'aquests dipòsits està relacionada amb valors del quocient Q_{ox}/Q_{red} propers a 1 en els experiments voltamètrics/*strippings*. Percentatges superiors de molibdè (fins a un 60%) impliquen la presència d'esquerdes en els dipòsits. La morfologia dels dipòsits Co-Mo és nodular, mentre que els dipòsits de Co pur obtinguts a partir d'un bany sulfat-citrat són aciculars. Làmines primes (~0.2 μm) Co-Mo amb un 15-35% Mo presenten una estructura parcialment amorfa, mentre que làmines homòlogues de Co pur són cristal·lines. La mesura de les propietats magnètiques revela que la introducció de molibdè a les capes de cobalt produeix una disminució clara de la coercitivitat. La

magnetització de saturació, però, també disminueix i ho fa de forma gradual a mesura que augmenta el percentatge de molibdè.

4.2 Mecanisme de l'electrodeposició de cobalt-molibdè

4.2.1 Finalitat

Després de confirmar la viabilitat del procés d'electrodeposició, es va estudiar el mecanisme de codeposició induïda de cobalt i molibdè.

En primer lloc es va fer un estudi electroquímic a baixos potencials/densitats de corrent per obtenir informació de les etapes del procés de deposició a pH=6.6. Es van utilitzar concentracions variables de $CoSO_4$ i de Na_2MoO_4 en solució i l'elèctrode de carboni vitri com a elèctrode de treball. Es va dur a terme una caracterització qualitativa *ex situ* de les espècies intermèdies de molibdè generades durant el procés de deposició amb l'objectiu de correlacionar la informació recollida de les tècniques de caracterització de superfície utilitzades amb els resultats electroquímics.

En segon lloc es va testar un model teòric desenvolupat en el grup de recerca per explicar el fenomen de la codeposició induïda. Es va testar la capacitat del model per *reproduir* les corbes j-t enregistrades a diferents potencials a partir de solucions que contenien 0.2 mol dm^{-3} citrat, 0.1 mol dm^{-3} $CoSO_4$ i una concentració variable de Na_2MoO_4 (0.002-0.006 mol dm^{-3}). Es van preparar dipòsits de Co-Mo i de Co pur (a partir d'un bany en absència de molibdat) sobre carboni vitri a temps molt curts de deposició per determinar la geometria dels nuclis formats, així com la velocitat de nucleació. A partir de l'ajust de les corbes experimentals es pretenia calcular paràmetres relacionats amb la cinètica de nucleació i creixement.

En darrer lloc es va estudiar la influència dels components del bany i del pH sobre el procés de deposició. Es va estudiar per separat l'efecte de l'agent complexant, del Co(II) i del molibdat mitjançant experiments voltamètrics i cronoamperomètrics. Es van preparar

dipòsits a diferents concentracions de citrat sòdic i valors de pH distints per tal de conèixer com afecten aquests paràmetres a la naturalesa dels dipòsits (homogeneïtat, morfologia...). Atès que la manera com té lloc la descàrrega dels metalls depèn dels complexos que existeixen en solució, es va utilitzar l'espectroscòpia Raman per determinar les espècies presents a pH=6.6 i a pH=4.0. A partir de l'examen de tota la informació recollida, es van proposar les etapes involucrades en la deposició de Co-Mo en les condicions experimentals assajades.

Els resultats detallats d'aquest capítol s'inclouen en els següents articles:

Detection and characterization of molybdenum oxides formed during the initial stages of cobalt-molybdenum electrodeposition
J. Appl. Electrochem. 33 (2003) 245

Extracting deposition parameters for cobalt-molybdenum alloy from potentiostatic current transients
Phys. Chem. Chem. Phys. 6 (2004) 1340

Influence of the bath composition and the pH on the induced cobalt-molybdenum electrodeposition
J. Electroanal. Chem. 556 (2003) 137

Detection and characterization of molybdenum oxides formed during the initial stages of cobalt-molybdenum electrodeposition

Journal of Applied Electrochemistry **33**: 245–252, 2003.

Detection and characterization of molybdenum oxides formed during the initial stages of cobalt–molybdenum electrodeposition

E. GÓMEZ*, E. PELLICER and E. VALLÉS
Laboratori de Ciència i Tecnologia Electroquímica dels Materials (LCTEM), Departament Química Física. Facultat de Química. Universitat de Barcelona. Martí i Franquès, 1. 08028 Barcelona, Spain
*(*author for correspondence, fax: +34 93 4021231, e-mail: e.gomez@qf.ub.es)*

Received 19 August 2002; accepted in revised form 15 December 2002

Key words: cobalt–molybdenum, electrodeposition, induced codeposition, molybdenum oxides

Abstract

The initial stages of cobalt–molybdenum electrodeposition on a vitreous carbon electrode were studied to obtain information about the mechanism of cobalt–molybdenum induced codeposition. Solutions containing cobalt sulphate, sodium molybdate and sodium citrate at pH 6.6 were used. A first step in the mechanism of alloy deposition is proposed. This step takes into account the formation of molybdenum(IV) oxides over which Co–Mo alloy may be only deposited if sufficient potential is applied. Co–Mo electrodeposition occurs through an early stage involving low reduction current, related to the formation of molybdenum oxides, followed by a later stage in which the reduction current suddenly increases, corresponding to alloy codeposition. When a low potential is applied, a continuous coloured molybdenum oxide film is formed on the electrode and Co–Mo is not deposited. To induce the alloy deposition on the 'oxide film' it is necessary to apply more negative potentials than a threshold value, which depends on the composition of the electrolytic bath. By increasing molybdate concentration in solution, the 'threshold potential' shifts to more negative values. Intermediate molybdenum oxides were characterized using scanning electron microscopy (SEM), compositional analysis, Raman measurements and Auger and X-ray photoelectron spectroscopies.

1. Introduction

Alloys containing molybdenum are of interest because of their hardness, thermal and corrosion resistance and magnetic properties. They also offer good catalytic properties for hydrogen evolution [1–4]. Electrodeposition is a useful method to obtain these alloys. Molybdenum cannot be electrodeposited alone from aqueous solutions [5], but can be obtained by electrodeposition as an alloy, such as combined with an iron-group metal (induced codeposition).

Several studies have examined the induced codeposition mechanism between the molybdenum and an iron-group element and various hypotheses centred specially on Ni–Mo codeposition have been put forward [6–9]. Podlaha et al. extended the proposed sequence of steps for Ni–Mo codeposition [8, 9] to the codeposition of all iron group-molybdenum [10]. They suggested the formation of an intermediate, which involves an iron-group element that may act as a catalyst for the reduction of a proposed molybdenum oxide intermediate.

Previously, we studied the Co–Mo electrodeposition from a citrate-sulfate bath in order to obtain alloys that exhibit soft magnetic behaviour [11]. Baths with high cobalt(II)/molybdate ratios, greater than $[Co(II)]/[MoO_4^{2-}] = 6$, were used due to the great ability of the molybdenum to incorporate in the deposit. During the electrochemical study of the process two distinct responses were obtained in potentiostatic experiments depending on the applied potential. As a result of this unexpected behaviour, we decided, in the present work, to analyse the first stages of Co–Mo electrodeposition. This study aims to clarify the Co–Mo mechanism, by characterising the electrochemical response and the films produced in the initial stages of the reduction process. Improved knowledge of the deposition mechanism will facilitate the final objective of preparing Co–Mo deposits with desired magnetic properties.

2. Experimental details

Electrochemical measurements were taken from a conventional thermostatted three-electrode cell, using a microcomputer-controlled potentiostat/galvanostat (model 273, EG&G) or an Autolab with PGSTAT30 equipment and GPES software. The temperature was maintained at 25 °C. The chemicals used were $CoSO_4 \cdot 7H_2O$, $Na_2MoO_4 \cdot 2H_2O$ and $Na_3C_6H_5O_7 \cdot 2H_2O$, all of analytical grade. All solutions were freshly

prepared with water which was first doubly distilled and then treated with a Millipore Milli Q system. Citrate was always maintained at 0.2 mol dm^{-3}. The pH was adjusted to 6.6. Before each experiment the solutions were deaerated by argon bubbling and maintained under argon atmosphere during the recording of the experimental curves.

The working electrode used was a vitreous carbon (Metrohm) rod of 2 mm in diameter. It was polished to a mirror finish using alumina of distinct grades (3.75 and 1.87 μm) and cleaned ultrasonically for 2 min in water. The counter electrode was a platinum spiral. The reference was a Ag|AgCl|NaCl 1 mol dm^{-3} electrode mounted in a Luggin capillary containing 0.5 mol dm^{-3} Na_2SO_4 solution. All potentials are referred to this electrode.

Voltammetric experiments were carried out initially scanning in the negative direction. Only one cycle was run in each voltammetric experiment. Chronoamperometric experiments were done by stepping the potential from an initial value at which no process occurred to a value at which the reduction process occurred. Deposits were obtained under moderate stirring at 60 rpm.

The morphology of the deposits was examined with a Hitachi S 2300 or with a Leica Cambridge Stereoscan S-360 scanning electron microscopes. Elemental composition was determined using an X-ray analyser incorporated in the Leica equipment (EDS). For quantitative analysis, standards of pure molybdenum and pure cobalt, previously polished, were used before each experimental determination.

For chemical analysis, the films were dissolved in 5 ml of a 1% nitric acid solution and the resultant samples were then analysed by inductively coupled plasma mass spectrometry (ICP-MS). Measurements were made in a Perkin-Elmer spectrometer Elan 6000. Certified standard solutions of cobalt and molybdenum ions containing rhodium as internal standard were used to calibrate the instrument.

Raman measurements were performed at room temperature with a Jobin Yvon T64000 spectrometer coupled with an Olympus metallographic microscope, using the green line of an Ar^+ laser ($\lambda = 514.5$ nm) as excitation light and working in subtractive mode. The dispersive microprobe was constituted by three monocromators. The samples were exposed to laser powers between 4 and 10 mW with spot size was 1 μm.

Auger spectroscopy measurements were done with a PHI 670 scanning Auger nanoprobe system, which allowed a controlled sputtering of the samples and, simultaneously, the in-depth measurement of the chemical composition. The beam energy of the electron gun was selected at 10 kV and with a current of 10 nA. The level of vacuum was kept below 10^{-7} pa. To ensure that measurements were taken in a flat central region of the crater, the sputter area was larger than that scanned by the electron beam.

X-ray photoelectron spectroscopy (XPS) measurements were performed with a PHI 5600 multitechnique system, using standard AlK_α radiation, with a resolution of 0.1 eV.

3. Results

3.1. *Electrochemical study*

A first electrochemical study of the electrodeposition process was performed using solutions with 0.1 mol dm^{-3} Co(II) and different molybdate concentrations ranged between 0 and 0.015 mol dm^{-3}. The voltammetric response (Figure 1) showed that the gradual increase in molybdate concentration in solution advanced the appearance of the sharp reduction current increase, which was related in previous work to the Co–Mo deposition process [11]. When the voltammetric response previous to the onset of alloy deposition was zoomed (picture inside of Figure 1), a zone of low reduction current was detected (zone I) followed by the beginning of alloy deposition (zone II). By increasing the molybdate concentration the current related to zone I was enhanced.

For all solutions, by reversing the negative scan at more negative potentials than those corresponding to the beginning of alloy deposition, a typical nucleation loop was detected. A clear oxidation peak centred between −250 and −300 mV was recorded during the positive scan.

For these solutions, in the chronoamperometric experiments, two distinct shapes of the j/t transient were observed, depending on the applied potential. At low negative potentials, the j/t transients showed a monotonic current increase, even when the deposition time was increased to several hours, with a low charge involved (Figure 2, curves (a) and (b)). Applying more negative potentials, the j/t transients showed an initial zone of relatively low current followed by a sudden slope change (Figure 2, curve (c)). The length of time for

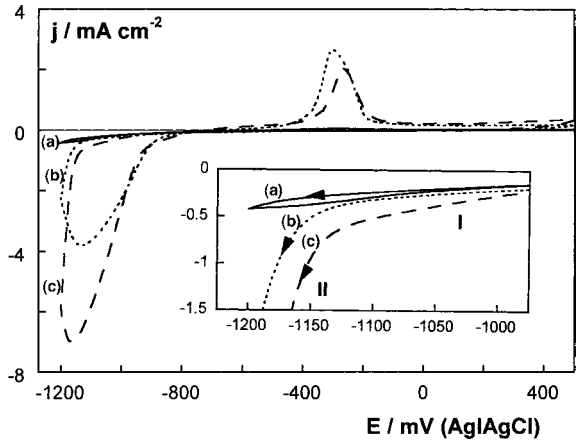

Fig. 1. Cyclic voltammograms of 0.1 mol dm^{-3} $CoSO_4$ + x mol dm^{-3} Na_2MoO_4 + 0.2 mol dm^{-3} $Na_3C_6H_5O_7$ solution. $v = 50$ mV s^{-1}. Cathodic limit −1200 mV. (a) $x = 0$, (b) $x = 0.005$, (c) $x = 0.015$. Under quiescent conditions.

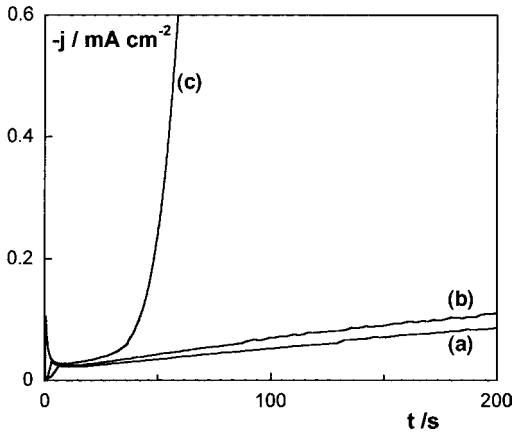

Fig. 2. j/t transients of a 0.1 mol dm^{-3} $CoSO_4$ + 0.012 mol dm^{-3} Na_2MoO_4 + 0.2 mol dm^{-3} $Na_3C_6H_5O_7$ solution. Starting potential −500 mV. Final potential: (a) −950 mV, (b) −960 mV, (c) −1000 mV. $\omega = 60$ rpm.

Table 1. Threshold potential of different electrolytic baths containing 0.2 mol dm^{-3} $C_6H_5Na_3O_7$, 0.1 mol dm^{-3} $CoSO_4$ and a variable molybdate concentration

$[MoO_4^{2-}]$ /mol dm^{-3}	$-E_{threshold}$ /mV
0.005	960
0.012	975
0.015	985
0.018	1000
0.035	1050
0.150	1160

the first zone gradually decreased as the applied potentials were made more negative.

For each bath, a potential value at which the potentiostatic response changed drastically – from the behaviour observed in curves (a) and (b) to the behaviour observed in curve (c) – was found. Therefore, it seemed that a minimum potential value had to be applied to detect the appearance of the sharp current increase during the reduction process. This threshold value was a function of bath composition (Table 1), being more negative as the molybdate concentration in solution increased.

3.2. *Characterization of deposits*

Different samples were prepared potentiostatically from the solutions tested in Section 3.1 applying, for each bath, potentials which were at most, 20 mV more negative than the threshold potential. This narrow range of potential was selected in order to ensure clear observation of the first part of the j/t transient in the chronoamperometric experiments.

When samples obtained at the onset of the second part of the j/t transient (Figure 3A, points (a) and (b)) were imaged by SEM, rounded crystallites distributed homogeneously on the substrate were observed (Figure 3B and C). EDS analysis revealed that the crystallites corresponded to a Co–Mo alloy.

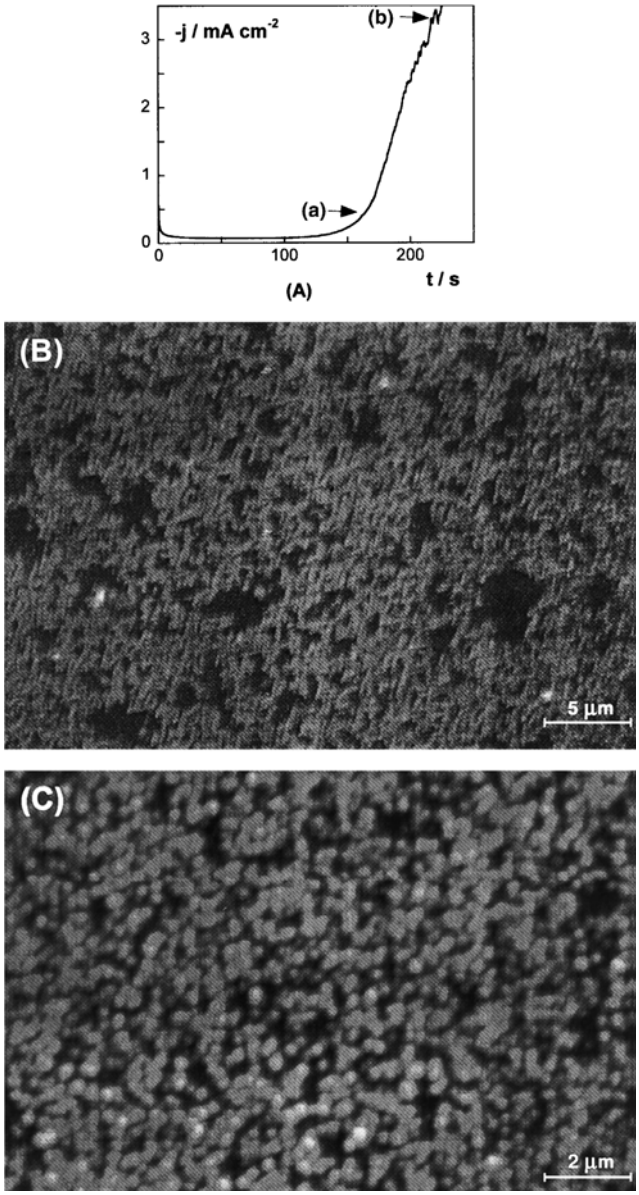

Fig. 3. (A) j/t transient at −980 mV from the solution of Figure 2. (B) and (C) SEM images of deposits corresponding to points (a) and (b) of Figure 3A.

When these images were zoomed between the crystallites, it appeared that a thin film had grown under the nuclei. To characterize this initial film, samples obtained at more positive potentials than the corresponding threshold value were prepared. These potentials were selected to ensure that monotonic j/t transients and long deposition times (thousand seconds) were applied to obtain a sufficient amount of the film (Figure 4A). In these conditions, coloured shiny films were obtained (green, blue or dark red).

SEM micrographs of these samples showed very fine-grained cracked films (Figure 4B). EDS analysis revealed the presence of mainly molybdenum and oxygen, accompanied by a very little cobalt (Figure 4C). Moreover, the significant carbon signal showed that the films were very thin. Chemical ICP-MS analysis of the solutions obtained after dissolving the films corroborated the

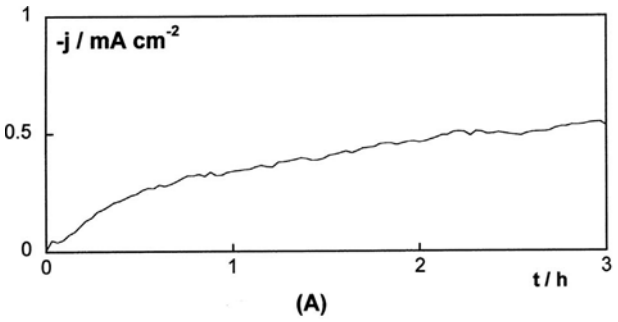

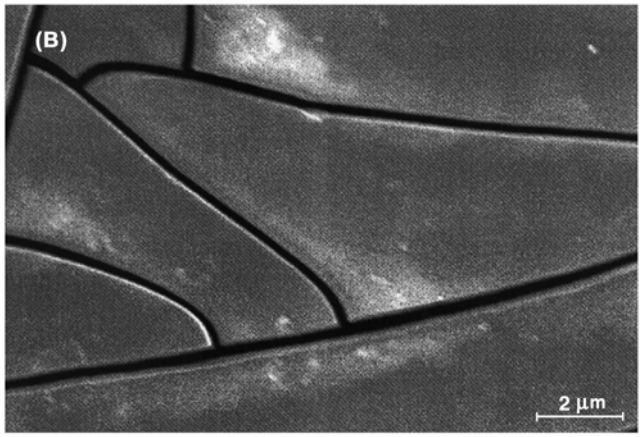

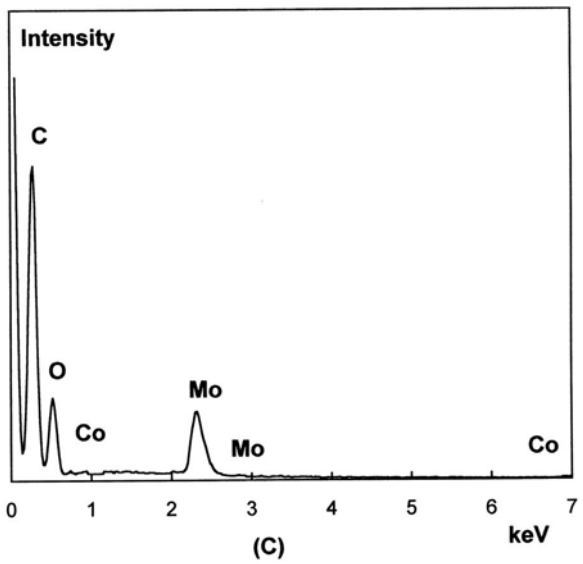

Fig. 4. (A) j/t transient of a film obtained from 0.1 mol dm^{-3} $CoSO_4$ + 0.012 mol dm^{-3} Na_2MoO_4 + 0.2 mol dm^{-3} $Na_3C_6H_5O_7$ solution at −930 mV during 3 h. (B) Corresponding SEM picture of the film. (C) Corresponding EDS microanalysis.

almost unique presence of molybdenum as a metal in these films (Table 2, samples 1–3). Furthermore, ICP-MS analysis revealed that the presence of Co in the deposit increased greatly when the potential applied to produce the film was very close to the corresponding threshold (Table 2, sample 4).

Auger experiments were carried out to characterize the species on the surface. Successive cycles with increasing sputter time were run and the spectra corresponding to the substrate (carbon) and to the three possible elements of the film (cobalt, molybdenum and oxygen) were recorded (Figure 5). These experiments indicated that the film was composed mainly of molybdenum and oxygen, the cobalt signal being at quasi-noise level. Carbon was observed even at low sputtering times due to cracking of the films. Similar results were obtained by XPS measurements (Figure 6).

Table 2. ICP-MS analysis of solutions obtained after dissolving oxide films in 5 ml of 1% nitric acid. The baths employed for preparing the films contained 0.2 mol dm^{-3} $C_6H_5Na_3O_7$, 0.1 mol dm^{-3} $CoSO_4$ and a variable molybdate concentration

Sample	$[MoO_4^{2-}]$ /mol dm^{-3}	$-E$ /mV	ppb Mo	ppb Co
1	0.012	920	152.9	5.9
2		930	140.7	6.8
3	0.035	990	170.3	12.0
4		1040	250.0	90.0

Films were prepared potentiostatically, E being the applied potential.

These analyses indicated that the films were formed of molybdenum oxides/hydroxides. For all the films an apparent atomic Mo:O ratio around 1:1 was obtained from the EDS (Figure 4C) and XPS spectra (Figure 6). In order to explain these unexpected results, similar analyses from standards of stoichiometric molybdenum compounds containing molybdenum and oxygen were performed. For this kind of compound the analyses revealed that, under our experimental conditions, preferential sputtering occurred, leading to a Mo:O lower than the theoretical one. Therefore the stoichiometric Mo:O ratio was not possible to deduce by means of these techniques.

To attempt to clarify the nature of the 'molybdenum oxides' obtained by reduction, before Co–Mo electrodeposition, Raman spectroscopy was used. The Raman spectra of various films showed a similar peak-response and no significant differences attributed to colour were observed (Figure 7A). A broad peak centred on 740 cm^{-1} was recorded for all the samples, and was accompanied by peak/s ranging between 500–580 cm^{-1} (Figure 7A and B, curve (a)). These peaks were clearly related to the presence of molybdenum(IV) oxide in the deposit [12, 13]. The peaks, especially in the interval 500–580 cm^{-1}, were very sensitive to laser power and, after subsequent scans, their definition diminished, being undetectable in some cases. The group of peaks corresponding to Mo(VI) oxide [14] always appeared in the spectra. Their presence was more evident as both the number of scans and the laser power were increased, especially for those that appeared around 950 cm^{-1} and under 250 cm^{-1}.

However, Raman spectra recorded from samples at which cobalt–molybdenum codeposition had been started did not show the peaks, related to Mo(IV) oxide, centred at 740 and 550 cm^{-1} (Figure 7B, curve (b)). A new peak about 660 cm^{-1} appeared, which was possible to assign to Co–Mo interaction [12]. This peak increased in intensity with samples obtained at longer deposition time.

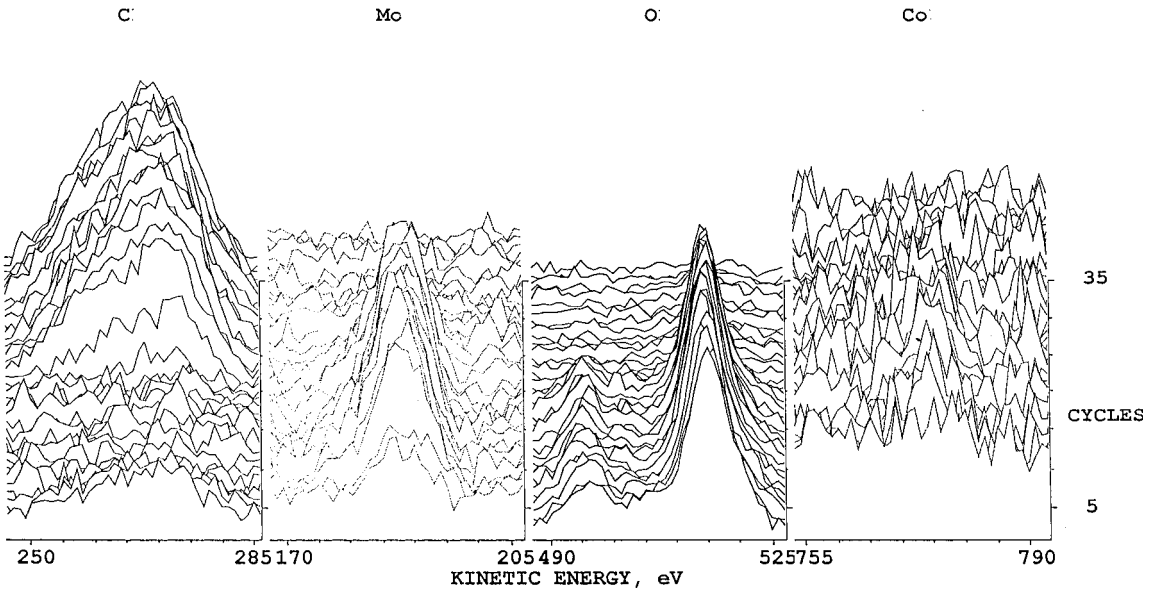

Fig. 5. Auger depth profiles of a film obtained from 0.1 mol dm^{-3} $CoSO_4$ + 0.012 mol dm^{-3} Na_2MoO_4 + 0.2 mol dm^{-3} $Na_3C_6H_5O_7$ solution at −930 mV during 3 h.

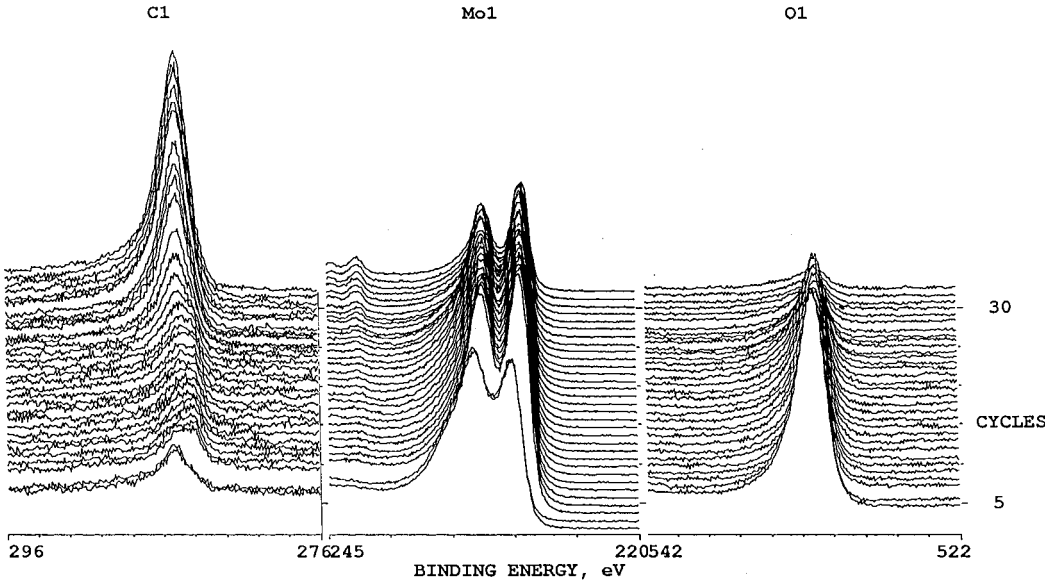

Fig. 6. XPS depth profiles of the same film in Figure 5.

Samples prepared at potentials slightly more positive than the threshold value led, after several hours, to an incipient Co–Mo alloy formation upon the molybdenum oxide film (Figure 8). Obviously, this kind of sample did not correspond to a homogeneous deposit, but they were useful to demonstrate that cobalt–molybdenum deposition took place over the oxide film.

3.3. *Influence of Co(II) concentration on oxide formation*

As the current related to oxide formation increased with increasing molybdate concentration in solution, baths with high molybdate concentrations were tested in order to proceed later to examine the possible influence of Co(II) on molybdenum oxide formation.

Figure 9 shows the voltammetric response when molybdate concentration was raised to 0.15 mol dm^{-3}. During the cathodic scan, a quasi-plateau related to oxide formation appeared (zone I), followed by a sharp reduction current increase (zone II). Reversing the scan, whether at the onset of the second process (curve (a)) or at more negative potentials (curve (b)), a broad oxidation band was recorded from −800 mV. This oxidation current was greatly minimised under stirring conditions. Lengthening the positive scan to more positive potentials, a very small peak around −125 mV was recorded, related to cobalt–molybdenum oxidation. The charge involved in this peak was always very low (i.e., it was not sensitive to the cathodic limit).

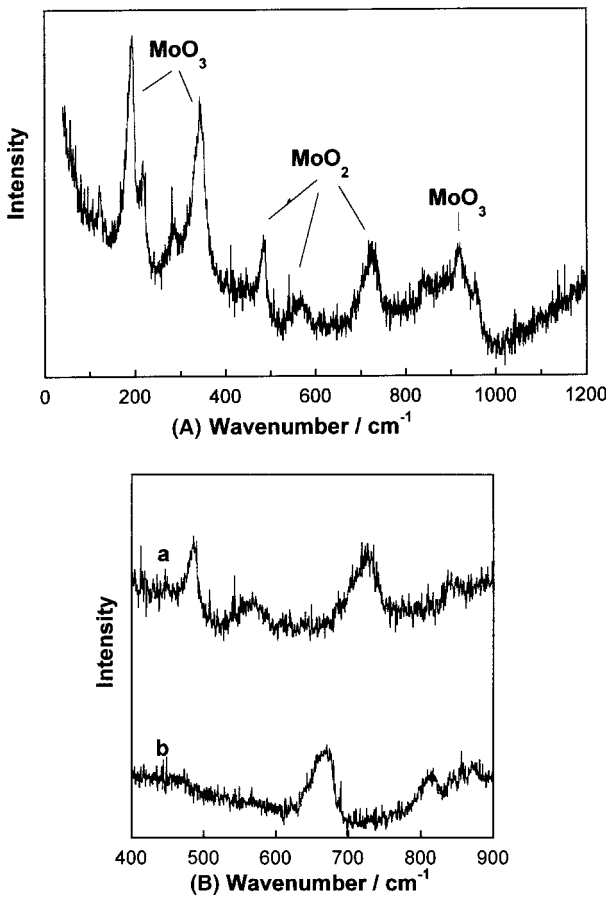

Fig. 7. Raman spectra of the films obtained from: (A) 0.1 mol dm^{-3} $CoSO_4$ + 0.012 mol dm^{-3} Na_2MoO_4 + 0.2 mol dm^{-3} $Na_3C_6H_5O_7$ solution at −930 mV during 3 h. (B) curve (a) zoom detail between 400 cm^{-1} and 900 cm^{-1} of the (A) spectrum. Curve (b): 0.1 mol dm^{-3} $CoSO_4$ + 0.005 mol dm^{-3} Na_2MoO_4 + 0.2 mol dm^{-3} $Na_3C_6H_5O_7$ solution at −980 mV during 1600 s.

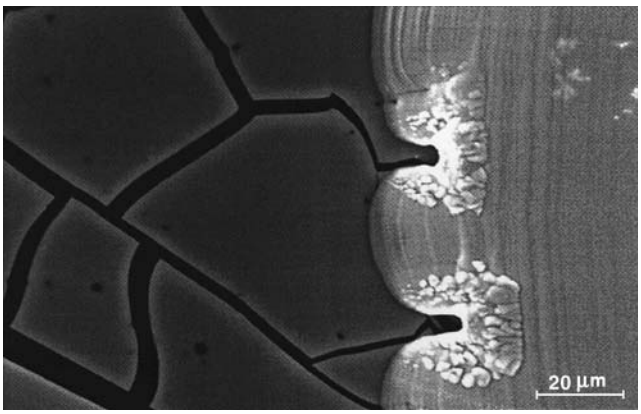

Fig. 8. SEM image of a deposit obtained from the same solution of Figure 2 at −960 mV during 10 h. Left part: molybdenum oxides, right part: Co–Mo alloy, 30% Mo.

The study of Co(II) influence on molybdenum oxides formation was performed at 0.15 mol dm^{-3} MoO_4^{2-}, because the voltammetric plateau ensured a large range of potentials at which only oxide formation occurred. Figure 10 shows a collection of voltammograms recorded from solutions containing a variable Co(II) concentration (between 0 and 0.12 mol dm^{-3}) at fixed cathodic limit of −1100 mV. Voltammetric curves showed that Co(II) in solution clearly favoured the onset of molybdenum oxide formation, this being more evident at concentrations >0.05 mol dm^{-3} (curves (d) and (e)). Only a broad band was recorded during the positive scan and the oxidation charge involved increased with increasing Co(II) concentration.

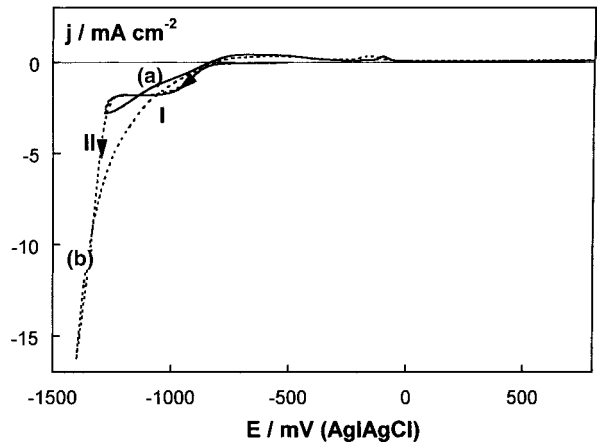

Fig. 9. Cyclic voltammograms of 0.1 mol dm^{-3} $CoSO_4$ + 0.15 mol dm^{-3} Na_2MoO_4 + 0.2 mol dm^{-3} $Na_3C_6H_5O_7$ solution. v = 50 mV s^{-1}. Cathodic limit: (a) −1300 mV, (b) −1400 mV. Under quiescent conditions.

The corresponding chronoamperometric curves, recorded at −900 mV (Figure 11), show, on the one hand a smooth current increase of the j/t transient for Co(II)-free solutions (curve (a)) and a clear enhancement of the reduction process when Co(II) was present in solution (curve (b)). On the other hand, Figure 9 shows that large current densities were reached as Co(II) concentration in solution was increased (curves (b) and (c)).

Various molybdenum oxide films were prepared at low deposition potentials and were compared with those obtained from solutions containing 0.1 mol dm^{-3} $CoSO_4$ (Section 3.2). In contrast to what was observed

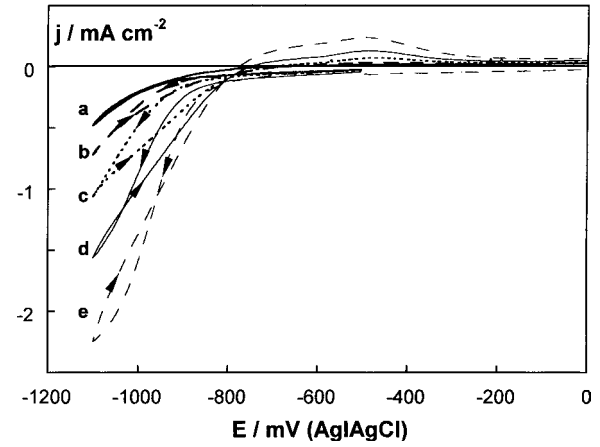

Fig. 10. Cyclic voltammograms of x mol dm^{-3} $CoSO_4$ + 0.15 mol dm^{-3} Na_2MoO_4 + 0.2 mol dm^{-3} $Na_3C_6H_5O_7$ solution. v = 50 mV s^{-1}. Cathodic limit −1100 mV. (a) $x = 0$, (b) $x = 0.024$, (c) $x = 0.045$, (d) $x = 0.065$, (e) $x = 0.085$. Under quiescent conditions.

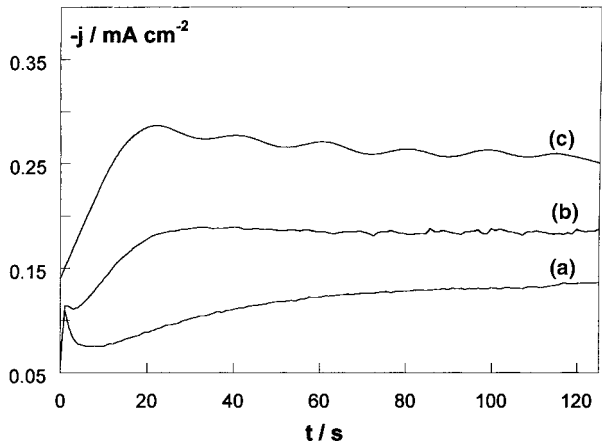

Fig. 11. j/t transients of x mol dm^{-3} $CoSO_4$ + 0.15 mol dm^{-3} Na_2MoO_4 + 0.2 mol dm^{-3} $Na_3C_6H_5O_7$ solution at −900 mV: (a) $x = 0$, (b) $x = 0.024$, (c) $x = 0.045$. Under quiescent conditions.

Table 3. Current efficiency (η) of the molybdenum oxides formation process

$[MoO_4^{2-}]$ /mol dm^{-3}	[Co(II)] /mol dm^{-3}	$-E$ /mV	η /%
0.012	0.1	930	3.8
	0		1.3
	0.1	920	5.3
	0		2.1
0.10	0.1	950	3.1
	0		0.9

Oxide films were prepared potentiostatically from solutions containing 0.2 mol dm^{-3} $C_6H_5Na_3O_7$.

in the first case, films prepared from Co(II)-free solutions were clearly pale-coloured. Table 3 shows the current efficiency of the process involved in preparing molybdenum oxide films. The current efficiency values (η) were deduced by comparing the theoretical reduction charge during deposition with the amount of molybdenum obtained from ICP-MS analysis. The same deposition potential was selected to assure a comparable hydrogen evolution reaction for both kinds of solution, although, in the case of Co(II)-free solutions, it was necessary to increase the deposition time to attain similar deposition charges. The results showed that, at fixed MoO_4^{2-} concentration and applied potential, the efficiency of the process was higher for solutions containing Co(II). However, the low efficiency involved in all cases confirmed that the molybdenum oxide films were very catalytic to hydrogen evolution.

4. Discussion and conclusions

Results obtained have demonstrated that molybdenum(IV) oxides are formed as a first step in induced cobalt–molybdenum codeposition.

A relationship between the electrochemical response during the deposition and the kind of deposit formed on the electrode has been found. The two reduction zones detected in voltammetric experiments are related to molybdenum oxides (zone I) and alloy (zone II) formation, respectively. Chronoamperometric experiments are in agreement with these results. Alloy formation takes place over an initial molybdenum oxide but for Co–Mo alloy deposition a 'threshold potential' is necessary, and at more positive potentials than this critical value, only molybdenum oxides are formed as a consequence of the reduction process.

A combination of the characterisation techniques and the electrochemical studies constitutes a successful way of detecting the previous molybdenum oxide formation during induced cobalt–molybdenum electrodeposition. The SEM shows the formation of a thin film on the electrode substrate, over which cobalt–molybdenum begins to deposit. Results obtained from EDS, Auger and XPS techniques have demonstrated that molybdenum oxides are formed at potentials lower than that for Co–Mo deposition. Molybdenum(IV) oxide formation has been demonstrated by Raman experiments. However, it is not possible to rule out the presence of Mo(VI) oxides, probably produced by oxidation of the freshly deposited molybdenum intermediate oxides.

The coloured molybdenum(IV) oxides obtained at low potentials from Co(II)-molybdate baths may correspond to substoichiometric molybdenum oxides, whose colour is related to the presence of oxygen vacancies [16]. For these oxides an associated intercalation reaction [17] is favoured. During electrochemical formation, ions in solution are inserted into the film (protons, sodium or cobalt ions). When an initial film of molybdenum oxide is formed, significant hydrogen evolution occurs and the possible inclusion of protons may lead to the formation of blue molybdenum oxide [18]. Moreover, the incorporation of some cobalt ions in the films prepared from solutions containing Co(II) may explain their deep colour in comparison to the pale ones obtained from Co(II)-free solutions. At a fixed deposition charge, films produced from Co(II)-free solutions were thinner than those obtained in the presence of Co(II) because of lower current efficiency. In order to discover if colour variation was dependent on film thickness, various samples from Co(II)-free baths were prepared with increasing deposition charge or deposition time. In all cases, films were pale-coloured. Therefore, colour variation could not be solely attributed to film thickness.

At our working pH, $CoCit^-$ is the predominant cobalt(II) species in solution [19, 20]. Then, the formation of molybdenum oxides can be catalysed by the $CoCit^-$ species:

$$MoO_4^{2-} + 2\,H_2O + 2\,e^- \xrightarrow{CoCit^-} MoO_2 + 4\,OH^- \qquad (1)$$

The high efficiency of molybdenum oxide formation when Co(II) is present in solution may be related to the simultaneous adsorption of $CoCit^-$ on the molybdenum oxides freshly deposited, thereby reducing the hydrogen evolution.

$$MoO_2 + CoCit^- \longrightarrow [MoO_2 - CoCit^-]_{ads} \quad (2)$$

However, the adsorption of Co(II) over the molybdenum oxide is not enough to promote molybdenum deposition. Only when sufficient potential is applied does the discharge of the molybdenum oxide to molybdenum metal take place.

The detection of the intermediate molybdenum oxides is in agreement with the mechanism proposed by Podlaha et al. for M–Mo electrodeposition [8–10], M being nickel, iron or cobalt, in which the first step is the reduction of MoO_4^{2-} to Mo(IV) by means of the collaboration of M(II)L (L being a ligand) to form an adsorbed intermediate $[M(II)(L)MoO_2]_{ads}$ species. Next, the formation of the Co–Mo alloy occurs through steps in which $CoCit^-$ is reduced to cobalt and $[MoO_2–CoCit^-]_{ads}$ is reduced to molybdenum.

$$CoCit^- + 2\,e^- \longrightarrow Co + Cit^{3-} \quad (3)$$

$$[MoO_2–CoCit^-]_{ads} + 2\,H_2O + 4\,e^- \longrightarrow Mo + CoCit^- + 4\,OH^- \quad (4)$$

At low molybdate concentration, alloy deposition occurs at more positive potentials than those corresponding to pure cobalt [11], probably because of the greater facility of cobalt to be deposited on the molybdenum oxides than on vitreous carbon. However, when the molybdate concentration is increased, the threshold potential is shifted to more negative values. This potential shift may be explained by the semiconducting nature of these molybdenum oxides. With increasing molybdate concentration in solution thicker molybdenum oxide films are formed, thereby making Co–Mo deposition more difficult. Moreover, as a result of the threshold potential shift, a greater hydrogen coevolution accompanies alloy deposition.

Depending on the counterbalance between the concentration of electrolyte and the deposition parameters, either Co–Mo deposits or molybdenum oxide films may be obtained. Although only a low current efficiency achieved during electrochemical preparation of oxide films, electrochemistry may constitute an alternative to physical methods like sputtering and PVD.

Acknowledgements

The authors thank the Serveis Cientificotècnics (Universitat de Barcelona) for the use of their equipment. This paper was supported financially by contract MAT 2000-0986 from the Comisión Interministerial de Ciencia y Tecnología (CICYT) and by the Comissionat of the Generalitat de Catalunya under Research Project 2001SGR00046. E. Pellicer also thanks the DURSI of the Generalitat de Catalunya for financial support.

References

1. Ch . Fan, D.L. Piron, A. Sleb and P. Paradis, *J. Electrochem. Soc.* **141** (1994) 382.
2. Ch. Fan, D.L. Piron and P. Paradis, *Electrochim. Acta* **39** (1994) 2715.
3. E. Chassaing, M.P. Roumegas and M.F. Trichet, *J. Appl. Electrochem.* **25** (1995) 667.
4. Ch. Chu and S. Wu, *J. Electrochem. Soc.* **147** (2000) 2190.
5. A. Brenner, 'Electrodeposition of Alloys', vols. 1 and 2 (Academic Press, New York, 1963).
6. H. Fukushima, T. Akiyama, S. Akagi and K. Higashi, *Trans Jpn. Inst. Met.* **20** (1979) 358.
7. E. Chassaing, K. Vu Quang and R. Wiart, *J. Appl. Electrochem.* **19** (1989) 839.
8. E.J. Podlaha and D. Landolt, *J. Electrochem. Soc.* **143** (1996) 885.
9. E.J. Podlaha and D. Landolt, *J. Electrochem. Soc.* **143** (1996) 893.
10. E.J. Podlaha and D. Landolt, *J. Electrochem. Soc.* **144** (1997) 1672.
11. E. Gómez, E. Pellicer and E. Vallés, *J. Electroanal. Chem.* **517** (2001) 109.
12. Z.J. Niu, S.B. Yao and S.M. Zhou, *J. Electroanal. Chem.* **455** (1998) 205.
13. Y. Zeng, Z. Li, M. Ma and S. Zhou, *Electrochem. Commun.* **2** (2000) 36.
14. T. Ivanova, K.A. Gesheva and A. Szekeres, *J. Solid Stat. Electrochem.* **6** (2002) [online March 8].
15. P. Garrido, E. Gómez and E. Vallés, *J. Electroanal. Chem.* **441** (1998) 147.
16. V.K. Sabhapathi, M. Hussain, P.S. Reddy, P. Ramakrishna Reddy, S. Uthanna, B.S. Naidu and P. Jayarama Reddy, *Phys. Status Solidi (a)* **148** (1995) 167.
17. J. Scarminio, A. Lourenço and A. Gorenstein, *Thin Solid Films* **302** (1997) 66.
18. S. Liu, Q. Zhang, E. Wang and S. Dong, *Electrochem. Comm.* **1** (1999) 365.
19. S.S. El Rehim, S.M. El Wahaab, M.A.M. Ibrahim and M.M. Dankeria, *J. Chem. Technol. Biotechnol.* **73** (1998) 369.
20. D.R. Lide (Ed.), 'Handbook of Chemistry and Physics', 77th edn. (CRC Press New York, 1996–1997), pp. 8–50.

Extracting deposition parameters for cobalt-molybdenum alloy from potentiostatic current transients

RESEARCH PAPER

PCCP
www.rsc.org/pccp

Extracting deposition parameters for cobalt–molybdenum alloy from potentiostatic current transients

E. Gómez, Z. G. Kipervaser, E. Pellicer and E. Vallés*

Departament de Química Física, Laboratori d'Electrodeposició i Corrosió (Electrodep), Universitat de Barcelona, Martí i Franquès 1, E-08028, Barcelona, Spain. E-mail: e.valles@ub.edu; Fax: +34 93 4021231

Received 20th November 2003, Accepted 15th January 2004
First published as an Advance Article on the web 10th February 2004

In a previous paper a model for the potentiostatic current transients during induced cobalt–molybdenum alloy deposition was developed and tested in a few experimental conditions. Hemispherical geometry was assumed for the alloy crystallites. Here the model is studied in a wider range of experimental situations, in which the potential and the molybdate concentration are varied. It is verified that the model can be applied to the new set of variables. However, at the lowest molybdate concentrations the theoretical parameters do not agree with the experimental findings. This is attributed to changes in the geometry of the crystallites, which are conical rather than hemispherical. The consistency of the model in these conditions is also tested. The model correctly predicts that the system tends to follow the pattern found in charge-transfer controlled Co deposition as molybdate concentration in solution decreases. Pure Co without molybdenum was also deposited. SEM images showed that the pure Co deposits have sharp points. In comparison to alloy deposition, which is instantaneous, the pure-Co deposition is progressive. The difference in the nucleation kinetics may be caused by the molybdenum oxide layer, which is deposited before the alloy. The oxide layer may change the electrochemical properties of the substrate and therefore modify the nucleation kinetics.

Introduction

Cobalt–molybdenum electrodeposition is induced since molybdenum is not deposited from aqueous solution by itself.[1] It discharges only in conjunction with the deposition of another metal. The electrodeposition of cobalt–molybdenum has been studied in a sulfate–citrate bath on vitreous carbon electrode.[2] Low molybdate concentrations were used to obtain Co–Mo alloys with relatively low molybdenum percentages due to the substantial ability of molybdenum to incorporate in the deposits. Co–Mo electrodeposition occurs through an intermediate step which involves the formation of molybdenum oxides.[3]

In order to describe the Co–Mo deposition, a model was recently developed to interpret the potentiostatic curves corresponding to fixed concentrations and moderate deposition potentials.[4] Alloy deposition was modelled taking into account that it is preceded by the formation of molybdenum oxides.

Here we examine whether the model is valid for a range of molybdate concentrations and potentials, and calculate the nucleation and growth parameters for each concentration. High deposition potentials were chosen to minimise the time during which only molybdenum oxides are formed on the electrode, so that alloy deposition begins almost immediately.

The model

The model is described in detail elsewhere[4] and may be summarised as follows:

(1) It is assumed that the total current density of the Co–Mo electrodeposition process $j(t)$ can be expressed by eqn. (1)

$$j(t) = \begin{cases} j_{Ox}(t) \Rightarrow 0 \le t \le t_A \\ j_{Co}(t - t_A) + j_{Mo}(t - t_A) \Rightarrow t_A \le t \end{cases} \quad (1)$$

where $j_{Ox}(t)$, $j_{Co}(t)$ and $j_{Mo}(t)$ correspond to the molybdenum oxides, cobalt and molybdenum current densities, respectively. Eqn. (1) reflects the fact that only molybdenum oxides are deposited during t_A. After t_A, the alloy starts to be deposited. In this study the experimental conditions were chosen to minimise t_A.

(2) The Mo deposition occurs in two steps: oxide formation followed by their reduction to metallic Mo. Since both processes accelerate after t_A, we cover both steps in one term: $j_{Mo}(t)$.

(3) We assume that $j_{Mo}(t)$ is a mixed controlled process, with a rate constant of deposition, k_{Mo} (cm s^{-1}) since the interfacial reactions have an important role in the Mo deposition. Mixed controlled systems are defined by both the diffusion process and the charge transfer.

(4) It is assumed that $j_{Co}(t)$ is charge-transfer controlled because of the high concentration of Co in the solution, in comparison with the molybdate concentration. Moreover, Mo oxide deposition takes some time ($\le t_A$), which allows the bulk Co concentration near the electrode to be recovered.

(5) In our range of molybdate concentrations and at short deposition times (several seconds), the alloy composition was practically constant, even under stationary conditions.[4] We therefore assume that the mass fraction of Co deposited, m_{Co}, divided by the total mass of the deposit is constant, $\alpha = m_{Co}/(m_{Co} + m_{Mo})$. The molar volumes of Co and Mo in the alloy, $V^A_{m_{Co}} = \chi M_{Co}/\alpha$ and $V^A_{m_{Mo}} = \chi M_{Mo}/(1-\alpha)$, are also assumed to be constant, defining $\chi = [\alpha/\rho_{Co} + (1-\alpha)/\rho_{Mo}]$. M_{Co} and M_{Mo} are the molar masses (g mol^{-1}) of Co and Mo, respectively, and ρ_{Co} and ρ_{Mo} are their corresponding densities (g cm^{-3}).

(6) Hemispherical geometry is assumed for the crystallites of alloy. The model takes into account the possible overlap of the crystallites.

(7) Either possible nucleation law, progressive or instantaneous, is possible through the adoption of eqn. (2) for the nuclei density

$$N(t) = N_0[1 - \exp(-At)], \quad (2)$$

DOI: 10.1039/b315057g

N_0 (cm^{-2}) being the maximum nuclei density and A the nuclei activation rate (s^{-1}). If A is high, eqn. (2) converges to the instantaneous case. If A is low, it converges to the progressive case.

Taking into account the above assumptions, expressions for $j_{Mo}(t)$ and $j_{Co}(t)$ were deduced,[4] resulting in eqns. (3) and (5), respectively

$$j_{Mo}(t) = \zeta \int_0^t \exp(-Au)H(t-u)\mathrm{d}u \times \frac{1-\exp\left\{-\eta \int_0^t \frac{\exp(-Au)H(t-u)\mathrm{d}u}{\exp[Q^2(t-u)]\mathrm{erfc}[Q(t-u)^{1/2}]}\right\}}{\eta \int_0^t \frac{\exp(-Au)H(t-u)}{\exp[Q^2(t-u)]\mathrm{erfc}[Q(t-u)^{1/2}]}\mathrm{d}u} \quad (3)$$

where

$$H(t) = \left[\left(a_{Mo}^2 + b_{Mo}\,t\right)^{1/2} - 2a_{Mo} + \frac{a_{Mo}^2}{\left(a_{Mo}^2 + b_{Mo}\,t\right)^{1/2}}\right], \quad (4)$$

the function erfc(x) is the complementary error function,[5] z_{Mo} is the number of electrons transferred by the Mo ions, and F is the Faraday constant. In order to simplify the notation we define: $\eta = 2\pi D_{Mo} N_0 A/k_{Mo}$ and $\zeta = z_{Mo}FD_{Mo}c_{Mo}(2\pi N_0 A)^2/k_{Mo}$, $Q = k_{Mo}/D_{Mo}^{1/2}$, $a_{Mo} = D_{Mo}/k_{Mo}$, $b_{Mo} = 2D_{Mo}c_{Mo}V_{m_{Mo}}^{A}$ D_{Mo} is the diffusion coefficient of the molybdate in the solution.

$$j_{Co}(t) = \gamma \int_0^{R(t)} \int_0^{v(u=0)} \exp\{-A[t-T(y,v)]\}v\mathrm{d}v \times \exp\left\{\lambda \int_0^{v(u=0)} [1-\exp(-A(t-T(y,v)))]v\mathrm{d}v\right\}\mathrm{d}y \quad (5)$$

where $\gamma = 2\pi z_{Co}FN_0A/V_{m_{Co}}{}^{A},$, $\lambda = 2\pi N_0$, $T(y,v) = \{[(y^2+v^2)^{1/2} + a_{Mo}]^2 - a_{Mo}^2\}/b_{Mo}$, z_{Co} is the number of electrons transferred by the Co ions, $v(u=0) = [R^2(t) - y^2]^{1/2}$, and $R(t) = (a_{Mo}^2 + b_{Mo}t)^{1/2} - a_{Mo}$.

The theoretical expression for the j–t curves during the Co–Mo alloy deposition is obtained by substituting eqns. (3) and (5) into eqn. (1).

Experimental details

Solutions contained 0.1 mol dm^{-3} $CoSO_4$, 0.2 mol dm^{-3} $Na_3C_6H_5O_7$ and a concentration of Na_2MoO_4 ranging between 0.002 and 0.006 mol dm^{-3}. The solution pH was 6.6. All solutions were prepared from analytical grade reagents and water which was doubly distilled and then treated with a Milipore-Milli Q system. Before each experiment the solutions were de-aerated with argon.

Chronoamperometric experiments were performed in a thermostatted three-electrode cell using an Autolab with PGSTAT30 equipment and GPES software. The temperature was maintained at 25 °C.

The working electrode was a 2 mm-diameter vitreous carbon rod electrode (Metrohm). It was polished to a mirror finish before each experiment using alumina of different grades (3.75 and 1.85 μm) and cleaned ultrasonically for 2 min in water before each experiment. The reference electrode was Ag/AgCl/1 mol dm^{-3} NaCl mounted in a Luggin capillary containing 0.5 mol dm^{-3} Na_2SO_4 solution. All potentials were referred to this electrode. The counter electrode was a platinum spiral.

Potentiostatic transients were recorded from −500 mV to a final potential at which alloy deposition occurs. Deposit composition was determined with an X-ray analyser incorporated in a Leica Cambridge Stereoscan S-360 scanning electron microscope. The deposits were examined on a Hitachi 2300 scanning electron microscope.

Results and discussion

The potentiostatic transients of Co–Mo deposition were recorded applying −1100, −1150, −1250 and −1275 mV, at each of the three molybdate concentrations analysed: 0.002, 0.004 and 0.006 mol dm^{-3}. At the least negative potentials, the j–t transient can be described by an initial low current, a sudden increase after about 3–4 s and a stabilisation of the current followed by a slow decrease (Fig. 1(A)). The first part of the curves can be attributed to the formation of molybdenum oxides and the sudden increase is assigned to alloy deposition.[3] For a fixed potential, the deposition current clearly increases with molybdate concentration.

When the deposition potential is decreased, the process accelerates and the alloy deposition current is detected immediately after the first deposition times (Fig. 1(B)).

To fit the experimental curves using eqns. (3) and (5) it is necessary to determine N_0, A, k_{Mo} and α. The values of α were measured experimentally. The analysis of the deposits confirmed that, in our range of the deposition times, the deposit composition (and thus α) was practically constant. Moreover,

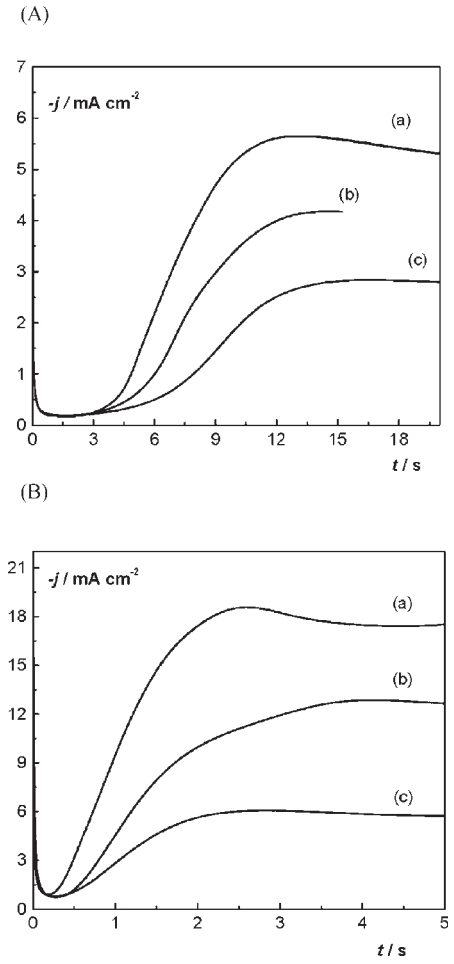

Fig. 1 (A) j–t Curves of Co–Mo alloy deposition at $E = -1100$ mV from a 0.1 mol dm^{-3} $CoSO_4$ + 0.2 mol dm^{-3} $Na_3C_6H_5O_7$ + x mol dm^{-3} Na_2MoO_4 solution: (a) $x = 0.006$, (b) $x = 0.004$ and (c) $x = 0.002$. (B) j–t Curves of Co–Mo alloy deposition at $E = -1275$ mV from a 0.1 mol dm^{-3} $CoSO_4$ + 0.2 mol dm^{-3} $Na_3C_6H_5O_7$ + x mol dm^{-3} Na_2MoO_4 solution: (a) $x = 0.006$, (b) $x = 0.004$ and (c) $x = 0.002$.

for each molybdate concentration, similar α values were obtained for the different applied potentials. This observation corroborates that, for the Co–Mo system, there is little influence of the deposition potential on the alloy composition.[6] In principle, N_0, A and k_{Mo} could be obtained by the best fit procedure, but the j–t curves were well fitted by the instantaneous case. This result was expected since high potentials were used in the experiments. Then, it was assumed that A is high, leading eqns. (3) and (5) to converge to the instantaneous case.

A good fit of the j–t transients is observed from the previous assumptions (Fig. 2). Table 1 lists the experimental values of α and the N_0 and k_{Mo} values corresponding to these fits.

Table 1 shows that for each molybdate concentration k_{Mo} increases as the potential decreases, as expected. However, at a fixed potential, although k_{Mo} is similar for 0.006 and 0.004 mol dm^{-3} molybdate concentrations, it is lower for the 0.002 mol dm^{-3} solution. Moreover, although the nuclei density is almost constant for 0.006 and 0.004 mol dm^{-3} concentrations, N_0 increases by one order of magnitude for the 0.002 mol dm^{-3} solution. Therefore, although a good fit is attained for all molybdate concentrations, the lowest molybdate concentration shows anomalous behaviour.

In order to understand the results for the 0.002 mol dm^{-3} solution, the consistency of the model was tested. It was assumed that a gradual decrease of molybdate concentration reduces the contribution of $j_{Mo}(t)$, so the j–t curve is well represented by the approximation

$$j(t) \approx j^*_{Co}(t), \quad (6)$$

where $j^*_{Co}(t)$ is the current density of Co, assuming that the crystallites have hemispherical geometry and that the deposition is charge-transfer controlled,[7]

$$J^*_{Co}(t) = 2 z_{Co} F k_{Co} p t \exp(-p t^2) \int_0^t \exp(p u^2) \mathrm{d}u, \quad (7)$$

where $p = \pi N_0 (M_{Co} k_{Co}/\rho_{Co})^2$, and k_{Co} (mol cm^{-2} s^{-1}) is the rate of crystal growth of Co. Note that k_{Co} and k_{Mo} have different units.

To verify approximation (6), the curves of 0.002 mol dm^{-3} molybdate concentration were fitted with eqn. (7) (Fig. 3). It is also necessary to calculate the values of the crystal growth rate of cobalt in the alloy, k^A_{Co} (mol cm^{-2} s^{-1}), because this parameter is hidden in eqn. (5). In ref. 4 an expression for k^A_{Co} as a function of the other parameters is developed

$$k^A_{Co}(t) = \frac{b_{Mo}}{2 V^A_{m_{Co}} (a^2_{Mo} + b_{Mo} t)^{1/2}}. \quad (8)$$

Table 1 Extracted N_0 and k_{Mo} values from the j–t alloy deposition transients through eqn. (1)

	$[MoO_4^{2-}] = 0.006$ mol dm^{-3}, $\alpha = 0.78$		$[MoO_4^{2-}] = 0.004$ mol dm^{-3}, $\alpha = 0.81$		$[MoO_4^{2-}] = 0.002$ mol dm^{-3}, $\alpha = 0.9$	
E/mV	$10^{-11} N_0$/ cm^{-2}	$10^4 k_{Mo}$/ cm s^{-1}	$10^{-11} N_0$/ cm^{-2}	$10^4 k_{Mo}$/ cm s^{-1}	$10^{-12} N_0$/ cm^{-2}	$10^4 k_{Mo}$/ cm s^{-1}
−1275	4.5	17.5	4.5	17	4	7.7
−1250	4.5	12.5	4.5	13	5	6.7
−1150	4.5	6.2	4.5	6.2	2.15	4.15
−1100	4	5.1	4	4.95	1	3.6

Using the parameters of Table 1 to plot eqn. (8), k^A_{Co} can be considered constant at the time studied here. Table 2 lists the parameters extracted from the fit of the 0.002 mol dm^{-3} molybdate concentration curves, using eqns. (1) and (6).

Taking into account the close values of N_0 and k^A_{Co} and k_{Co} in Table 2, four conclusions arise: (1) eqn. (6) describes well the system for low molybdate concentrations which suggests that in these conditions eqn. (7) is a good approximation. (2) Eqn. (1) converges to eqn. (7) for low molybdate concentrations. (3) Since eqn. (7) represents charge-transfer controlled deposition, this agreement indicates that the Co deposition is charge-transfer controlled in the presence of low molybdate concentrations. (4) As eqn. (7) is the instantaneous expression for charge-transfer controlled systems, this result suggests that, in this case, nucleation is instantaneous. If nucleation were progressive, the nuclei density would be a function of time, according to eqn. (2), and it is unlikely to have the same N_0 as an instantaneous description.

Since the model seems to be consistent for low molybdate concentrations, then the anomalous behaviour observed in Table 1 can be attributed to a change in the Co–Mo electrodeposition process when very low molybdate concentrations are present in solution. To corroborate this hypothesis, a study of the pure-cobalt deposition from similar electrodeposition conditions was made. We expected to observe intermediate features between the pure-cobalt deposition, the Co–Mo electrodeposition process from the 0.002 mol dm^{-3} solution and the Co–Mo deposition from greater molybdate concentrations.

At a fixed applied potential, the pure Co deposition process is slower than that of the alloy (Fig. 4). To obtain information about the deposition process of pure cobalt in the sulfate–citrate medium, the transients were analysed theoretically. In principle, it was assumed that the Co deposition regime does

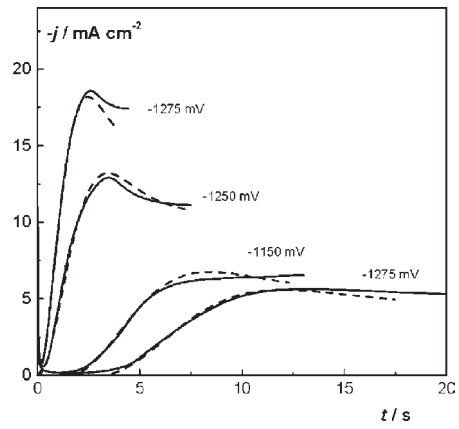

Fig. 2 j–t Curves of Co–Mo alloy deposition from 0.1 mol dm^{-3} $CoSO_4$ + 0.2 mol dm^{-3} $Na_3C_6H_5O_7$ + 0.006 mol dm^{-3} Na_2MoO_4 solution. Experimental (—) and theoretical (---) curves. The fitting parameters are in Table 1.

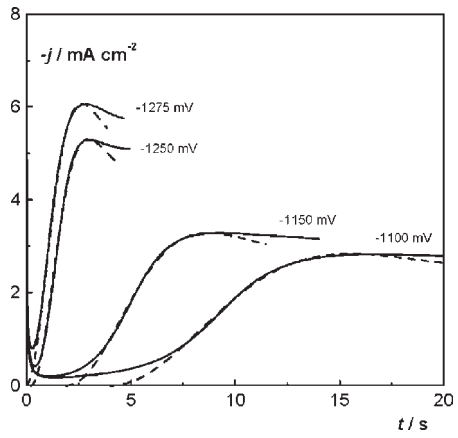

Fig. 3 j–t Curves of Co–Mo alloy deposition from 0.1 mol dm^{-3} $CoSO_4$ + 0.2 mol dm^{-3} $Na_3C_6H_5O_7$ + 0.002 mol dm^{-3} Na_2MoO_4 solution; experimental (—) and theoretical (---) curves. The fitting parameters are in Table 1.

Table 2 Comparison of the fitting parameters N_0, k^{A}_{Co} and k_{Co} obtained through eqns. (1) and (6) for $[MoO_4^{2-}] = 0.002$ mol dm^{-3}; k^{A}_{Co} is calculated with eqn. (8)

	Eqn. (1)		Eqn. (6)	
E/mV	$10^{-12}N_0$/ cm^{-2}	$10^{8}k^{A}_{Co}$/ mol cm^{-2} s^{-1}	$10^{-12}N_0$/ cm^{-2}	$10^{8}k_{Co}$/ mol cm^{-2} s^{-1}
−1275	4	2.26	4	2.35
−1250	5	1.96	4.5	2.05
−1150	2.15	1.22	2	1.28
−1100	1	1.05	1	1.1

not change in the absence of molybdate, nor its geometry. Unfortunately, the fitting using eqn. (7) does not confirm these hypotheses, nor does the expression for progressive, charge-transfer controlled systems with hemispherical geometry of the crystallites.[7]

Since Co deposition curves are far from the alloy curves, this suggests that the pure Co deposition occurs in a different way from the alloy deposition. To test this assumption, the pure-Co curves were fitted with diffusion[8] and mixed[4] controlled deposition models. However, neither of these models fit the pure Co deposition curves obtained in sulfate–citrate medium. The reason why the models of diffusion-controlled processes did not fit these curves can be gleaned from Fig. 4, where the Cottrell equation (dashed line) is plotted together with the Co j–t curves. The maxima of the experimental curves are far from Cottrell behaviour. With the mixed control models the fittings were slightly better, although not satisfactory.

These poor fittings may have been attributable to the shape of the crystallites, because the models used above assume hemispherical geometry. To verify this, SEM images were performed for c_{Mo} equal to 0.006, 0.002 and 0 mol dm^{-3} (Fig. 5). The images revealed that the crystallites became more pointed as the molybdate concentration diminished. The deposits obtained from a 0.002 mol dm^{-3} Mo concentration are not hemispherical, which could explain the anomalous values of N_0 and k_{Mo}. It is also confirmed that the pure Co deposits are far from hemispherical.

The sharp points observed in the pure-Co SEM images were conical rather than hemispherical. According to this, the curves of Co (in citrate) deposition were studied assuming that the crystallites grow as cones, the deposition process being

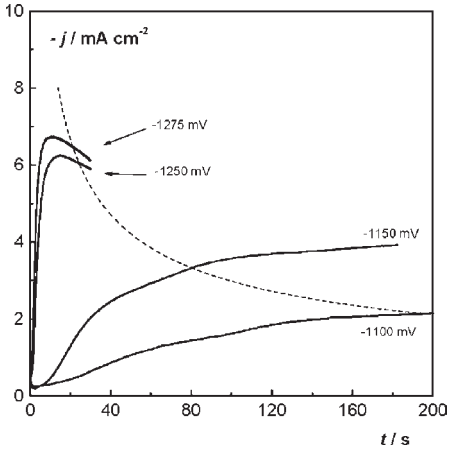

Fig. 4 j–t Curves of Co deposition from 0.1 mol dm^{-3} $CoSO_4 + 0.2$ mol dm^{-3} $Na_3C_6H_5O_7$ solution. Experimental curves (—). The dashed line corresponds to the Cottrell equation for these experimental conditions. The value of D_{Co} used in the Cottrell equation is 7×10^{-6} cm s^{-1}.

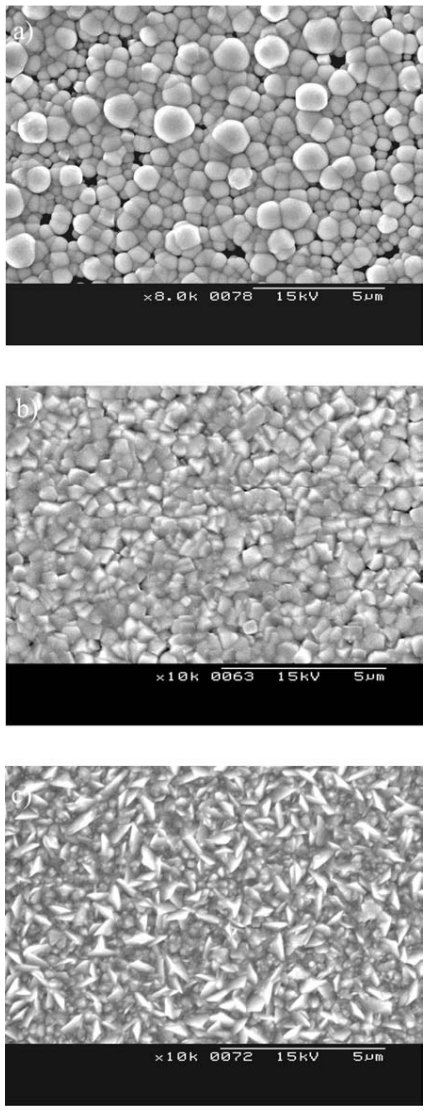

Fig. 5 SEM images of the deposits obtained from 0.1 mol dm^{-3} $CoSO_4 + 0.2$ mol dm^{-3} $Na_3C_6H_5O_7 + x$ mol dm^{-3} Na_2MoO_4 solutions: (a) $x = 0.006$, (b) $x = 0.002$ and (c) $x = 0$.

charge-transfer controlled,[9]

$$j^{**}_{Co}(t) = z_{Co}Fk^{n}_{Co} \times \left\{1 - \exp\left[-P\left(t^2 - \frac{2t}{A} + \frac{2}{A^2} - \frac{2}{A^2}\exp(-At)\right)\right]\right\}, \quad (9)$$

where $P = \pi M_{Co}k^{l}_{Co}N_0/\rho_{Co}$, k^{n}_{Co} and k^{l}_{Co} are the normal and the lateral rates of growth (mol cm^{-2} s^{-1}). Eqn. (9) takes into account both possibilities for the reduction of the nuclei density. Fig. 6 shows the best fits of the Co j–t curves with eqn. (9) and the values of the parameters are listed in Table 3.

The reduction of the molybdate concentration increases N_0 but, as expected, the values of k^{A}_{Co} and k^{n}_{Co} are similar (Tables 3 and 1). However, the curves for −1150 and −1100 mV have no clear maximum and so they could contain errors. This behavior could be caused by hydrogen contribution. The main difference between the pure Co deposition and the Co deposition in the alloy lies in the values of A, which indicate that nucleation is progressive. This could explain the slower behaviour of Co deposition in citrate media.

As nucleation is progressive in the absence of molybdate but instantaneous with 0.002 mol dm^{-3} molybdate concentration, it is concluded that small quantities of molybdate alter the

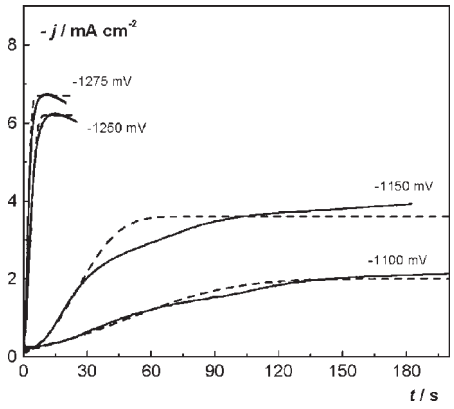

Fig. 6 *j–t* Curves of Co deposition from 0.1 mol dm^{-3} $CoSO_4 + 0.2$ mol dm^{-3} $Na_3C_6H_5O_7$ solution; experimental (—) and theoretical (---) curves plotted from eqn. (9). The fitting parameters are listed in Table 3.

Table 3 Fitting parameters of the pure-Co deposition, assuming conical geometry for the crystallites, eqn. (9)

E/mV	$10^{-12}N_0$/ cm^{-2}	A/s^{-1}	$10^8 k^n_{Co}$/ mol cm^{-2} s^{-1}	$10^8 k^l_{Co}$/ mol cm^{-2} s^{-1}
−1275	10	0.04	3.35	3.35
−1250	9	0.01	3.1	3.1
−1150	4	0.001	1.8	0.8
−1100	1	0.001	1	0.4

nucleation kinetics. This is consistent with the finding that Mo deposition involves a first step of oxide formation. This oxide layer could alter the nucleation behaviour, so the substrate may have different electrochemical properties.

Conclusions

The model proposed for Co–Mo deposition has been tested for different experimental conditions, through variations of the potential and the molybdate concentration. Although the model fitted a progressive pattern for low or moderate deposition potentials,[4] the experimental conditions used here led to an instantaneous pattern and therefore it is verified that the model can also be applied to the second case.

Moreover, the consistency of the model for low molybdate concentrations has been tested. It was assumed that low molybdate concentrations would make $j(t)$ converge to a charge-transfer controlled deposition of Co, $j^*_{Co}(t)$. This convergence is verified.

In spite of the above conclusion, low molybdate concentrations change the morphology of the crystallites, which become sharper as the concentration decreases. In addition, the nucleation changes from progressive (pure Co) to instantaneous (Co with molybdate). This change can be understood by assuming that the first Mo oxide step alters the electrochemical properties of the substrate.

The main parameters extracted from the curve fitting can be described as follows:

(1) k_{Mo} depends on the potential. For the set of alloy curves tested, it increases as E is more negative.

(2) At molybdate concentrations for which the applicability of the model is demonstrated, N_0 is low dependent on both the molybdate concentration and the applied potential.

(3) The values of k_{Mo} and N_0 for the 0.002 mol dm^{-3} solution are one order of magnitude higher than expected, if we compare them with those of the other solutions. These differences are explored and they are attributed to changes in the geometry of the crystallites. SEM images of the 0.002 mol dm^{-3} solution showed that the crystallites are conical rather than hemispherical. This could lead to erroneous fitting parameters.

Acknowledgements

The authors thank the Serveis Cientificotècnics (Universitat de Barcelona) for the use of their equipment. This paper was supported financially by contract MAT 2000-0986 from the Comisión Interministerial de Ciencia y Tecnología (CICYT) and by the Comissionat of the Generalitat de Catalunya under Research Project 2001 SGR 00046.

References

1 A. Brenner, *Electrodeposition of Alloys*, Academic Press, New York, 1963, vols. 1–2.
2 E. Gómez, E. Pellicer and E. Vallés, *J. Electroanal. Chem.*, 2001, **517**, 109.
3 E. Gómez, E. Pellicer and E. Vallés, *J. Appl. Electrochem.*, 2003, **33**, 245.
4 E. Gómez, Z. G. Kipervaser and E. Vallés, *J. Electroanal. Chem.*, 2003, **557**, 9–18.
5 W. Press, S. Teukolsky, W. T. Vetterling and B. P. Flannery, *Numerical Recipes in Fortran*, Cambridge University Press, Cambridge, 2nd edn., 1996.
6 E. Gómez, E. Pellicer and E. Vallés, *J. Solid State Electrochem.,* in press.
7 M. Y. Abyaneh, *Electrochim. Acta*, 1982, **27**, 1329.
8 L. Heerman and A. Tarallo, *J. Electroanal. Chem.*, 1999, **470**, 70.
9 M. Y. Abyaneh, *J. Electroanal. Chem.*, 2002, **530**, 82.

Influence of the bath composition and the pH on the induced cobalt-molybdenum electrodeposition

Available online at www.sciencedirect.com
SCIENCE DIRECT®
Journal of Electroanalytical Chemistry 556 (2003) 137–145
Journal of Electroanalytical Chemistry
www.elsevier.com/locate/jelechem

Influence of the bath composition and the pH on the induced cobalt–molybdenum electrodeposition

Elvira Gómez *, Eva Pellicer, Elisa Vallés

Laboratori d'Electrodeposició i Corrosió (Electrodep), Departament de Química Física, Facultat de Química, Universitat de Barcelona, Martí i Franquès, 1, E-08028 Barcelona, Spain

Received 13 February 2003; received in revised form 14 April 2003; accepted 3 May 2003

Abstract

Experimental electrodeposition parameters (pH, cobalt(II), citrate and molybdate concentrations) were varied in order to analyse their influence on induced cobalt–molybdenum codeposition. Voltammetry was the main technique used. In Co–Mo electrodeposition an initial molybdenum oxide layer is formed, over which the alloy is deposited. The process depends on the nature of the species in solution. At quasi-neutral pH, $CoCit^-$ is the main Co(II) species when there is sufficient complexing agent. Thus, cobalt is deposited as a result of the reduction of $CoCit^-$, and molybdenum is reduced from MoO_4^{2-} to MoO_2. This intermediate oxide evolves to molybdenum via the formation of $[MoO_2–CoCit^-]_{ads}$. In acidic media, molybdate complexes with citrate, so molybdenum oxides are formed from $H_rMoO_4Cit^{[5-r]}$. On the other hand, cobalt is deposited mainly by CoHCit reduction. $CoCit^-$/CoHCit and molybdenum oxides are reduced simultaneously, so cobalt nuclei are always needed to induce the codeposition.

Keywords: Cobalt–molybdenum; Magnetic alloy; Induced codeposition mechanism; Electrodeposition

1. Introduction

Deposits of molybdenum alloys are hard and protect the substrate from corrosion [1–3]. Currently, they are of considerable interest due to their possible application in magnetic devices.

The formation of Co–Mo deposits by electrodeposition is an induced process [4]. This means that cobalt ions are necessary for the reduction of molybdate species, which is incomplete in aqueous solution. The interaction between Co(II) and molybdate is not fully understood.

The influence of electrodeposition conditions on the alloy composition has been studied [5–8] and certain mechanisms have been proposed [9–12] for M–Mo systems (M = Co, Fe, Ni). The most probable hypothesis involves the formation of an adsorbed intermediate, a cobalt–molybdenum oxide complex, which then permits subsequent reduction to molybdenum [11,12]. It remains to be established why molybdenum deposition is so strongly favoured, as the Mo/Co ratio in the deposit is higher than the corresponding $[MoO_4^{2-}]$/[Co(II)] ratio in solution.

We analysed the general trends of cobalt–molybdenum deposition in a sulphate–citrate bath at pH 6.6 at two molybdate concentrations [13]. This bath always led to deposits with molybdenum percentages above 15%. We found that molybdenum incorporation in the cobalt deposit reduced the coercive force (H_c), but simultaneously decreased the saturation magnetisation (M_s). Our aim is to obtain soft cobalt–molybdenum deposits with the highest possible M_s values.

Here we examine the mechanism of codeposition of cobalt–molybdenum alloy by analysing the molybdate effect, with special attention to the pH and the concentrations of Co(II) and citrate.

* Corresponding author. Tel.: +34-93-402-1234; fax: +34-93-402-1231.
E-mail address: e.gomez@qf.ub.es (E. Gómez).

0022-0728/03/$ - see front matter © 2003 Elsevier B.V. All rights reserved.
doi:10.1016/S0022-0728(03)00339-5

2. Experimental

The electrochemical measurements were performed in a conventional three-electrode cell using a potentiostat/galvanostat, model 273 from EG&G or an Autolab with PGSTAT equipment and GPES software. The temperature was 25 °C. Chemicals used were $CoSO_4 \cdot 7H_2O$, $Na_2MoO_4 \cdot 2H_2O$, and $Na_3C_6H_5O_7 \cdot 2H_2O$, all of analytical grade. The pH was adjusted by adding H_2SO_4 to the solution. All solutions were freshly prepared with water which was distilled twice and then treated with a Millipore Milli Q system. The solutions were de-aerated by argon bubbling before each experiment and maintained under an argon atmosphere during the experiment.

For electrochemical experiments, the working electrode was a vitreous carbon (Metrohm) electrode of 0.0314 cm^2. It was polished to a mirror finish using alumina of two grades (3.75 and 1.85 μm) and cleaned ultrasonically for 2 min in water before each experiment. For deposit preparation, a copper substrate of 0.0314 cm^2 was used. The reference electrode was Ag/AgCl/1 M NaCl mounted in a Luggin capillary containing 0.5 M Na_2SO_4 solution. All potentials are referred to this electrode. The counter electrode was a platinum spiral.

Electrochemical experiments were performed in quiescent conditions. Voltammetric experiments were carried out at 50 mV s^{-1}, scanning initially towards negative potentials. Only one cycle was run in each voltammetric experiment. Chronoamperometric experiments were performed from an initial potential at which no process occurred to a potential at which reduction occurred.

Raman measurements were performed at room temperature with a Jobin Yvon T64000 spectrometer using the green line of an Ar^+ laser ($\lambda = 514.5$ nm) as the excitation light and working in subtractive mode. The macroRaman system was constituted by three monochromators. The samples were exposed to a laser power of 115 mW. The diameter of the spot was 0.1 mm.

For preparation of the deposits the solutions were stirred at 60 r.p.m. to avoid the depletion of the minority element (molybdenum) around the electrode and ensure homogeneous composition.

The deposits were examined with a Hitachi S-2300 scanning electron microscope (SEM). The elemental composition was determined with an X-ray analyser incorporated in a Leica Cambridge Stereoscan S-360 microscope. Standards of pure molybdenum and pure cobalt, previously polished, were used before each quantitative analysis. The efficiency of deposit preparation was calculated by comparing the deposition charge and the chemical analysis of the films. For chemical analysis, the deposits were dissolved in 5 ml of a 1% nitric acid solution and the resulting samples were analysed by inductively coupled plasma mass spectrometry (ICP-MS). Measurements were made in a Perkin Elmer spectrometer Elan 6000. Certified standard solutions of cobalt and molybdate ions containing rhodium as an internal standard were used to calibrate the instrument.

3. Results

3.1. Previous electrochemical study

A preliminary voltammetric study was carried out based on the individual response of each constituent of the bath: 0.1 M $CoSO_4$+0.2 M $C_6H_5Na_3O_7$+0.005 M Na_2MoO_4. The unadjusted pH of this bath was 6.6. This bath had already been tested [13].

When only 0.2 M $C_6H_5Na_3O_7$ was present in solution, no current between −1600 and +1200 mV was detected in the voltammetric response. Similarly, when 0.005 M Na_2MoO_4 was added to this solution no current was detected, even at −1500 mV (Fig. 1, curve a). Furthermore, no oxidation current was detected during the positive scan.

On the other hand, in a 0.1 M $CoSO_4$ solution, cobalt deposition began around −825 mV (Fig. 1, curve b). When the scan was reversed, the typical nucleation loop was detected, with a single oxidation peak centred at −40 mV. The addition of molybdate (0.005 M) to this solution shifted the onset of the main reduction process to more negative potentials (Fig. 1, curve c). In the positive scan, the typical nucleation loop was also recorded, followed by an oxidation peak centred at more negative potentials than that obtained from the $CoSO_4$ solution.

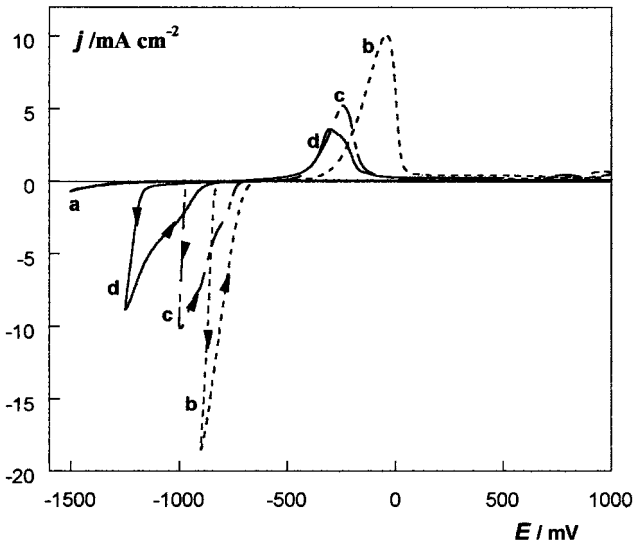

Fig. 1. Cyclic voltammograms of (a) 0.2 M $C_6H_5Na_3O_7$+0.005 M Na_2MoO_4, lower limit = −1500 mV; (b) 0.1 M $CoSO_4$, lower limit = −900 mV; (c) 0.1 M $CoSO_4$+0.005 M Na_2MoO_4, lower limit = −1000 mV; (d) 0.2 M $C_6H_5Na_3O_7$+0.1 M $CoSO_4$+0.005 M Na_2MoO_4; lower limit = −1300 mV.

The subsequent addition of citrate (0.2 M) shifted the onset of the reduction (Fig. 1, curve d) as a consequence of the cobalt complexation. The Co–Mo oxidation peak [13] appeared in the same potential range as the peak recorded from the citrate-free cobalt(II)+molybdate solution. No other oxidation current was recorded up to +1000 mV.

These results show the strong influence of the presence of both molybdate and citrate in solution on the cobalt. In order to quantify these influences, the effect of the bath components on the cobalt–molybdenum electrodeposition was studied.

3.2. Influence of citrate on the deposition process

Two kinds of voltammetric responses were observed as a function of the citrate concentration range.

For Co(II)+molybdate solutions in the presence of citrate (up to 0.04 M), deposition began slightly earlier than in its absence. Moreover, when the negative scan was reversed, the typical nucleation loop was again observed at low negative limits (Fig. 2). At more negative potentials a reduction peak, clearly influenced by mass transport, preceded a sharp current increase attributed to hydrogen evolution. During the positive scan, when short negative limits were applied, a distorted peak appeared around −250 mV. The maximum of this peak moved to more positive potentials as the scan was reversed at more negative values. This oxidation peak developed to a clear double peak when the lower limit was −1400 mV.

Gradual additions of citrate (>0.04 M) shifted the onset of reduction to more negative values (Table 1). The reduction peak observed at low citrate concentrations, prior to the sharp current increase, moved to more negative potentials until it was indistinguishable from the current attributable to hydrogen evolution. At all concentrations a distorted oxidation peak covering between −400 and −150 mV was recorded during the positive scan. Moreover, the gradual shift to more negative potentials decreased the voltammetric Q_{ox}/Q_{red} ratio. This ratio was always lower than 1 since alloy deposition was simultaneous to hydrogen evolution.

So, the presence of small amounts of citrate in the Co(II)+molybdate solutions favoured the deposition process, while the start was delayed at higher concentrations.

Table 1
Potential of the onset of the deposition process (E_i) and Q_{ox}/Q_{red} ratio deduced from voltammograms obtained applying a lower limit $E_c = E_i - 50$ mV

$[C_6H_5Na_3O_7]$/M	$-E_i$/mV	Q_{ox}/Q_{red}
0	965	0.67
0.02	950	0.88
0.04	948	0.92
0.08	975	0.90
0.12	1035	0.94
0.16	1120	0.87
0.2	1130	0.60
0.5	1350	<0.1
1.0	1390	<0.1

$[Co(II)] = 0.1$ M, $[MoO_4^{2-}] = 0.005$ M.

3.3. Influence of Co(II) on the deposition process

The influence of Co(II) on Co–Mo deposition was assessed by voltammetry in solutions containing fixed

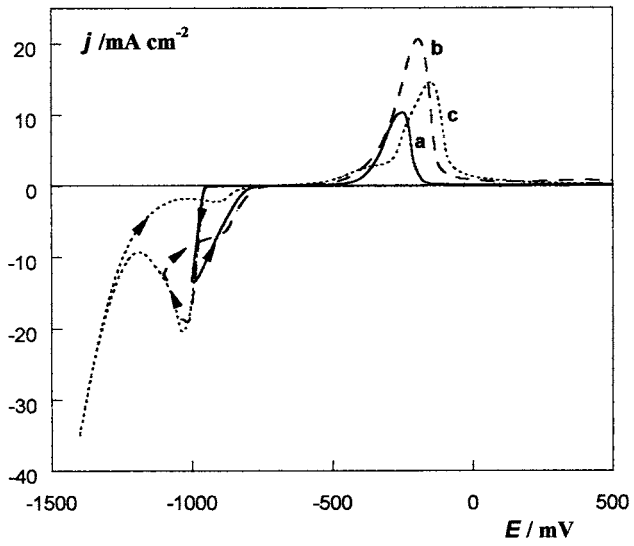

Fig. 2. Cyclic voltammogram of 0.04 M $C_6H_5Na_3O_7$+0.1 M $CoSO_4$+0.005 M Na_2MoO_4. Lower limit: (a) −1000 mV, (b) −1100 mV, (c) −1400 mV.

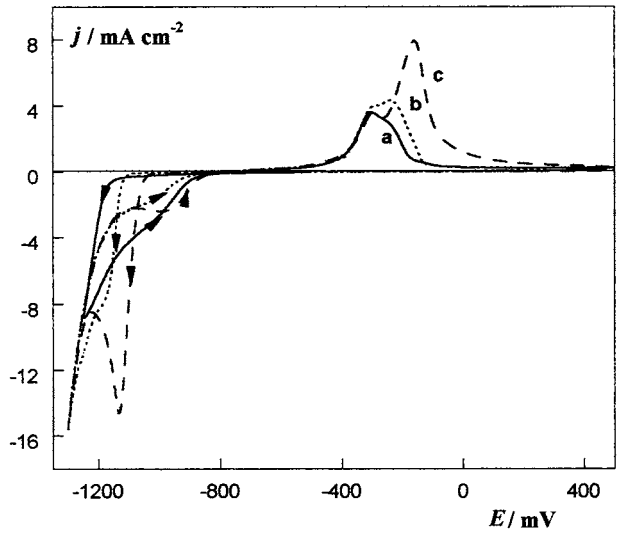

Fig. 3. Cyclic voltammograms of 0.2 M $C_6H_5Na_3O_7$+x M $CoSO_4$+0.005 M Na_2MoO_4 solution. (a) $x = 0.1$, (b) $x = 0.14$, (c) $x = 0.2$.

molybdate (0.005 M) and citrate (0.2 M) concentrations (Fig. 3).

As the Co(II) concentration was increased the reduction current appeared earlier. For 0.14 M $CoSO_4$ a shoulder appeared (Fig. 3, curve b). When the Co(II) concentration was 0.2 M, a sharp peak, with the typical shape of a diffusion-controlled process, was observed (Fig. 3, curve c). For all concentrations a clear double oxidation peak was recorded during the positive scan. The charge associated with the more positive peak increased progressively with Co(II) concentration. This behaviour was similar to that described in the previous section, attributed to the cobalt(II)/citrate concentration ratio in solution. When there was an insufficient citrate concentration in solution to complex all the cobalt(II), a clear reduction peak, probably caused by the reduction of non-complexed cobalt, was always observed prior to the coevolution of hydrogen.

3.4. Influence of molybdate concentration on the deposition

Molybdate concentration was varied from 0 to 0.15 M for solutions containing 0.2 M citrate and 0.1 M cobalt(II).

As the molybdate concentration in solution increased from 0 to 0.025 M, the voltammetric current appeared at less negative potentials. The addition of molybdate up to 0.005 M (Fig. 4 curves a and b) shifted the onset of deposition to more positive potentials, but further addition reduced this effect (Fig. 4, curves c and d). In the first reduction part of these voltammograms, a low current was detected at less negative potentials than −1160 mV (Fig. 4 zoom). This current, which increased at higher molybdate concentrations, was due to molybdenum oxide formation [14] before alloy deposition. During the positive scan, the broad oxidation band recorded from molybdate-free cobalt–citrate solution evolved to a double oxidation peak when molybdate was present. On increasing the molybdate concentration, the double peak became a quasi-single peak and the Q_{ox}/Q_{red} ratio decreased.

However, when the molybdate concentration was 0.035 M, the main voltammetric reduction current was delayed (Fig. 4, curve e). Furthermore, when the molybdate concentration was ~0.1 M, the shape of the voltammogram changed (Fig. 5): a quasi-plateau attributed to the formation of molybdenum oxide was recorded [14]. Moreover, the current due to Co–Mo deposition was shifted to more negative values. In this case, a smooth band, probably related to hydrogenated species, followed by a small oxidation peak, was recorded during the positive scan. So, although low molybdate concentrations favoured alloy deposition, higher concentrations led to the formation of molybdenum oxides, which hindered Co–Mo deposition.

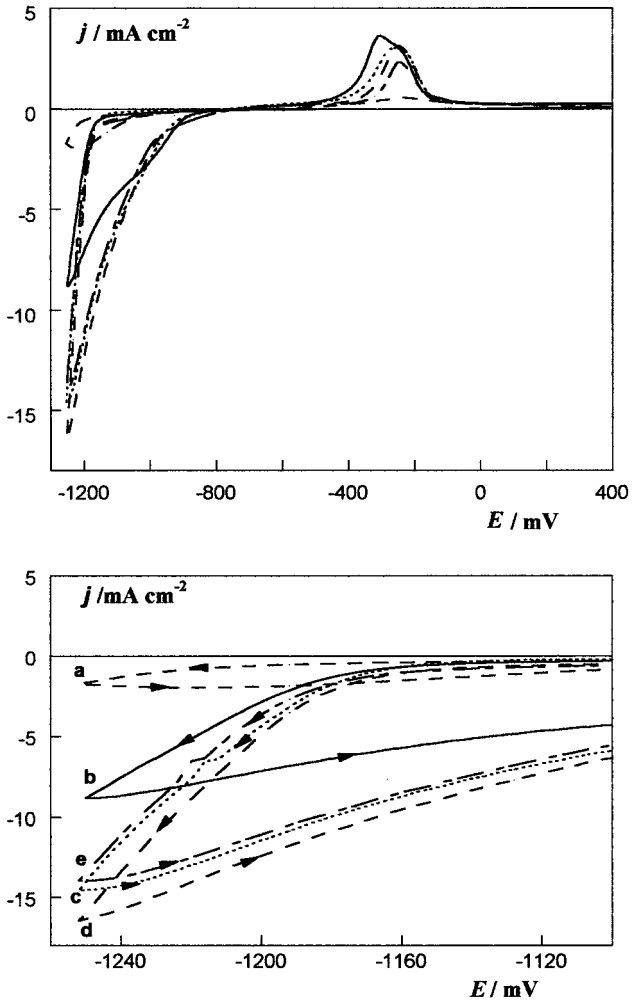

Fig. 4. Cyclic voltammograms and magnified detail of 0.2 M $C_6H_5Na_3O_7$+0.1 M $CoSO_4$+x M Na_2MoO_4. Lower limit = −1300 mV. (a) $x = 0$, (b) $x = 0.005$, (c) $x = 0.010$, (d) $x = 0.025$, $x = 0.035$.

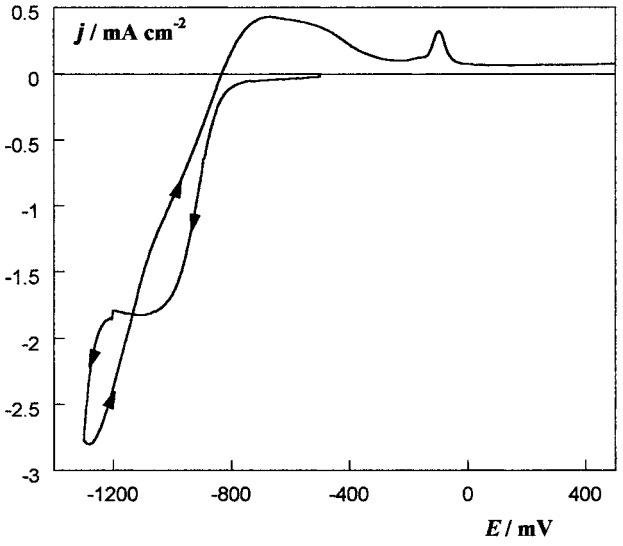

Fig. 5. Cyclic voltammograms of 0.2 M $C_6H_5Na_3O_7$+0.1 M $CoSO_4$+ 0.15 M Na_2MoO_4. Lower limit = −1300 mV.

For these solutions a parallel potentiostatic study was performed at fixed potential but at varying molybdate concentrations. The first part of the j–t transients showed a small current, followed by a sharp increase (Fig. 6). The shape of the j–t transient paralleled the voltammetric response: the first part was attributed to molybdenum oxide formation and the increase was attributed to alloy deposition [13]. An increase of the molybdate concentration to 0.012 M raised both currents (oxide formation and alloy deposition) but delayed the latter (Fig. 6, curves a and b). However, when the molybdate concentration was above 0.012 M, although the oxide formation current gradually increased, Co–Mo deposition was progressively delayed (Fig. 6, curves c–e). For example, at $[MoO_4^{2-}] = 0.021$ M, the main process did not occur during the experiment (300 s); deposition did not start until more negative potentials were applied.

However, for all the molybdate concentrations studied, the response of j–t transients to the applied potential was normal when deposition of the Co–Mo alloy began [13].

3.5. Influence of pH on the deposition process

First, two solutions at different pH were compared (Fig. 7). At pH 4.0 the deposition began at less negative potentials than at pH 6.6 and a reduction peak was recorded, followed by a sharp current increase (Fig. 7, curves a and b). The reduction peak was similar to that observed previously (Sections 3.2 and 3.3). Moreover, at pH 4.0, a greater current was seen at high magnification

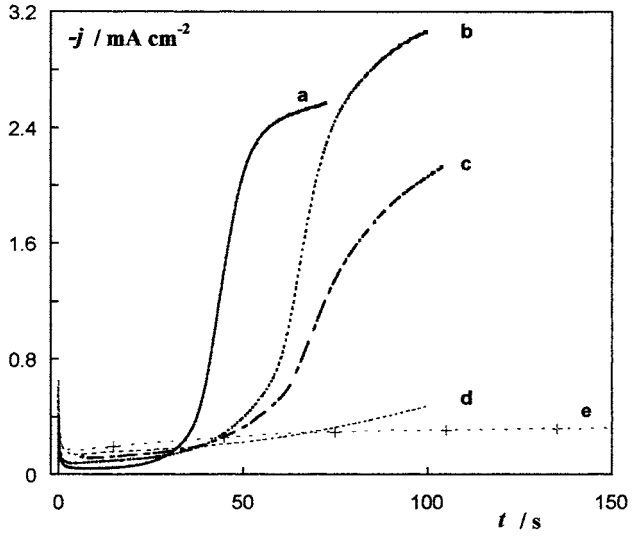

Fig. 6. j–t transient of 0.2 M $C_6H_5Na_3O_7$+0.1 M $CoSO_4$+x M Na_2MoO_4 solution. Starting potential = −500 mV. Final potential = −1000 mV. (a) $x = 0.005$, (b) $x = 0.012$, (c) $x = 0.014$, (d) $x = 0.018$, (e) $x = 0.021$.

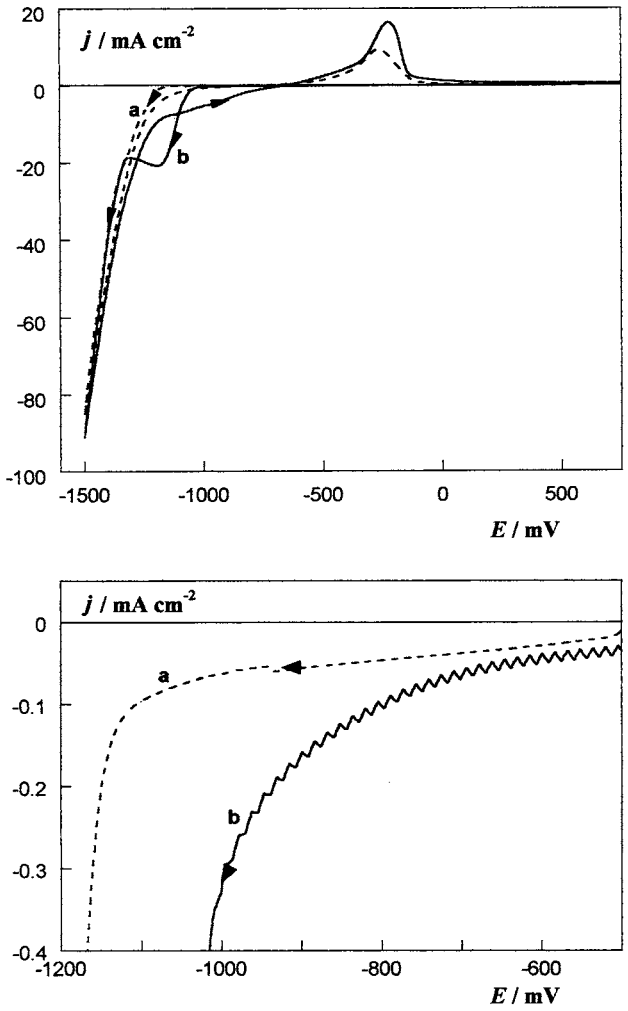

Fig. 7. Cyclic voltammograms and magnified detail of 0.2 M $C_6H_5Na_3O_7$+0.1 M $CoSO_4$+0.005 M Na_2MoO_4 solution. (a) pH 6.6, (b) pH 4.0. Magnified detail inside the figure.

(Fig. 7 zoom), attributable to molybdenum oxide formation. When the negative scan was reversed at a similar lower limit, a double oxidation peak was obtained in both cases.

A collection of voltammograms was recorded at a fixed lower limit and bath composition but with varying pH of the solution (Fig. 8). The Co–Mo deposition process was slightly favoured by lowering the pH from 6.6 to 5.1. No other differences were found when the voltammetric scan was extended to more negative potentials. At pH < 4.7 the onset of the voltammetric current advanced and a reduction peak gradually developed. Moreover, the charge involved in the first reduction process was increased by lowering the pH (Fig. 8, curves c and d). The positive scan revealed a double peak: the charge associated with the more positive peak increased progressively as the pH decreased.

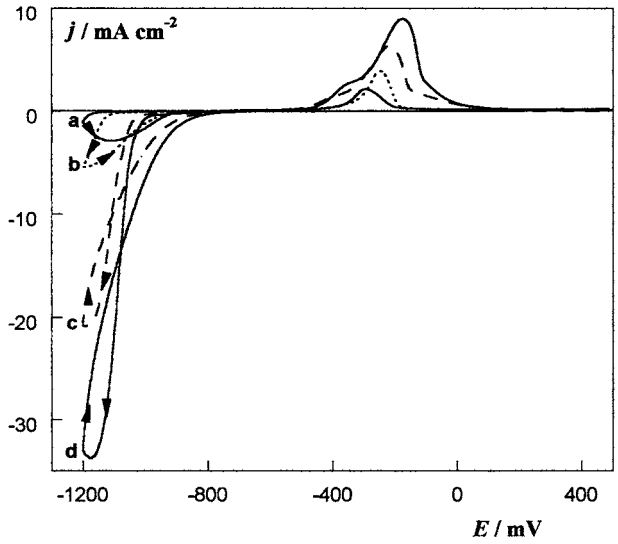

Fig. 8. Cyclic voltammograms of 0.2 M $C_6H_5Na_3O_7$ + 0.1 M $CoSO_4$ + 0.005 M Na_2MoO_4 solution. Lower limit = −1200 mV. (a) pH 6.6, (b) pH 5.3, (c) pH 4.0, (d) pH 3.4.

3.6. Characterisation of the deposits

Several deposits were prepared from 0.1 M $CoSO_4$ + 0.005 M Na_2MoO_4 at different citrate concentrations and pH values.

The examination by SEM revealed that the deposits were neither homogeneous nor coherent when they were formed from citrate-free solution or from solutions containing a low citrate concentration (Fig. 9). A cracked molybdenum oxide film had formed on the vitreous carbon electrode and some cobalt or Co–Mo islands (< 10% Mo) had grown over this film. When a metallic substrate was used no coherent deposits were obtained.

According to this result, 0.2 M citrate assured coherent homogeneous Co–Mo deposits, and this concentration was therefore chosen for subsequent assays. Cobalt–molybdenum samples were prepared in order to compare the pH dependence of the deposits with the results of the previous study. Deposits were prepared galvanostatically on copper substrates since thick deposits could not be obtained on vitreous carbon.

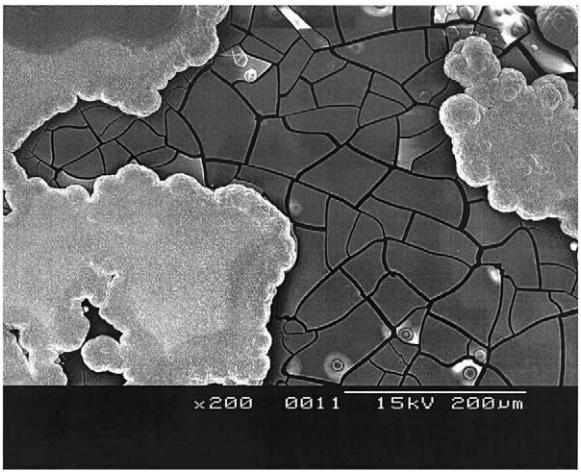

Fig. 9. SEM micrograph of a deposit obtained galvanostatically at −15.9 mA cm^{-2} under stirred conditions on vitreous carbon. 0.01 M $C_6H_5Na_3O_7$ + 0.1 M $CoSO_4$ + 0.005 M Na_2MoO_4 solution. pH 6.6.

At pH 6.6 and low current density (−3.2 mA cm^{-2}), deposits with a fluffy appearance (Fig. 10A) and molybdenum percentages ∼23% were obtained at high current efficiency (∼80%). When higher negative current densities were applied, the molybdenum percentage in the deposit increased slightly.

At pH 4.0 lower molybdenum percentages (8–11%) and efficiencies were achieved. These deposits were also fluffy, tending to nodular (Fig. 10B) as the molybdenum percentage was increased.

At citrate concentrations above 0.4 M, thin, cracked deposits were obtained, even at pH 6.6, as a consequence of the simultaneous hydrogen evolution.

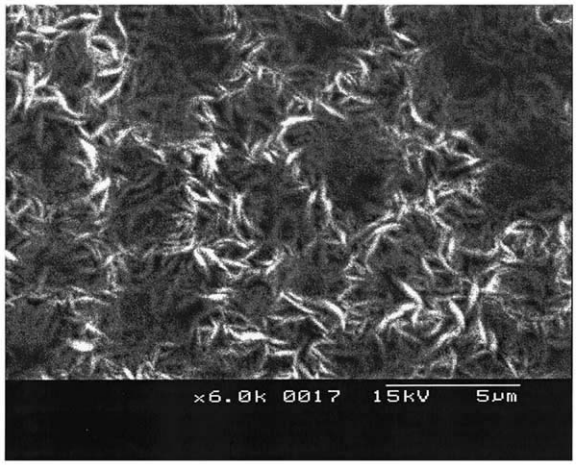

(A)

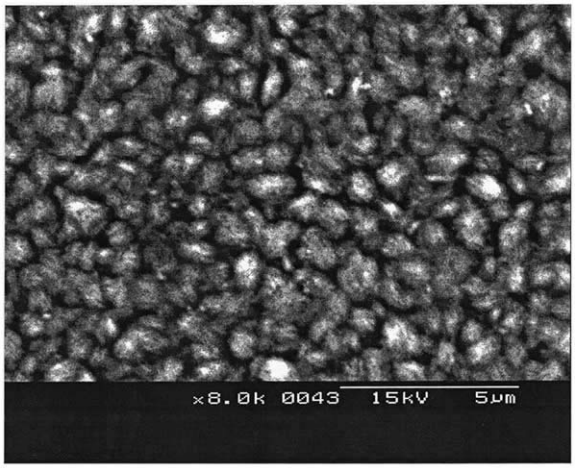

(B)

Fig. 10. SEM micrographs of thick cobalt–molybdenum deposits obtained galvanostatically at −3.2 mA cm^{-2} under stirred conditions. 0.2 M $C_6H_5Na_3O_7$ + 0.1 M $CoSO_4$ + 0.005 M Na_2MoO_4 solution. (A) pH 6.6, 23% Mo. (B) pH 4.0, 11% Mo.

3.7. Species in solution

Since different behaviour was observed in solutions at pH 4.0 and 6.6, a study was made of the species present in solution.

The nature of the cobalt species in solutions containing a citrate medium is well known [15]. In order to identify, at these pH, the main molybdate species when molybdate and citrate coexist, the Raman spectra of a 0.2 M $C_6H_5Na_3O_7$+0.1 M $CoSO_4$+0.1 M Na_2MoO_4 solution were acquired. A high molybdate concentration was maintained in order to reveal possible differences in Raman profiles. Only one scan was run between 850 and 1050 cm^{-1}, since the molybdate–citrate or molybdate–molybdate main interactions appeared in this range. At pH 6.6 a band at 899 cm^{-1} assigned to MoO_4^{2-} [16] and a clear sharp peak at 983 cm^{-1} assigned to SO_4^{2-} were observed (Fig. 11 curve a). At pH 4.0 the bands at 899 and 983 cm^{-1} were detected, together with a new band at 936 cm^{-1} (Fig. 11, curve b). This band, which appeared only at pH 4.0, was attributed to the presence of $H_rMoO_4Cit^{[5-r]}$ species [16,17].

Although the molybdate concentration was higher than in the voltammetric studies, these results show that complexation between citrate and molybdate species does not occur at pH 6.6.

4. Discussion and conclusions

Non-homogeneous deposits are formed in the absence of citrate. A molybdenum oxide film coexists with islands of cobalt. The molybdenum oxide formation hinders Co(II) reduction but it does not block it. As a result the onset of deposition is delayed and the cobalt phase is more prone to oxidation than that obtained in the absence of molybdate. This is probably due to the simultaneous incorporation of hydrogen in the deposit, leading to cobalt hydride species.

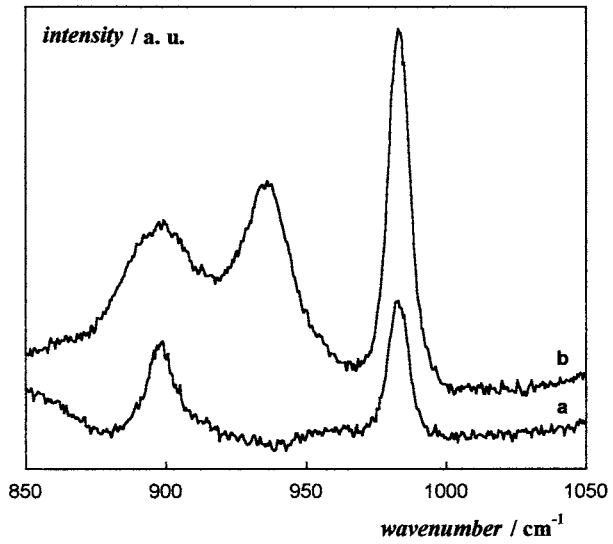

Fig. 11. Raman spectra of 0.2 M $C_6H_5Na_3O_7$+0.1 M $CoSO_4$+0.1 M Na_2MoO_4 solution. (a) pH 6.6, (b) pH 4.0.

To prepare Co–Mo deposits, citrate must be present, although an appropriate concentration is essential to assure homogeneous films. If the citrate concentration is much lower than [Co(II)], deposits are not coherent. The addition of citrate to the bath permits the gradual formation of homogeneous coherent deposits. On the other hand, when the citrate concentration is 0.5 M, coatings are cracked and irregular.

When the molybdate concentration is increased, the layer of molybdenum oxides is thicker. As they are semiconductors, this increase in thickness delays the onset of alloy deposition to more negative potentials, at which deposition is accompanied by hydrogen evolution.

The degree of protonation of the citrate depends on the pH, which therefore determines the ratio of the possible cobalt–citrate complexes in solution [15]. Under the conditions tested, when citrate doubles the 0.1 cobalt(II) concentration, $CoCit^-$ is predominant at pH 6.6, whereas its percentage in solution falls to 40% at pH 4.0, HCoCit then being the main species. On the other hand, molybdenum is involved in a great number of complex equilibria. The Raman spectra confirmed that the molybdenum species are also pH dependent. While at pH 6.6 the main molybdate species is MoO_4^{2-}, the predominant molybdate species at pH 4.0 is $H_rMoO_4Cit^{[5-r]}$. The r value is increased by lowering the pH of the electrolytic bath [16], and the complexation between molybdate and citrate is stronger, as demonstrated by the corresponding complex formation constants ($HMoO_4Cit^{4-}$, $\log K_1 = 8.08$; $H_2MoO_4Cit^{3-}$ $\log K_2 = 6.27$; $H_3MoO_4Cit^{2-}$ $\log K_3 = 21.74$). In acidic media, the presence of $CoSO_4$ does not break the molybdate–citrate complexes [16].

The advance of the voltammetric current at pH 4.0 indicates that the cobalt species present in solution are more electroactive than that at pH 6.6. This means that HCoCit, the main species at pH 4.0, deposits more easily than $CoCit^-$.

On the other hand, at a fixed complexing agent concentration, the increase of cobalt(II) concentration facilitates the onset of deposition. Similarly, when the citrate concentration is raised, Co(II) complexation is favoured, so deposition is delayed due to the shift of the equilibrium potentials. The voltammetric results suggest that cobalt deposition plays an important role in the cobalt–molybdenum alloy deposition.

According to these influences, different stages of the Co–Mo electrodeposition process could be written, depending on the pH.

In a previous study, the detection of molybdenum oxides in quasi-neutral sulphate–citrate baths allowed

us to propose, as a first stage of Co–Mo deposition, the formation of molybdenum oxide, favoured by the presence of $CoCit^-$ in solution [14]:

$$MoO_4^{2-} + 2H_2O + 2e^- \overset{CoCit^-}{\rightarrow} MoO_2 + 4OH^- \quad (1)$$

Thereafter, both MoO_2 and $CoCit^-$ evolved to Co–Mo alloy through the formation of an adsorbate intermediate, previously proposed [11,12]:

$$CoCit^- + 2e^- \rightarrow Co + Cit^{3-} \quad (2)$$

$$CoCit^- + MoO_2 \rightarrow [MoO_2{-}CoCit^-]_{ads} \quad (3)$$

$$[MoO_2{-}CoCit^-]_{ads} + 2H_2O + 4e^- \rightarrow Mo + CoCit^- + 4OH^- \quad (4)$$

The results presented here, at pH 6.6, indicate that Co and Mo deposit simultaneously, but the presence of a small amount of metallic cobalt (Eq. (2)) is necessary to induce the reduction of the adsorbed intermediate (Eq. (4)).

$$MoO_2 + CoCit^- \rightarrow [MoO_2 - CoCit^-]_{ads} \overset{Co}{\rightarrow} Mo \quad (5)$$

When MoO_4^{2-} and Co^{2+} are present in solution (without citrate), only MoO_2 and Co are detected in the deposit. However, the addition of low citrate concentrations (up to ~ 0.04 M) leads to the formation of MoO_2 and Co–Mo alloy on the electrode. Under these conditions, the main electroactive species in solution are MoO_4^{2-} and Co^{2+}, but the solution also contains a low concentration of $CoCit^-$. Therefore, although MoO_2 and Co would be deposited from the main species, the low concentration of $CoCit^-$ would be enough to form $[MoO_2{-}CoCit^-]_{ads}$ over the Co nuclei. As alloy formation is favoured with respect to pure-cobalt deposition, a slight advance of the reduction process is observed in voltammetric experiments for solutions with low molybdate concentration with respect to a citrate cobalt sulphate bath.

The necessary presence of cobalt nuclei is corroborated by the behaviour observed when [citrate] > [Co(II)]. Under these conditions, all cobalt(II) is in the form of $CoCit^-$, and cobalt deposition is delayed with respect to non-complexed Co^{2+}. Moreover, the formation of $[MoO_2{-}CoCit^-]_{ads}$ might be favoured due to the high value of $[CoCit^-]$. However, this intermediate evolves to Mo simultaneously with cobalt deposition since only a current due to Co–Mo alloy formation is detected in voltammetric experiments at more negative potentials than those observed for low citrate concentrations.

Therefore, the reduction of molybdenum oxides to molybdenum from the $[MoO_2{-}CoCit^-]_{ads}$ intermediate can occur when some initial cobalt has been deposited on the electrode. This proposal is consistent with previous results [14], in which molybdenum oxides evolved to molybdenum only if a sufficient potential was applied, which might also be necessary to induce cobalt formation.

Co–Mo deposition at pH 4.0 shows different behaviour. In solutions containing 0.2 M citrate and 0.1 M $CoSO_4$, the electroactive species are CoHCit, $CoCit^-$ and $H_rMoO_4Cit^{[5-r]}$. The reaction proposed for the molybdenum oxide formation from this species is:

$$H_rMoO_4Cit^{[5-r]} + (5-r)H^+ + 2e^- \rightarrow MoO_2 + 2H_2O + HCit^{2-} \quad (6)$$

leading to a greater molybdenum oxide current than at pH 6.6, probably as a consequence of the higher H^+ concentration.

Cobalt formation can occur from the two complexed species of cobalt mentioned above, although the process:

$$CoHCit + 2e^- \rightarrow Co + HCit^{2-} \quad (7)$$

might be more favoured than the reduction from $CoCit^-$ (Eq. (2)), as it is expected that the species with the lower negative charge deposits more easily. Voltammetric experiments support this proposal because the reduction current appears at more positive potentials than at pH 6.6. In the same way as occurs at pH 6.6, when cobalt nuclei are initially formed on the electrode, the adsorbed intermediate can evolve to molybdenum, leading to the formation of Co–Mo alloy.

On the other hand, the voltammetric results indicate that the presence of molybdate in the bath (with or without citrate) favours the oxidation of the deposit. This suggests that more easily oxidised phases than those obtained from a sulphate bath are formed. Probably the ability to oxidise may be caused by the presence of molybdenum in the deposit. However, since this behaviour was also observed in the absence of citrate, conditions under which molybdenum does not deposit, the presence of hydrogen in the deposits cannot be ruled out.

Voltammetric experiments always show a double oxidation peak. When the experimental conditions favour the increase of free $[Co^{2+}]$ in solution, the charge associated with the peak at more positive potentials increases. Under these conditions, greater cobalt percentages in the Co–Mo deposits are achieved. This finding suggests that this voltammetric peak corresponds to a Co–Mo phase that is richer in cobalt than that oxidised at more negative potentials.

These results point out that, at a given pH, the concentration ratio of the species determines the electrochemical behaviour and the kind of deposit obtained. Cobalt incorporation in the deposit is enhanced both by increasing Co(II) and by decreasing citrate concentrations. Lowering the pH has a similar effect, although it implies a loss of process efficiency due to greater hydrogen coevolution.

The information gleaned from the tendencies observed may allow us to predict how Co–Mo electrodeposition begins and, therefore, to decide whether the kind of deposit that we might obtain will have the properties that we are seeking.

Acknowledgements

The authors thank the *Serveis Cientificotècnics (Universitat de Barcelona)* for the use of their equipment. This paper was supported financially by contract MAT 2000-0986 from the *Comisión Interministerial de Ciencia y Tecnología (CICYT)* and by the *Comissionat* of the *Generalitat de Catalunya* under Research Project 2001 SGR 00046. E. Pellicer also thanks the DURSI of the *Generalitat de Catalunya* for financial support.

References

[1] K.H. Jürgen Buschow, R.W Cahn, M.C. Flemings, B. Ilschner, E.J. Kramer, S. Mahajan (Eds.), Encyclopedia of Materials Science of Technology, vol. 2, Elsevier, Amsterdam, 2001.
[2] R.B. Rebak, P. Crook, Critical factors in localized corrosion III, 98-17, The Electrochemical Society Proceedings Series, Pennington, NJ, 1999, p. 289.
[3] V.Q. Kinh, E. Chassaing, M. Saurat, Electrodep. Surf. Treat. 3 (1975) 205.
[4] A. Brenner, Electrodeposition of Alloys, vol. 1–2, Academic Press, New York, 1963.
[5] M. Cherkaoui, E. Chassaing, K.Vu Quang, Plat. Surf. Finish. 74 (1987) 50.
[6] C.C. Nee, W. Kim, R. Weil, J. Electrochem. Soc. 135 (1988) 1100.
[7] E. Chassaing, M.P. Roumegas, M.F. Trichet, J. Appl. Electrochem. 25 (1995) 667.
[8] E.J. Podlaha, D. Landolt, J. Electrochem. Soc. 143 (1996) 885.
[9] J. Crousier, M. Eyraud, J.P. Crousier, J.M. Roman, J. Appl. Electrochem. 22 (1992) 749.
[10] E. Chassaing, K.Vu. Quang, R. Wiart, J. Appl. Electrochem. 19 (1989) 839.
[11] E.J. Podlaha, D. Landolt, J. Electrochem. Soc. 143 (1996) 893.
[12] E.J. Podlaha, D. Landolt, J. Electrochem. Soc. 144 (1997) 1672.
[13] E. Gómez, E. Pellicer, E. Vallés, J. Electroanal. Chem. 517 (2001) 109.
[14] E. Gómez, E. Pellicer, E. Vallés, J. Appl. Electrochem. (2003), in press.
[15] Stability constants of metal-ion complexes. Section B: Organic Ligands. Douglas D. Perrin (Ed). IUPAC Chemical Data Series 22, Pergamon Press, Exeter, 1983.
[16] K. Murase, H. Ando, E. Matsubara, T. Hirato, Y. Awakura, J. Electrochem. Soc. 147 (2000) 2210.
[17] J.J. Cruywagen, E.A. Rohwer, G.F.S. Wessels, Polyhedron 14 (1995) 3481.

4.2.3 Resum de resultats

El procés de codeposició induïda Co-Mo és similar a pH=6.6 i pH=4.0, per bé que les espècies de partida existents en solució són diferents (en condicions d'excés de citrat respecte de Co(II), $CoCit^-$ i MoO_4^{2-} són les espècies majoritàries a pH=6.6 i CoHCit i $H_rMoO_4Cit^{[5-r]}$ a pH=4.0). La descàrrega del molibdat sempre té lloc a través de la formació d'un òxid de molibdè que s'adsorbeix sobre l'elèctrode. Aquest intermedi evoluciona fins a molibdè metàl·lic només en el cas que s'apliqui un potencial suficientment negatiu. Per a cada composició del bany existeix un potencial llindar per damunt del qual és possible d'obtenir únicament l'òxid de molibdè. Si s'apliquen potencials més negatius que el potencial llindar, aleshores la descàrrega del molibdat és completa i s'obté l'aliatge Co-Mo. La reducció d'òxid de molibdè a molibdè metàl·lic té lloc sobre una petita quantitat de cobalt metàl·lic dipositat inicialment sobre l'elèctrode.

El mecanisme proposat a pH=6.6 és el següent:

$$CoCit^- + 2e^- \rightarrow Co + Cit^{3-}$$

$$MoO_4^{2-} + 2H_2O + 2e^- \xrightarrow{CoCit^-} MoO_2 + 4OH^-$$
$$CoCit^- + MoO_2 \rightarrow \left[MoO_2 - CoCit^-\right]_{ads}$$
$$\left[MoO_2 - CoCit^-\right]_{ads} + 2H_2O + 4e^- \xrightarrow{Co} Mo + CoCit^- + 4OH^-$$

A pH=4.0, la deposició de Co té lloc majoritàriament a partir de l'espècie CoHCit:

$$CoHCit + 2e^- \rightarrow Co + HCit^{2-}$$

I la reducció de molibdat per formar l'òxid de molibdè té lloc a partir d'un complex molibdat-citrat:

$$H_rMoO_4Cit^{[5-r]} + (5-r)H^+ + 2e^- \rightarrow MoO_2 + 2H_2O + HCit^{2-}$$

on *r* depèn del grau de protonació de l'agent complexant.

El temps d'inducció observat en les corbes j-t està relacionat amb la formació d'òxids de molibdè. En augmentar la concentració de molibdat en solució el temps d'inducció s'allarga. A més, un increment important de la concentració de molibdat condueix a la formació d'una major quantitat d'òxids de molibdè, la qual cosa retarda l'inici de la deposició de l'aliatge com a conseqüència de la seva naturalesa semiconductora.

En absència de citrat no és possible d'obtenir dipòsits Co-Mo homogenis. La descàrrega de molibdat no és completa i en els dipòsits es detecta la presència d'òxid de molibdè i illes de cobalt. Una concentració apropiada d'agent complexant en solució és essencial per garantir l'obtenció de dipòsits coherents.

El model teòric proposat per a la deposició Co-Mo té en compte la formació d'òxids de molibdè intermedis i proposa, com a premisses que: la deposició de cobalt està controlada per la transferència de càrrega, la deposició de molibdè està governada per la transferència de càrrega seguit d'un control per difusió, la geometria dels cristalls Co-Mo és hemiesfèrica i la seva composició no és funció de la concentració de molibdat en l'interval 0.002-0.006 mol dm^{-3}. Les corbes j-t calculades d'acord amb una nucleació instantània s'ajusten a les corbes experimentals, la qual cosa demostra la validesa de les premisses. Tanmateix, en el cas de la concentració més baixa de molibdat, apareixen discordances entre les corbes experimentals i calculades, la qual cosa és fàcilment interpretable tenint en compte que el règim de nucleació és aleshores progressiu i les imatges de SEM dels dipòsits mostren que la geometria dels cristalls tendeix a ser cònica.

4.3 Preparació i caracterització de capes i microestructures Co-Mo

4.3.1 Finalitat

Un cop conegut el mecanisme d'electrodeposició, es va procedir a la caracterització d'electrodipòsits Co-Mo obtinguts a partir de diferents banys sulfat-citrat. Els dipòsits es van preparar en condicions d'agitació suau sobre substrats d'aplicació més àmplia (grafit, coure i Si/capa llavor).

En primer lloc es van preparar dipòsits a partir del bany 0.2 mol dm^{-3} citrat + 0.1 mol dm^{-3} $CoSO_4$ + 0.005 mol dm^{-3} Na_2MoO_4, pH=6.6, prèviament estudiat des del punt de vista electroquímic. Es va fer un examen exhaustiu de la influència de la tècnica de deposició (potenciostàtica o galvanostàtica), de la naturalesa del substrat, del gruix del dipòsit i del potencial de deposició sobre la morfologia i estructura dels dipòsits. Per tal de conèixer com afecta l'estructura cristal·lina a les propietats magnètiques dels dipòsits, es va enregistrar la corba d'histèresi magnètica en camp paral·lel i en camp perpendicular de dipòsits amb un percentatge de molibdè similar però diferents des del punt de vista estructural.

Per tal d'aconseguir incorporacions discretes de molibdè als dipòsits, es va investigar la possibilitat de disminuir el pH del bany i augmentar la concentració de Co(II). Es van dissenyar diferents banys electrolítics que conduïssin a dipòsits amb percentatges de molibdè baixos i es va determinar l'eficiència de corrent en cada cas. En funció de la qualitat dels dipòsits obtinguts, es van escollir el/s bany/s més adequats per obtenir dipòsits Co-Mo magnèticament tous.

Finalment es van preparar dipòsits sobre substrats Si/capa llavor a fi d'avaluar-ne la seva compatibilitat amb la tecnologia del silici. Es van caracteritzar les capes Co-Mo obtingudes i es va determinar la velocitat

de creixement de l'aliatge. A fi de reduir tensions en els dipòsits, es va investigar la possibilitat d'usar un agent antiestressant com la sacarina i d'augmentar la temperatura del bany. En darrer lloc, es van utilitzar substrats base silici litografiats amb resines d'entre 2 i 20 μm d'alçada per examinar la selectivitat de la deposició. El perfil de les microestructures Co-Mo alliberades es va resseguir mitjançant les tècniques de perfilometria interferomètrica i d'AFM.

Els resultats detallats d'aquest capítol s'inclouen en els següents articles:

Properties of Co-Mo coatings obtained by electrodeposition at pH=6.6
J. Solid State Electrochem. 8 (2004) 497

Electrodeposition of soft-magnetic cobalt-molybdenum coatings containing low molybdenum percentages
J. Electroanal. Chem. 568 (2004) 29

Microstructures of soft-magnetic cobalt-molybdenum alloy obtained by electrodeposition on seed layer/silicon substrates
Electrochem. Commun. 6 (2004) 853

Developing plating baths for the production of cobalt-molybdenum films
Surf. Coat. Technol. 197 (2005) 238

Properties of Co-Mo coatings obtained by electrodeposition at pH 6.6

J Solid State Eletrochem (2004) 8: 497–504
DOI 10.1007/s10008-004-0495-z

ORIGINAL PAPER

Elvira Gómez · Eva Pellicer · Xavier Alcobé
Elisa Vallés

Properties of Co-Mo coatings obtained by electrodeposition at pH 6.6

Received: 22 March 2003 / Accepted: 6 June 2003 / Published online: 5 March 2004

Abstract Cobalt-molybdenum coatings were prepared by electrodeposition in a sulfate-citrate bath and their morphology, structure and magnetic properties were analysed. Concentrations of 0.1 mol dm^{-3} $CoSO_4$ and 0.005 mol dm^{-3} Na_2MoO_4 at pH 6.6 led to Co-Mo deposits of 20–23% Mo that can be grown to several microns over graphite or copper substrates. At low deposition potentials or current densities, the deposits presented a close-packed hexagonal structure (hcp) that evolved to a (100) + (110) preferred orientation and acicular morphology as the deposit thickness increased. When the deposition potential or the current density was made more negative, a mixed crystalline + amorphous structure was obtained. The degree of crystallinity depended on the thickness: thin films were more amorphous than the thicker ones. Co-Mo deposits showed lower saturation magnetization (M_s) and coercivity (H_c) than the pure cobalt deposits. The crystalline + amorphous films showed the lowest H_c values (around 40 Oe).

Keywords Cobalt-molybdenum alloy · Electrodeposition · Magnetic films · X-ray diffraction

Introduction

Magnetic materials of iron group metals have wide applications in industry, mainly in micro-electromechanical systems (MEMS) and magnetic storage devices. The presence of molybdenum modifies their magnetic properties [1, 2] and improves their hardness and corrosion resistance [3, 4, 5]. These new properties make iron group metal-molybdenum alloys promising materials for microelectronic applications.

Interest in the electrodeposition of molybdenum with iron group metals has thus increased. Codeposition of molybdenum with iron group metals is induced, since complete reduction of molybdenum in aqueous solutions does not occur in the absence of an iron group metal [6]. Several studies have examined the anomalous electrodeposition of Ni-Mo [7, 8, 9, 10, 11, 12, 13, 14, 15], especially in a citrate medium, although there are fewer reports on Co-Mo or Fe-Co deposition [16, 17, 18].

In a previous study [2] the Co-Mo electrodeposition from a sulfate-citrate bath was explored. The percentage of Mo in the deposits was up to 60%, although the films were highly stressed. It was claimed that the presence of Mo led to soft magnetic behaviour.

A more recent study of the influence of bath composition and pH on the electrochemical behaviour of Co-Mo deposition suggested that the equilibria between the species in solution played an important role. It was found that alloy deposition occurred through different stages depending on the pH of the bath, which affected the composition of the final deposit [19]. We fixed the working pH at 6.6 to decrease simultaneous hydrogen evolution. In the present study, bath composition was fixed at 0.1 mol dm^{-3} cobalt sulfate and 0.005 mol dm^{-3} sodium molybdate. Citrate concentration was adjusted at 0.2 mol dm^{-3} in order to complex cobalt(II); higher citrate concentrations hinder the codeposition and decrease the efficiency of the process [19]. Molybdate concentration was kept low to prevent large Mo incorporation in the deposits, which would decrease the saturation magnetization of the coating.

The aim of the present study was to examine the influence of various electrodeposition parameters on the properties of the deposit at this fixed bath composition. We tested the deposition over a range of substrates in order to improve the film adherence and we analysed the

E. Gómez · E. Pellicer · E. Vallés (✉)
Electrodep, Departament de Química Física,
Universitat de Barcelona, Martí i Franquès 1,
08028 Barcelona, Spain
E-mail: e.valles@qf.ub.es
Tel.: +34-93-4021234
Fax: +34-93-4021231

X. Alcobé
Serveis Cientificotècnics, Universitat de Barcelona,
Lluis Solé i Sabaris 1–3, 08028 Barcelona, Spain

influence of the thickness and the electrodeposition conditions on structure and magnetic properties, since our main interest was the preparation of homogeneous films with soft magnetic behaviour.

Experimental

The electrochemical measurements were performed in a conventional three-electrode cell using a microcomputer-controlled Autolab potentiostat/galvanostat with PGSTAT30 equipment and GPES software. All chemicals used were of analytical grade. Solutions were freshly prepared with water that was first doubly distilled and then treated with a Millipore Milli-Q system. Before and during the experiments, solutions were de-aerated with argon. The temperature was maintained at 25 °C.

The morphology of the deposits was examined with a Hitachi S 2300 scanning electron microscope. Elemental composition was determined with an X-ray analyser incorporated in a Leica Cambridge Stereoscan S-360 scanning electron microscope. The efficiency of deposition was calculated by comparing the reduction charge and the results of chemical analysis of the films. For chemical analysis, the deposits were dissolved in 5 mL of 1% nitric acid solution and samples were analysed by inductively coupled plasma mass spectrometry (ICP-MS). Measurements were made in a Perkin-Elmer spectrometer Elan 6000. Certified standard solutions of cobalt and molybdate ions containing rhodium as an internal standard were used to calibrate the instrument.

The thickness of the deposits was measured on a Zeiss Axiovert 405M microscope.

X-ray diffraction (XRD) phase analysis was performed in a Philips MRD diffractometer in low-resolution parallel beam optics. The Cu-K_α radiation ($\lambda = 1.5418$ Å) was selected by means of a diffracted-beam flat graphite monochromator. Diffractograms were obtained in the 20–100° 2θ range with a step of 0.05° and a measuring time of 5″ per step. The magnetic measurements were performed with a Manics DSM8 pendulum-type magnetometer at room temperature or with a SQUID magnetometer.

Vitreous carbon ($r = 1.0$ mm), graphite ($r = 4.1$ mm) and copper ($r = 1.0$ mm) rods were used as working electrodes. The vitreous carbon electrode was polished to a mirror finish before each experiment using alumina of different grades (3.75 and 1.85 μm) and cleaned ultrasonically for 2 min in water. Copper and graphite electrodes were also polished before each experiment using sandpaper (2400 and 4000) and, later, damp alumina (0.3 μm). The reference electrode was an Ag/AgCl/1 mol dm^{-3} NaCl electrode mounted in a Luggin capillary containing 0.5 mol dm^{-3} Na_2SO_4 solution. All potentials are referred to this electrode. The counter electrode was a platinum spiral.

During electrodeposition the solution was gently stirred ($\omega = 60$ rpm) to avoid the depletion of the minority species (molybdate) to the electrode and to ensure homogeneous composition of the deposits.

Results and discussion

Electrochemical study

The general behaviour of Co-Mo deposition was analysed on vitreous carbon, graphite and copper substrates to identify the best electrode for thick-adherent coatings. Voltammetric, chronoamperometric and chronopotentiometric studies were carried out for this purpose.

The redox process was similar in all substrates, but the electrodes behaved differently in the reduction (Fig. 1). Copper was the most active substrate and

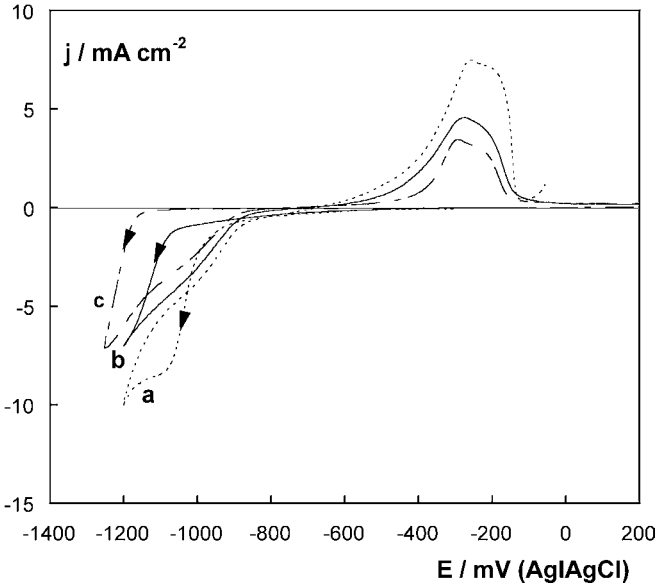

Fig. 1 Cyclic voltammograms of a 0.1 mol dm^{-3} $CoSO_4 + 0.2$ mol dm^{-3} $Na_3C_6H_5O_7 + 0.005$ mol dm^{-3} Na_2MoO_4, pH 6.6, solution (Co-Mo solution): (*a*) copper, (*b*) graphite and (*c*) vitreous carbon electrodes; scan rate 50 mV s^{-1}

vitreous carbon was the slowest. Alloy deposition started at around −900 mV for copper, at −1050 mV for graphite and at −1150 mV for the vitreous carbon electrode. A complex oxidation peak was observed in all cases, at around −200 mV. According to this, it seemed that alloy deposits could be obtained in a similar way over the different substrates, although the potential necessary to start the deposition process was different for each electrode.

To test the adherence of Co-Mo deposits on those substrates, various samples were prepared at long deposition times. When deposits were obtained potentiostatically on the vitreous carbon electrode, there were deformations in the *j–t* curves in spite of stirring (Fig. 2A) and the films were cracked (Fig. 2B). At longer deposition times the deposits fell off the substrate (Fig. 2C). Vitreous carbon was therefore ruled out. Graphite or copper substrates were suitable because the deposits did not detach even for thick coatings.

Characterization of the cobalt-molybdenum deposits

According to the results earlier obtained, Co-Mo deposits of several microns were prepared on graphite or copper electrodes. Morphological, compositional and structural characterization was carried out for each sample. Our main objective was focused on controlling the structure of the deposits, because it is known that structure and magnetic properties are usually related. Graphite electrodes were more useful because their greater area improved the resolution of the response.

Pure cobalt deposits were prepared from a molybdate-free bath in order to compare them with the Co-Mo

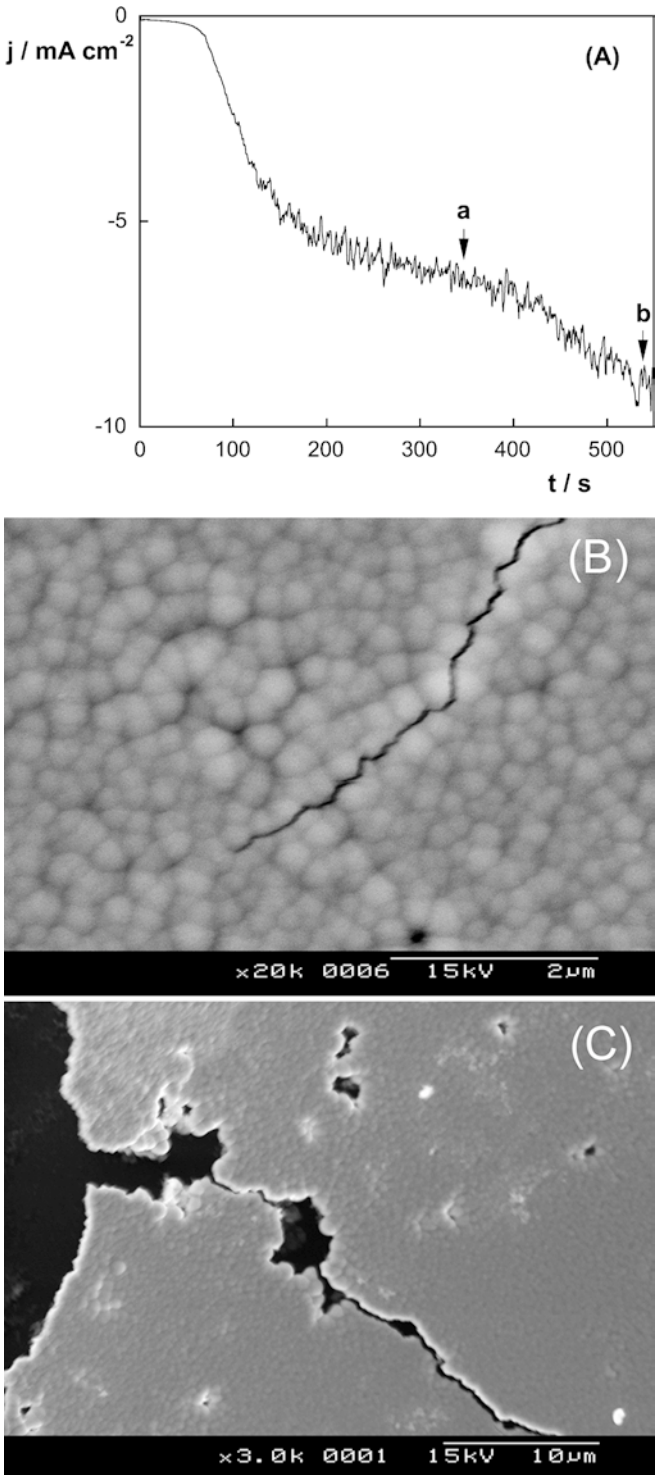

Fig. 2 **A** *j–t* transient from −500 mV to −980 mV; 60 rpm, vitreous carbon electrode, Co-Mo solution. **B**, **C** SEM images of the deposits obtained at points *a* and *b* of **A**, respectively

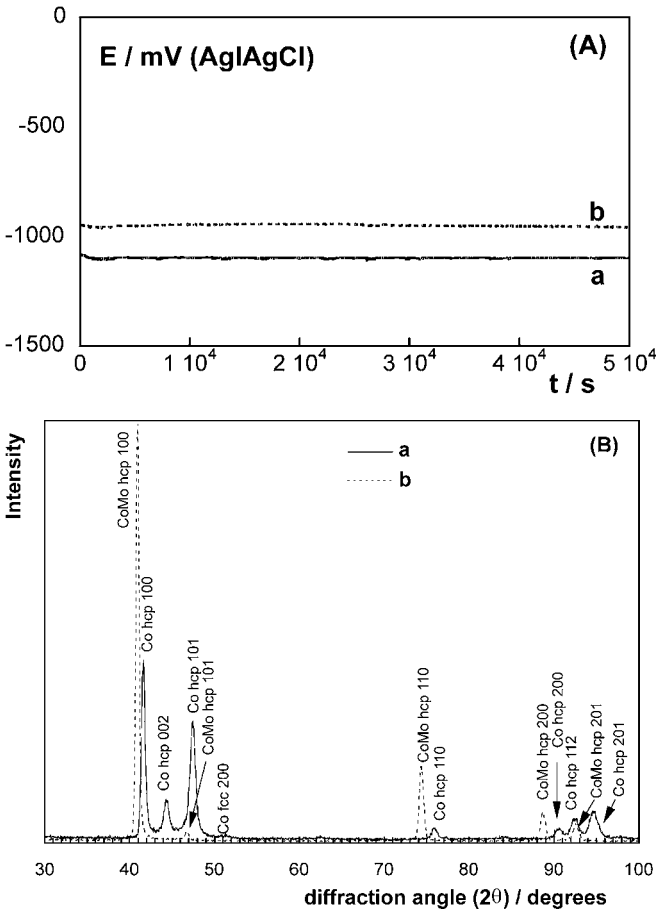

Fig. 3 **A** *E–t* transients recorded applying −3.2 mA cm^{-2}, graphite electrode, 60 rpm: (*a*) cobalt deposit obtained from a 0.1 mol dm^{-3} $CoSO_4$ + 0.2 mol dm^{-3} $Na_3C_6H_5O_7$, pH 6.6, solution; (*b*) Co-Mo deposit of 23% Mo obtained from the Co-Mo solution. **B** X-ray diffractograms of the deposits from **A**; 140 C cm^{-2}, 32 µm

deposits. Potentials or current densities were chosen to give similar deposition rates.

Figure 3 shows the diffractograms of cobalt and cobalt-molybdenum (~23% Mo) deposits obtained at a similar deposition rate ($j = -3.2$ mA cm^{-2}) and the corresponding chronopotentiometric curves. The potential related to pure cobalt deposition evolved to a more negative value than that corresponding to Co-Mo deposition (Fig. 3A), because alloy deposition was favoured [2]. The diffractograms showed narrow peaks, revealing the crystalline nature of the deposits (Fig. 3B). For pure cobalt, the main peaks corresponded to a close-packed hexagonal structure (hcp), whereas a small peak around $2\theta = 51.5°$ is attributed to face-centred cubic (fcc) cobalt deposited next to the main hcp structure.

The diffractogram of a Co-Mo deposit shows a pure hcp structure, although the position and relative height of the peaks are different from the pure cobalt deposit. The peaks of the hexagonal structure were shifted to lower values corresponding to an increase of the cell parameters, as a consequence of the incorporation of molybdenum. The cell parameters of this hexagonal structure were calculated after fit profile and least-squares refinement, leading to values of $a = 2.550$ Å and $c = 4.125$ Å, greater than those for pure cobalt ($a = 2.507$ Å, $c = 4.092$ Å). Moreover, the Co-Mo deposit showed greater orientation, the *hk*0 being the main diffraction peaks. The practical absence

of peaks with $l \neq 0$ indicated that the [001] crystallographic direction was nearly parallel to the substrate surface.

In a previous study, thinner (0.2 μm) Co-Mo deposits with an amorphous structure had been obtained [2]. In contrast, Co-Mo deposits of several microns prepared in the present work had a crystalline structure. Since the former were prepared potentiostatically and using a vitreous carbon electrode, we explored the influence of deposition parameters on the structure of the Co-Mo coatings.

Influence of deposition technique and the substrate nature

For all the conditions tested, potentiostatic and galvanostatic techniques led to equivalent electrochemical parameters: when a current density value j_1 was applied, the potential reached a stationary value E_1; analogously, when E_1 was the potential value applied, the stationary current recorded from the j–t transient was j_1. Moreover, by comparing the deposits obtained with both techniques, the same morphology and composition were found.

For example, irrespective of the technique, thick Co-Mo deposits corresponded to an acicular morphology when a graphite substrate was used (Fig. 4). The process was highly efficient for these deposits (around 85%).

On the other hand, the galvanostatic transients of Co-Mo deposition over graphite and copper electrodes at the same current density (−3.2 mA cm^{-2}) showed that practically the same stabilization potential was attained in both cases. The deposits obtained on copper substrate at long deposition times showed the same morphology and composition as those obtained over the graphite electrode.

When the diffractograms of the thick Co-Mo deposits obtained through the potentiostatic/galvanostatic technique and over the copper/graphite substrate were compared, similar profiles were also observed (Fig. 5). An hcp structure with $hk0$ main peaks was always obtained. The position of these peaks did not change, as corresponds to a given value of the molybdenum percentage. Similar results were obtained when potentials lower than −1000 mV were used.

Influence of the deposit thickness

When deposits obtained at different deposition times for a given potential value were analysed, it was corroborated that the composition of the coatings did not change with the deposition time, due to the stirring conditions. However, the morphology and structure presented some differences as a function of the reduction charge. Thick Co-Mo coatings had the morphology shown in Fig. 4, while thinner coatings presented the morphology shown in Fig. 6A. Figure 6B shows the corresponding X-ray diffractograms. A relationship between the change in the morphology and the structure was observed. As the thickness of the deposit increased, the hcp structure increased its preferred orientation, leading to a structure with a clear (100) + (110) preferred orientation. At the same time, the morphology changed from a polyhedral grain to acicular.

Influence of the deposition potential

The influence of the deposition rate on the morphology and structure of the coatings was analysed by means of the variation of the deposition potential, because the deposition rate increases as the applied potential is more

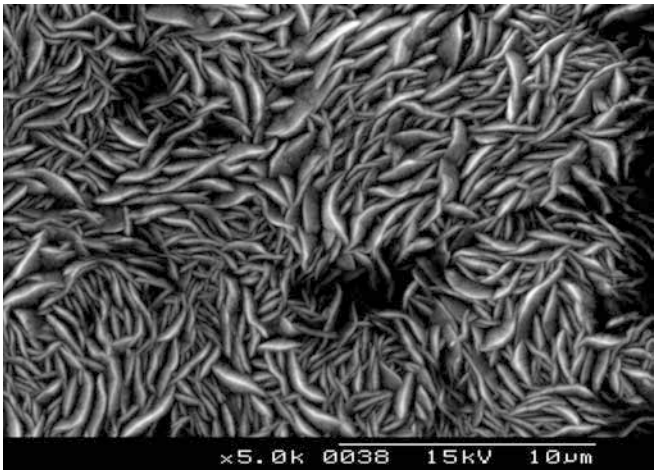

Fig. 4 SEM image of a deposit obtained at −940 mV during 55,000 s; 23% Mo, 32 μm, Co-Mo solution, 60 rpm, graphite electrode

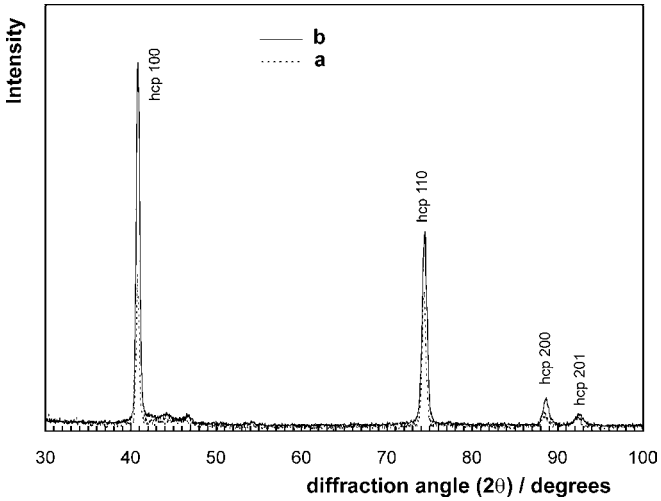

Fig. 5 X-ray diffractograms of the deposits obtained at −3.2 mA cm^{-2} from the Co-Mo solution; 60 rpm: (*a*) copper electrode, (*b*) graphite electrode

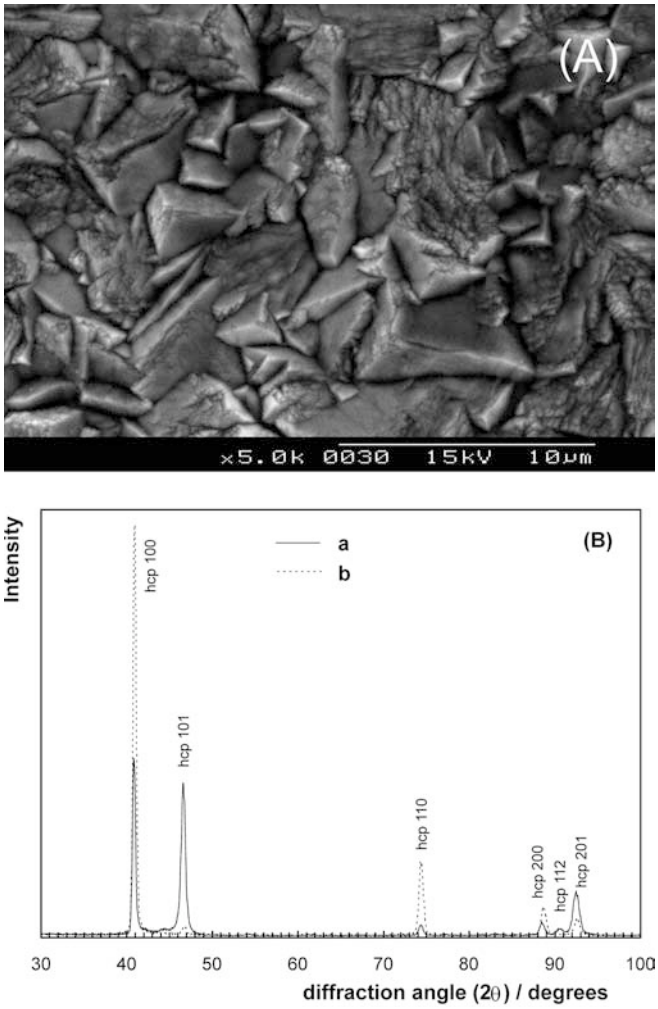

Fig. 6 **A** SEM micrograph of the deposits obtained at −940 mV from the Co-Mo solution; 60 rpm, graphite electrode, 8 μm. **B** X-ray diffractograms of Co-Mo deposits with (*a*) 8 μm and (*b*) 32 μm

negative. In the potential range studied, the applied potential had little effect on the composition (Table 1). However, a clear decrease of the deposit thickness was obtained by making more negative the deposition potential as a consequence of the lowering of the efficiency (η).

The morphology, composition and crystalline structure of the deposits obtained at a fixed charge (20 C cm^{-2}) were studied. Deformations in the *j*–*t* transients were observed for potentials equal to or more negative than −1000 mV (Fig. 7A), probably attributable to simultaneous hydrogen evolution. At deposition potentials less negative than −1000 mV, non-cracked coatings were obtained (Fig. 7B, image a), showing the previously described polyhedral morphology for thin Co-Mo films. In contrast, stressed and cracked deposits were obtained from −1000 mV (Fig. 7B, images b and c). Diffractograms of deposits obtained at different potentials showed some differences, as can be observed in the magnified X-ray diffractograms in the range 35–60° 2θ (Fig. 7C). For the deposits obtained at −940 mV,

Table 1 Molybdenum percentages in Co-Mo coatings obtained at different deposition potentials

$-E$ (mV)	% Mo	η (%)
930	21	85
940	23	88
970	20	75
1000	22	53
1100	23	13
1200	22	6

the narrow 100, 002 and 101 peaks of the hexagonal structure can be observed next to small peaks of the substrate. For those obtained at −1000 mV, there were small 100 and 101 peaks corresponding to a hexagonal crystalline structure, peaks corresponding to a graphite substrate and a very wide peak (3.5° 2θ) centred on 44.5° 2θ and attributed to an amorphous Co-Mo phase [2]. Thus, at this potential, the deposit seems to have a mixed crystalline and amorphous structure. The diffractogram of the deposit obtained at −1100 mV mainly showed peaks of the substrate and a wide peak attributed to the amorphous phase. Thus, a decrease of the deposition potential, i.e. an increase of the deposition rate, favoured the formation of less crystalline deposits. For the crystalline + amorphous samples, the presence of cracks or a non-compact structure allowed the observation of the substrate peaks in the diffractogram.

At higher deposition charges of around 150 C cm^{-2}, for which deposits of several microns were obtained, XRD revealed the formation of crystalline deposits at −940 and −1000 mV. On the other hand, a mixture of crystalline + amorphous phases was detected at −1100 mV, since the 100 peak of the hcp structure and the wide peak attributed to the amorphous structure were detected (Fig. 8). This result evidenced that, at the intermediate deposition potential (−1000 mV), the crystallinity increased with the deposit thickness. In contrast, for the deposits prepared at $E < -1000$ mV, the structure was not affected by the deposit thickness.

Magnetic behaviour of Co-Mo films

Since different Co-Mo structures were observed as a function of the deposition potential (or current density), deposits of several microns were prepared to analyse their magnetic properties. A graphite electrode and high thicknesses were selected to facilitate separation of the coatings from the substrate.

The magnetic properties were determined by recording hysteresis loops (Fig. 9). The easy axis is the in-plane direction of the parallel film. For a parallel applied field ($H_{\parallel}$) a large saturation field ($H_{s_{\parallel}}$) of about 9 kOe was required to align the magnetization in the film plane and a low remanence value was observed. The results obtained under a perpendicular field ($H_{\perp}$) were similar, except that the saturation field ($H_{s\perp}$) was about 20 kOe. These features indicated strong uniaxial

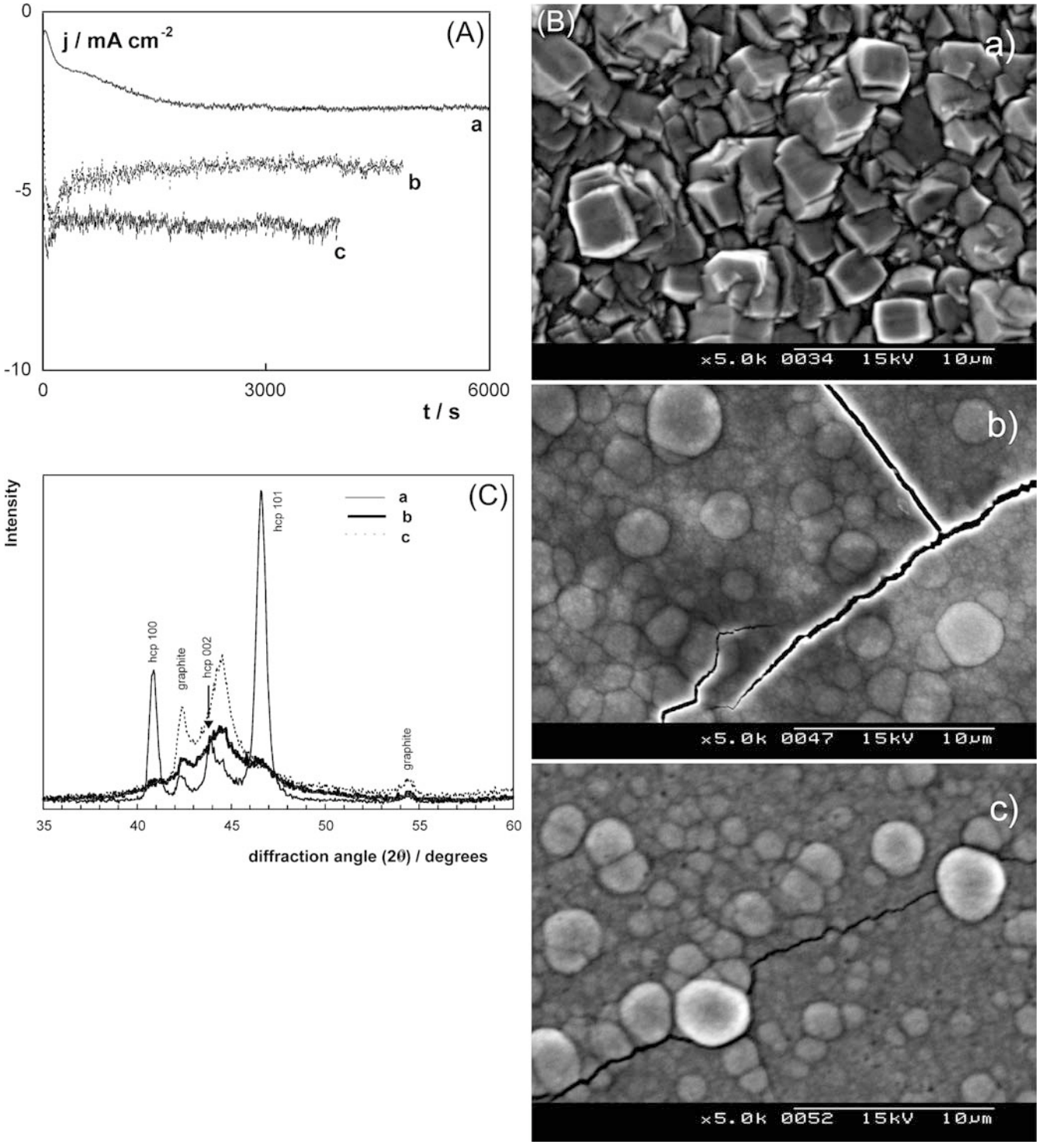

Fig. 7 **A** *j–t* transients of the Co-Mo solution; 60 rpm, graphite electrode: (*a*) −940, (*b*) −1000, (*c*) −1100 mV. **B** SEM images of the deposits obtained from **A**; 20–23% Mo, 20 C cm^{-2}: (*a*) 4.6 µm, (*b*) 2.7 µm, (*c*) 0.8 µm. **C** X-ray diffractograms of these deposits

anisotropy, in addition to the usual shape anisotropy [20].

The value of the uniaxial anisotropy constant (K) and the angle θ of the resulting anisotropy with respect to the film normal may be found using the expressions [21]:

$$H_{S\|} = 2K\cos^2\theta/M_S \quad (1)$$

and:

$$H_{S\|} + H_{S\perp} = 4\pi M_S + 2K/M_S \quad (2)$$

where M_s is the saturation magnetization. Values of $K \approx 6.4\times10^6$erg cm^{-3} and $\theta = 55°$ were found.

A strong uniaxial anisotropy was observed for the Co-Mo samples, as expected for an hcp structure and

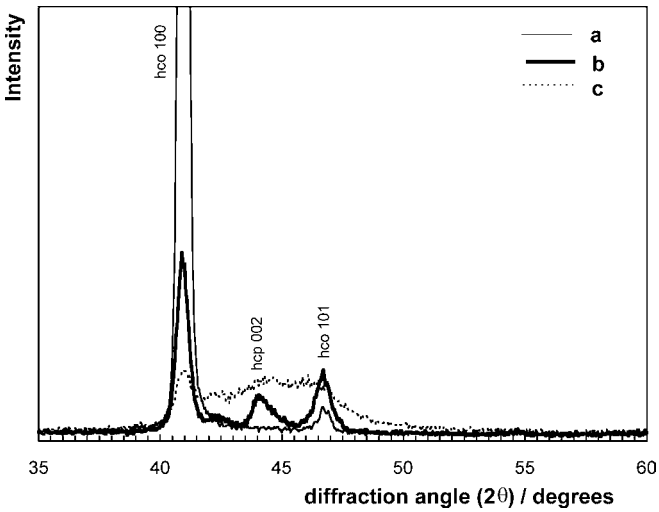

Fig. 8 X-ray diffractograms of deposits obtained under the same conditions as in Fig. 7 but with a greater charge: (*a*) −940, (*b*) −1000, (*c*) −1100 mV; 150 C cm^{-2}; (*a*) 35 μm, (*b*) 20 μm, (*c*) 6.5 μm

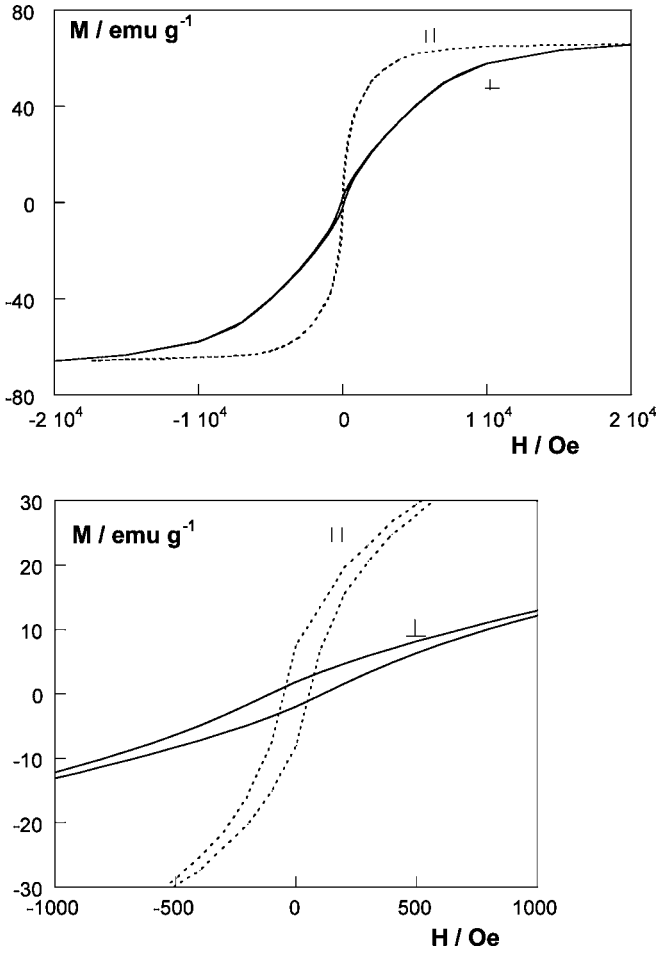

Fig. 9 Parallel and perpendicular hysteresis loops for a deposit obtained from Co-Mo solution; 60 rpm, graphite electrode, −3.2 mA cm^{-2}, 22% Mo, 40 μm

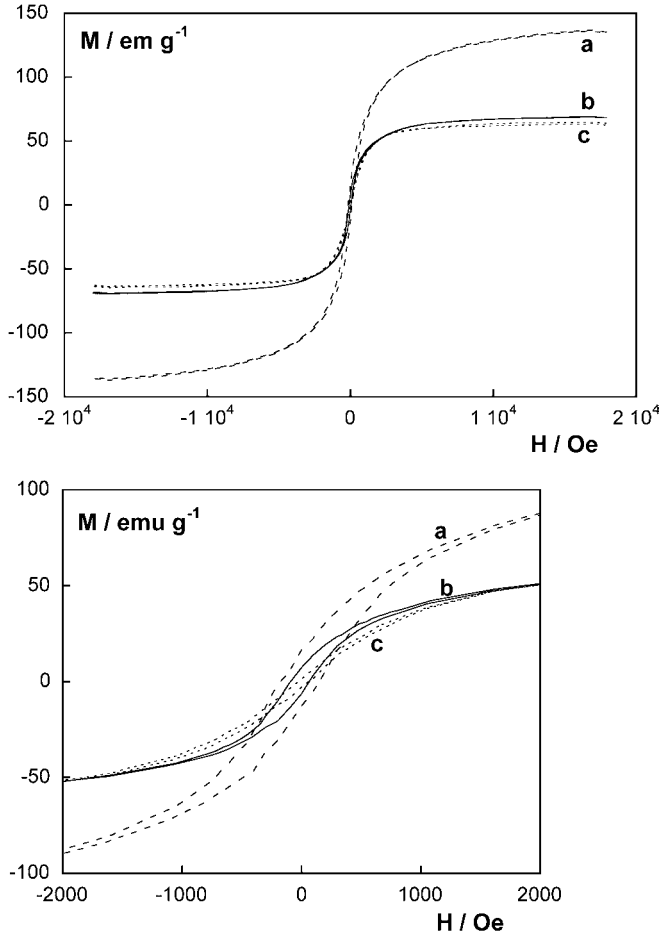

Fig. 10 Magnetization versus magnetic field applied for the deposits obtained at 60 rpm over a graphite electrode: (*a*) 0.1 mol dm^{-3} $CoSO_4$ + 0.2 mol dm^{-3} $Na_3C_6H_5O_7$, pH 6.6 solution, −1120 mV, 37 μm; (*b*) Co-Mo solution, −940 mV, 35 μm; (*c*) Co-Mo solution, −1100 mV, 6.5 μm

high textured films. However, the K value obtained was greater than that corresponding to pure hcp cobalt ($K = 4.5\times10^6$ emu cm^{-3}) [20], probably due to the residual stress and distortions caused by the presence of molybdenum in the crystalline lattice of cobalt.

The magnetization curves of Co-Mo deposits were compared with those corresponding to pure cobalt deposits obtained from a molybdate-free solution and prepared at similar deposition rates (Fig. 10). For the pure cobalt coating with an hcp structure, a saturation magnetization of 135 emu g^{-1} was obtained, which corresponded to a bulk cobalt response. The coercivity value (H_c) was around 160 Oe.

For cobalt-molybdenum deposits, a clear decrease of the saturation magnetization was observed, around 65 emu g^{-1}. This value was approximately constant for deposits prepared at different deposition rates, because they contained similar molybdenum percentages.

Moreover, the introduction of molybdenum in the deposits caused a clear decrease of the coercivity of the coatings. The Co-Mo films were soft, with coercivities in the range 70–40 Oe. The deposits obtained at potentials

no more negative than −1000 mV (or at current densities no more negative than -5 mA cm^{-2}) showed similar values of coercivity (around 70 Oe). However, deposits prepared at more negative values of the current density or the potential (until −1200 mV) showed a lower coercivity (around 40 Oe), revealing that amorphous + crystalline coatings presented the lowest value of any of these films.

Conclusions

Electrodeposition is a suitable way to obtain Co-Mo magnetic deposits over different substrates from a sulfate-citrate bath at pH 6.6. As deduced from voltammetric experiments, the start of the alloy deposition over vitreous carbon is delayed with respect to graphite and copper electrodes. Copper and graphite are useful to prepare Co-Mo coatings of several microns, whereas vitreous carbon favours detachment of the films.

The bath used, although it contains a low concentration of molybdate, leads to cobalt-molybdenum deposits of 20–23% Mo. This percentage is slightly dependent on the deposition potential or the current density applied. It is possible to maintain a constant composition through the thickness of the coating using moderate stirring of the solution during the deposition. No influence of the substrate (copper/graphite) or the preparation technique has been detected on the properties of the Co-Mo films. Co-Mo coatings of an hcp structure have been always obtained, and the cell parameters are clearly greater than those for the hexagonal cobalt. The films evolve with thickness to a structure with a clear (100) + (110) preferred orientation, showing an acicular morphology.

However, the properties (morphology, structure and magnetic properties) of the cobalt-molybdenum coatings are dependent on the deposition rate. The incorporation of molybdenum in the cobalt coatings leads to a decrease of both saturation magnetization and coercivity, with respect to the values for pure cobalt. The value of the saturation magnetization was constant for a fixed molybdenum percentage, but the value of the coercivity was also dependent on the crystalline structure of the films. Low deposition rates (low deposition potentials or current densities) favoured the formation of homogeneous crystalline deposits with a coercivity approximately constant. However, when high deposition rates were used to prepare the films, cracked coatings were obtained, with a mixed crystalline + amorphous structure and a lower coercivity than those for pure crystalline ones.

For the solution studied, the selection of both coating thickness and deposition potential (or current density) allows us to control the crystalline nature of the Co-Mo deposits. A decrease of the crystallinity improves the soft magnetic behaviour of the Co-Mo coatings.

Acknowledgements The authors thank the Serveis Cientificotècnics (Universitat de Barcelona) for the use of their equipment, the Servei de Magnetoquímica (Universitat de Barcelona) and Dr B. Martínez of Institut de Ciència de Materials de Barcelona (ICMAB) for magnetic measurements. This paper was supported financially by contract MAT 2000-0986 from the Comisión Interministerial de Ciencia y Tecnología (CICYT) and by the Comissionat of the Generalitat de Catalunya under Research Project 2001 SGR 00046. E.P. also thanks the DURSI of the Generalitat de Catalunya for financial support.

References

1. Taylor WP, Schneider M, Baltes H, Allen MG (1997) In: Proceedings of the international conference on solid-state sensors and actuators, Transducers'97, Chicago. Transducer, Chicago, pp 1445
2. Gómez E, Pellicer E, Vallés E (2001) J Electroanal Chem 517:109
3. Kinh VQ, Chassaing E, Saurat M (1975) Electrodep Surf Treat 3:205
4. Friend WZ (1980) Corrosion of nickel and nickel alloys. Wiley-Interscience, New York, pp 95–135, 248
5. Yao SW, Zeng Y, Guo HT (1994) Surf Tech (Japan) 45:643
6. A. Brenner (1963) Electrodeposition of alloys, vols 1–2. Academic Press, New York
7. Nee CC, Kim W, Weil R (1988) J Electrochem Soc 135:1100
8. Chassaing E, Vu Quang K, Wiart R (1989) J Appl Electrochem 19:839
9. Crousier J, Eyraud M, Crousier JP, Roman JM (1992) J Appl Electrochem 22:749
10. Chassaing E, Roumegas MP, Trichet MF (1995) J Appl Electrochem 25:667
11. Podhala EJ, Landolt D (1996) J Electrochem Soc 143:885
12. Podhala EJ, Landolt D (1996) J Electrochem Soc 143:893
13. Hu CC, Weng CY (2000) J Appl Electrochem 30:499
14. Murase K, Ando H, Matsubara E, Hirato T, Awakura Y (2000) J Electrochem Soc 147:2210
15. Zeng Y, Li Z, Ha M, Zhen S (2000) Electrochem Commun 2:36
16. Beltowska-Lehman E (1990) J Appl Electrochem 20:132
17. Podhala EJ, Landolt D (1997) J Electrochem Soc 144:1672
18. Niu ZJ, Yao SB, Zhou SM (1998) J Electroanal Chem 455:205
19. Gómez E, Pellicer E, Vallés E (2003) J Electroanal Chem 556:137
20. Klavunde KJ (2001) Nanoscale materials in chemistry. Wiley-Interscience, New York
21. Xiao JQ, Chien CL, Gavrin A (1996) J Appl Phys 79:5309

Electrodeposition of soft-magnetic cobalt-molybdenum coatings containing low molybdenum percentages

Available online at www.sciencedirect.com
SCIENCE DIRECT®
Journal of Electroanalytical Chemistry 568 (2004) 29–36
Journal of Electroanalytical Chemistry
www.elsevier.com/locate/jelechem

Electrodeposition of soft-magnetic cobalt–molybdenum coatings containing low molybdenum percentages

Elvira Gómez, Eva Pellicer, Elisa Vallés *

Electrodep, Departament de Química Física, Universitat de Barcelona, Martí i Franquès 1, 08028 Barcelona, Spain

Received 29 September 2003; accepted 9 December 2003
Available online 10 May 2004

Abstract

Electrodeposition of cobalt–molybdenum alloys has been optimised to obtain coatings that show low coercivity and high saturation magnetisation. For this purpose, low molybdenum percentages were required ($\leqslant 10\%$). Solutions containing a fixed sodium citrate concentration (0.2 mol dm^{-3}) and variable concentrations of $CoSO_4$ and Na_2MoO_4 were tested. 0.1 mol dm^{-3} $CoSO_4$ + 0.005 mol dm^{-3} Na_2MoO_4 or 0.3 mol dm^{-3} $CoSO_4$ + 0.012 mol dm^{-3} Na_2MoO_4 solutions, both at pH 4, were useful to obtain Co–Mo coatings of several microns with a molybdenum percentage $\leqslant 10\%$, although higher process efficiency was obtained from the second solution. These coatings showed a fluffy morphology and a close-packed hexagonal structure (hcp) with (1 1 0) + (1 0 0) preferred orientation. These films exhibited a soft magnetic behaviour and their coercivity (H_c) was clearly lower than that corresponding to pure-cobalt deposits and they maintained, moreover, high saturation magnetisation (M_s).

Keywords: Cobalt–molybdenum alloy; Electrodeposition; XRD; Magnetic films

1. Introduction

Electrodeposition is a useful method to obtain metallic coatings, which satisfy many properties such as hardness, corrosion resistance, catalytic properties, etc. In this regard, the preparation of cobalt alloys, which exhibit a soft magnetic behaviour, has been gaining importance because these materials are needed for microelectronic devices [1–9]. Molybdenum incorporation in cobalt alloys is one way to achieve a soft magnetic response of the material [10].

In a previous paper [11] we obtained homogeneous non-stressed 20–25% Mo cobalt–molybdenum deposits from a sulphate–citrate bath at pH 6.6. Those deposits showed low coercivity but also lower saturation magnetisation than pure-cobalt. To obtain Co–Mo coatings with low coercivity but high saturation magnetisation, lower molybdenum percentages are desirable. Previous experiments demonstrated that molybdenum incorporation in the deposits was constrained by decreasing the pH [12].

Here we examine the electrochemical response of various solutions at low pH as well as the characterisation of the Co–Mo deposits obtained. Baths tested contained a fixed sodium citrate concentration (0.2 mol dm^{-3}). The cobalt sulphate concentration ranged between 0.1 and 0.3 mol dm^{-3} and sodium molybdate was varied between 0.005 and 0.012 mol dm^{-3} to prevent high molybdenum incorporation in the deposits.

2. Experimental

The study of the electrodeposition process and deposit preparation was performed in a conventional three-electrode cell using a microcomputer-controlled Autolab potentiostat/galvanostat with PGSTAT30 equipment and GPES software. Solutions contained $CoSO_4$, $Na_3C_6H_5O_7$ and Na_2MoO_4, all of analytical grade. The pH was adjusted to 4.0 by adding H_2SO_4. All solutions were freshly prepared with water, which was first doubly distilled and then treated with a Millipore

* Corresponding author. Tel.: +34-93-402-1234; fax: +34-93-402-1234.
E-mail address: e.valles@ub.es (E. Vallés).

0022-0728/$ - see front matter © 2004 Published by Elsevier B.V.
doi:10.1016/j.jelechem.2003.12.032

Milli Q system. Before and during the experiments, solutions were deaerated with argon. The temperature was maintained at 25 °C.

For the electrochemical study, the working electrode was a vitreous carbon (Metrohm) electrode of 0.0314 cm^2. It was polished to a mirror finish before each experiment using alumina of different grades (3.75 and 1.85 μm) and cleaned ultrasonically for 2 min in water. For deposit preparation, copper (John Matthey 99.99%, 0.720 cm^2) and graphite (Alfa Aesar, 0.352 cm^2) electrodes were used. They were polished before each experiment using sandpaper (2400 and 4000) followed by damp alumina of 0.3 μm. The reference electrode was an Ag|AgCl|1 mol dm^{-3} NaCl electrode mounted in a Luggin capillary containing 0.5 mol dm^{-3} Na_2SO_4 solution. All potentials are referred to this electrode. The counter electrode was a platinum spiral.

Voltammetric experiments were carried out at 50 mV s^{-1}, scanning initially from −500 mV towards negative potentials. Only one cycle was run in cyclic voltammetric experiments. Two linear sweep voltammetries (partial scans) were combined in some cases to obtain complementary information.

For preparation of the deposits, the solution was stirred moderately ($\omega = 60$ rpm) to avoid the depletion of the minority species (molybdate) to the electrode during the experiments and to maintain homogeneous deposit composition.

The morphology of the deposits was examined with scanning electron microscopy, using Hitachi S 2300 equipment. Deposit composition was determined with an X-ray analyser incorporated in a Leica Cambridge Stereoscan S-360 scanning electron microscope using standards of pure molybdenum and pure cobalt before each quantitative analysis.

X-ray diffraction (XRD) phase analysis was performed on a Philips MRD diffractometer with low-resolution parallel beam optics. The Cu Kα radiation ($\lambda = 1.5418$ Å) was selected by means of a diffracted beam flat graphite monochromator. 2θ diffractograms were obtained in the 2θ range of 20–100° with a step range of 0.05° and a measuring time of 5″ per step. The magnetic measurements were performed with a Manics DSM8 pendulum-type magnetometer at room temperature.

The efficiency of deposit preparation was calculated from measurement of the thickness of the deposits (using a Zeiss Axiovert 405 M Microscope).

3. Results and discussion

3.1. Voltammetric study

According to previous knowledge of the influence of pH on the composition of cobalt–molybdenum deposits [12], various baths adjusted to pH 4.0 were tested. The Co(II) concentration was varied from 0.1 to 0.3 mol dm^{-3} as it was expected that the molybdenum content in the deposits would also be reduced by increasing Co(II) concentration in solution.

The electrochemical response of a solution containing 0.3 mol dm^{-3} $CoSO_4$ + 0.005 mol dm^{-3} Na_2MoO_4 + 0.2 mol dm^{-3} $Na_3C_6H_5O_7$ was analysed by means of the voltammetric technique (Fig. 1). A reduction peak prior to a sharp current increase attributable to hydrogen evolution was recorded during the negative scan. When the scan was reversed at lower limits prior to the hydrogen coevolution current, a single peak was recorded during the positive scan. In contrast, when the scan was reversed at higher negative limits, a double peak was recorded. This behaviour was observed for all Co(II) concentrations studied.

In order to determine the nature of this double oxidation peak, which appeared at large negative limits, two linear sweep voltammetries were combined: a negative going scan sweep, followed by an oxidation scan performed from an initial potential at which no current was detected. Fig. 2 shows that the peak at more negative potentials was enhanced when deposition continued in the positive going sweep.

The two combined linear sweep voltammetries were used to analyse the oxidation response when different negative limits were applied (Fig. 3(A)). A single oxidation peak was recorded when the negative limit was fixed at potentials prior to the reduction peak or at potentials for which the reduction peak was developed (Fig. 3(B), curve a). The oxidation of deposits formed by scanning to more negative potentials showed a shoulder-shape positive current prior to the main peak (Fig. 3(B), curves b, c). At even more negative lower limits a double peak was recorded accompanied by a clear decrease of the Q_{ox}/Q_{red} ratio (Fig. 3(B), curve d).

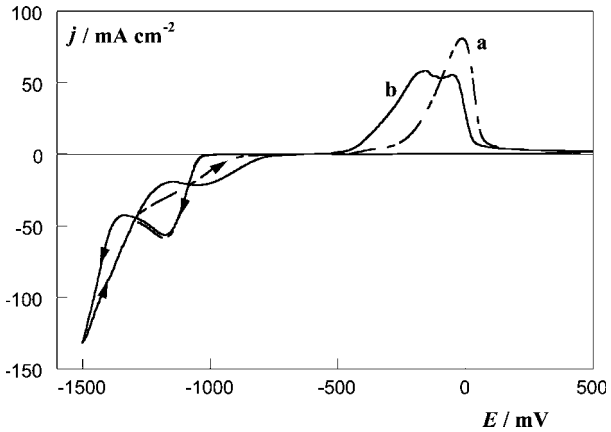

Fig. 1. Cyclic voltammograms of a 0.3 mol dm^{-3} $CoSO_4$ + 0.2 mol dm^{-3} $Na_3C_6H_5O_7$ + 0.005 mol dm^{-3} Na_2MoO_4 solution. Quiescent conditions. Lower limit (E_c) = (a) −1300 mV and (b) −1500 mV.

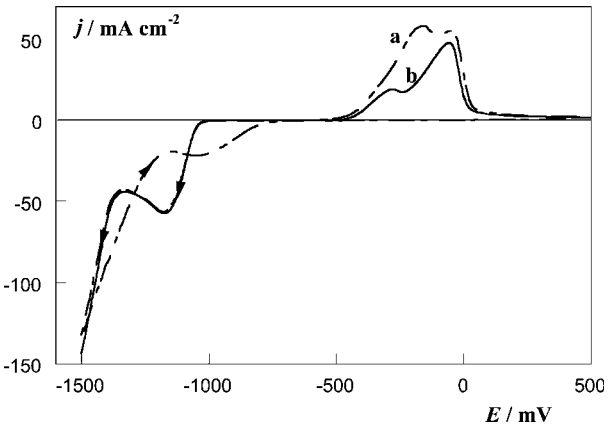

Fig. 2. 0.3 mol dm^{-3} $CoSO_4$ + 0.2 mol dm^{-3} $Na_3C_6H_5O_7$ + 0.005 mol dm^{-3} Na_2MoO_4 solution. Quiescent conditions. (a) Cyclic voltammogram, $E_c = -1500$ mV; (b) combined linear sweep voltammetries (reduction scan to $E_c = -1500$ mV + oxidation scan from −500 mV).

For deposits formed in a single scan towards large negative limits, in some experiments the potential was held during the oxidation scan. When the potential was held at a value close to the onset of the oxidation, the peak at more negative potentials disappeared and that at more positive potentials remained in the same position (Fig. 4). As these peaks were independent, it seemed that they were related to the formation of two different types of Co–Mo deposit.

When cyclic voltammetries were recorded while stirring the solution, the reduction peak evolved to a plateau, revealing that it was influenced by mass transport (Fig. 5). The oxidation of the deposit began at more positive potentials than those corresponding to quiescent conditions and only a single peak was recorded. This result revealed that the supply of electroactive species to the electrode favoured the formation of a more homogeneous deposit, which was oxidised in a single peak.

For a fixed Co(II) concentration, voltammetric studies from solutions with a variable molybdate concentration were performed. Fig. 6(A) shows that, at low negative limits, the general trends of the electrochemical response were maintained when the molybdate concentration was increased from 0.005 to 0.012 mol dm^{-3}. A reduction peak was observed during the negative scan and only a single oxidation peak was obtained in the positive scan. However, this oxidation peak moved to more negative potentials as the molybdate concentration was increased, corresponding to the formation of Co–Mo deposits with higher molybdenum percentages [13]. In contrast, different features were observed when the negative limit was raised to potentials at which the hydrogen evolution current was significant (Fig. 6(B)). A single oxidation peak was recorded for $[MoO_4^{2-}] = 0.012$ mol dm^{-3}, even under quiescent conditions, whereas the double peak mentioned above was observed for $[MoO_4^{2-}] = 0.005$ mol dm^{-3}. This result made it evident that a more homogeneous deposit was formed for molybdate concentrations greater than 0.005 mol dm^{-3}.

Zooming the reduction zone of the voltammetry of Fig. 6, a low current attributed to molybdenum oxide formation [14] was observed. Moreover, a tiny shoulder appeared (Fig. 7(A), continuous line). None of these features was observed when a reduction scan from a molybdate-free solution was performed (Fig. 7(A), dashed line). In order to investigate the nature of this shoulder, various negative scans in the range of these low currents were carried out, followed by the corresponding oxidation scans. At the negative limits for which the shoulder developed, an oxidation peak centred at −200 mV was recorded (Fig. 7(B), curve a). The oxidation peak of a pure cobalt deposit formed at low reduction charges in citrate media appeared in the same position (Fig. 7(B), curve c). Meanwhile, for more negative lower limits the oxidation peak, attributed to Co–Mo oxidation, was centred at −250 mV (Fig. 7(B), curve

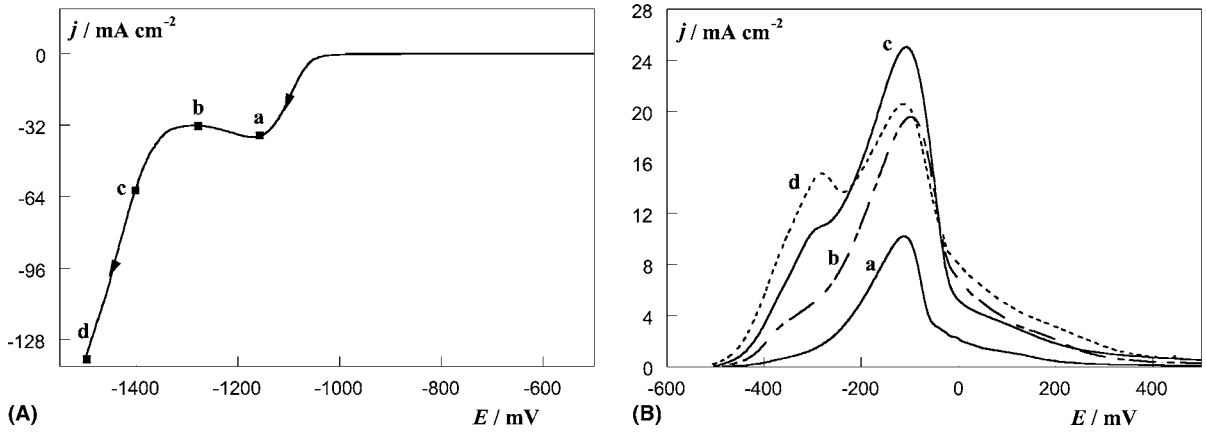

Fig. 3. 0.2 mol dm^{-3} $CoSO_4$ + 0.2 mol dm^{-3} $Na_3C_6H_5O_7$ + 0.005 mol dm^{-3} Na_2MoO_4 solution. Quiescent conditions. Combined linear sweep voltammetries. (A) Reduction scans to E_c = (a) −1175 mV, (b) −1300 mV, (c) −1400 mV and (d) −1500 mV. (B) Corresponding oxidation scans from −550 mV.

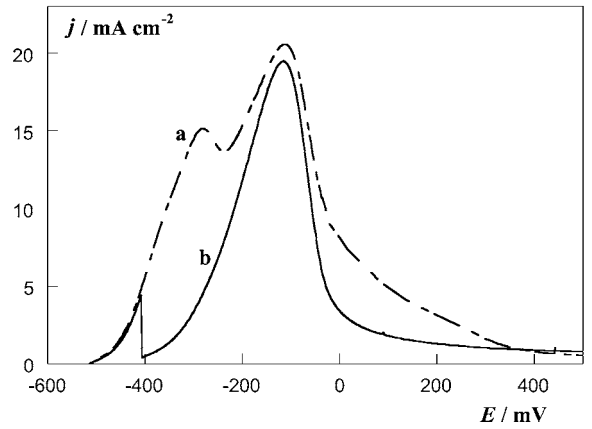

Fig. 4. 0.2 mol dm^{-3} $CoSO_4$ + 0.2 mol dm^{-3} $Na_3C_6H_5O_7$ + 0.005 mol dm^{-3} Na_2MoO_4 solution. Quiescent conditions. (a) Oxidation scan from −550 mV of a deposit formed during a reduction scan to $E_c = -1500$ mV, (b) oxidation scan holding the potential at −400 mV during 60 s of a deposit obtained under the same conditions.

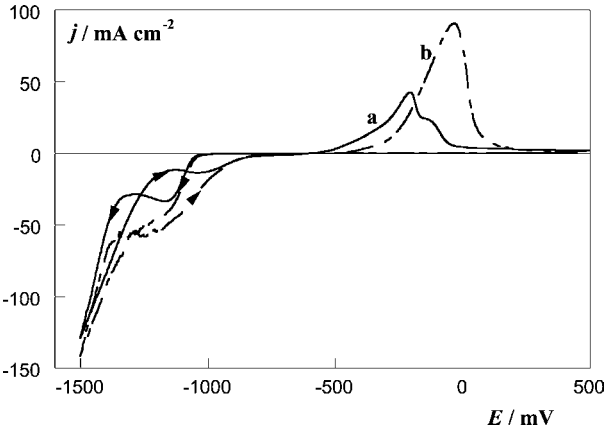

Fig. 5. Cyclic voltammograms of a 0.2 mol dm^{-3} $CoSO_4$ + 0.2 mol dm^{-3} $Na_3C_6H_5O_7$ + 0.005 mol dm^{-3} Na_2MoO_4 solution. $E_c = -1500$ mV. (a) Quiescent conditions, (b) stirred conditions.

b). Obviously, the position of these peaks corresponded to low reduction charges, since they shifted, as usual, to more positive potentials when the reduction charge increased. These results were in accord with the proposed mechanism for Co–Mo electrodeposition [12]. This proposal suggests that the presence of a small amount of cobalt nuclei on the intermediate molybdenum oxides is always necessary to induce alloy deposition. Complementary galvanostatic experiments at very low current densities revealed that the typical nucleation spike appeared after a previous reduction process assigned to molybdenum oxide formation [14] (Fig. 8, curves a and b). When a more negative current density was applied, only a nucleation spike attributed to Co–Mo, which appeared at shorter deposition times, was observed (Fig. 8, curve c).

The Q_{ox}/Q_{red} ratio was estimated for different bath compositions from the two combined linear sweep voltammetries (negative going sweep of the reduction scan + oxidation scan) (Table 1). For a $[MoO_4^{2-}] = 0.005$ mol dm^{-3}, the Q_{ox}/Q_{red} ratio increased strongly when the Co(II) concentration was raised from 0.1 to 0.2 mol dm^{-3} and increased slightly from 0.2 to 0.3 mol dm^{-3}. For a 0.3 mol dm^{-3} Co(II) concentration, the Q_{ox}/Q_{red} ratio decreased slightly when the molybdate concentration was increased moderately. In all cases, a low Q_{ox}/Q_{red} ratio was observed at very low negative limits, for which molybdenum oxide formation was important, and these intermediates were hardly oxidised [13]. On the other hand, Q_{ox}/Q_{red} was also low at very negative lower limits as a consequence of considerable hydrogen evolution. However, for each bath composition, there was always a potential range at which deposits could be prepared with reasonable efficiency.

3.2. Preparation and characterisation of deposits

Deposits were prepared mainly galvanostatically to facilitate control of the deposited charge. All deposits

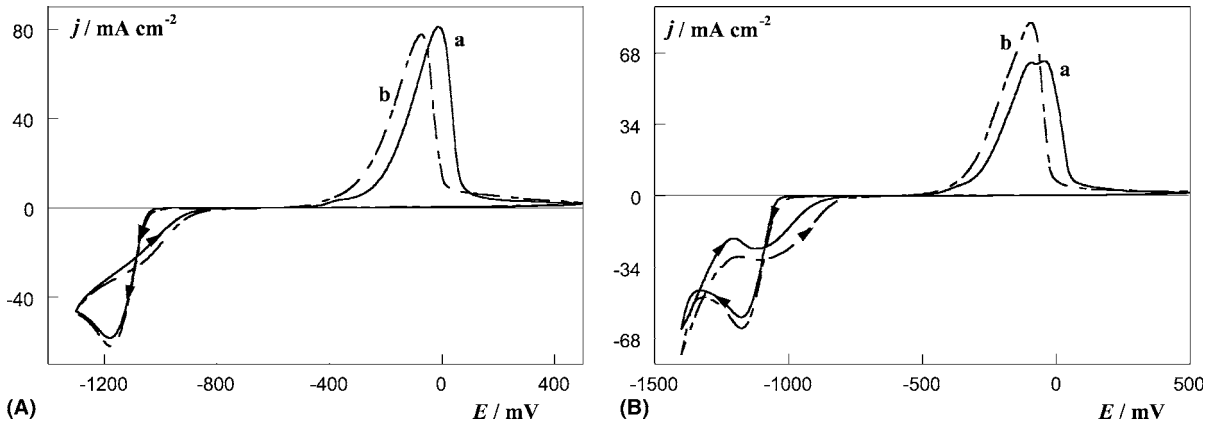

Fig. 6. Cyclic voltammograms of a 0.3 mol dm^{-3} $CoSO_4$ + 0.2 mol dm^{-3} $Na_3C_6H_5O_7$ + x mol dm^{-3} Na_2MoO_4 solution. Quiescent conditions. (a) $x = 0.005$, (b) $x = 0.012$. (A) $E_c = -1300$ mV. (B) $E_c = -1500$ mV.

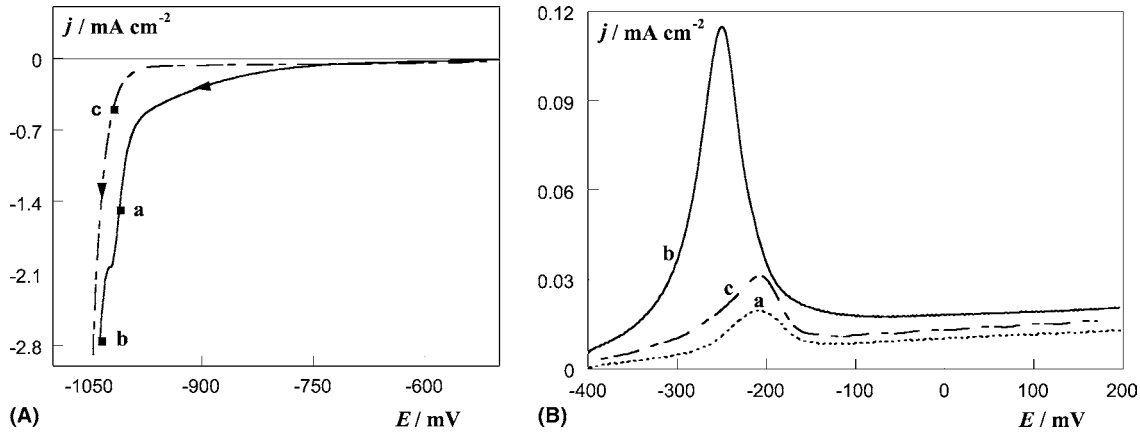

Fig. 7. (A) Reduction scans to E_c = (a) −1018 mV, (b) −1035 mV of a 0.3 mol dm^{-3} $CoSO_4$ + 0.2 mol dm^{-3} $Na_3C_6H_5O_7$ + 0.012 mol dm^{-3} Na_2MoO_4 solution and (c) E_c = −1030 mV of a 0.3 mol dm^{-3} $CoSO_4$ + 0.2 mol dm^{-3} $Na_3C_6H_5O_7$ solution. Quiescent conditions. (B) Corresponding oxidation scans from −400 mV.

were obtained under a moderate stirring of the solution (ω = 60 rpm) as it was demonstrated in voltammetric experiments that it was necessary to maintain the flux of the species to the electrode, thereby obtaining deposits of homogeneous composition. Copper or graphite substrates were used since thick deposits could not be prepared on vitreous carbon [11]. Compositional analysis of samples prepared from the baths previously studied revealed, as a general trend, that the molybdenum content in Co–Mo deposits was low, dependent on the applied current density in acidic media (Table 2). Moreover, the efficiency of deposition increased in direct proportion to Co(II) concentration. This result was in agreement with previous voltammetric experiments.

Our experimental conditions led to deposits with molybdenum percentages that ranged between <3% and 10% Mo. The molybdenum percentage increased directly with molybdate concentration and indirectly with Co (II) concentration. Moreover, a practically constant composition was observed for different deposition charges, revealing that the stirring conditions used were adequate to assure a constant composition throughout the thickness of the deposit (Table 3).

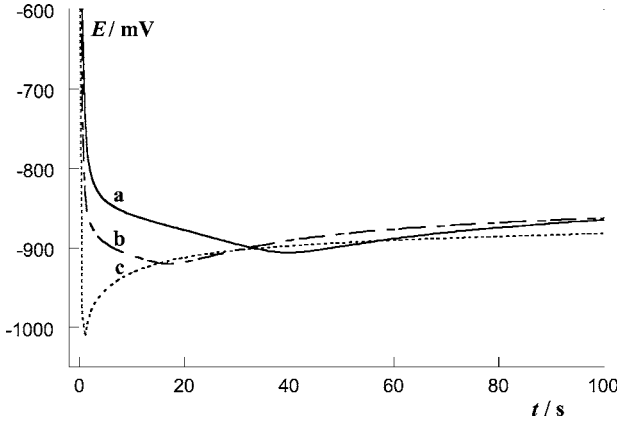

Fig. 8. E–t transients recorded from a 0.3 mol dm^{-3} $CoSO_4$ + 0.2 mol dm^{-3} $Na_3C_6H_5O_7$ + 0.012 mol dm^{-3} Na_2MoO_4 solution. Quiescent conditions. (a) −160 μA cm^{-2}, (b) −255 μA cm^{-2} and (c) −796 μA cm^{-2}.

Deposits with very low molybdenum percentages (lower than 5%) were black and showed an needle-like morphology, very similar to that corresponding to pure-cobalt (Fig. 9(A)). Deposits with molybdenum percentages ranging between 5 and 10% were less dark, tending

Table 1
Q_{ox}/Q_{red} ratios obtained from voltammetric experiments as a function of the lower limit for different electrolyte concentrations

Q_{ox}/Q_{red}	−E (mV)						
	1040	1050	1070	1100	1160	1225	1500
[Co(II)] = 0.1 M $[MoO_4^{2-}]$ = 0.005 M	–	–	–	0.01	0.23	0.24	0.15
[Co(II)] = 0.2 M $[MoO_4^{2-}]$ = 0.005 M	–	0.09	0.35	0.50	0.70	0.70	0.60
[Co(II)] = 0.3 M $[MoO_4^{2-}]$ = 0.005 M	0.10	0.39	0.50	0.67	0.82	0.84	0.47
[Co(II)] = 0.3 M $[MoO_4^{2-}]$ = 0.012 M	0.16	0.30	0.42	0.60	0.87	0.85	0.39

$[Na_3C_6H_5O_7]$ = 0.2 M.

Table 2
Molybdenum percentages (%Mo) and efficiency values (η) for Co–Mo deposits obtained galvanostatically

[Co(II)] (mol dm^{-3})	[MoO_4^{2-}] (mol dm^{-3})	$-j$ (mA cm^{-2})	$-E$ (mV)	% Mo	η (%)
0.1	0.005	6.3	970	9	15
		12.5	1180	10	23
0.3	0.005	6.4	920	3	60
		9.5	955	3	54
		15.9	1015	3	47
		23	1070	<3	56
0.3	0.012	6.4	880	9	43
		9.5	935	7	46
		15.9	980	5	67
		23.9	1015	5	74

j was the applied current density and E was the stabilised potential. [$Na_3C_6H_5O_7$] = 0.2 mol dm^{-3}.

Table 3
Molybdenum percentages (%Mo) of various Co–Mo coatings obtained galvanostatically, j being the applied current density and Q the reduction charge

[Co(II)] (mol dm^{-3})	$-j$ (mA cm^{-2})	$-Q$ (C cm^{-2})	% Mo
0.1	6.3	64	10
		670	9
	12.7	64	9
		400	9
		670	10
0.3	9.5	37	3
		476	3
	15.9	24	3
		420	3

[$Na_3C_6H_5O_7$] = 0.2 mol dm^{-3}, [MoO_4^{2-}] = 0.005 mol dm^{-3}.

to a fluffy appearance as the molybdenum percentage increased (Fig. 9(B)).

In all cases, the diffractograms of Co–Mo deposits of several microns ($\geqslant$ 50 μm) ranging from 3% to 10% Mo showed narrow peaks, revealing the crystalline nature of the deposits, which can be assigned to a close-packed hexagonal structure (hcp) with a (1 1 0) + (1 0 0) preferred orientation (Fig. 10). The cell parameters of this hexagonal structure were obtained after a fit profile and least square refinement, leading to values very similar to those of cobalt. The peaks of the hexagonal structure gradually shifted to lower values than those corresponding to cobalt as a consequence of the molybdenum incorporation in the deposit. Deposits showing a crystallographic direction parallel to the substrate surface (an hcp structure with $hk0$ main peaks) were obtained as the molybdenum percentage increased. The parameter c could not be determined for deposits in the range of the highest molybdenum percentages because no diffraction peaks with $l \neq 0$ were observed.

The peak profile analysis was performed using pseudo-Voight functions, and the full width at half maximum (FWHM) was refined for every peak. Table 4 lists the FWHM values for the different diffraction peaks and the adjusted cell parameters for two samples. A slight increase of the width of the peaks was observed by increasing the molybdenum percentage, probably as a consequence of the stress produced in the crystalline lattice when molybdenum was incorporated in the deposit.

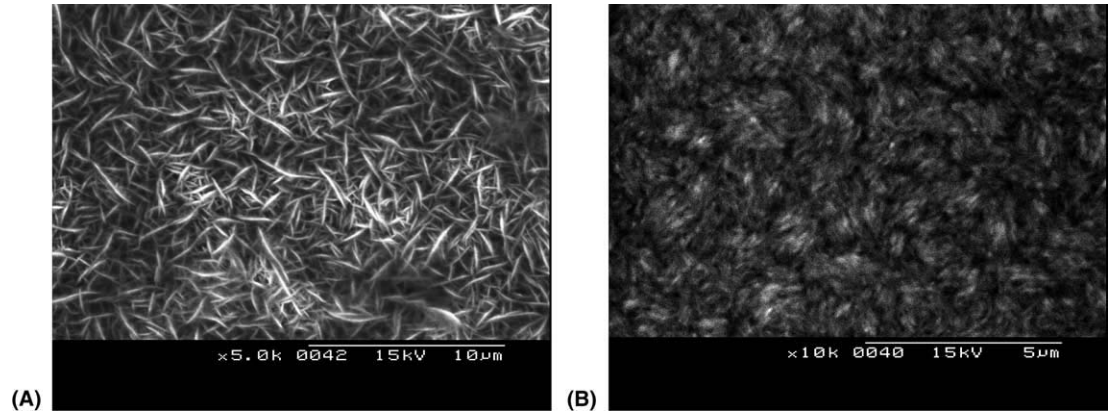

Fig. 9. SEM micrographs of Co–Mo deposits obtained galvanostatically under stirred conditions (ω = 60 rpm). (A) 0.3 mol dm^{-3} $CoSO_4$ + 0.2 mol dm^{-3} $Na_3C_6H_5O_7$ + 0.005 mol dm^{-3} Na_2MoO_4 solution. $j = -32$ mA cm^{-2}, 3% Mo. (B) 0.1 mol dm^{-3} $CoSO_4$ + 0.2 mol dm^{-3} $Na_3C_6H_5O_7$ + 0.005 mol dm^{-3} Na_2MoO_4 solution. $j = -8$ mA cm^{-2}, 8% Mo.

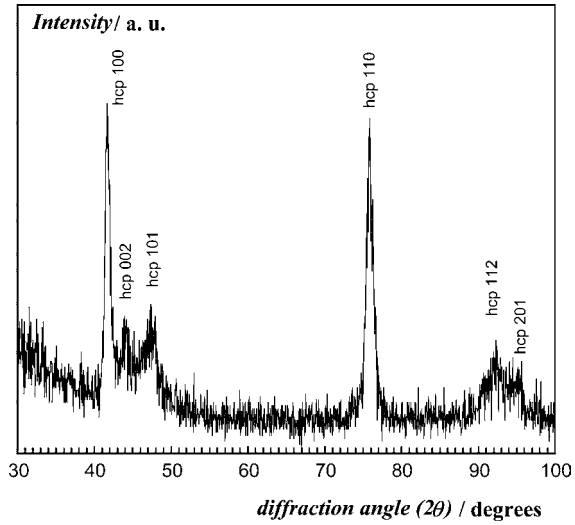

Fig. 10. X-ray diffractogram of Co–Mo deposits with a molybdenum percentage $3 \leqslant \%\ \mathrm{Mo} \geqslant 10$.

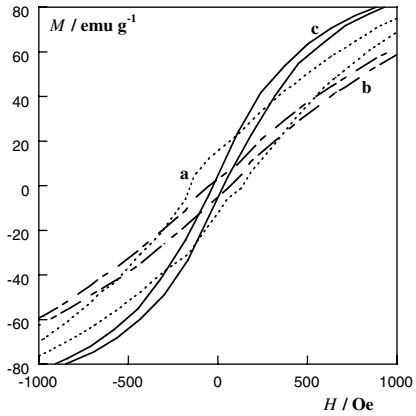

Fig. 11. Magnetisation vs. magnetic field applied and magnified detail of deposits obtained from (a) 0.3 mol dm^{-3} $CoSO_4 + 0.2$ mol dm^{-3} $Na_3C_6H_5O_7$ solution, (b) 0.3 mol dm^{-3} $CoSO_4 + 0.2$ mol dm^{-3} $Na_3C_6H_5O_7 + 0.012$ mol dm^{-3} Na_2MoO_4 solution. 5% Mo, (c) 0.1 mol dm^{-3} $CoSO_4 + 0.2$ mol dm^{-3} $Na_3C_6H_5O_7 + 0.005$ mol dm^{-3} Na_2MoO_4 solution. 9% Mo.

Table 4
FWHM values for the diffraction peaks and cell parameters obtained from diffractograms corresponding to Co–Mo coatings of different molybdenum content

	FWHM (º)								
	100	002	101	110	200	112	201	a (Å)	c (Å)
3% Mo	0.63	1.32	2.46	1.02	1.47	1.67	1.96	2.504	4.112
9% Mo	0.67	1.52	–	1.31	1.51	–	–	2.513	–

Magnetic measurements of the samples previously characterised by XRD were carried out by taking hysteresis loops. Co–Mo deposits of $\%\mathrm{Mo} < 5\%$ exhibited H_c values very close to those of homologous pure-Co deposits, revealing that very low molybdenum percentages in cobalt deposits did not promote changes in the magnetic response. The coercivity clearly decreased as the molybdenum percentage increased in the range of 5–10% (Fig. 11). At the same time, the saturation magnetisation decreased slightly from the M_s value corresponding to a pure-cobalt deposit. Under these conditions, Co–Mo deposits obtained from different bath compositions but containing the same molybdenum percentage led to practically identical M_s and H_c values.

4. Conclusions

The voltammetric study allows us to choose the deposition potential range, the stirring conditions, and the molybdate concentration in order to prepare homogeneous Co–Mo deposits with low molybdenum percentages successfully. A single oxidation peak in voltammetric experiments revealed the formation of homogeneous deposits. For this purpose, solutions should be stirred moderately, especially when the molybdate concentration is kept at quasi "homeopathic" quantities (0.005 mol dm^{-3}) since depletion of molybdate around the electrode is unavoidable when quiescent conditions are used. Moreover, hydrogen evolution was minimised at slightly negative potentials since, under these conditions, the process was more efficient and porous hydrogenated deposits did not form.

The voltammetric study combined with galvanostatic experiments also provided experimental support for the previously suggested sequence of steps for Co–Mo electrodeposition [12]. The initial formation of intermediate molybdenum oxides was demonstrated both by voltammetric and galvanostatic curves when working at low current densities. Moreover, the shoulder that appeared in the negative scan of the voltammetric curves was related to the subsequent nucleation of cobalt to induce the alloy deposition over the oxides.

At pH 4.0, for a fixed 0.2 mol dm^{-3} citrate concentration, the fraction of free Co^{2+} calculated from the corresponding complexation constants increases from ~4% for $[\mathrm{Co(II)}] = 0.1$ mol dm^{-3} to 40% for

[Co(II)] = 0.3 mol dm^{-3}. An increase of free Co^{2+} concentration in solution caused an advance of the onset of the deposition process and an increase of the voltammetric Q_{ox}/Q_{red} ratio. This resulted in a greater current efficiency for deposit preparation when [Co(II)] = 0.3 mol dm^{-3}.

For each bath composition, a potential range, in which Co–Mo deposits could be prepared with moderate or high current efficiency, was found. At deposition potentials below this range, molybdenum oxides form on the electrode, thereby hindering the alloy deposition [12]. Moreover, deposition potentials over this optimum range should also be avoided since hydrogen evolution diminishes the current efficiency and the deposit homogeneity considerably.

Co–Mo deposits with a molybdenum percentage between 5 and 10% showed an excellent soft-magnetic behaviour. In comparison to Co–Mo deposits with higher molybdenum percentages (~23%) obtained in previous work [11], we have here maintained the saturation magnetisation close to the value exhibited by pure-Co deposits.

The morphology and structure of those Co–Mo coatings poor in molybdenum were quite similar to those of pure cobalt, although some changes were promoted when the molybdenum percentage was increased over 5%. Morphological and structural changes were linked to changes in the magnetic response and it seemed that a minimum percentage of molybdenum was necessary to observe a clear diminution of the coercivity.

Acknowledgements

The authors thank the Serveis Cientificotècnics (Universitat de Barcelona) and the Servei de Magnetoquímica (Universitat de Barcelona) for the use of their equipment. This paper was supported financially by contract MAT 2000–0986 from the *Comisión Interministerial de Ciencia y Tecnología (CICYT)* and by the *Comissionat* of the *Generalitat de Catalunya* under Research Project 2001 SGR 00046. E. Pellicer also thanks the DURSI of the *Generalitat de Catalunya* for financial support.

References

[1] M. Onoda, K. Shimizu, T. Tsuchiya, T. Watanabe, J. Mag. Mag. Mater. 126 (1993) 595.
[2] T. Osaka, Electrochim. Acta 42 (1997) 3015.
[3] T. Osaka, T. Sawaguchi, F. Mizutani, T. Yokoshima, M. Takai, Y. Okinaka, J. Electrochem. Soc. 146 (1999) 3295.
[4] F.E. Rasmussen, J.T. Ravnkilde, P.T. Tang, O. Hansen, S. Bouwska, in: Eurosensors XIV, 14th European Conference on Solid State Transducers 2000, Denmark, p. 915.
[5] T. Osaka, Electrochim. Acta 45 (2000) 3311.
[6] I. Tabakovic, S. Riemer, V. Inturi, P. Jallen, A. Thayer, J. Electrochem. Soc. 147 (2000) 219.
[7] Y.K. Kim, H.Y. Son, Y.S. Choi, K.S. Moon, K.H. Sunwoo, J. Appl. Phys. 87 (2000) 5413.
[8] H.-S. Nam, T. Yokoshima, T. Nakanishi, T. Osaka, Y. Yamazaki, D.N. Lee, Thin Solid Films 384 (2001) 288.
[9] I. Tabakovic, V. Inturi, S. Riemer, J. Electrochem. Soc. 149 (2002) C18.
[10] W. P. Taylor, M. Schneider, H. Baltes, M. G. Allen, in: Proceedings of the International Conference on Solid-State Sensors and Actuators, Transducers '97, Chicago, 1997.
[11] E. Gómez, E. Pellicer, X. Alcobe, E. Vallés, J. Solid State Electrochem., in press.
[12] E. Gómez, E. Pellicer, E. Vallés, J. Electroanal. Chem. 556 (2003) 137.
[13] E. Gómez, E. Pellicer, E. Vallés, J. Electroanal. Chem. 517 (2001) 109.
[14] E. Gómez, E. Pellicer, E. Vallés, J. Appl. Electrochem. 33 (2003) 245.

Microstructures of soft-magnetic cobalt-molybdenum alloy obtained by electrodeposition on seed layer/silicon substrates

Available online at www.sciencedirect.com
SCIENCE DIRECT®
Electrochemistry Communications 6 (2004) 853–859
electrochemistry communications
www.elsevier.com/locate/elecom

Microstructures of soft-magnetic cobalt–molybdenum alloy obtained by electrodeposition on seed layer/silicon substrates

Elvira Gómez, Eva Pellicer, Elisa Vallés *

Electrodep, Departament de Química Física, Universitat de Barcelona, Martí i Franquès 1, E-08028 Barcelona, Spain

Received 2 June 2004; received in revised form 15 June 2004; accepted 16 June 2004
Available online 2 July 2004

Abstract

Cobalt–molybdenum alloy containing ~10% molybdenum, which has promising applications in magnetic devices, was deposited on silicon-based substrates. A solution containing 0.2 mol dm^{-3} $C_6H_5Na_3O_7$ + 0.3 mol dm^{-3} $CoSO_4$ + 0.012 mol dm^{-3} Na_2MoO_4 at pH = 4.0 and 25 °C was used to prepare Co–Mo coatings, which showed a soft-magnetic response. A constant deposition rate of 7.7 μm h^{-1} was achieved under stirring. White-light interferometry and AFM techniques were used to measure the thickness of Co–Mo coatings, with identical results. White-light interferometry also revealed smooth surfaces. Deposition was highly selective on mask devices and deposits were crack-free up to ~7 μm. Vertical walls and well-defined profiles of the coatings were obtained. At higher thickness cracks appeared and the Co–Mo layers detached. The stress was reduced by increasing the temperature and adding saccharine to the bath.

Keywords: Cobalt–molybdenum alloy; Electrodeposition; White-light interferometry; AFM; MEMS

1. Introduction

The preparation of magnetic materials of iron-group metals has received attention because they have wide applications in industry, mainly in micro-electromechanical systems (MEMS) and magnetic storage devices. Cobalt alloys with soft-magnetic behaviour have been studied with a view to microelectronic devices [1–5].

One of the most interesting applications is the use of thin films with minimum coercivity and maximum saturation magnetisation for magnetic actuation in MEMS. Electrodeposition has proved to be a valid method to prepare magnetic materials. Although Ni–Fe permalloy is the most common alloy used in MEMS applications [6], cobalt alloys can also be incorporated in MEMS devices [7,8] due to their magnetic properties [9–11].

We demonstrated in a previous study that the presence of molybdenum in cobalt coatings led to a soft-magnetic response [12], so they could be used in magnetic devices such as sensors and actuators. Cobalt–molybdenum (Co–Mo) alloys can be obtained by electrodeposition according to an induced process, since molybdenum is not fully reduced in aqueous solution in the absence of an inductor metal (Co, Fe, Ni).

We have previously reported the electrochemical behaviour of the cobalt–molybdenum system in baths with a range of compositions and pH [13,14]. Among the baths we developed, the best soft-magnetic response was achieved at acid pH with $[Co(II)]/[MoO_4^{2-}] \approx 25$ [14]. Here we examine the possibility of preparing these coatings on silicon-based substrates. We also analyse the properties of these deposits and of test structures used in primary studies for MEMS development. Analyses were mainly focused on growth rate and surface roughness. In the case of test

* Corresponding author. Tel.: +34-93-402-12-34; fax: +34-93-402-12-31.
E-mail address: e.valles@ub.edu (E. Vallés).

1388-2481/$ - see front matter © 2004 Elsevier B.V. All rights reserved.
doi:10.1016/j.elecom.2004.06.011

structures, the surface topography was recorded to assess the selectivity of deposition.

2. Experimental

The study of the electrodeposition process and deposit preparation was performed in a conventional three-electrode cell using a microcomputer-controlled potentiostat/galvanostat Autolab with PGSTAT30 equipment and GPES software. A 0.2 mol dm^{-3} $C_6H_5Na_3O_7$ + 0.3 mol dm^{-3} $CoSO_4$ + 0.012 mol dm^{-3} Na_2MoO_4 solution was used, all reagents being of analytical grade. The saccharine was also of analytical grade. The pH was adjusted to 4.0 by adding H_2SO_4. All solutions were freshly prepared with water which was first doubly distilled and then treated with a Millipore Milli Q system. Before the experiments solutions were de-aerated with argon and maintained under argon atmosphere during the preparation of the deposits. The temperature was maintained at 25 °C except for the experiments concerning to the temperature influence study.

For electrochemical study modified p-type 4–40 Ω cm ⟨1 0 0⟩ silicon samples were used as working electrodes. The reference electrode was an Ag/AgCl/1 mol dm^{-3} NaCl electrode mounted in a Luggin capillary containing 0.5 mol dm^{-3} Na_2SO_4 solution. All potentials are referred to this electrode. The counter electrode was a platinum spiral.

The silicon surfaces were prepared for better adhesion and minimum mechanical stress by IMB–CNM.CSIC (Centro Nacional de Microelectrónica). A Ti(1000 Å)/Ni(500 Å) seed layer was sputtered on a previously grown phosphosilicate glass (PSG) layer 1 μm thick. This seed layer supplied an electrical connection for the electrodeposition process. The flat silicon-based substrates were cleaned with ethanol and then rinsed in water before each experiment. Deposits were prepared on the silicon-based substrates mentioned above and on silicon-based substrates on which an UV photoresist microstructure had been previously patterned. The photolithographic process was also performed using IMB–CNM technology.

Voltammetric experiments were performed in quiescent conditions at 50 mV s^{-1}, scanning initially from −400 mV towards negative potentials. Only one cycle was run in cyclic voltammetric experiments.

For preparation of the deposits, the solution was gently stirred ($\Omega = 60$ rpm) to avoid the depletion of the minority species (molybdate) to the electrode during the experiments and to maintain homogeneous deposit composition.

The morphology of the deposits was examined by scanning electron microscopy (SEM) and their composition was determined by energy dispersive X-ray spectroscopy (EDS). The efficiency of deposit preparation was estimated by comparing the deposited charge and the ICP–MS analysis of the samples obtained after chemical dissolution of the films in a 1% HNO_3 solution. X-ray diffraction (XRD) analysis was performed on a Siemens D-500 diffractometer. The magnetic measurements were performed with a Manics DSM8 pendulum-type magnetometer at room temperature.

The roughness (rms) of the deposits was measured using a white-light interferometer from Zygo Corporation. For deposit thickness below 6 μm, atomic force microscopy (AFM) analysis of the step height and the surface profile was carried out. For this purpose, an AFM Nanoscope III-A instrument was used in tapping mode. White-light interferometry was also used for step height analysis and surface profiling, especially for deposit thickness over 6 μm. In this case, samples were covered with Au using a high-vacuum system to minimise the great difference in reflectivity between the deposit and the substrate before measurement.

3. Results

3.1. Preparation and properties of cobalt–molybdenum coatings on flat silicon-based substrates

The voltammetric response of a $C_6H_5Na_3O_7$ 0.2 mol dm^{-3} + $CoSO_4$ 0.3 mol dm^{-3} + Na_2MoO_4 0.012 mol dm^{-3} solution at pH = 4.0 was recorded on silicon-based substrate (Fig. 1). The metallic seed-layer favoured the start of the deposition respect to vitreous carbon electrode [14]. Deposit oxidation appeared as a single peak as seen on vitreous carbon. However, oxidation took place slightly earlier on silicon-based substrate and a lower Q_{ox}/Q_{red} was observed. According to these results, Co–Mo deposition seemed to be feasible on a silicon-based substrate. In order to corroborate

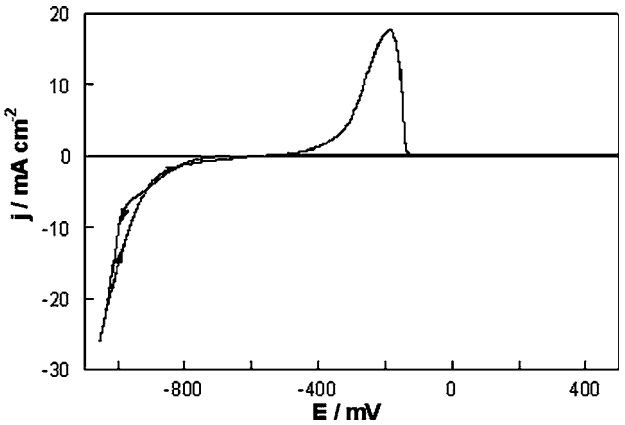

Fig. 1. Cyclic voltammogram of the working solution on Si/SiO_2/Ti(1000 Å)/Ni(500 Å) electrode, 50 mV s^{-1}, $E_i = -400$ mV and $E_c = -1050$ mV.

alloy formation and to establish its morphology and composition, various coatings were prepared either potentiostatically or galvanostatically. Under stirring conditions, the same electrochemical parameters were obtained irrespective of the technique used: when a current density j_1 was applied, the stationary potential value was E_1; analogously, when a potential value E_1 was applied, the stationary current density was j_1.

Moderate deposition potentials or current densities were selected because low deposition potentials favour only the formation of molybdenum oxides [15], whereas very negative deposition potentials induce hydrogen evolution.

EDS analysis confirmed that coatings were composed of cobalt and molybdenum. The deposits showed a fluffy appearance as already seen on graphite and copper substrates [14] (Fig. 2(a)). Next, the potential/current density was optimised to obtain Co–Mo deposits with a molybdenum percentage around 10% on seed layer/silicon substrate (Fig. 2(b)). In these conditions, the chemical analysis of the deposits showed that relatively high current efficiencies (~70%) were obtained.

White-light interferometry was useful to demonstrate that deposits of an appreciable thickness were formed on the seed layer/silicon substrate (Fig. 3(a) and (b)).

Fig. 4(a) shows the diffractogram of cobalt–molybdenum (~10%) deposits over silicon seed-layer substrate. For better analysis of the samples, the Co–Mo films were detached from the electrode and mounted on a silicon substrate in order to avoid the diffraction peaks of Ni and Ti seed-layers. In these conditions, only the peaks corresponding to the deposited film were observed, next to a small peak centred around 69°2θ and attributed to silicon. Coating peaks corresponded to crystalline deposits of a hexagonal close-packed structure (hcp) with hk0 main peaks. Therefore, deposits showed a crystallographic direction parallel to the substrate. The position of the diffraction peaks was shifted to lower °2θ values respect to those of pure cobalt (Fig. 4(b)), as corresponds to molybdenum presence in the deposits.

The coercivity exhibited by Co–Mo coatings with around 10% of molybdenum was 70 Oe (Fig. 5), while pure-cobalt coatings obtained from a sulphate–citrate bath at the same current range conditions showed a coercivity of 140 Oe [14]. Moreover, the saturation magnetisation was close to that of the pure-cobalt deposits, since a decrease of 15% was observed.

In order to study the roughness variation, the thickness and the quality of the coatings, a set of Co–Mo

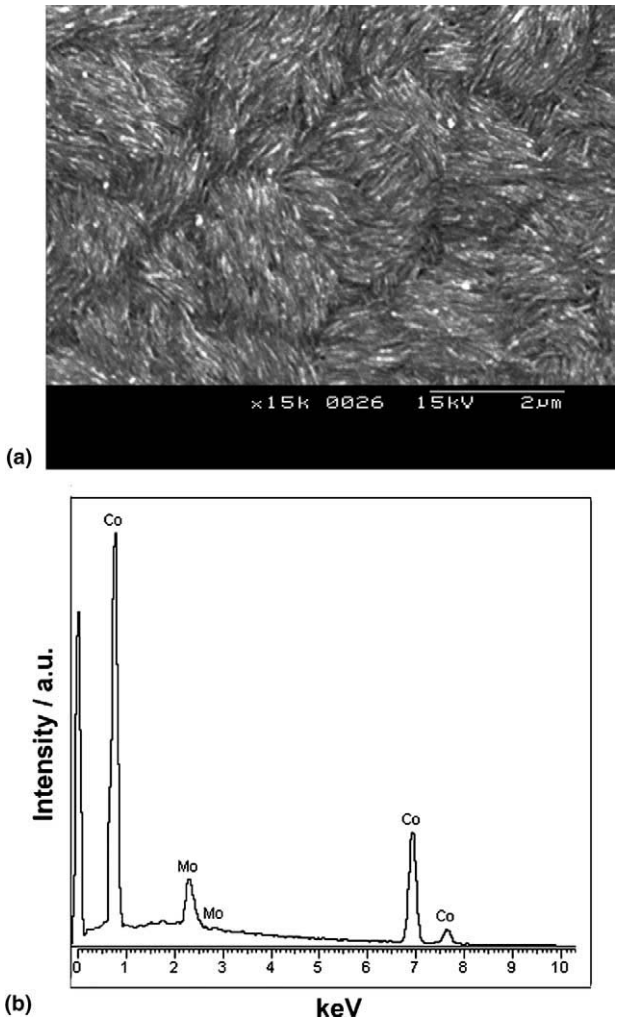

Fig. 2. (a) SEM image and (b) EDS analysis of a deposit obtained potentiostatically at $E = -920$ mV during 2500 s. 9% Mo. (Quantification using L lines of cobalt and molybdenum.)

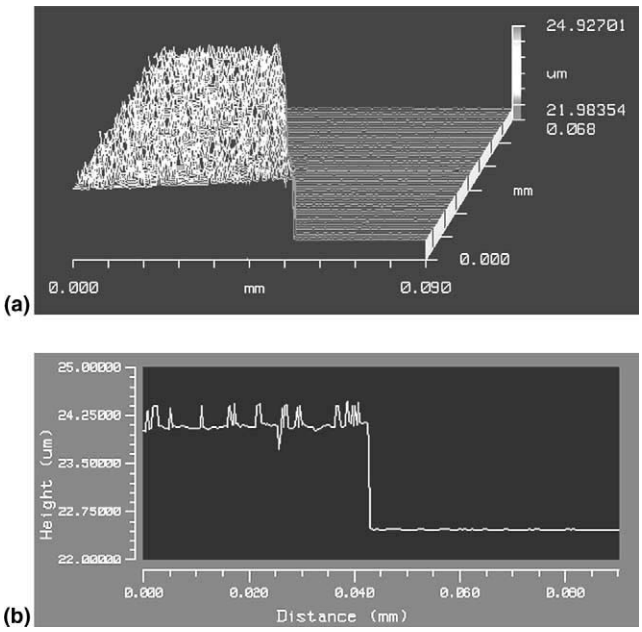

Fig. 3. (a) 3D surface profile and (b) step height profile, both obtained by interferometry, of a Co–Mo deposit obtained potentiostatically at $E = -920$ mV for 700 s.

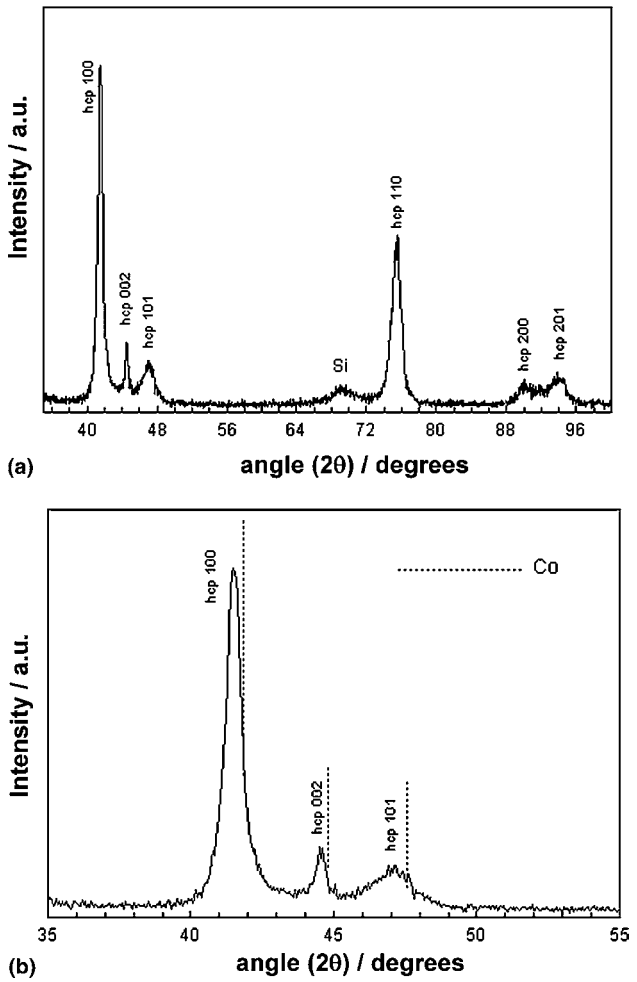

Fig. 4. (a) X-ray diffractogram of a Co–Mo deposit containing 10% molybdenum obtained at $E = -920$ mV during 3000 s. (b) Magnified detail in the range 35–55°2θ.

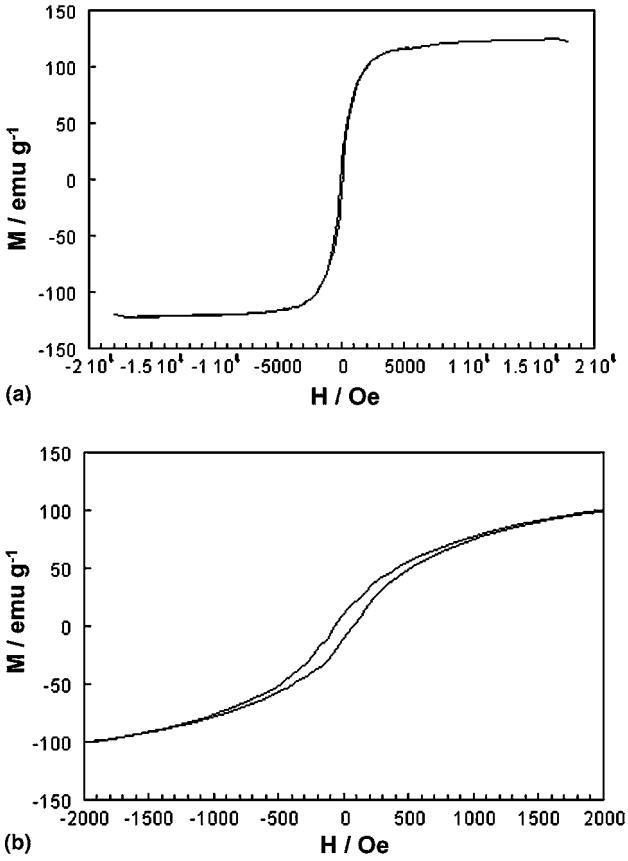

Fig. 5. (a) Magnetisation versus magnetic field. (b) Magnified detail of a Co–Mo deposit with 10% molybdenum.

samples was prepared by applying a fixed potential but different deposition times. These deposits were coherent and crack-free. The roughness of the samples was low at short deposition times, near to the value for the substrate (rms$\sim$8 nm), and it increased with the deposition time, achieving a quasi-stationary value (Table 1).

To estimate the growth rate of the Co–Mo alloy in the conditions chosen, the deposit thickness at different deposition times was measured using white-light interferometry or AFM. The step height between the substrate and the deposit was determined for each coating. Similar results were obtained by the two techniques. The growth rate of the Co–Mo alloy was around 7.7 μm h^{-1}.

3.2. Preparation and properties of cobalt–molybdenum deposits on photolithographed silicon-based substrates

The selectivity of deposition was tested using photolithographed silicon-based substrates. Different heights of the UV photoresist (2, 8 and 20 μm) patterned on silicon-based substrates were used. After the electrodeposition step, the photoresist was removed by acetone.

Deposition was highly selective as shown by surface profiles obtained from white-light interferometry and AFM. Co–Mo alloy filled the conductor zones in such a way that the shape of the test patterns were retained (Fig. 6).

The growth rate of cobalt–molybdenum on masks was also estimated from the thickness of various samples obtained at a fixed potential but at different deposition times. Co–Mo growth rate on mask devices was similar to the value observed on flat silicon-based substrates (Fig. 7).

Table 1
Rms average of Co–Mo coatings obtained potentiostatically ($E = -920$ mV) at different deposition times

t/s	rms/nm
0	8
30	21
100	11
250	14
415	37
700	66
830	53
1040	60

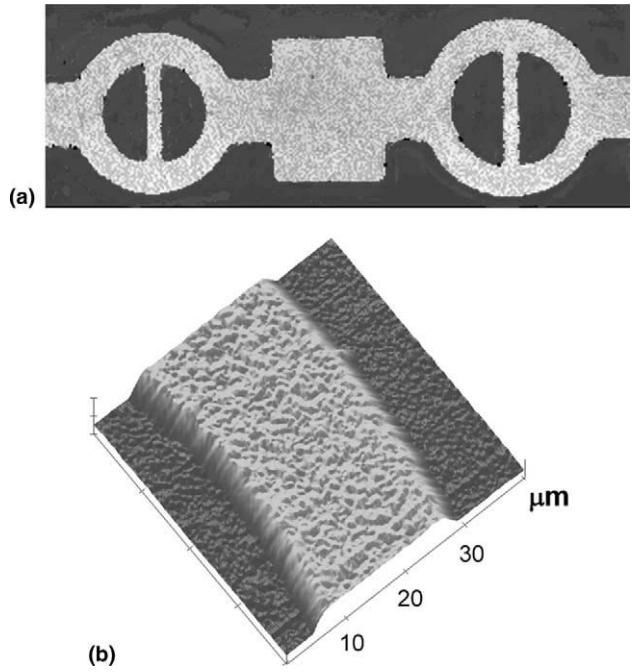

Fig. 6. (a) 2D surface profile and (b) 3D AFM image of a magnified detail of a Co–Mo microstructure prepared at $E = -920$ mV for 1000 s. Measured thickness = 2 μm.

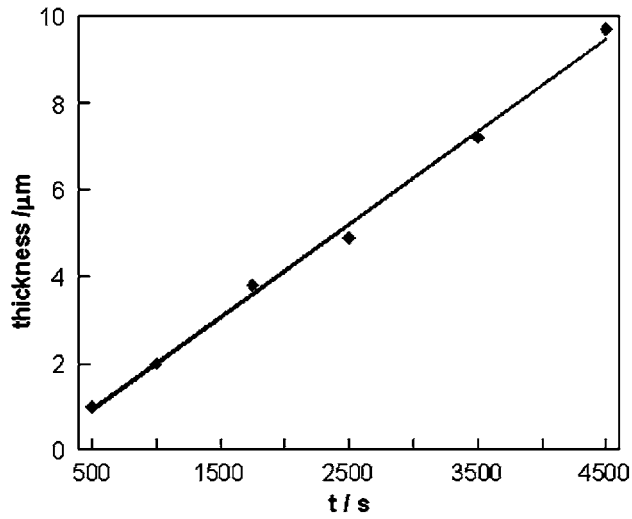

Fig. 7. Dependence of the thickness of the Co–Mo microstructures on deposition time Mask of 20 μm photoresist. Applied potential: −920 mV.

Patterns with different spacing-to-opening ratios were tested (Fig. 8(a)), revealing that the vertical profile of the test patterns were always retained, although the growth of the Co–Mo alloy was hindered when the cavities were narrow. In this case, surface profiles revealed an irregular filling of the structures (Fig. 8(b) and (c)).

Thick Co–Mo deposits (>7 μm) showed incipient cracks and slight detachment from the substrate. Although deposit detachment was attributed to the stress,

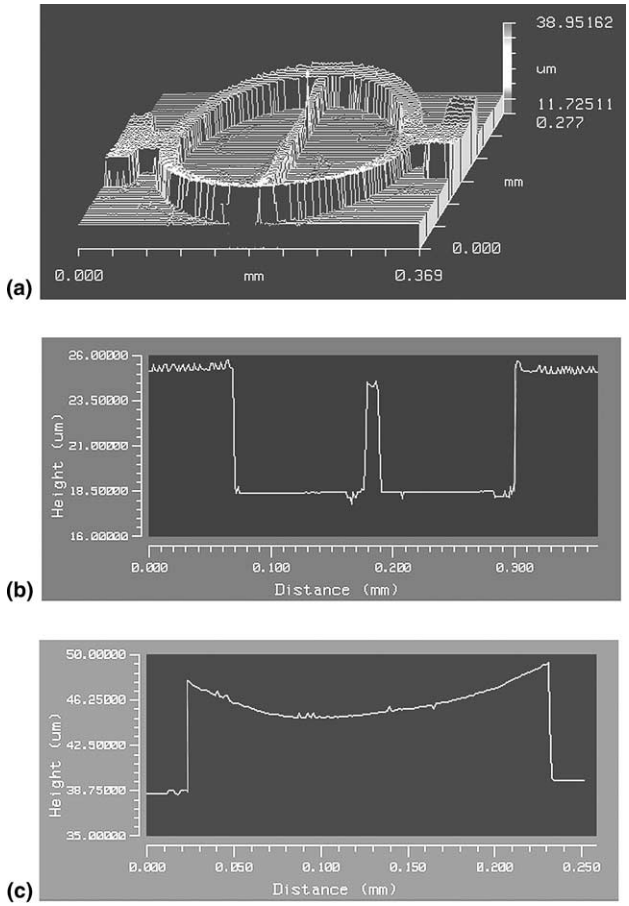

Fig. 8. (a) 3D profile, (b) step height from left to right and (c) step height from top to bottom obtained by interferometry of a Co–Mo sample prepared at $E = -920$ mV for 3500 s. Measured thickness = 7 μm.

it was favoured by the exposure to a high vacuum system when samples were covered by an Au film.

3.3. Effect of temperature and saccharine on the final quality of cobalt–molybdenum deposits

In order to minimise the stress observed for Co–Mo deposits obtained at high deposition times, the effect of introducing 1 $g\,l^{-1}$ saccharine to the bath and increasing the temperature were tested. It is known that saccharine has an antistress effect.

At each temperature a potential range was selected to prepare Co–Mo samples under a comparable current density to that used for coatings prepared from the bath at 25 °C and saccharine-free. High deposition times were chosen to obtain thick deposits. EDS analysis revealed that Mo content in the coatings hardly varied (7–10%) in the temperature range studied (25–40 °C). As expected the hysteresis magnetic curve did not change, since the molybdenum percentage was constant in the temperature range studied.

Co–Mo coatings prepared at up to 33 °C showed comparable thickness to coatings obtained at 25 °C and

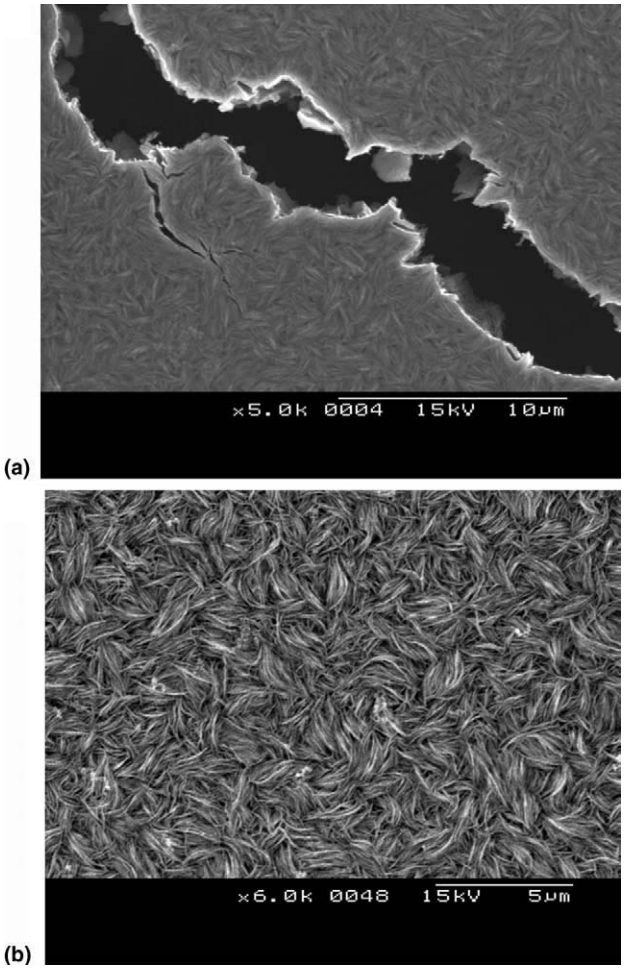

Fig. 9. SEM images of a Co–Mo layer obtained potentiostatically from the working solution on flat silicon-based substrate at (a) 25 °C, $E = -920$ mV, $t = 6000$ s, 12.7 μm and (b) 30 °C, 1 $g\,l^{-1}$saccharine, $E = -905$ mV, 6000 s, 12.3 μm.

saccharine-free. SEM images revealed that the new deposits did not show cracks (Fig. 9). With further increase of the temperature the appearance of the deposits was worse. In this case, surface profiling revealed hydrogen pitting, especially at 40 °C. Moreover, the thickness was lower than expected.

In order to understand why the current efficiency decreased when the bath was maintained at around 40 °C, cathodic polarization curves were recorded scanning at 1 $mV\,s^{-1}$ in a blank solution. The response to hydrogen evolution was compared when using the flat silicon-based substrate and a Co–Mo deposit previously deposited over the silicon as working electrodes. While the cathodic current corresponding to hydrogen formation was always low for the substrate, it increased with temperature when a ''Co–Mo electrode'' was used. Fig. 10 shows that, for the ''Co–Mo electrode'', the current attributed to hydrogen formation increased considerably when the bath temperature rose from 35 to 40 °C. Moreover, the polarisation curve corresponding to 40 °C showed fluctuations due to strong hydrogen evolution. Studies on

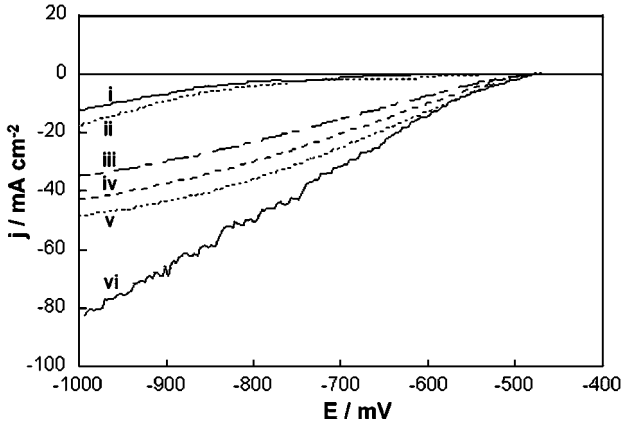

Fig. 10. Cathodic polarisation curves obtained from a 0.2 $mol\,dm^{-3}$ $C_6H_5Na_3O_7$ + 0.3 $mol\,dm^{-3}$ Na_2SO_4 solution at pH = 4.0 over flat silicon-based substrate at (i) 25 °C, (ii) 40 °C and over Co–Mo deposit at (iii) 25 °C, (iv) 30 °C, (v) 35 °C, (vi) 40 °C. The Co–Mo deposit was prepared at $E = -920$ mV for 3600 s at 25 °C.

similar systems such as Ni–Mo point out that the incorporation of non-metallic elements (particularly H) is considerable when electrodeposition takes place from a sulphate–citrate bath at $T \geqslant 40$ °C [16].

4. Discussion and conclusions

Sulphate–citrate solutions containing cobalt (II) and molybdate favour the induced Co–Mo electrodeposition, also over $Si/SiO_2/Ti$(1000 Å)/Ni(500 Å) substrates. The preparation of homogeneous Co–Mo alloys with low molybdate percentage (~10% molybdenum) is possible with a high $[Co(II)]/[MoO_4^{2-}]$ ratio, pH around 4 and some non-complexed cobalt (II) in solution. Deposits prepared in these conditions showed soft-magnetic response and high saturation magnetisation.

Voltammetric experiments showed that the reduction process was advanced on silicon-based substrate respect to vitreous carbon and the deposit oxidised at a slightly more negative potential. A major incorporation of hydrogen in the film formed on seed-layer during a single voltammetric scan could explain why it oxidizes earlier, since nickel catalyses hydrogen evolution. This also explains why the Q_{ox}/Q_{red} ratio is slightly lower on silicon-based substrate than on vitreous carbon. Although the voltammetric behaviour on silicon-based substrates showed few differences, the kind of deposit obtained, either potentiostatically or galvanostatically, was similar as on graphite or copper substrates [14]. Fluffy deposits with smooth surfaces ($\sim 11 \leqslant$ rms $\leqslant \sim 60$) were obtained with a constant deposition rate on silicon-based substrates and over those which were previously photolithographed.

High selectivity was obtained in all the samples, irrespective of the photoresist used. The aspect ratio was reasonably good for both thin and thick masks. How-

ever, the latter were irregularly filled when the spacing-to-opening ratio was high, probably because the current distribution was not uniform [17].

For deposit thickness up to ~7 μm, the plated coatings were crack-free and showed good adherence. The aspect of thicker Co–Mo coatings was improved by increasing the deposition temperature and by adding saccharine to the bath. However, since hydrogen evolution was enhanced with the plating temperature, a slight increase in temperature is recommended. When the formation of hydrogen was important, as occurred at 40 °C, the efficiency of Co–Mo deposition decreased and deposits showed hydrogen pitting.

Acknowledgements

The authors thank the Serveis Cientificotècnics (Universitat de Barcelona) and the Servei the Magnetoquímica (Universitat de Barcelona) for the use of their equipment. The authors also thank the CNM for the silicon-based substrates supply. This paper was supported financially by contract MAT 2003-09483-C02-01 from the *Comisión Interministerial de Ciencia y Tecnología (CICYT)* and by the *Comissionat* of the *Generalitat de Catalunya* under Research Project 2001 SGR 00046. E. Pellicer also thanks the DURSI of the *Generalitat de Catalunya* for financial support.

References

[1] T. Osaka, Electrochim. Acta 45 (2000) 3311.
[2] I. Tabakovic, S. Riemer, V. Inturi, P. Jallen, A. Thayer, J. Electrochem. Soc. 147 (2000) 219.
[3] Y.K. Kim, H.Y. Son, Y.S. Choi, K.S. Moon, K.H. Sunwoo, J. Appl. Phys. 87 (2000) 5413.
[4] H.-S. Nam, T. Yokoshima, T. Nakanishi, T. Osaka, Y. Yamazaki, D.N. Lee, Thin Solid Films 384 (2001) 288.
[5] I. Tabakovic, V. Inturi, S. Riemer, J. Electrochem. Soc. 149 (2002) C18.
[6] M. Ruan, J. Shen, C.B. Wheeler, in: Proceedings of MEMS '01, Interlaken, Switzerland, 2001.
[7] M. Duch, J. Esteve, E. Gómez, R. Pérez-Castillejos, E. Vallés, J. Electrochem. Soc. 149 (2002) C201.
[8] M. Duch, J. Esteve, E. Gómez, R. Pérez-Castillejos, E. Vallés, J. Micromech. Microeng. 12 (2002) 400.
[9] N. Fenineche, O. El Kedim, C. Coddet, Surf. Coat. Technol. 48 (1991) 948.
[10] J.S. Judge, J.R. Morrison, D.E. Speliotis, J. Appl. Phys. 36 (1965) 948.
[11] E. Gómez, E. Vallés, J. Appl. Electrochem. 29 (1999) 805.
[12] E. Gómez, E. Pellicer, X. Alcobé, E. Vallés, J. Sol. Stat. 8 (2004) 497.
[13] E. Gómez, E. Pellicer, E. Vallés, J. Electroanal. Chem. 556 (2003) 137.
[14] E. Gómez, E. Pellicer, E. Vallés, J. Electroanal. Chem. 568 (2004) 29.
[15] E. Gómez, E. Pellicer, E. Vallés, J. Appl. Electrochem. 33 (2003) 245.
[16] E. Chassaing, K. Vu Quang, M.E. Baumgärtner, M.J. Funk, Ch.J. Raub, Surf. Coat. Technol. 53 (1992) 257.
[17] R.V. Shenoy, M. Datta, L.T. Romankiv, J. Electrochem. Soc. 143 (1996) 2305.

Developing plating baths for the production of cobalt-molybdenum films

Available online at www.sciencedirect.com
SCIENCE DIRECT
Surface & Coatings Technology 197 (2005) 238–246
SURFACE & COATINGS TECHNOLOGY
www.elsevier.com/locate/surfcoat

Developing plating baths for the production of cobalt–molybdenum films

Elvira Gómez*, Eva Pellicer, Elisa Vallés

Electrodep, Departament de Química Física, Universitat de Barcelona, Martí i Franquès 1, E-08028 Barcelona, Spain

Received 26 March 2004; accepted in revised form 24 September 2004
Available online 26 November 2004

Abstract

A set of plating baths for obtaining soft-magnetic cobalt–molybdenum (Co–Mo) films with 5–11 wt.% Mo was tested. Free Co^{2+} concentration in solution seemed to determine the quality of the electrodeposited films. Coherent, compact Co–Mo films were obtained under a current efficiency up to ~70% in baths with ~40% free Co^{2+}. By contrast, low concentrations of free Co^{2+} reduced current efficiency in the preparation of the deposits, while excess concentrations of free Co^{2+} resulted in cracked films. Backscattered electron images demonstrated that good-quality Co–Mo films grew layer by layer. Such growth was linked to both structural and magnetic properties. The coatings presented a crystallographic direction parallel to the substrate. Moreover, a high uniaxial anisotropy constant and an angle of the resulting anisotropy of 62° were determined by magnetic measurements. The selectivity of deposition was verified on photolithographed silicon-based substrates.

Keywords: Cobalt–molybdenum alloy; Electrodeposition; White-light interferometry; AFM

1. Introduction

The preparation of cobalt alloys by electrodeposition has been gaining importance in recent years due to their magnetic properties [1–11]. In this regard, the introduction of molybdenum to the cobalt coating results in a material that presents good soft-magnetic properties [12]. The codeposition of molybdenum is not easily achieved because molybdenum is only completely reduced in aqueous solution when an inductor metal is present in the plating bath. However, when this condition is satisfied, molybdenum incorporation in the deposits is considerable. We have previously demonstrated that the molybdenum content must be restrained in order to achieve maximum saturation magnetisation and minimum coercivity [13]. A very low molybdate concentration in solution is sufficient to obtain deposits with 5–11 wt.% Mo, considered the most appropriate quantity for use in microelectronic devices [13].

Here, several baths for producing Co–Mo films with low molybdenum percentages were tested. Citrate–Co(II)–molybdate baths, adjusted to a pH<5, were used because acidic media have been found to minimise molybdenum incorporation into the cobalt films [14]. The deposit quality obtained from each bath was evaluated. Various substrates (vitreous carbon, copper, graphite, and flat silicon-based substrates) were used as cathodes. Furthermore, the selectivity of deposition was tested using photolithographed silicon-based substrates given that the main application of the plated films lies in the microelectromechanical systems (MEMS).

2. Experimental

Deposit preparation was performed in a conventional three-electrode cell using a microcomputer-controlled potentiostat/galvanostat Autolab with PGSTAT30 equipment and GPES software. The chemicals used were $C_6H_5Na_3O_7 \cdot 2H_2O$, $CoSO_4 \cdot 7H_2O$, $Na_2MoO_4 \cdot 2H_2O$, and saccharine. All reagents were of analytical grade. All solutions were freshly prepared with water which had first been doubly distilled and then treated with a Millipore Milli Q system. Before the experiments, solutions were deaerated with argon and maintained under argon atmosphere while the deposits were prepared.

* Corresponding author. Tel.: +34 93 402 12 34; fax: +34 402 12 31.
E-mail address: e.gomez@ub.edu (E. Gómez).

0257-8972/$ - see front matter © 2004 Elsevier B.V. All rights reserved.
doi:10.1016/j.surfcoat.2004.09.017

Table 1
Bath composition, plating conditions, and kind of deposit obtained

No.	Bath	[Co(II)]/[citrate] analytical	pH	T (°C)	−E range (mV)	%Mo	Deposit quality
I	$C_6H_5Na_3O_7$ 0.2 M+$CoSO_4$ 0.1 M+Na_2MoO_4 0.005 M	0.5	4.0	25	970–1180	10−5	Coherent films
II	$C_6H_5Na_3O_7$ 0.2 M+$CoCl_2$ 0.1 M+Na_2MoO_4 0.005 M	0.5	4.0	25	880–940	8−7	Very smooth films
III	$C_6H_5Na_3O_7$ 0.2 M+$CoSO_4$ 0.3 M+Na_2MoO_4 0.012 M	1.5	4.0	25	880–1015	11−5	Coherent films
IVa	$C_6H_5Na_3O_7$ 0.2 M+$CoSO_4$ 0.3 M+Na_2MoO_4 0.012 M+1 g/l saccharin	1.5	4.0	30	865–1000	10−7	Coherent films
IVb	$C_6H_5Na_3O_7$ 0.2 M+$CoSO_4$ 0.3 M+Na_2MoO_4 0.012 M+1 g/l saccharin	1.5	4.0	40	840–870	10−8	Coherent films
V	$C_6H_5Na_3O_7$ 0.2 M+$CoSO_4$ 0.5 M+Na_2MoO_4 0.005 M	2.5	4.9	25	850–855	13−10	Cracked films
VI	$C_6H_5Na_3O_7$ 0.2 M+$CoSO_4$ 0.5 M+Na_2MoO_4 0.005 M	2.5	4.0	25	825–845	6−4	Cracked films

Vitreous carbon (Metrohm, 0.0314 cm^2), copper (John Matthey 99.99%, 0.0314 cm^2), graphite (Alfa Aesar, 0.352 cm^2), and modified p-type 4–40 Ω cm ⟨100⟩ silicon samples were used as working electrodes. The vitreous carbon electrode was polished to a mirror finish before each experiment using alumina of different grades (3.75 and 1.85 μm), and then cleaned ultrasonically for 2 min in water. Graphite electrodes were polished using sandpaper (2400 and 4000), followed by damp alumina of 0.3 μm and then cleaned ultrasonically in water. The reference electrode was an Ag/AgCl/1 mol dm^{-3} NaCl electrode mounted in a Luggin capillary containing 0.5 mol dm^{-3} Na_2SO_4 solution. All potentials refer to this electrode. The counter electrode was a platinum spiral.

The silicon surfaces were prepared for better adhesion and minimum mechanical stress by IMB-CNM.CSIC (Centre Nacional de Microelectrònica). A Ti(1000 Å)/Ni(500 Å) seed layer was sputtered on a previously grown, 1-μm-thick phosphosilicate glass (PSG) layer. This seed layer supplied an electrical connection for the electrodeposition process. The flat silicon-based substrates were cleaned with ethanol and then rinsed in water before each experiment. Either flat silicon-based substrates or patterned silicon-based substrates were used to prepare Co–Mo deposits. The photolithographic process was also performed using IMB-CNM technology.

For preparing the deposits, the solution was gently stirred (ω=60 rpm) to avoid the depletion of the minority species (molybdate) to the electrode during the experiments and to maintain homogeneous deposit composition.

Deposit morphology was examined by scanning electron microscopy (SEM) and deposit composition was determined by energy-dispersive X-ray spectroscopy (EDS). The efficiency of deposit preparation was estimated by comparing the deposited charge and the ICP-MS analysis of the samples obtained after chemical dissolution of the films. X-ray diffraction (XRD) analysis was performed on a Philips MRD diffractometer.

The magnetic measurements were performed with two different equipment sets: a Manics DSM8 pendulum-type magnetometer and a SQUID magnetometer. Measurements were performed at room temperature in all cases to test the magnetic properties of the films in these conditions.

The roughness (rms) of the deposits was measured using a white-light interferometer (Zygo). For deposit thickness below 6 μm, atomic force microscopy (AFM) analysis of the step height and the surface profile was carried out. For this

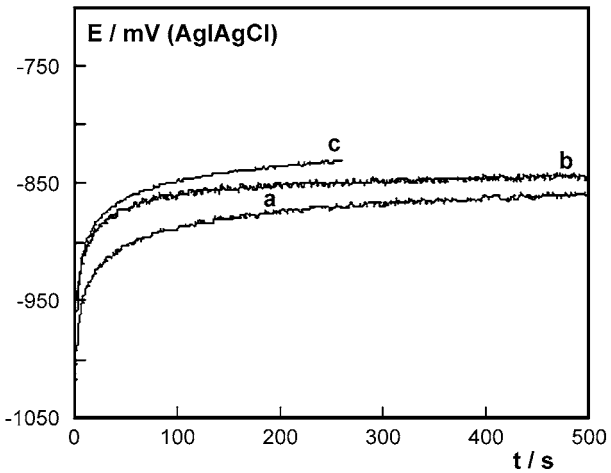

Fig. 1. Galvanostatic curves obtained from (a) bath II, (b) bath V, and (c) bath VI over the vitreous carbon electrode at −3.18 mA cm^{-2}. ω=60 rpm.

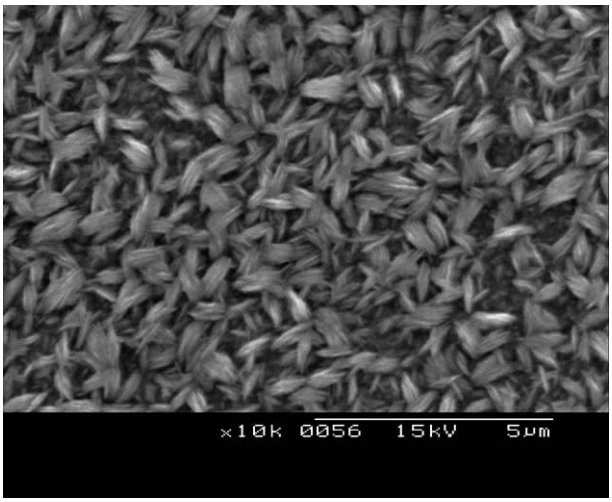

Fig. 2. SEM image of a Co–Mo deposit obtained galvanostatically from bath V at −4.8 mA cm^{-2} during 400 s. ω=60 rpm.

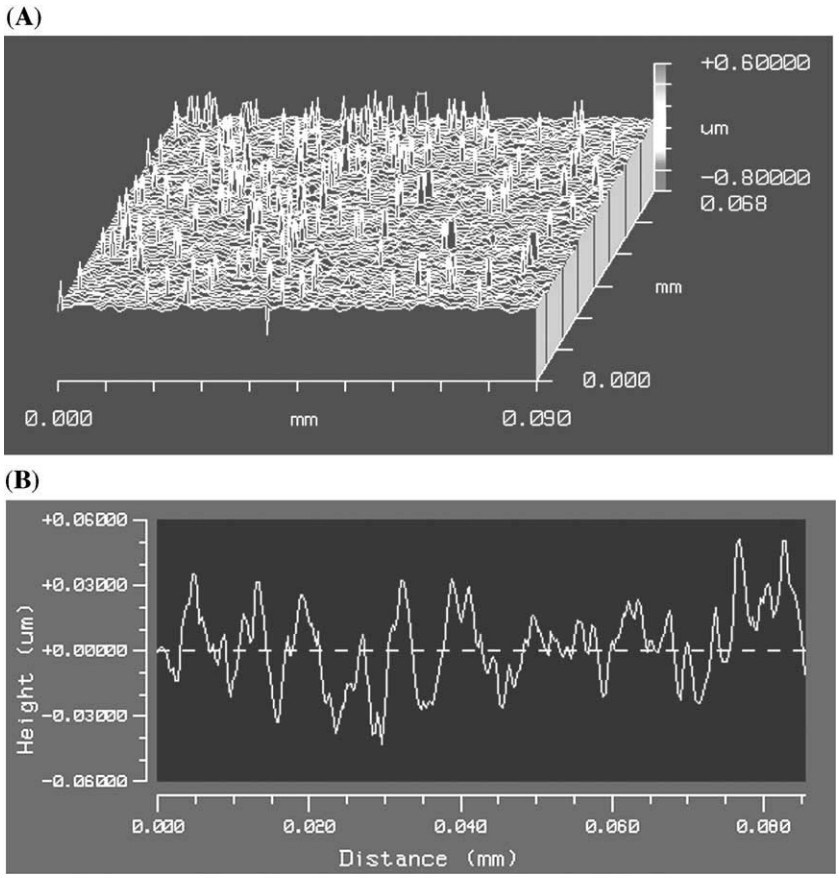

Fig. 3. (A) 3-D surface profile and (B) roughness profile obtained by white-light interferometry of a Co–Mo deposit obtained potentiostatically from bath IVa. E=−905 mV, t=4000 s, 10 wt.% Mo. rms average=43 nm.

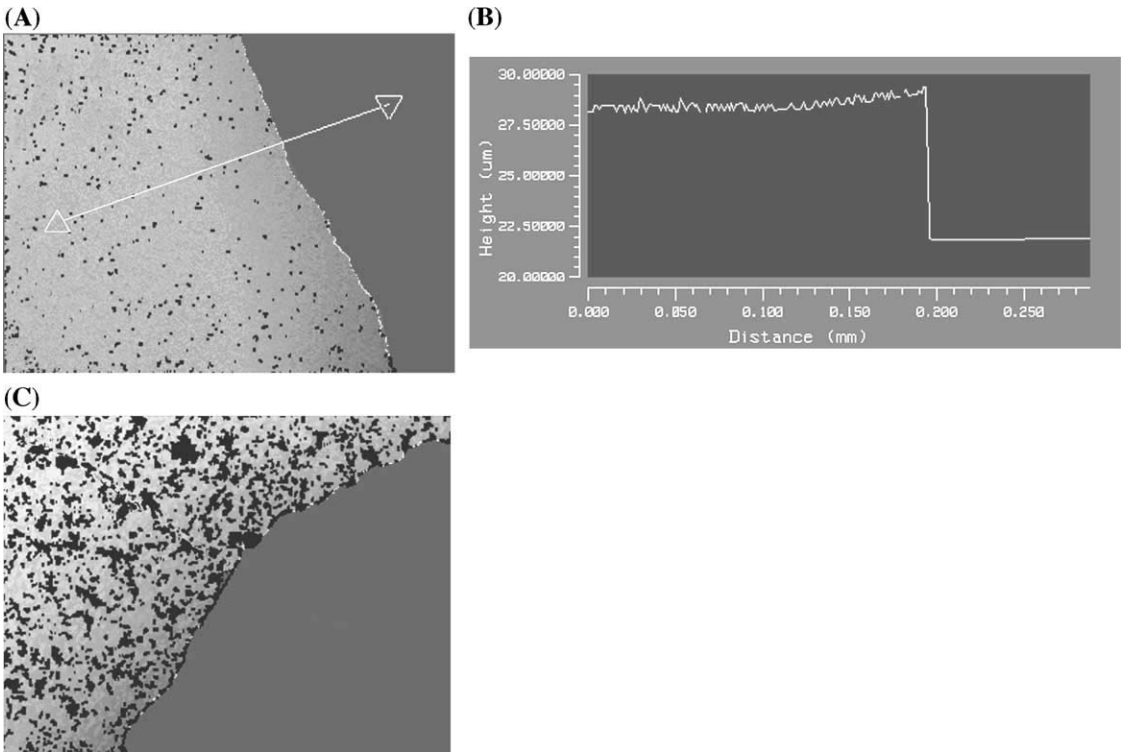

Fig. 4. (A) 2-D surface profile and (B) step height measurement of a Co–Mo deposit obtained from bath IVa at −905 mV during 6000 s and (C) 2-D surface profile of a Co–Mo deposit obtained from bath IVb at −870 mV during 6000 s. Deposit thickness: ~6.5 μm in both cases.

purpose, an AFM Nanoscope III-A instrument was used in tapping mode. Prior preparation of the samples was not required. White-light interferometry was also used for step height analysis and surface profiling, especially for deposit thicknesses over 6 μm. However, in such cases, samples were covered with Au using a high-vacuum system to minimise the great difference in reflectivity between the deposit and the substrate before measurement.

3. Results

3.1. Plating bath design

Several baths used in producing Co–Mo films with low molybdenum percentages (around 4–13 wt.% Mo) were developed (Table 1). The concentration of electroactive species, the pH, and the temperature were varied in order to regulate the molybdenum content in the deposits. Vitreous carbon, copper, graphite, and flat silicon-based substrates were used to prepare Co–Mo coatings either potentiostatically or galvanostatically. For each bath, a potential/current density range was selected in order to achieve the desired molybdenum content. This range was hardly dependent on the substrate nature [13,15]. Although Co–Mo electrodeposition occurs once a threshold potential that is related to the initial formation of molybdenum oxides has been reached [16], the subsequent formation of an alloy layer nullifies any possible substrate effect for long deposition times.

More negative potentials were needed in sulphate that is in chloride media to attain similar molybdenum percentages. Moreover, a reduction in the [Co(II)]/[citrate] ratio in solution meant the use of more negative potentials. Fig. 1 shows the galvanostatic curves obtained from three of the baths over a vitreous carbon electrode. The nucleation spike appeared at more positive potentials and the potential also stabilised at more positive values as the Co(II) concentration in solution increased (curves a and c). For a given solution, a pH increase caused a shift in the stabilised potential towards more negative values (curves b and c).

Copper, graphite, and flat silicon-based substrate electrodes were found to be more suitable for preparing thick Co–Mo coatings, while the film became detached on the vitreous carbon electrode, especially in the cases of baths V and VI.

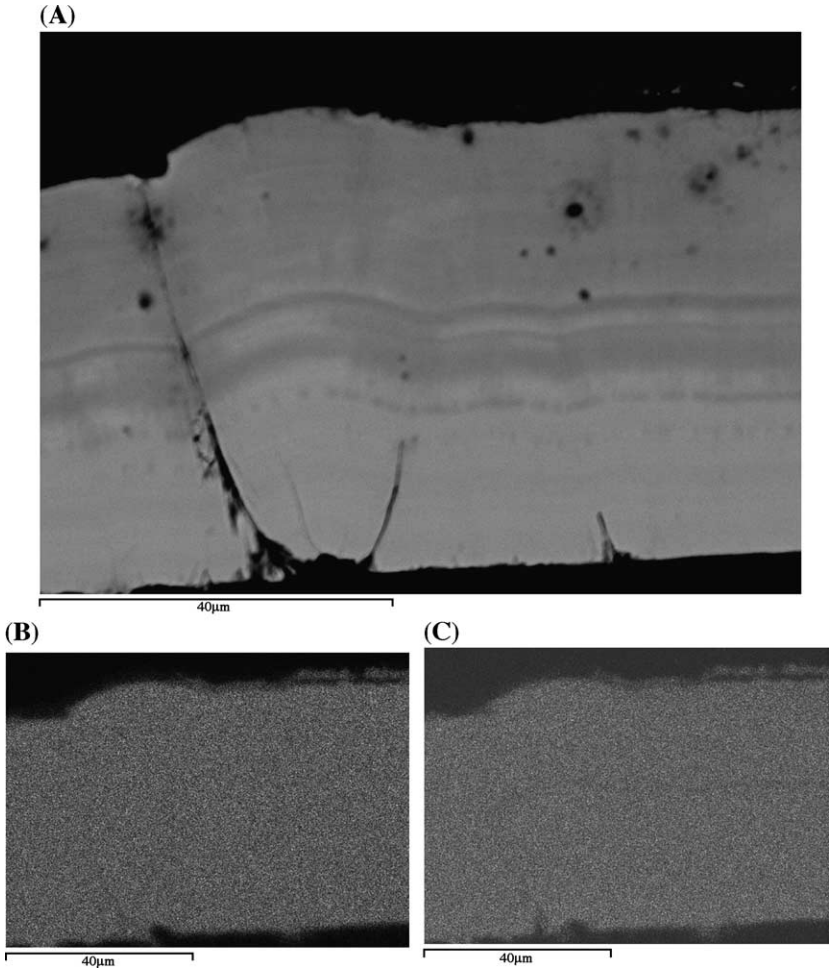

Fig. 5. (A) Backscattered electron image, (B) mapping of cobalt, and (C) mapping of molybdenum of the cross-section of a Co–Mo alloy obtained from bath III at −900 mV over graphite, 11 wt.% Mo. Film thickness=50 μm.

EDS analysis of the coatings allowed us to establish a relationship between the applied potential and the molybdenum percentage in the alloy. In all the baths studied, the molybdenum percentage fell as the potential/current density was made more negative.

From the SEM examination of deposits, it was deduced that the analytical [Co(II)]/[citrate] ratio in solution was highly influential in determining their eventual appearance. A low [Co(II)]/[citrate] ratio (baths I, III, IVa, and IVb) led to compact, coherent films, whereas a high ratio (baths V and VI) led to cracked films. When cobalt chloride (bath II) was used instead of cobalt sulphate, deposit quality was found worse.

The effects of temperature and the simultaneous addition of an additive on a given bath were also examined. A small increase in bath temperature reduced slightly Co–Mo coating stress. Films obtained from bath IVa were crack-free, whereas those obtained from bath III exhibited incipient cracking. However, a further increase in temperature did not improve film appearance because hydrogen pitting was detected (bath IVb).

3.2. Properties of Co–Mo coatings

The morphology of Co–Mo coatings containing 5–11 wt.% Mo showed a fluffy appearance independent from the bath used (Fig. 2). The morphology was also unaffected by deposition time, as coatings that had been prepared over several hours did not present any variation in appearance. However, the morphology was affected by molybdenum content. The fluffy appearance became acicular in deposits with a molybdenum percentage below 5 wt.%. Baths that resulted in cracked (V and VI) or very smooth films (II) were discarded. Previous results have shown molybdenum oxide formation to be the main reduction process at low reduction potentials. This oxide formation blocks alloy deposition and diminishes current efficiency [16]. Thus, bath VI suffers another drawback because the preparation of deposits in the range 6–11 wt.% Mo means the use of potentials close to the threshold value. Therefore, given that the use of more positive potentials will enhance molybdenum oxide formation, bath VI was considered of little practical application.

The current efficiency of coherent deposits was determined. An efficiency of 15–23% was obtained for baths I and IVb, while it ranged between 40 and 70% for baths III and IVa. In all cases, deposition efficiency decreased as the applied potential was more negative.

Coatings with a thickness of 4 μm and more were deposited on flat silicon-based substrates. In these conditions, a roughness between 40 and 60 nm was observed in those deposits prepared in baths I, III, IVa, and IVb (Fig. 3). However, in certain zones of the deposits prepared from baths I and IVb, higher roughness values were recorded, due it would seem to hydrogen pitting. Deposit thicknesses were determined from the step height between the Co–Mo film and the substrate (Fig. 4A and B). Because the increase in temperature favoured hydrogen evolution, the two-dimensional (2-D) surface profiling obtained by white-light interferometry was useful for revealing hydrogen pitting in the deposits (Fig. 4C).

In order to examine the growth of the coherent deposits, SEM images of the deposit cross-sections were taken. For this purpose, deposits were embedded in resin. This was then carefully removed by mechanical polishing until the deposit section was exposed to view. The images of the deposit section obtained from backscattered electrons showed bright and dark bands, arranged alternatively and parallel to the substrate (Fig. 5A). SEM mapping of the deposit section was carried out to discard the possibility that the composition differed from one layer to another. Fig. 5B and C shows the distribution of cobalt and molybdenum, respectively, in the alloy. These mappings failed to show the band structure observed in the backscattered electron image, but rather revealed completely uniform distribution of spots. Thus, the existence of layers could not be attributed to a variation in alloy composition through the deposit thickness.

When the structure of the deposits obtained from baths I–IVb was analysed by X-ray diffraction, the diffractograms

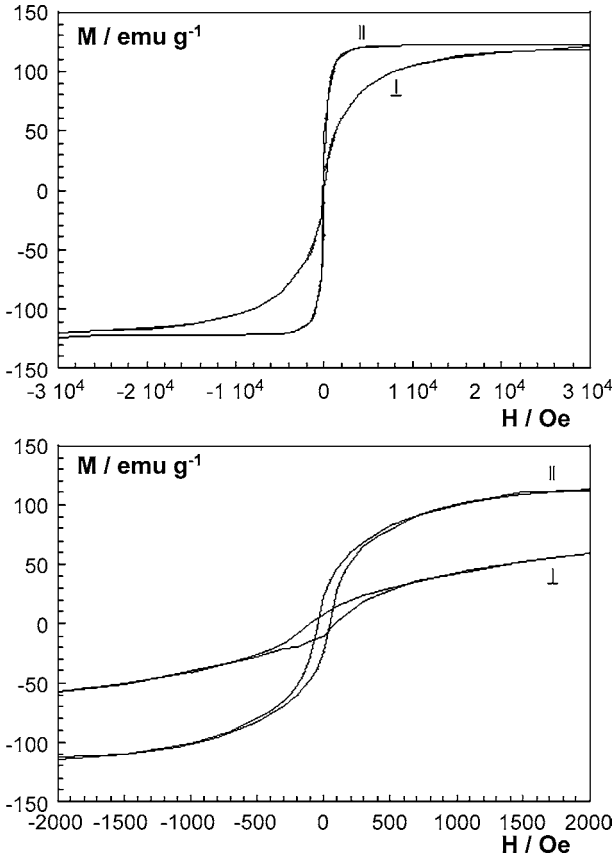

Fig. 6. Parallel and perpendicular hysteresis loops and corresponding zoomed details for a deposit obtained from bath IVa at −905 mV (10 wt.% Mo) on flat silicon-based substrate. Film thickness=30 μm.

revealed that the Co–Mo deposits (5–11 wt.% Mo) were crystalline with a close-packed hexagonal structure (hcp). Moreover, the deposits presented a crystallographic direction that was parallel to the substrate. The (110)+(100) were the preferred orientations. For deposits of similar compositions, no differences were observed as a function of the anion-type, saccharine presence or bath temperature. The position of the diffractogram peaks shifted to low 2θ values in relation to pure cobalt. From the equilibrium-phase diagram of Co–Mo [17], at room temperature, the ϵ-Co phase was able to dissolve substantial amounts of molybdenum. Because the atomic radius of Mo is greater than that of Co, the lattice of the ϵ-Co phase expanded because of the presence of dissolved molybdenum.

The electrodeposited films were separated from the substrate so as to measure their magnetic properties. When the films were introduced into a capsule in the pendulum-type magnetometer and the magnetic field was applied, they immediately oriented themselves in the magnetic field direction. Here, the response was similar to that observed for measurements made with the SQUID when the applied field was parallel to the film (Fig 6). This spontaneous orientation of the film parallel to the magnetic field revealed a strong uniaxial anisotropy, in addition to the usual shape anisotropy expected for these films [18]. From the parallel and perpendicular hysteresis loops obtained with the SQUID, very different values of the saturation fields (H_s) were observed for parallel ($H_{s||}$=7.5 Oe) and perpendicular ($H_{s\perp}$=30 Oe) fields. Thus, an easier magnetization in the parallel-applied field ($H_{s||}$) was observed. A high uniaxial anisotropy constant K can be evaluated [19] from these values leading to a value of 1.3×10^7 emu cm^{-3}. The calculated angle θ of the resulting anisotropy with respect to the film normal was 62°.

Similar magnetic responses were observed for deposits with the same molybdenum percentage, but originating from different baths (I, III, IVa, and IVb). For films of ~10 wt.% Mo, a saturation magnetization (M_s) of about 120 emu g^{-1} was obtained, which was slightly lower than that of pure hcp-deposited cobalt from a sulphate–citrate bath at pH=4

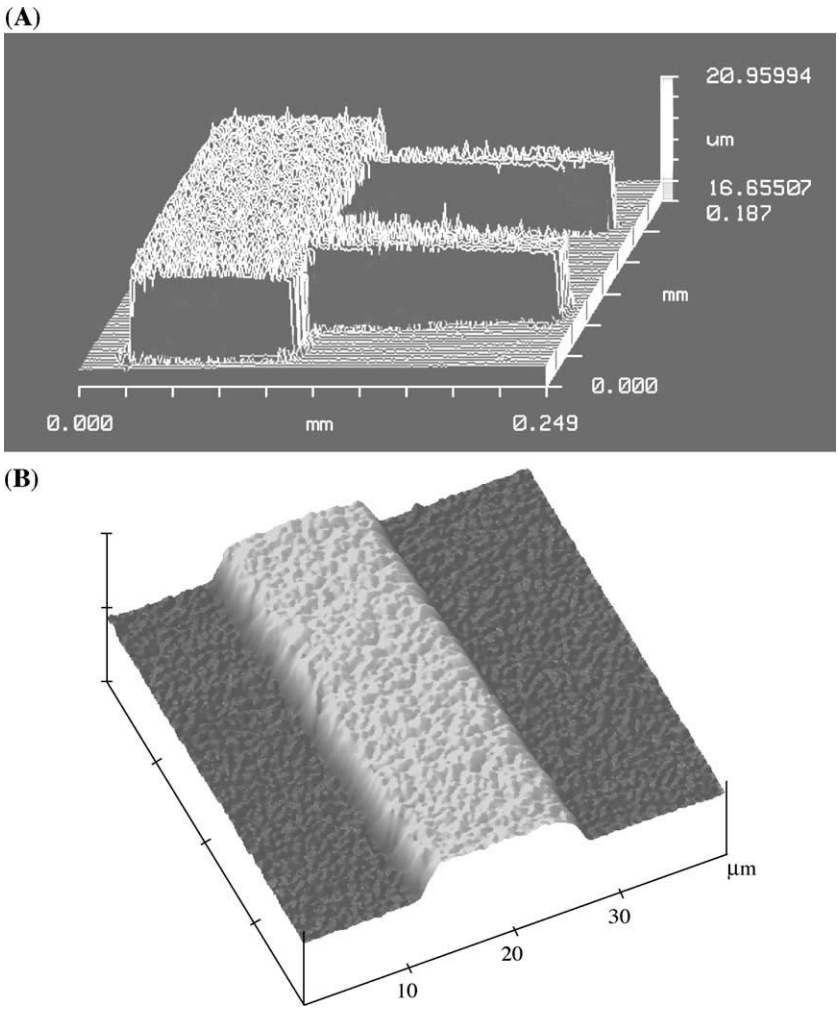

Fig. 7. (A) 3-D surface profile obtained by interferometry and (B) magnified detail obtained by AFM of a Co–Mo microstructure obtained from bath IVa at −905 mV (10 wt.% Mo) after etching a positive UV photoresist. Microstructure thickness=2.9 µm.

(M_s=138 emu g^{-1}). M_s is an intrinsic magnetic property, dependent only on the film composition. Fairly constant coercivities (H_c) were observed. The H_c values for the samples, measured from the hysteresis loops obtained from pendulum-type magnetometer or SQUID using a parallel field, were in the range of 40–70 Oe (~160 Oe for deposited cobalt).

3.3. Selectivity of deposition

After verifying the quality of Co–Mo deposits obtained from baths I, III, IVa, and IVb, the selectivity of deposition on photolithographed silicon-based substrates was tested. For this purpose, UV photoresists from 2 to 20 μm were used in order to obtain plated Co–Mo microstructures of different thicknesses. Furthermore, Co–Mo deposition was examined for either positive or negative photoresist patterned on silicon-based substrates. The photoresist was removed using acetone following electrodeposition. The profiling of the Co–Mo microstructures was determined by white-light interferometry and AFM techniques. Deposition only took place on the conductive areas of the substrate (Fig. 7) and the resulting microstructures presented vertical walls. Deposits of several micrometers were crack-free and no substrate detachment was observed (Fig. 8). However, in order to obtain microstructures of similar thickness, higher deposition charges flowed during film preparation in baths I and IVb. Moreover, for these baths, enhanced hydrogen pitting was observed with increasing microstructure thickness.

4. Discussion and conclusions

Different baths were developed in our laboratory in order to produce to Co–Mo deposits that gave soft-magnetic response. A low molybdate concentration was chosen as what were required were molybdenum percentages around 5–11 wt.%. Coherent Co–Mo deposits that were obtained presented an important, additional magnetic anisotropy owing to the presence of texture in the coatings. The angle value of the resulting anisotropy ($\theta \approx 62^\circ$) revealed that this anisotropy was sufficiently parallel to the film and that it was in accordance with a texture (110)+(100) observed in X-ray measurements.

The quality of Co–Mo deposits was closely connected with the analytical [Co(II)]/[citrate] ratio in solution. A [Co(II)]/[citrate]<1 caused a shift in the onset of deposition towards more negative potentials. This shift meant that the current efficiency involved in deposit preparation was

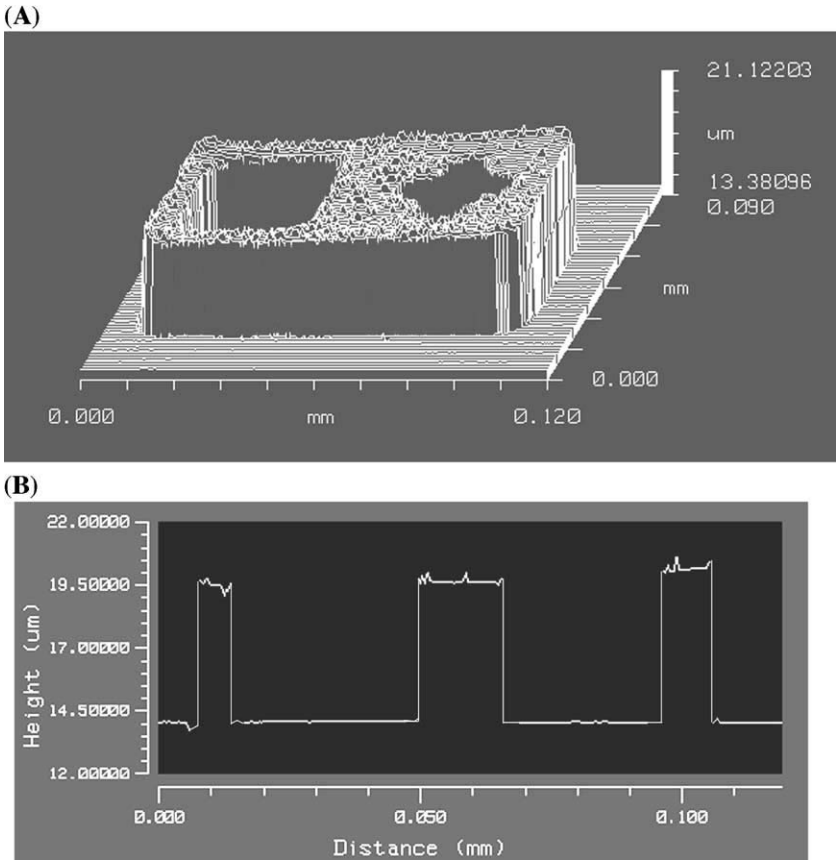

Fig. 8. (A) 3-D surface profile and (B) step height from left to right obtained by interferometry of a Co–Mo microstructure obtained from bath IVa at −915 mV (9 wt.% Mo) after etching a negative UV photoresist. Microstructure thickness=5.6 μm.

lower, given the enhanced nature of hydrogen evolution. By contrast, a [Co(II)]/[citrate]>2 resulted in cracked deposits, a consequence, it would seem, of an excessively high deposition rate.

Taking into account the molar fraction of cobalt(II) species present in each bath, calculated from the corresponding stability constants [20], it would seem that a certain free Co^{2+} content in solution is needed to guarantee the formation of compact Co–Mo deposits under a reasonably high current efficiency. The baths that led to good Co–Mo deposits had 40% free Co^{2+} in solution (Fig. 9A). By contrast, the percentage of free Co^{2+} was around 4% for baths I and II (Fig. 9B) and around 60% for baths V and VI (Fig. 9C). In these conditions, the free Co^{2+} content in solution is excessively low in the first two cases and excessively high in the second two. Furthermore, it also seems that too much free Co^{2+} content is more harmful than too little because the quality of deposits obtained from bath I was acceptable while the quality of those obtained from baths V and VI was not acceptable.

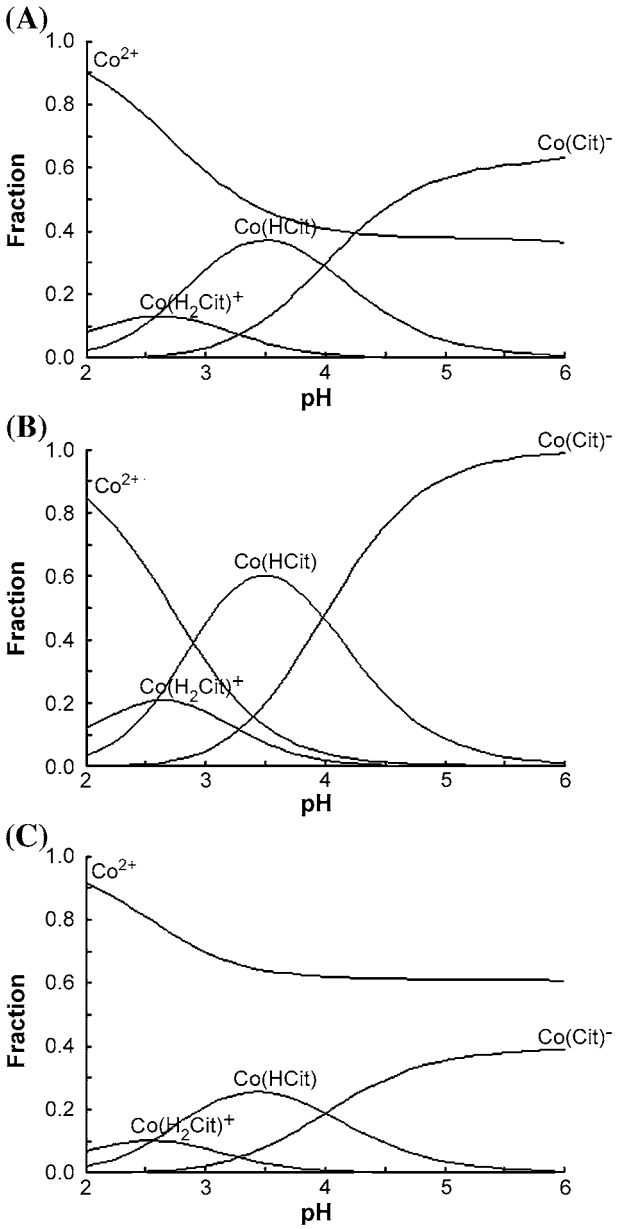

Fig. 9. Diagram of Co(II)–citrate complexes present in solution for (A) 0.3, (B) 0.1, and (C) 0.5 mol dm^{-3} Co(II). [$C_6H_5Na_3O_7$]=0.2 mol dm^{-3}.

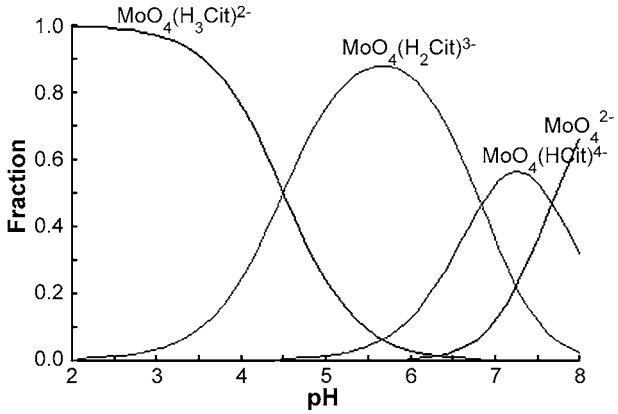

Fig. 10. Diagram of molybdate–citrate complexes present in solution for a 0.2 mol dm^{-3} $C_6H_5Na_3O_7$. Valid for a molybdate concentration between 0.005 and 0.012 mol dm^{-3}.

The mechanism explaining Co–Mo deposition at pH=6.6 has been outlined elsewhere [14]. In acidic media, the formation of molybdate–citrate complexes is favoured respect to pH=6.6 [20] by the presence of citrate species with lower negative charges (Fig. 10). Because the interaction between molybdate and citrate species is necessary for the reduction of molybdate to MoO_2, the intermediate step of molybdenum oxide formation is completed more readily at pH=4.0 than at pH=6.6. This in turn accelerates the subsequent formation of the alloy.

The appearance of coatings obtained from a chloride–citrate bath was worse than that of coatings obtained from a sulphate–citrate bath. This was probably the result of the adsorption of chloride ions on the Co–Mo deposit during electrodeposition [21]. Thus, it seems chloride adsorption blocks alloy growth.

Acknowledgements

The authors wish to thank the Serveis Cientificotècnics (Universitat de Barcelona) and the Servei de Magnetoquímica (Universitat de Barcelona) for the use of their equipment. The authors also thank the CNM for supplying silicon-based substrates. This paper was supported by contract MAT 2003-09483-C02-01 from the Comisión Interministerial de Ciencia y Tecnología (CICYT) and by the Comissionat of the Generalitat de Catalunya under Research Project 2001 SGR 00046. E. Pellicer also thanks the DURSI of the Generalitat de Catalunya for financial support.

References

[1] P.L. Cavallotti, A. Vicenzo, M. Bestetti, S. Franz, Surf. Coat. Technol. 169–170 (2003) 76.
[2] D. Kim, D.-Y. Park, B.-Y. Yoo, P.T.A. Sumodjo, N.V. Myung, Electrochim. Acta 48 (2003) 819.
[3] N.V. Myung, D.Y. Park, M. Schwarz, K. Nobe, H. Yang, C.-K. Yang, J.W. Judy, Proc. Electrochem. Soc. PV2000-29 (2000) 506.
[4] T. Osaka, T. Sawaguchi, F. Mizutani, T. Yokoshima, M. Takai, Y. Okinaka, J. Electrochem. Soc. 146 (1999) 3295.
[5] F.E. Rasmussen, J.T. Ravnkilde, P.T. Tang, O. Hansen, S. Bouwska, Eurosensors XIV, 14th European Conference on Solid State Transducers 2000, Denmark, 2000, p. 915.
[6] T. Osaka, Electrochim. Acta 45 (2000) 3311.
[7] Y.K. Kim, H.Y. Son, Y.S. Choi, K.S. Moon, K.H. Sunwoo, J. Appl. Phys. 87 (2000) 5413.
[8] H.S. Nam, T. Yokoshima, T. Nakanishi, T. Osaka, Y. Yamazaki, D.N. Lee, Thin Solid Films 384 (2001) 288.
[9] I. Tabakovic, V. Inturi, S. Riemer, J. Electrochem. Soc. 149 (2002) C18.
[10] N. Fenineche, O. El Kedim, C. Coddet, Surf. Coat. Technol. 48 (1991) 948.
[11] E. Gómez, E. Vallés, J. Appl. Electrochem. 29 (1999) 805.
[12] W.P. Taylor, M. Schneider, H. Baltes, M.G. Allen, Proceedings of the International Conference on Solid-State Sensors and Actuators, Transducers '97, Chicago, 1997.
[13] E. Gómez, E. Pellicer, E. Vallés, J. Electroanal. Chem. 568 (2004) 29.
[14] E. Gómez, E. Pellicer, E. Vallés, J. Electroanal. Chem. 556 (2003) 137.
[15] E. Gómez, E. Pellicer, X. Alcobé, E. Vallés, J. Sol. Stat. Electrochem. 8 (2004) 497.
[16] E. Gómez, E. Pellicer, E. Vallés, J. Appl. Electrochem. 33 (2003) 245.
[17] M. Hansen, Constitution of Binary Alloys, Mc Graw Hill, New York, 1958.
[18] Nanoscale Materials in Chemistry. In: K.J. Klavunde (Ed.), Wiley Interscience, J. Wiley and Sons, New York, 2001.
[19] J.Q. Xiao, C.L. Chien, A. Gavrin, J. Appl. Phys. 79 (1996) 5309.
[20] Stability constants of metal-ion complexes. Section B: Organic Ligands. Douglas D. Perrin (Ed). IUPAC Chemical Data Series 22, Pergamon Press, Exter, 1983.
[21] E. Gómez, M. Marín, F. Sanz, E. Vallés, J. Electroanal. Chem. 422 (1997) 139.

4.3.3 Resum de resultats

A pH=6.6 és possible obtenir dipòsits Co-Mo de vàries micres de gruix sobre elèctrodes de coure o grafit, els quals afavoreixen una major adherència dels dipòsits que l'elèctrode de carboni vitri. S'ha comprovat que la morfologia i composició d'aquests dipòsits és independent de la tècnica de deposició aplicada i de la naturalesa del substrat. El contingut de molibdè a les capes és força constant i s'obtenen percentatges del 20-25% quan s'apliquen potencials de deposició en l'interval de –930 a –1200 mV. Per contra, la morfologia i l'estructura sí que depenen del potencial/densitat de corrent aplicat. A baixos potencials/densitats de corrent els dipòsits presenten una estructura hexagonal compacta (hcp) amb una orientació preferent (100)+(110) i una morfologia acicular. A potencials/densitats de corrent més negatius els dipòsits exhibeixen una estructura parcialment amorfa. Aquest canvi estructural afecta a la resposta magnètica, de manera que els dipòsits parcialment amorfs presenten valors d'H_c inferiors. A més, les làmines Co-Mo s'orienten més ràpidament sota l'acció d'un camp magnètic paral·lel.

Per tal d'obtenir valors petits d'H_c però alhora una M_s propera a la del Co pur, calen dipòsits amb percentatges de molibdè inferiors. Una disminució del pH del bany afavoreix una menor incorporació de molibdè als dipòsits. Així, a partir del bany 0.2 mol dm^{-3} citrat + 0.1 mol dm^{-3} $CoSO_4$ + 0.005 mol dm^{-3} Na_2MoO_4 a pH=4.0 és possible obtenir dipòsits amb un percentatge de Mo inferior a l'11%. Tanmateix, l'eficiència de corrent que acompanya el procés de deposició és baixa. Triplicant la concentració de Co(II) en solució i augmentant la concentració de molibdat fins a 0.012 mol dm^{-3} és possible obtenir dipòsits amb un contingut de molibdè similar i una eficiència de corrent superior (η=40-70%). S'ha comprovat que una agitació suau a ω=60 rpm és suficient per assegurar una composició constant en tot el perfil del dipòsit. L'augment de l'eficiència de corrent sembla que està relacionat amb la presència d'una certa quantitat

òptima de Co^{2+} lliure en solució (~40%). Làmines Co-Mo amb un gruix ≥50 μm preparades a partir d'ambdós banys presenten una estructura hcp i una orientació preferent (110)+(100). La mínima incorporació de molibdè a les capes necessària per provocar una disminució clara d'H_c és del 5% ($H_{c\ Co\text{-}Mo}$=40-70 Oe versus $H_{c\ Co}$=160 Oe). Els dipòsits amb 5-11% Mo són foscos i la seva morfologia és de tipus llanós. A més, també s'observa que la magnetització en camp paral·lel és més ràpida que en camp perpendicular, la qual cosa està relacionada amb un creixement a capes de l'aliatge i l'orientació cristal·logràfica preferent (hk0).

S'ha comprovat que l'ús de concentracions de Co(II) superiors a 0.3 mol dm^{-3} o la substitució de $CoSO_4$ per $CoCl_2$ empitjora la qualitat dels dipòsits. D'entre els banys dissenyats en el laboratori, la dissolució 0.2 mol dm^{-3} citrat + 0.3 mol dm^{-3} $CoSO_4$ + 0.012 mol dm^{-3} Na_2MoO_4 a pH=4.0 és la més adient per preparar dipòsits Co-Mo coherents amb un contingut baix de molibdè.

Els dipòsits Co-Mo són compatibles amb la tecnologia del silici. Poden obtenir-se, sobre substrats Si/capa llavor i a partir del bany escollit, làmines Co-Mo amb unes propietats similars a les exhibides per dipòsits preparats sobre grafit o coure. En aquestes condicions, la velocitat de creixement de l'aliatge és de 7.7 μm h^{-1} i els dipòsits resultants presenten una baixa rugositat. La deposició és altament selectiva i les microestructures Co-Mo preparades sobre substrats base silici litografiats conserven perfectament el relleu esbossat per la resina. El *farcit* de les cavitats conductores és homogeni i les parets laterals són verticals. Quan el gruix de les microestructures és superior a 7 μm, tanmateix, s'observen esquerdes incipients i un cert desarrelament del dipòsit. L'addició d'1 g l^{-1} de sacarina al bany i un lleuger augment de la temperatura (fins a 35ºC) permet de minimitzar-ne l'estrès. S'ha comprovat que increments superiors de la temperatura del bany no són recomanables puix que afavoreixen l'evolució d'hidrogen.

4.4 Mecanisme de l'electrodeposició de cobalt-níquel-molibdè

4.4.1 Finalitat

Abans de procedir a la preparació de dipòsits ternaris Co-Ni-Mo, es va estimar convenient fer un estudi del mecanisme d'electrodeposició dels sistemes Co-Ni i Co-Ni-Mo en medi sulfat-citrat. L'objectiu d'aquest estudi era determinar si la presència de Ni(II) en el bany alterava el mecanisme suggerit per a la deposició de l'aliatge Co-Mo o, per contra, continuaven essent vàlides les etapes proposades. Per a l'estudi del procés de deposició Co-Ni es van utilitzar solucions a pH=4.0 que contenien una concentració total de cations metàl·lics igual a 0.3 mol dm^{-3} en una relació [Ni(II)]:[Co(II)]=5:1 i una concentració variable de citrat sòdic (0.1-0.5 mol dm^{-3}). Es va utilitzar la tècnica LSV per tal d'obtenir informació in situ de les espècies dipositades inicialment sobre l'elèctrode de carboni vitri, aplicant límits molt curts en els escombrats catòdics. Es van dur a terme anàlisis químiques (ICP-MS) de les espècies dipositades en aquestes condicions per avalar els resultats experimentals.

Un cop analitzada la naturalesa de la deposició Co-Ni en medi sulfat-citrat, l'objectiu més immediat fou elucidar les etapes involucrades en la deposició del sistema ternari Co-Ni-Mo. Per fer aquest estudi es van utilitzar banys ajustats a pH 4.0 i 6.6, amb una relació [Ni(II)]:[Co(II)]=5:1, 0.2 mol dm^{-3} citrat sòdic i una concentració baixa de molibdat (0.005 o 0.012 mol dm^{-3}). Es van utilitzar també les tècniques de LSV i ICP-MS per obtenir informació de les espècies dipositades inicialment sobre l'elèctrode. Així mateix, es va fer una caracterització *ex situ* (SEM, AFM, perfilometria interferomètrica) en condicions d'incipient creixement de l'aliatge Co-Ni-Mo sobre les espècies intermèdies generades durant el procés d'electrodeposició.

Finalment es va dur a terme un estudi dels òxids de molibdè intermedis formats durant els processos d'electrodeposició dels

sistemes Co-Mo i Co-Ni-Mo. Amb aquest estudi es pretenia conèixer quin és el tipus d'òxid de molibdè capaç d'evolucionar fins a molibdè metàl·lic per formar l'aliatge binari Co-Mo o el ternari Co-Ni-Mo i el rang de pH de treball més adequat per propiciar la reducció d'òxid de molibdè a molibdè metàl·lic. Es van preparar capes suficientment gruixudes d'aquests òxids de molibdè sobre l'elèctrode vidre/ITO o Si/capa llavor i es van caracteritzar mitjançant UV-Vis, XPS i difracció de raigs X. Així mateix, es va dur a terme un estudi paral·lel de la formació d'òxids de molibdè en absència de citrat i de metalls inductors amb l'objectiu de detectar quines són les diferències (color, estat d'oxidació, estructura cristal·lina...) respecte dels produïts com a intermedis durant el procés de deposició de Co-Mo i Co-Ni-Mo.

Els resultats detallats d'aquest capítol s'inclouen en els següents articles:

An approach to the first stages of cobalt-nickel-molybdenum electrodeposition in sulphate-citrate medium
J. Electroanal. Chem. 580 (2005) 222

Intermediate molybdenum oxides involved in binary and ternary induced electrodeposition
J. Electroanal. Chem. 580 (2005) 238

An approach to the first stages of cobalt-nickel-molybdenum electrodeposition in sulphate-citrate medium

Available online at www.sciencedirect.com
SCIENCE DIRECT®
Journal of Electroanalytical Chemistry 580 (2005) 222–230
Journal of Electroanalytical Chemistry
www.elsevier.com/locate/jelechem

An approach to the first stages of cobalt–nickel–molybdenum electrodeposition in sulphate–citrate medium

Elvira Gómez, Eva Pellicer, Elisa Vallés *

Electrodep, Departament de Química Física, Universitat de Barcelona, Martí i Franquès 1, E-08028 Barcelona, Spain

Received 27 July 2004; received in revised form 21 December 2004; accepted 10 January 2005
Available online 5 May 2005

Abstract

The first stages of Co–Ni and Co–Ni–Mo deposition in sulphate–citrate medium at pH 4.0 were analysed. In both cases, the formation of non-hydrogenated nickel on the electrode before alloy deposition was detected by linear sweep voltammetry and inductively coupled plasma mass spectrometry. Co–Ni electrodeposition was anomalous since the Co/Ni ratio in the alloy was higher than the corresponding [Co(II)]/[Ni(II)] ratio in solution. The adsorption of Co(II) over the initial nickel could explain the anomalous codeposition, which persisted with the addition of molybdate to the Co–Ni bath. However, the formation of intermediate molybdenum oxides also took place. A mechanism has been proposed to describe the sequence of steps for Co–Ni–Mo electrodeposition. Under our conditions, the alloy is formed mainly from free Co^{2+} and Ni^{2+} cations, whereas molybdate is reduced firstly to molybdenum oxide from $MoO_4(H_3Cit)^{2-}$ and, secondly, $NiCit^-$ catalyses the subsequent reduction to molybdenum metal of the intermediate $[MoO_2–NiCit^-]_{ads}$ species.

Keywords: Cobalt–nickel–molybdenum alloy; Electrodeposition; Molybdenum oxides

1. Introduction

Cobalt alloys have received attention in recent years due to their magnetic properties [1–6]. In our laboratory, we have obtained by electrodeposition cobalt–molybdenum alloys from a sulphate–citrate medium. Co–Mo deposits with different molybdenum percentages were obtained by varying the composition and the pH of the electrolytic bath. It was found that small amounts of molybdenum (~11% wt) into the deposits led to a soft-magnetic response of the material. These percentages were achieved from baths that contained some non-complexed Co(II) in solution and were adjusted to a pH 4.0 [7,8].

The properties of the Co–Mo alloy could be modified or extended by the introduction of a third element in the alloy. In this line, the introduction of nickel to the Co–Mo deposits might improve their corrosion resistance.

However, the influence of nickel on Co–Mo electrodeposition is unknown and probably complex since Co–Mo deposition is an induced process. Since changes in the electrodeposition mechanism due to the presence of nickel in the solution could induce changes in the final properties of the coatings, a preliminary study of the electrodeposition mechanism of the ternary cobalt–nickel–molybdenum system seems appropriate.

Thus, the goal of this study consists in establishing the stages of ternary Co–Ni–Mo deposition in a sulphate–citrate medium. Cyclic voltammetry and linear sweep voltammetry (LSV) experiments were used to provide in situ information of the species formed on the electrode at the onset of the reduction processes. Complementary chemical analyses were performed to characterise the species gradually deposited. The

* Corresponding author. Tel.: +34 93402 1234; fax: +34 93402 1231.
E-mail address: e.valles@ub.edu (E. Vallés).

0022-0728/$ - see front matter © 2005 Elsevier B.V. All rights reserved.
doi:10.1016/j.jelechem.2005.01.038

knowledge of the mechanism of the ternary electrodeposition will be useful to control the alloy preparation.

2. Experimental

The study of the electrodeposition process and deposit preparation was performed in a conventional three-electrode cell using a microcomputer-controlled potentiostat/galvanostat Autolab with PGSTAT30 equipment and GPES software. Solutions contained $CoSO_4$, $NiSO_4$, $Na_3C_6H_5O_7$ and Na_2MoO_4, all of analytical grade. The pH was adjusted to either 4.0 or 6.6 by adding H_2SO_4. All solutions were freshly prepared with water which was first doubly distilled and then treated with a Millipore Milli Q system. Before the experiments, solutions were de-aerated by strong argon bubbling over an extensive period of time in order to avoid the formation of hydroxides of the metals presents in solution during electrodeposition. The temperature was maintained at 25 °C.

For electrochemical study, a vitreous carbon (Metrohm) of 0.0314 cm^2 was used as working electrode. It was polished to a mirror finish before each experiment using alumina of different grades (3.75 and 1.85 μm) and cleaned ultrasonically for 2 min in water. The reference electrode was an Ag/AgCl/1 mol dm^{-3} NaCl electrode mounted in a Luggin capillary containing 0.5 mol dm^{-3} Na_2SO_4 solution. All potentials are referred to this electrode. The counter electrode was a platinum spiral.

Voltammetric experiments were performed under quiescent conditions at 50 mV s^{-1}, scanning initially from −500 mV towards negative potentials. Only one cycle was run for each experiment. Combined linear sweep voltammetries (negative scan under stirring + positive scan under quiescent conditions) were also carried out at 50 mV s^{-1}. The positive scan was performed in the same solution as used to record the reduction scan since the oxidation response was the same as that observed in a blank solution.

Deposits were prepared under stirring conditions (60 rpm) either on vitreous carbon electrode or on indium tin oxide (ITO) thin films sputtered on glass plates (thickness of ITO layer = 25 nm). The resistivity of 1 cm × 1 cm ITO/glass plates was 200 Ω between two opposite edges. Deposit morphology was examined with scanning electron microscopy, using a Hitachi S 2300 or a Field Emission Hitachi 4100. Deposit composition was determined by chemical analysis of the films obtained. For this purpose, films were dissolved in 1% nitric acid and the resulting solutions were analysed by inductively coupled plasma mass spectrometry (ICP-MS).

The roughness (rms) and the surface profiling of the films were measured using a white-light interferometer (Zygo Corporation). The AFM technique was also used working in tapping mode.

3. Results

3.1. Preliminary voltammetric study

The voltammetric response of a 0.2 mol dm^{-3} $Na_3C_6H_5O_7$ + 0.3 mol dm^{-3} $CoSO_4$ + 0.005 mol dm^{-3} Na_2MoO_4 solution at pH 4.0 was compared with the response of another solution at the same pH in which most of the Co(II) was substituted by Ni(II): 0.05 mol dm^{-3} $CoSO_4$ + 0.25 mol dm^{-3} $NiSO_4$. The Ni(II)-free solution was chosen as a reference since its voltammetric response has already been studied [7]. The presence of Ni(II) in the bath caused a shift of the onset of deposition to more negative potentials (Fig. 1). A lower slope of the reduction current was also observed during the negative scan. At all cathodic limits the Q_{ox}/Q_{red} ratio was always clearly lower for the bath that contained Ni(II), as usually occurs when depositing nickel due to its intrinsic hard oxidation [9–12].

3.2. Voltammetric study of molybdate-free solutions

Although many researchers have studied the behaviour of the Co–Ni system in simple baths (chloride, sulphate, sulphamate, Watts…), its behaviour in a sulphate–citrate medium has been less thoroughly investigated as it is not usually necessary to use complexing agents to induce the codeposition of cobalt and nickel. The influence of Ni(II) presence in a sulphate–citrate bath containing Co(II) was therefore analysed by means of cyclic voltammetry and linear sweep voltammetry (LSV) to study the general trends of the mechanism of Co–Ni alloy formation in this medium. Different citrate concentrations were used in order to achieve different complexation degrees for the metallic cations. The [Ni(II)]:[Co(II)] ratio was fixed at 5:1.

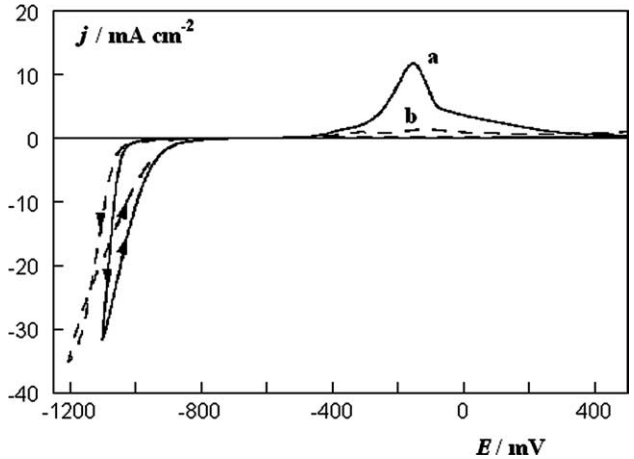

Fig. 1. Cyclic voltammetry of (a) 0.2 mol dm^{-3} $Na_3C_6H_5O_7$ + 0.3 mol dm^{-3} $CoSO_4$ + 0.005 mol dm^{-3} Na_2MoO_4 solution, pH 4.0 and (b) 0.2 mol dm^{-3} $Na_3C_6H_5O_7$ + 0.05 mol dm^{-3} $CoSO_4$ + 0.25 mol dm^{-3} $NiSO_4$ + 0.005 mol dm^{-3} Na_2MoO_4 solution, pH 4.0.

The cyclic voltammetry revealed that the onset of the electrodeposition process was delayed by increasing citrate concentration in solution (Fig. 2). During the positive scan, a low oxidation current was recorded in all cases.

The first stages of Co–Ni deposition at various citrate concentrations were analysed by means of two combined LSV (negative scan + positive scan). The negative going sweep was performed scanning from −500 mV to more negative limits. Those limits were selected according to the onset of alloy deposition previously determined by cyclic voltammetry. Values prior to the sharp current increase were applied since our purpose was to determine the species initially deposited on the electrode. The potential was held constant for a controlled time when the cathodic limit was reached in order to increase the amount of deposited species and, therefore, obtain an appreciable oxidation response. The positive scan was performed immediately after the reduction, scanning from a potential at which no current was detected towards more positive potentials.

At these very small cathodic limits, the corresponding positive scans showed a peak placed at positive potentials (Fig. 3A). A greater oxidation peak was observed for the lowest citrate concentration. In all cases, when the cathodic limit was extended to more negative potentials, an oxidation peak developed at negative potentials, which was attributed to Co–Ni alloy oxidation (Fig. 3B). In order to determine the nature of the peak placed at positive potentials, the LSV response of a 0.2 mol dm^{-3} $Na_3C_6H_5O_7$ + 0.3 mol dm^{-3} $NiSO_4$ solution was analysed since it seemed to correspond to the oxidation of nickel amounts formed initially on the electrode. For this solution, a peak at around +60 mV was recorded during the positive going sweep after the reduction scan to very small cathodic limits (Fig. 4, curve a). This peak can be attributed to the oxidation of non-hydrogenated nickel (also called massive nickel) [13,14]. When a more negative limit was applied, a new peak placed at −195 mV appeared (Fig. 4, curve b), attributable to the oxidation of hydrogenated nickel [13,14]. Therefore, we concluded that a small amount of massive Ni was formed initially on the electrode as a previous stage of Co–Ni electrodeposition. Table 1 lists the ICP-MS results corresponding to samples prepared from the 0.2 mol dm^{-3} $Na_3C_6H_5O_7$ + 0.25 mol dm^{-3} $NiSO_4$ + 0.05 mol dm^{-3} $CoSO_4$ solution by means of negative scans to different cathodic limits. When very small cathodic limits were applied, the solutions obtained after dissolving the film formed on the electrode were Ni(II)-rich. At slightly more negative cathodic limits, the Co(II) content in solution began to be significant to the detriment of Ni(II) content. At even more negative cathodic limits, the solutions were Co(II)-rich. Since the Co and Ni levels detected by ICP-MS were, in some cases, of the same order of magnitude as the detection limits of the technique, the ICP-MS data actually provided semi-quantitative information of the species formed on the electrode.

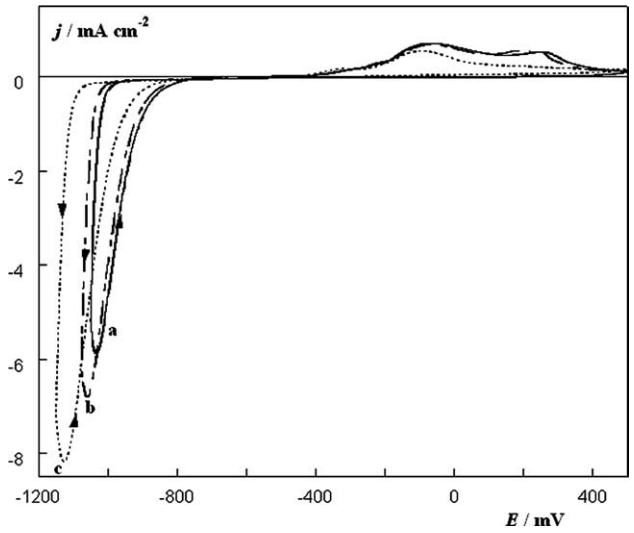

Fig. 2. Cyclic voltammetry of a x mol dm^{-3} $Na_3C_6H_5O_7$ + 0.05 mol dm^{-3} $CoSO_4$ + 0.25 mol dm^{-3} $NiSO_4$ solution at pH 4.0. (a) x = 0.1, (b) x = 0.2, (c) x = 0.4.

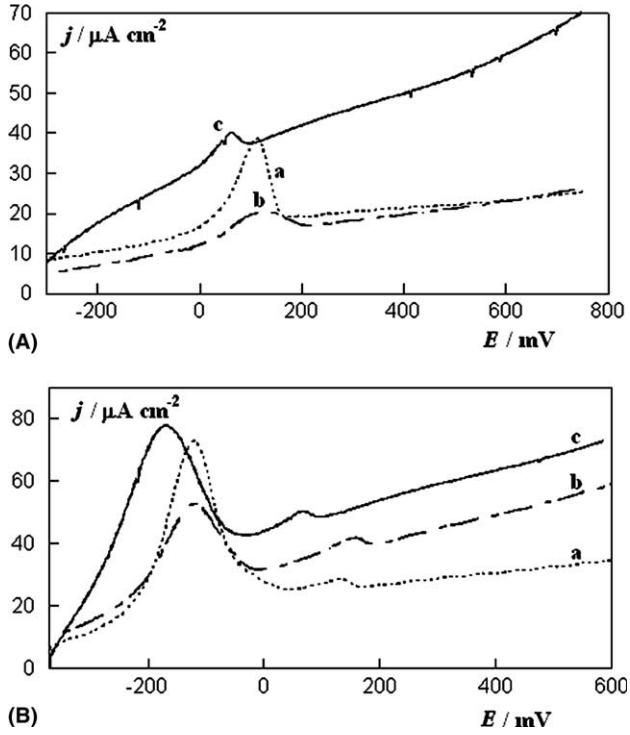

Fig. 3. Oxidation scans corresponding to cathodic linear sweep voltammetries performed on a x mol dm^{-3} $Na_3C_6H_5O_7$ + 0.05 mol dm^{-3} $CoSO_4$ + 0.25 mol dm^{-3} $NiSO_4$ solution at pH 4.0. (A) (a) x = 0.1, cathodic limit = −770 mV, t_{hold} = 10 min, (b) x = 0.2, cathodic limit = −770 mV, t_{hold} = 10 min and (c) x = 0.4, cathodic limit = −880 mV, t_{hold} = 10 min. (B) (a) x = 0.1, cathodic limit = −820 mV, t_{hold} = 5 min, (b) x = 0.2, cathodic limit = −820 mV, t_{hold} = 10 min and (c) x = 0.4, cathodic limit = −880 mV, t_{hold} = 12 min.

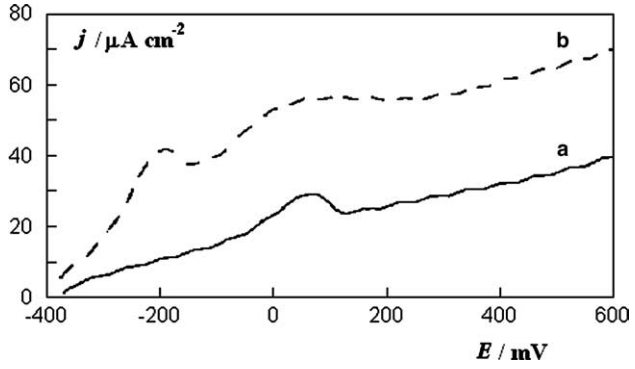

Fig. 4. Oxidation scans corresponding to cathodic linear sweep voltammetries performed on a 0.2 mol dm^{-3} $Na_3C_6H_5O_7$ + 0.3 mol dm^{-3} $NiSO_4$ solution at pH 4.0. (a) Cathodic limit = −800 mV, t_{hold} = 10 min and (b) cathodic limit = −897 mV, t_{hold} = 5 min.

Table 1
ICP-MS analysis of samples prepared by reduction scan over a vitreous carbon electrode from the 0.2 mol dm^{-3} $Na_3C_6H_5O_7$ + 0.05 mol dm^{-3} $CoSO_4$ + 0.25 mol dm^{-3} $NiSO_4$ solution at pH 4.0

$-E_c$ (mV)	t_{hold} (min)	[Ni(II)] (μg l^{-1})	[Co(II)] (μg l^{-1})	% Ni	% Co
730	10	0.33	0.05	86.8	13.2
820	4	0.56	0.09	86.2	13.8
878	6	1.20	2.38	33.5	66.5

According to these results, Co–Ni codeposition occurred through the formation of small amounts of non-hydrogenated Ni on the electrode, over which alloy deposition took place. Since the Co/Ni ratio in the alloy was much larger than the corresponding [Co(II)]/[Ni(II)] ratio in solution, Co–Ni electrodeposition was anomalous in sulphate–citrate medium.

3.3. Voltammetric study of Co–Ni–Mo solutions

After establishing the sequence of steps involved in Co–Ni electrodeposition, we studied a 0.2 mol dm^{-3} $Na_3C_6H_5O_7$ + 0.05 mol dm^{-3} $CoSO_4$ + 0.25 mol dm^{-3} $NiSO_4$ + 0.005 mol dm^{-3} Na_2MoO_4 solution to determine the stages of Co–Ni–Mo deposition. Cyclic voltammetry was used to determine whether the formation of intermediate molybdenum oxides occurred as in Co–Mo solutions [15], irrespective of the presence of Ni(II). The addition of molybdate to the bath led to the appearance of a low reduction current prior to the sharp current increase during the negative scan (Fig. 5). The low reduction current was attributed to molybdenum oxide formation as occurs in a Co–Mo bath [15,16], while the sharp current increase was likely due to Co–Ni–Mo alloy deposition. A low oxidation current was also recorded during the positive scan.

The LSV experiments performed at the first stages of electrodeposition led to similar results as those obtained

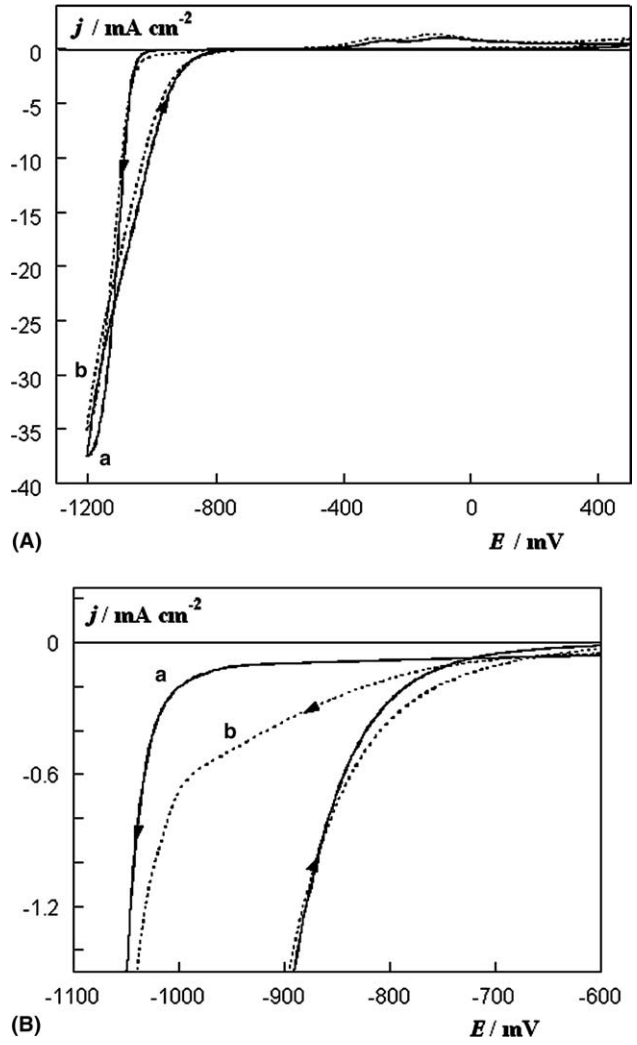

Fig. 5. (A) Cyclic voltammetry of a 0.2 mol dm^{-3} $Na_3C_6H_5O_7$ + 0.05 mol dm^{-3} $CoSO_4$ + 0.25 mol dm^{-3} $NiSO_4$ + x mol dm^{-3} Na_2MoO_4 solution at pH 4.0. (a) x = 0, (b) x = 0.005. (B) Magnified detail of the reduction zone.

from the Co–Ni bath. An oxidation peak placed at positive potentials was recorded when small cathodic limits were applied (Fig. 6, curve a). This peak was attributed to the oxidation of massive Ni formed initially on the electrode. When a more negative cathodic limit was applied, a peak centred at −165 mV and attributed to Co–Ni–Mo alloy oxidation was recorded during the positive going sweep (Fig. 6, curve b). Complementary chemical analysis of films prepared by means of negative scans to small cathodic limits showed that they mainly contained Ni (Table 2), whereas films prepared whilst scanning to more negative potentials were formed of a Co–Ni–Mo alloy of ~14% Ni. Thus, the anomalous behaviour of the Co–Ni system persisted despite the addition of molybdate to the bath.

However, oxide formation could not be demonstrated by LSV experiments since molybdenum oxides

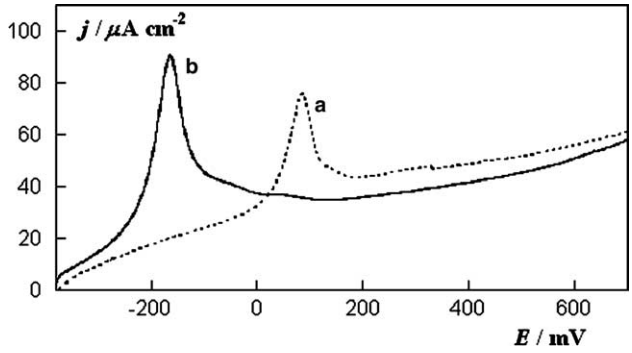

Fig. 6. Oxidation scans corresponding to cathodic linear sweep voltammetries performed on a 0.2 mol dm^{-3} $Na_3C_6H_5O_7$ + 0.05 mol dm^{-3} $CoSO_4$ + 0.25 mol dm^{-3} $NiSO_4$ + 0.005 mol dm^{-3} Na_2MoO_4 solution at pH 4.0. (a) Cathodic limit = −714 mV, t_{hold} = 10 min and (b) cathodic limit = −860 mV, t_{hold} = 2 min.

Table 2
ICP-MS analysis of samples prepared by reduction scan over a vitreous carbon electrode from the 0.2 mol dm^{-3} $Na_3C_6H_5O_7$ + 0.05 mol dm^{-3} $CoSO_4$ + 0.25 mol dm^{-3} $NiSO_4$ + 0.005 mol dm^{-3} Na_2MoO_4 solution at pH 4.0

$-E_c$ (mV)	t_{hold} (min)	[Ni] (μg l^{-1})	[Co] (μg l^{-1})	[Mo] (μg l^{-1})	% Ni	% Co	% Mo
700	85	2.46	0.60	0.25	74.3	18.1	7.6
860	5	6.99	34.56	7.69	14.2	70.2	15.6

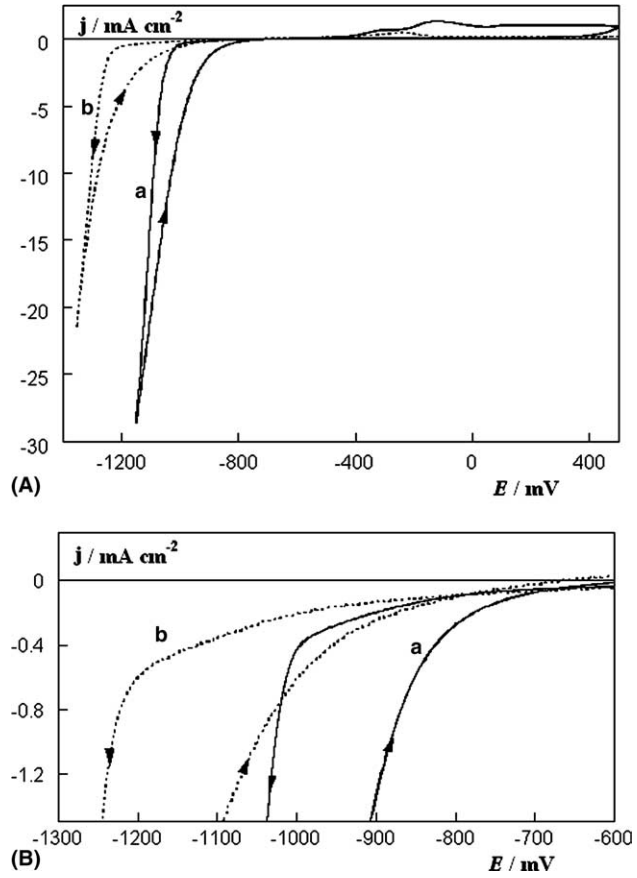

Fig. 7. (A) Cyclic voltammetry of (a) 0.2 mol dm^{-3} $Na_3C_6H_5O_7$ + 0.05 mol dm^{-3} $CoSO_4$ + 0.25 mol dm^{-3} $NiSO_4$ + 0.005 mol dm^{-3} Na_2MoO_4 solution, pH 4.0 and (b) 0.2 mol dm^{-3} $Na_3C_6H_5O_7$ + 0.0165 mol dm^{-3} $CoSO_4$ + 0.0835 mol dm^{-3} $NiSO_4$ + 0.012 mol dm^{-3} Na_2MoO_4 solution, pH 6.6. (B) Magnified detail of the reduction zone.

are hardly oxidised [15] and the molybdate concentration in solution was too low to obtain an appreciable amount of molybdenum oxides. In order to determine the possible formation of intermediate molybdenum oxides from the Co–Ni–Mo system, an electrolytic bath similar to those used to obtain molybdenum oxide films from a Co–Mo bath, was prepared [15]. Therefore, it was decided to raise the pH and decrease the [Ni(II)] + [Co(II)] to 0.1 but maintaining the 5:1 ratio. Simultaneously, the molybdate concentration in solution was increased to 0.012 mol dm^{-3}.

The voltammetric response of a 0.2 mol dm^{-3} $Na_3C_6H_5O_7$ + 0.0165 mol dm^{-3} $CoSO_4$ + 0.0835 mol dm^{-3} $NiSO_4$ + 0.012 mol dm^{-3} Na_2MoO_4 solution at pH 6.6 showed a greater reduction current corresponding to molybdenum oxide formation than that observed from the previous 0.2 mol dm^{-3} $Na_3C_6H_5O_7$ + 0.05 mol dm^{-3} $CoSO_4$ + 0.25 mol dm^{-3} $NiSO_4$ + 0.005 mol dm^{-3} Na_2MoO_4 solution at pH 4.0 (Fig. 7). The rise was attributed to the increase of molybdate concentration. This subtle feature was also observed in the binary Co–Mo deposition [16]. Furthermore, alloy deposition was delayed due to the decrease of non-complexed Co^{2+} and Ni^{2+} cations in solution, so the potential range for molybdenum oxide formation was enlarged.

The LSV experiments performed from the 0.2 mol dm^{-3} $Na_3C_6H_5O_7$ + 0.0165 mol dm^{-3} $CoSO_4$ + 0.0835 mol dm^{-3} $NiSO_4$ + 0.012 mol dm^{-3} Na_2MoO_4 solution at pH 6.6 did not show a peak placed at positive potentials when scanning to small negative cathodic limits. In contrast, an oxidation peak placed at negative potentials was recorded when scanning to more negative potentials. In order to characterise the species formed on the electrode before alloy formation, various samples were prepared potentiostatically applying small negative potentials. Lustrous coloured films (e.g. blue, red, green) were obtained in these conditions. When the films prepared at greater deposition charges were imaged by SEM, a cracked appearance we have previously linked to molybdenum oxides was observed (Fig. 8) [15]. Films prepared at lower deposition charges did not show cracks. Chemical analyses of molybdenum oxide films revealed that the resulting solutions contained ~90% molybdenum (Table 3), although cobalt and nickel were also detected, perhaps due to their inclusion in the molybdenum oxide structure [15]. For samples prepared scanning to more negative potentials, the ternary Co–Ni–Mo alloy with ~43% molybdenum was detected.

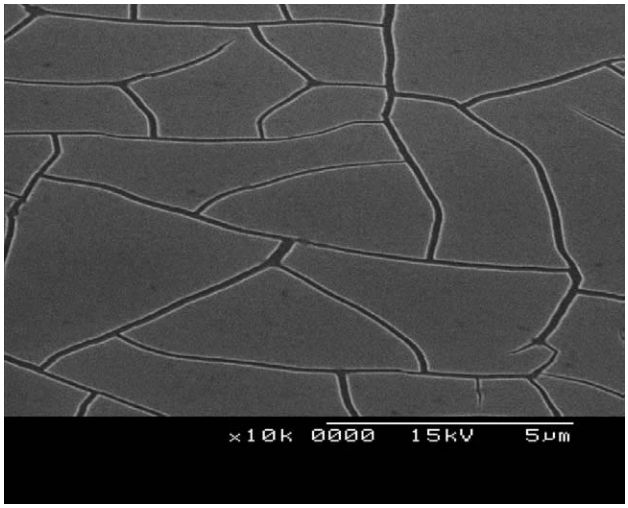

Fig. 8. SEM image of the film obtained potentiostatically from a 0.2 mol dm^{-3} $Na_3C_6H_5O_7$ + 0.0165 mol dm^{-3} $CoSO_4$ + 0.0835 mol dm^{-3} $NiSO_4$ + 0.012 mol dm^{-3} Na_2MoO_4 solution, pH 6.6, over vitreous carbon. Applied potential = −960 mV, t = 1500 s.

Table 3
ICP-MS analysis of samples prepared by reduction scan over a vitreous carbon electrode from the 0.2 mol dm^{-3} $Na_3C_6H_5O_7$ + 0.0165 mol dm^{-3} $CoSO_4$ + 0.0835 mol dm^{-3} $NiSO_4$ + 0.012 mol dm^{-3} Na_2MoO_4 solution at pH 6.6

$-E$ (mV)	t_{hold} (min)	[Ni] (µg l^{-1})	[Co] (µg l^{-1})	[Mo] (µg l^{-1})	% Ni	% Co	% Mo
960	8	2.91	4.62	72.69	3.6	5.8	90.6
990	4.5	1.97	3.81	34.41	4.9	9.5	85.6
1055	5	76.85	270.54	263.39	12.6	44.3	43.1

In order to increase the deposition area and to facilitate colour observation, a glass/ITO electrode was used. Several molybdenum oxide films were obtained applying more negative potentials than on vitreous carbon since the glass/ITO electrode was less active. Simultaneously, conditions under which Co–Ni–Mo alloy can grow over the molybdenum oxide film were also sought. Molybdenum oxide films obtained under a low deposition charge were crack-free (Fig. 9A), whereas the same cracked appearance as already seen by SEM (Fig. 9B) was observed when films of greater deposition charge were exposed to the interferometric light. A field emission SEM was used to image the formation of Co–Ni–Mo alloy islands over the initial molybdenum oxide film (Fig. 10). The AFM technique allowed us to determine the surface topography of these samples (Fig. 11). Therefore, a 'threshold' potential was necessary to induce the formation of alloy over molybdenum oxides as occurred with the binary Co–Mo system [15]. The roughness was very low for all the molybdenum oxide films analysed, independent of the charge flowed during their preparation. In contrast, the roughness of compact Co–Ni–Mo coatings prepared on the same substrate was notoriously greater (Fig. 12).

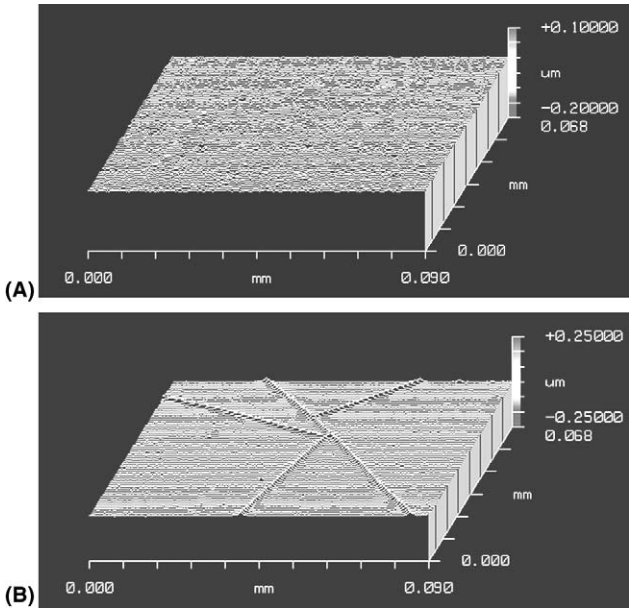

Fig. 9. 3D surface profile of molybdenum oxide films obtained potentiostatically from a 0.2 mol dm^{-3} $Na_3C_6H_5O_7$ + 0.0165 mol dm^{-3} $CoSO_4$ + 0.0835 mol dm^{-3} $NiSO_4$ + 0.012 mol dm^{-3} Na_2MoO_4 solution, pH 6.6, over glass/ITO electrode. Applied potential = −1010 mV. (A) Q = −0.89 C cm^{-2}, (B) Q = −1.66 C cm^{-2}.

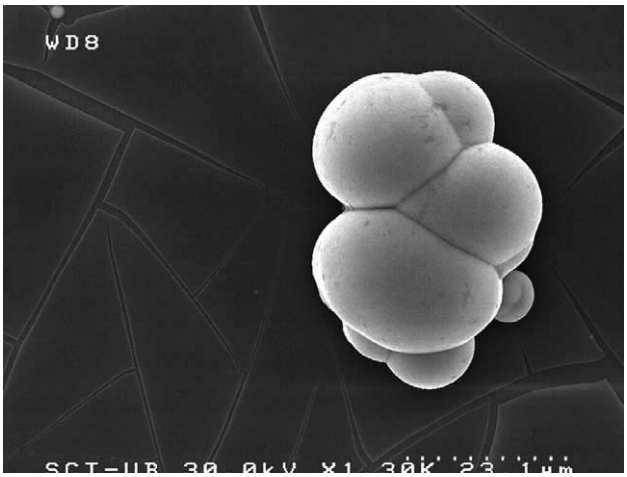

Fig. 10. FESEM image of a sample prepared from a 0.2 mol dm^{-3} $Na_3C_6H_5O_7$ + 0.0165 mol dm^{-3} $CoSO_4$ + 0.0835 mol dm^{-3} $NiSO_4$ + 0.012 mol dm^{-3} Na_2MoO_4 solution, pH 6.6, over glass/ITO electrode. Applied potential = −1080 mV, t = 13,800 s.

4. Discussion and conclusions

From the described experimental results, one can make certain conclusions regarding the mechanism of Co–Ni and Co–Ni–Mo deposition in the selected sulphate–citrate medium.

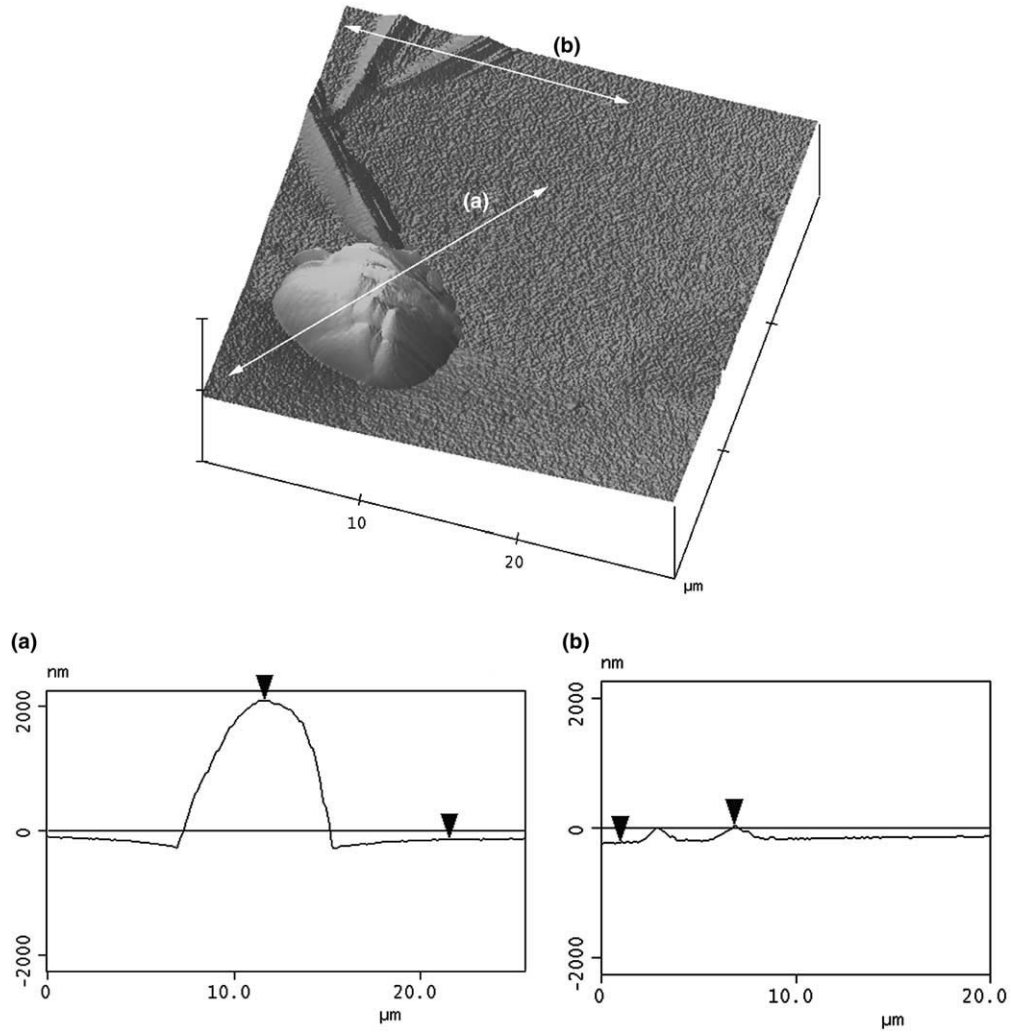

Fig. 11. AFM image of a sample prepared from a 0.2 mol dm^{-3} $Na_3C_6H_5O_7$ + 0.0165 mol dm^{-3} $CoSO_4$ + 0.0835 mol dm^{-3} $NiSO_4$ + 0.012 mol dm^{-3} Na_2MoO_4 solution, pH 6.6, over glass/ITO electrode. Applied potential = −1090 mV, t = 4800 s. (a) Surface profile of a Co–Ni–Mo island and (b) surface profile of molybdenum oxide film showing bulged cracks.

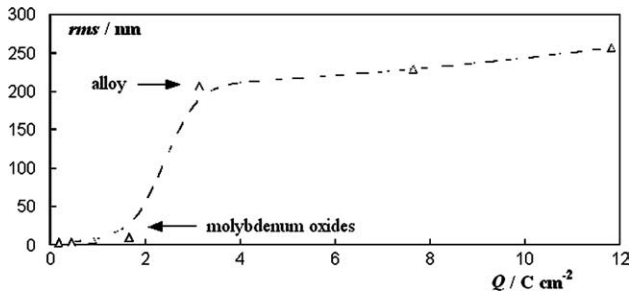

Fig. 12. rms average versus deposition charge of films obtained from a 0.2 mol dm^{-3} $Na_3C_6H_5O_7$ + 0.0165 mol dm^{-3} $CoSO_4$ + 0.0835 mol dm^{-3} $NiSO_4$ + 0.012 mol dm^{-3} Na_2MoO_4 solution, pH 6.6, over glass/ITO electrode. Potentials of −1010 and −1100 mV were applied for preparing molybdenum oxides and Co–Ni–Mo alloy, respectively.

Co–Ni codeposition is anomalous in a 0.2 mol dm^{-3} $Na_3C_6H_5O_7$ + 0.05 mol dm^{-3} $CoSO_4$ + 0.25 mol dm^{-3} $NiSO_4$, pH 4 solution. This behaviour has been observed in other baths [17–21], though differs from that seen in previous studies with a citrate medium at basic pH [22]. According to the equilibrium constants [23], the molar fractions (expressed in percentages) of the different species existing for each metal can be calculated: cobalt exists mainly in the form of free Co^{2+} (70%), whereas nickel mainly exists in the form of free Ni^{2+} (40%) and $NiCit^-$ (30%). The detection of massive nickel at small deposition potentials suggests a first stage of nickel deposition from Ni^{2+}, which is easier than deposition from $NiCit^-$:

$$Ni^{2+} + 2e^- \rightarrow Ni$$

Subsequent nickel deposition would be hindered by Co^{2+} adsorption over the initially deposited nickel. Simultaneously, cobalt deposition is enhanced, as has been proposed in chloride medium as a consequence of the catalytic effect of freshly electrodeposited nickel on cobalt deposition [19]. Thus, deposition of both cobalt

and nickel occurs from free cations. That of cobalt is catalysed, whilst that of nickel inhibited, leading to a greater proportion of cobalt in Co–Ni deposits.

For the 0.2 mol dm^{-3} $Na_3C_6H_5O_7$ + 0.05 mol dm^{-3} $CoSO_4$ + 0.25 mol dm^{-3} $NiSO_4$ + 0.005 mol dm^{-3} Na_2MoO_4, pH 4 solution, nickel mainly exists as Ni^{2+} (40%) and $NiCit^-$ (30%) [22], whereas Co^{2+} (75%) is the main species of cobalt, although $CoCit^-$ (10%) and CoHCit (10%) are also present in solution. Strong complexation between molybdate and citrate occurs [23], even in the presence of nickel and cobalt, $MoO_4(H_3Cit)^{2-}$ being the main species of molybdenum, as previously detected in Raman experiments [15].

Detection of massive nickel was also observed at small deposition potentials for the solution containing molybdate, revealing a primary nickel deposition from Ni^{2+}. After this initial nickel deposition, Co–Ni–Mo alloy deposition takes place. Alloy deposition also relies on free cation reduction. Simultaneously, reduction of $MoO_4(H_3Cit)^{2-}$ occurs, at pH 4, leading to molybdenum oxides, in a similar way as for Co–Mo deposition at the same pH [15]:

$$MoO_4(H_3Cit)^{2-} + 2H^+ + 2e^- \rightarrow MoO_2 + 2H_2O + HCit^{2-}$$

To reduce molybdenum oxides to molybdenum, an intermediate adsorbed species between molybdenum oxides and cobalt or nickel citrate complex is necessary. As $NiCit^-$ is the most abundant metal-citrate complex in solution, we propose, according to Landolt [24,25], that $NiCit^-$ catalyses molybdenum formation as follows:

$$NiCit^- + MoO_2 \rightarrow [MoO_2 - NiCit^-]_{ads}$$

$$[MoO_2 - NiCit^-]_{ads} + 2H_2O + 4e^- \rightarrow Mo + NiCit^- + 4OH^-$$

The detection of molybdenum oxides is difficult in the above Co–Ni–Mo solution, as there is no range of potentials at which only molybdenum oxide formation occurs.

In order to detect molybdenum oxides, a 0.2 ml dm^{-3} $Na_3C_6H_5O_7$ + 0.0165 mol dm^{-3} $CoSO_4$ + 0.0835 mol dm^{-3} $NiSO_4$ + 0.012 mol dm^{-3} Na_2MoO_4, pH 6.6 solution was used. Molybdate concentration was raised to enhance molybdenum oxide formation. The [Co(II)]/[Ni(II)] ratio in solution was maintained, though both concentrations were decreased to induce total complexation with citrate. Thus, cobalt and nickel reduction was delayed and it was possible to find a range of potentials, previous to Co–Ni–Mo deposition, at which only molybdenum oxides formation takes place. At this potential range and for a long deposition time, a detectable film of molybdenum oxides was formed and characterised.

Molybdenum oxide films prepared from this solution on ITO electrode exhibited a very low roughness (rms $\leqslant$ 13 nm), close to that of the substrate. Film stress was enhanced with the deposition charge leading to a cracked appearance easily observable through both SEM and white-light interferometry. Continuous Co–Ni–Mo coatings exhibited greater rms values. The formation of Co–Ni–Mo alloy over the molybdenum oxides was demonstrated by both FESEM and AFM techniques.

In conclusion, the deposition process of ternary Co–Ni–Mo system can be justified by a similar mechanism as Co–Mo deposition under similar conditions. Substitution of some cobalt in solution for nickel does not change the general trends of deposition. Only the detection of some initial nickel is observed, after which alloy deposition takes place. Moreover, cobalt and nickel maintain, in ternary deposition, the anomalous codeposition, as cobalt easily deposits at the expense of nickel. On the other hand, molybdenum deposition is induced by cobalt–nickel.

Acknowledgements

The authors wish to thank the Serveis Cientificotècnics (Universitat de Barcelona) for the use of their equipment. This paper was supported by contract MAT 2003-09483-C02-01 from the *Comisión Interministerial de Ciencia y Tecnología (CICYT)* and by the *Comissionat* of the *Generalitat de Catalunya* under Research Project 2001 SGR 00046. E. Pellicer would also like to thank the DURSI of the *Generalitat de Catalunya* for financial support.

References

[1] R.D. Srivastava, R.C. Mukerjee, J. Appl. Electrochem. 6 (1976) 321.
[2] P.J. Grundy, J. Phys. D: Appl. Phys. 31 (1998) 2975.
[3] M. Futamoto, N. Inaba, A. Nakamura, Y. Honda, Acta Mater. 46 (1998) 3777.
[4] G. Bordin, G. Buttino, A. Cecchetti, M. Poppi, J. Phys. D: Appl. Phys. 32 (1999) 1795.
[5] O. Gutfleisch, J. Phys. D: Appl. Phys. 33 (2000) R157.
[6] D. Landolt, J. Electrochem. Soc. 149 (2002) S9.
[7] E. Gómez, E. Pellicer, E. Vallés, J. Electroanal. Chem. 568 (2004) 29.
[8] E. Gómez, E. Pellicer, E. Vallés, Surf. Coat. Technol., in press.
[9] J.R. Vilche, A.J. Arvía, J. Electrochem. Soc. 123 (1976) 1061.
[10] R. Albalat, E. Gómez, C. Muller, M. Sarret, E. Vallés, J. Appl. Electrochem. 21 (1991) 709.
[11] E. Gómez, C. Muller, W.G. Proud, E. Vallés, J. Appl. Electrochem. 22 (1992) 872.
[12] C.Q. Cui, J.Y. Lee, J. Electrochem. Soc. 141 (1994) 2030.
[13] M. Fleischmann, A. Saraby-Reintjes, Electrochim. Acta 29 (1984) 69.
[14] A. Saraby-Reintjes, M. Fleischman, Electrochim. Acta 29 (1984) 557.

[15] E. Gómez, E. Pellicer, E. Vallés, J. Appl. Electrochem. 33 (2003) 245.
[16] E. Gómez, E. Pellicer, E. Vallés, J. Electroanal. Chem. 556 (2003) 137.
[17] A. BrennerElectrodeposition of Alloys, vol. 1–2, Academic Press, New York, 1963.
[18] S.S. Abd El-Rehim, A.M. Abd El-Halim, M.M. Osman, J. Appl. Electrochem. 15 (1985) 107.
[19] E. Gómez, J. Ramírez, E. Vallés, J. Appl. Electrochem. 28 (1998) 71.
[20] N. Zech, E.J. Podlaha, D. Landolt, J. Electrochem. Soc. 146 (1999) 2886.
[21] C. Hu, A. Bai, J. Electrochem. Soc. 149 (2002) C615.
[22] C. Fan, D.L. Piron, Electrochim. Acta 41 (1996) 1713.
[23] D.D. Perrin (Ed.), Stability constants of metal–ion complexes. Section B: Organic Ligands. IUPAC Chemical Data Series 22, Pergamon Press, Exeter, 1983.
[24] E.J. Podlaha, D. Landolt, J. Electrochem. Soc. 143 (1996) 893.
[25] E.J. Podlaha, D. Landolt, J. Electrochem. Soc. 144 (1997) 1672.

Intermediate molybdenum oxides involved in binary and ternary induced electrodeposition

Available online at www.sciencedirect.com
SCIENCE DIRECT®
Journal of Electroanalytical Chemistry 580 (2005) 238–244
Journal of Electroanalytical Chemistry
www.elsevier.com/locate/jelechem

Intermediate molybdenum oxides involved in binary and ternary induced electrodeposition

Elvira Gómez, Eva Pellicer, Elisa Vallés *

Electrodep, Departament de Química Física, Universitat de Barcelona, Martí i Franquès 1, E-08028 Barcelona, Spain

Received 31 January 2005; received in revised form 15 March 2005; accepted 17 March 2005
Available online 3 May 2005

Abstract

Molybdenum oxides have been produced by electrodeposition in sulphate medium from solutions containing molybdate, in the presence or in the absence of citrate, Co(II) and Co(II) + Ni(II). The goal of this work was the characterisation of intermediate molybdenum oxides able to progress to Co–Mo and/or Co–Ni–Mo electrodeposits. For this purpose, several oxide layers were prepared on ITO/glass and silicon-based substrates and characterised by UV–Vis, X-ray photoelectron spectroscopy and X-ray diffraction. The kind of molybdenum oxides that would evolve to the alloy presented a mixed valence state of Mo^{IV} and Mo^{V} and a certain degree of crystallinity. A yellow-brown-coloured film was observed when a continuous oxide layer was electrodeposited. Inclusion of small amounts of Co or Co + Ni occurred during oxide formation, thereby leading to doped molybdenum oxide layers. There would be two factors that determine the viability of the alloy deposition: the formation of reasonably reduced molybdenum oxides and the interaction between citrate and the other metals (cobalt, nickel) in solution. These requirements would be satisfied at solution pH > 2.

Keywords: Molybdenum oxides; Electrodeposition; Induced deposition; Cobalt–molybdenum; Cobalt–nickel–molybdenum

1. Introduction

The molybdenum oxides have been extensively investigated because they exhibit electrochromic and photochromic properties [1–10]. Indeed, they are known as catalysts or catalyst precursors for several reactions, gas sensors or energy storage devices (microbatteries). These oxide films are usually obtained by vacuum evaporation [11], sputtering [8], chemical vapour deposition [6,7,12] and anodic oxidation [13]. In recent years, the preparation of these materials by electrodeposition has attracted the interest of several investigators [9,14,15], but little work has been done regarding to the characteristics of their electroformation.

In our laboratory, molybdenum oxides were detected as intermediate species in both Co–Mo and Co–Ni–Mo electrodeposition. The codeposition of molybdenum with an iron-group element in aqueous solution is an induced process [16,17]. The discharge of molybdate to molybdenum metal occurs through the formation of intermediate molybdenum oxides [18,19]. In addition, the presence of a polycarboxylate in the bath is necessary to allow alloy formation [16]. A sequence of steps explaining both Co–Mo and Co–Ni–Mo processes in sulphate–citrate medium was proposed [20,21]. It was found that the reduction of molybdenum oxides towards molybdenum metal occurred in the presence of cobalt–citrate or nickel–citrate complexes, leading to alloy formation. Actually, molybdenum oxides only evolved towards the alloy if a more negative potential than a threshold value was applied [22].

* Corresponding author. Tel.: +34 93 403 92 38; fax: +34 93 402 12 31.
E-mail address: e.valles@ub.edu (E. Vallés).

0022-0728/$ - see front matter © 2005 Elsevier B.V. All rights reserved.
doi:10.1016/j.jelechem.2005.03.031

Thus, this paper deals with the characterisation of the molybdenum oxides deposited as intermediate species in Co–Mo or Co–Ni–Mo electrodeposition from different experimental conditions, particularly different bath compositions and pH values. The present study will allow us to determine the electrodeposition capability to know the kind of molybdenum oxide obtained. A comparison of the molybdenum oxides obtained in the presence or in the absence of citrate and the inductor metals (Co and Ni) in solution will be carried out. The pH range appropriate to form molybdenum oxides able to evolve to binary Co–Mo or ternary Co–Ni–Mo alloys will be likewise determined.

2. Experimental

Electrochemical measurements were performed using a conventional thermostatised three-electrode cell, by means an Autolab with PGSTAT30 equipment and GPES software. The temperature was maintained at 25 °C. The chemicals used were $CoSO_4 \cdot 7H_2O$, $NiSO_4 \cdot 6H_2O$, $Na_2MoO_4 \cdot 2H_2O$, and $Na_3C_6H_5Na_3O_7 \cdot 2H_2O$, all of analytical grade. The pH was adjusted by adding H_2SO_4. All solutions were freshly prepared with water first doubly distilled and then treated with a Millipore Milli Q system. The solutions were de-aerated by argon bubbling before each experiment and maintained under argon atmosphere during it.

Molybdenum oxides were prepared on ITO conducting glass plates or flat silicon-based (Si/Ti (1000 Å)/Ni (500 Å)) substrates depending on the characterisation technique used. Both working electrodes were cleaned with acetone and rinsed in water before using them. The counter electrode was a platinum spiral. The reference electrode was an Ag|AgCl|NaCl 1 mol dm^{-3} mounted in a Luggin capillary containing 0.5 mol dm^{-3} $NaSO_4$ solution. All potentials are referred to this electrode.

Voltammetric experiments were usually carried out under quiescent conditions at 50 mV s^{-1}, scanning initially towards negative potentials. Molybdenum oxide films were obtained under stationary conditions by means of the potentiostatic technique, stepping the potential from a value at which no process occurred to a value at which reduction occurred.

The UV–Vis absorbance spectra of the products were obtained using a UV–VIS 1603 spectrophotometer of Shimadzu, scanning in the visible region between 350 and 900 nm. The chemical state of the films was studied by X-ray photoelectron spectroscopy (XPS), with a PHI 5600 multitechnique system, using standard Al Kα radiation with a resolution of 0.1 eV. The take-off angle relative to the substrate was 45°. Charging effects were corrected by referring the binding energies to that of the C1s line at 284.8 eV. X-ray diffraction (XRD) was performed on a Siemens D-500 diffractometer.

3. Results and discussion

3.1. Initial study

3.1.1. Molybdate solutions

The voltammetric study of molybdate reduction was performed from solutions containing 0.2 mol dm^{-3} sodium molybdate at different pH. The onset of reduction process was notoriously shifted towards more positive potentials as the pH decreased (Fig. 1). Moreover, the shape of the voltammetric curve changed. At pH 6.6, both reduction and oxidation currents were very low. At pH 4.0, the voltammetric response was similar to pH 2.0: a plateau followed by a monotonic current increase was observed in the negative scan and a broad oxidation band centred at negative potentials was recorded in the positive scan. The oxidation current was minimised under stirring conditions (moderate argon flow) and, thus, it was attributed to the oxidation of hydrogen formed during the reduction. It is known that molybdenum oxides are catalytic to hydrogen evolution [23]. Moreover, it was found in a previous work that they are hardly oxidised [22]. A dramatic increase of the reduction current was observed at pH 1.0. A broad oxidation band was also observed at this pH, but placed at positive potentials. In this case, a blue film covered the electrode just by cycling once the potential.

According to the different features observed in the voltammetric response depending on the pH, it seemed that distinct species could be formed on the electrode during the reduction process. In order to gain a better understanding of the differences existing among them, an UV–Vis study of samples prepared potentiostatically from the previous solutions was carried out. For this purpose, 0.8 × 5 cm ITO/glass plates were used as working electrodes to facilitate visual checking of colour appearance. The applied potential was made more negative as the pH increased, but the same deposition charge flowed in all cases. A deep blue oxide film was obtained at pH 1.0, although dissolution of the film

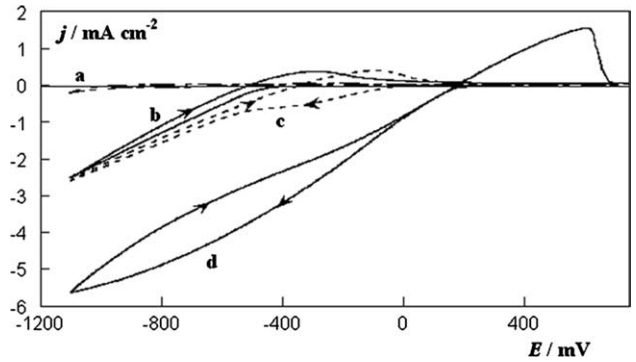

Fig. 1. Cyclic voltammetry of a 0.2 mol dm^{-3} Na_2MoO_4 solution at: (a) pH 6.6; (b) pH 4.0; (c) pH 2.0; (d) pH 1.0. Cathodic limit = −1100 mV. ITO/glass electrode.

occurred during electrodeposition. A non-uniform-coloured oxide film was obtained at pH 2.0. The brownish part of the film, close to the electrical connection, was adherent, whereas the blue part was not. Adherent yellow-brown oxide films were obtained at pH 4.0 and 6.6. Deconvolution of the UV–Vis spectra was done for each specimen by numerical fitting. The experimental spectra and the fitted Gaussian curves are shown in Fig. 2. Six Gaussian functions were necessary to fit the experimental spectra. The main absorption bands obtained after the deconvolution were in agreement with those reported in the literature for molybdenum oxides prepared by physical methods. The band A corresponded to an intense absorption in the UV region, although the end of the band had a contribution in the visible region. On the other hand, the bands C and D were assigned to Mo^{V} transitions [24,25]. The intensity of these bands increased as the films were prepared at higher pH values. Simultaneously, a systematic shift of C and D bands towards lower wavelengths was observed due to an increase of the Mo/O ratio [26] or an increase of the electron donation [27]. Thus, the formation of more reduced species took place just by increasing the solution pH.

An intense broad band (labelled E) was obtained at pH 1.0, which was attributed to $Mo^{VI} \rightarrow Mo^{V}$ transitions [15]. The E band shifted towards lower wavelengths as the pH increased, indicating again that a more reduced molybdenum oxide film was gradually deposited on the electrode, probably as a consequence of a minor proton insertion [15]. This band did not contribute at pH 4.0. The F band was attributed to an intervalence charge transfer (ICVT) of low reduced molybdenum oxides and it was placed in the IR region, around 970 nm. Some authors indicate that stoichiometries such as Mo_4O_{11} or Mo_9O_{26} would be responsible of this transition [25]. This band would not contribute at pH 6.6. The transition corresponding to band B (~422 nm) is unclear and not well understood, although Krylov et al. [28] suggested that it was due to the presence of oxygen vacancies in MoO_3 species. This meant that a small amount of MoO_3 will be always deposited on the electrode, even at quasi-neutral pH.

According to these results, the formation of mixed valence compounds with different stoichiometries depended on the pH. The brownish oxides formed at pH 4.0 and 6.6 would correspond to a molybdenum oxidation state equal or lower than Mo^{V}. At pH 2.0, the situation was more complex because a range of molybdenum oxidation states could be found because brownish and blue colours coexisted. This mixed situation was observed at any applied potential in the range of −400 and −1000 mV. In a similar way, the formation of blue films was always observed at pH 1.0 regardless of the applied potential. These films would be composed of low reduced molybdenum oxides. This finding suggested that the pH, rather than the applied potential, played an important role on the formation of different types of molybdenum oxides.

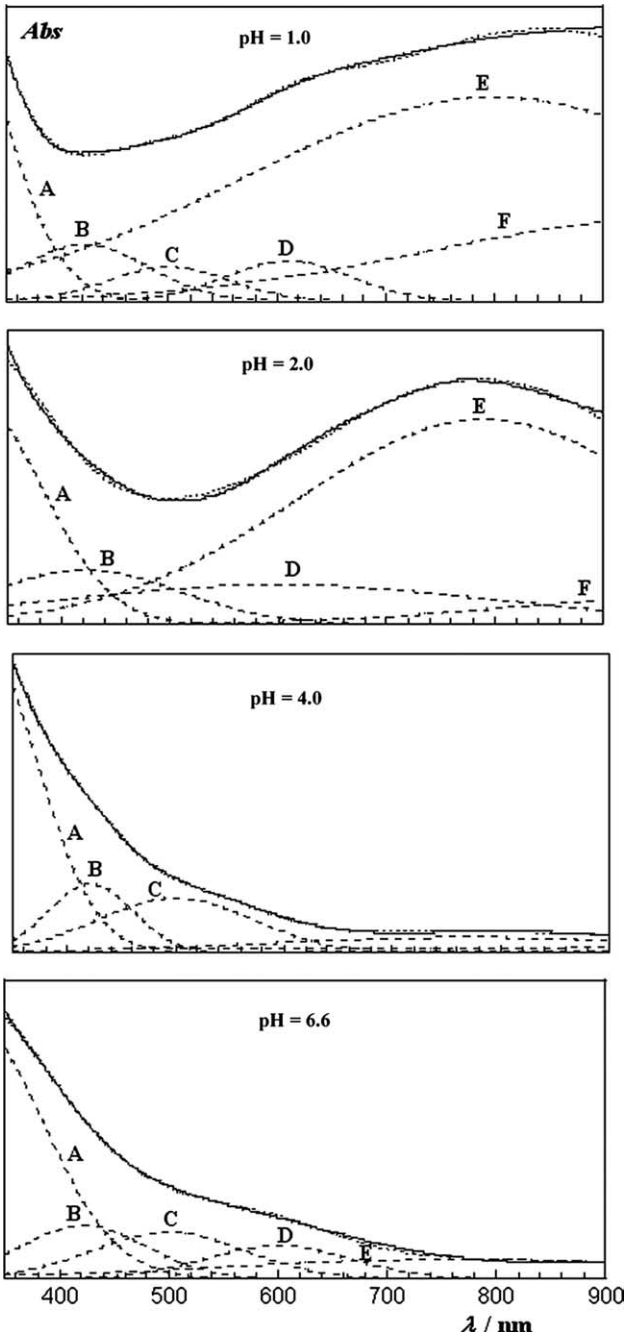

Fig. 2. UV–Vis spectra (—), fitted spectra (···) and their deconvoluted bands (- - -) of the samples obtained from 0.2 mol dm^{-3} Na_2MoO_4 solutions at different pH. The UV–Vis spectra are vertically shifted for better visualisation.

3.1.2. Addition of citrate, Co(II) and Co(II) + Ni(II)

Our next goal consisted on determining if both blue and brownish molybdenum oxide films could be completely reduced to metallic molybdenum in the presence

of citrate and the inductor metals (Co and Ni) to form Co–Mo and Co–Ni–Mo alloys. It was decided to analyse what happened when citrate and Co(II) or Co(II) + Ni(II) were gradually added to a molybdate solution at two different pH (1.0 and 6.6). Molybdate concentration was decreased up to 0.05 mol dm^{-3} in order to test the system under closer experimental conditions to those we currently used to electrodeposit the Co–Mo and Co–Ni–Mo alloys [29,30].

Blue molybdenum oxides were also formed from a 0.05 mol dm^{-3} molybdate solution at pH 1.0. These films grew rapidly although they were fragile and partially dissolved when rinsing in water. The corresponding UV–Vis spectrum showed the same bands mentioned in the Section 3.1.1, which would be compatible with the formation of $Mo^{VI/V}$ oxides. When 0.2 mol dm^{-3} citrate was added to the solution, the ITO/glass electrode was colourless after one or more voltammetric cycles. In order to determine if colourless molybdenum oxides were produced in these conditions, a collection of *j–t* curves were recorded (Fig. 3). The shape of the *j–t* curves was unusual. A monotonic current decrease was observed until a quasi-stationary value was achieved and after few seconds the current suddenly fell to zero, blocking the electrode. The sharp current decrease occurred earlier as the applied potential was made more negative. Although the formation of a poorly adherent, oxide film was observed during the current stabilisation stage, the ITO electrode was colourless at the end of the experiment. A characterisation of this oxide was not feasible since it did not adhere to the electrode. A similar behaviour was observed when Co(II) or Co(II) + Ni(II) were added to the citrate–molybdate solution: the formation of non-adherent species occurred and the electrode was blocked after a certain period of time. Therefore, the formation of Co–Mo or Co–Ni–Mo alloys films failed at pH 1.0.

On the other hand, brownish molybdenum oxide films were obtained from a 0.05 mol dm^{-3} molybdate solution at pH 6.6. Oxide formation also occurred when 0.2 mol dm^{-3} citrate was added to the solution,

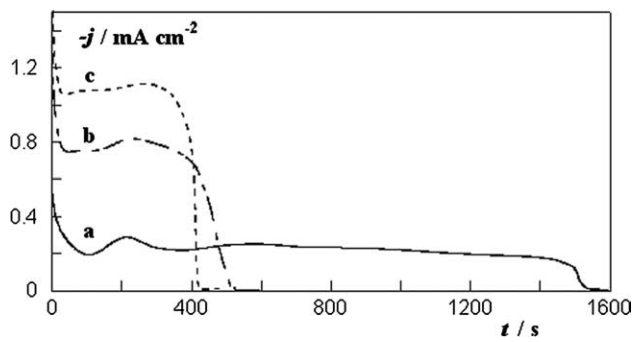

Fig. 3. *j–t* curves obtained from a 0.2 mol dm^{-3} $C_6H_5Na_3O_7$ + 0.05 mol dm^{-3} Na_2MoO_4 solution at pH 1.0. (a) $E = -850$ mV, (b) −925 mV, (c) −975 mV. ITO/glass electrode.

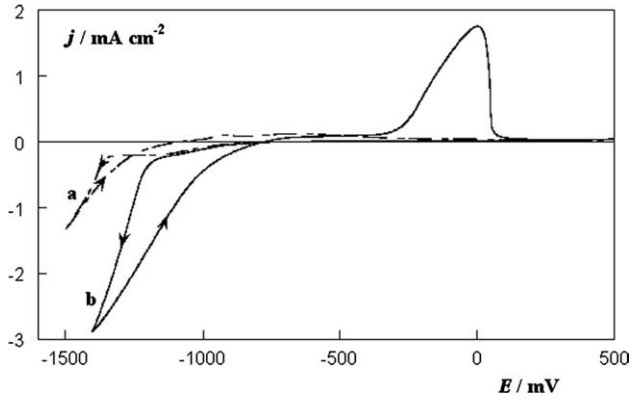

Fig. 4. Cyclic voltammetry of (a) 0.05 mol dm^{-3} Na_2MoO_4 solution, cathodic limit = −1500 mV and (b) 0.2 mol dm^{-3} $C_6H_5Na_3O_7$ + 0.1 mol dm^{-3} $CoSO_4$ + 0.05 mol dm^{-3} Na_2MoO_4 solution, cathodic limit = −1400 mV, pH 6.6. ITO/glass electrode.

although the growth rate greatly diminished. More negative potentials and long deposition times were used in the *j–t* experiments to obtain brownish molybdenum oxide films. Alloy formation took place at more negative potentials than a threshold value [22] when Co(II) or Co(II) + Ni(II) were subsequently added to the bath (Fig. 4). The sharp current increase recorded during the negative scan corresponded to alloy deposition, whereas the oxidation peak centred at −20 mV was attributed to its partial oxidation [20]. Indeed, the small reduction current observed before the sharp current increase revealed that molybdenum oxide formation also occurred. In a previous study [22], it was demonstrated by means the potentiostatic technique that molybdenum oxide films could be exclusively grown by applying a more positive potential than a threshold value. This threshold potential depended on the composition of the electrolytic bath. Oxides prepared either from the citrate–molybdate–Co(II) solution or from the citrate–molybdate–Co(II)–Ni(II) one were yellow-brown and showed a similar UV–Vis profile as that observed in the Fig. 2.

A similar electrochemical response was observed at lower molybdate concentrations (0.012 mol dm^{-3}), although current involved in oxide formation was lower. Yellow-brown oxide films were obtained at longer deposition times or higher deposition charges than those used from 0.05 mol dm^{-3} molybdate. Alloy formation also took place applying more negative potentials than a certain threshold value.

According to these results, it seemed that brownish molybdenum oxides enabled alloy formation.

3.2. Characterisation of the brownish molybdenum oxides

3.2.1. XPS study

A XPS study of the brownish oxide films was performed to confirm the molybdenum oxidation state.

They were prepared from a 0.2 mol dm^{-3} citrate + 0.1 mol dm^{-3} $CoSO_4$ + 0.012 mol dm^{-3} Na_2MoO_4 solution ('Co + Mo') and from a 0.2 mol dm^{-3} citrate + 0.0165 mol dm^{-3} $CoSO_4$ + 0.0835 mol dm^{-3} $NiSO_4$ + 0.012 mol dm^{-3} Na_2MoO_4 solution ('Co + Ni + Mo'). Both solutions were adjusted at pH 6.6. The XPS measurements were done of freshly prepared specimens in order to minimise their oxidation in air, thereby only detecting the species formed during the electrodeposition.

In all cases, a collection of molybdenum peaks was detected joined to the peaks corresponding to oxygen and carbon and those attributed to indium and tin of the glass/ITO substrate. Moreover, the samples obtained from the 'Co + Mo' solution showed small peaks that appeared at positions corresponding to cobalt. Similarly, the samples obtained from the 'Co + Ni + Mo' solution showed small cobalt and nickel peaks.

The molybdenum oxidation state was estimated by deconvolution of the peaks in the Mo3d region. The Mo3d spectrum typically consisted of a $Mo3d_{3/2}$–$Mo3d_{5/2}$ doublet due to the spin–orbit coupling. The components were spaced by a 3.13 eV difference. The shape of the doublet was Gaussian–Lorentzian type. The percentage of the Gaussian function used for the deconvolution was 80–90%.

For films prepared from the 'Co + Mo' solution, two well-resolved $Mo3d_{5/2}$ spectral lines at 229.5 and 230.6 eV were identified. The first one can be assigned to Mo^{IV} and the second one to mixed valence states of Mo^{IV} and Mo^{V}. Thus, a mixture of molybdenum oxides/hydroxides, mainly as Mo^{IV} and $Mo^{IV–V}$, was formed on the electrode. The inclusion of little amounts of cobalt, probably as Co^{2+} cation, occurred during the electrolytic formation of molybdenum oxides.

For films prepared from the 'Co + Ni + Mo' solution, a sole molybdenum compound was detected, corresponding to a $Mo3d_{5/2}$ peak centred at 231.0 eV and attributable to mixed valence states of Mo^{IV} and Mo^{V}. Inclusion of some Co^{2+} and a lower amount of Ni^{2+} also occurred during molybdenum oxide electrodeposition. The XPS data are summarised in Table 1.

Simultaneously, the XPS analysis of a blue molybdenum oxide film prepared from a bath that only contained molybdate at pH 1.0 was also performed. The corresponding spectral lines were compatible with a molybdenum oxidation state closer to Mo^{VI}.

Therefore, the XPS study allowed us to corroborate that the brownish films corresponded to a moderately reduced molybdenum oxidation state, which would be suitable for subsequent alloy formation.

3.2.2. XRD

The X-ray diffraction of the specimens previously characterised by XPS was carried out. Thicker freshly prepared molybdenum oxides were analysed. Flat silicon-based (Si/Ti/Ni) substrates were used instead of ITO/glass plates to improve oxide adherence.

The X-ray diffractograms of samples obtained from 'Co + Mo' and 'Co + Ni + Mo' solutions showed one sharp peak centred at 34°2θ attributable to the coated film, joined to some peaks corresponding to the seed-layer (Ni and Ti) and to the silicon response (Fig. 5a). Thus, the XRD analyses revealed the crystalline nature of these films. However, further assignation of the sharp peak to a specific molybdenum oxide structure was not possible. The citrate presence in the bath would induce the growth of molybdenum oxides with a certain degree of crystallinity, favoured by a low deposition rate. In order to verify this assumption, the X-ray diffraction of the blue molybdenum oxide formed from a citrate-free bath at a high deposition rate was carried out. The corresponding diffractogram showed two small broad bands centred at 28 and 54°2θ that revealed the amorphous nature of the coated film, next to the peaks of the substrate (Ti, Ni and Si) (Fig. 5b). Furthermore, when the surface of the blue molybdenum oxide was imaged by Field Emission Scanning Electron Microscopy (FESEM), no visible features were observed, indicating its amorphous nature and confirming that no grains were evident in the nanometric scale. According to this, citrate-free baths and low pH values would lead to non-crystalline structures because of a higher deposition rate.

3.3. Conclusions

Molybdenum oxide formation has been tested from solutions containing molybdate in either the presence or the absence of citrate, Co(II) and Co(II) + Ni(II).

Table 1
XPS binding energies of Mo 3d for freshly prepared molybdenum oxides

Bath	pH	$-E$ (mV)	XPS lines Mo $3d_{5/2}$ (eV)	Mo oxidation state
$C_6H_5Na_3O_7$ 0.2 M + $CoSO_4$ 0.1 M + Na_2MoO_4 0.012 M	6.6	990	229.5	Mo^{IV}
			230.6	Mo^{IV}/Mo^{V}
$C_6H_5Na_3O_7$ 0.2 M + $CoSO_4$ 0.0165 M + $NiSO_4$ 0.0835 M + Na_2MoO_4 0.012 M	6.6	1010	231.0	Mo^{IV}/Mo^{V}
Na_2MoO_4 0.2 M	1.0	325	232.3	Mo^{VI}
			233.6	—

E was the potential applied to obtain them.

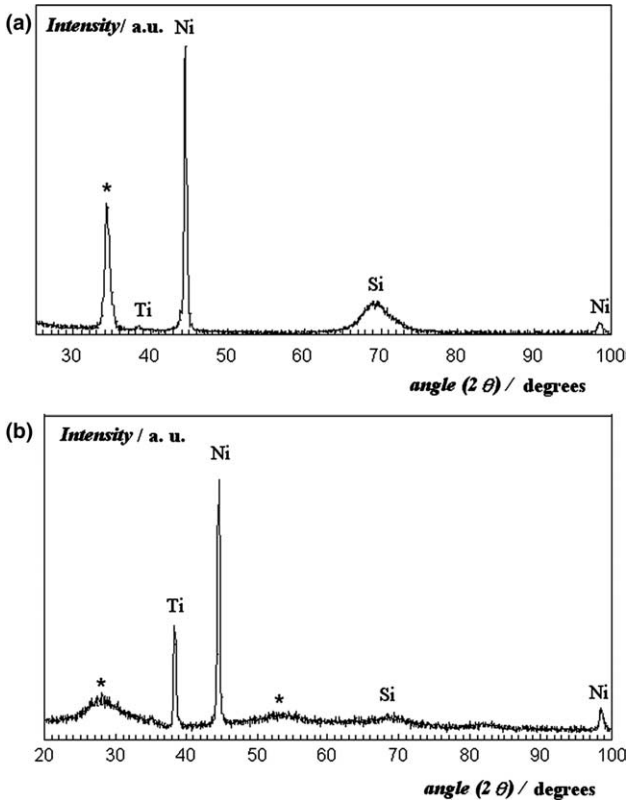

Fig. 5. X-ray diffractograms of samples obtained from (a) 0.2 mol dm^{-3} $C_6H_5Na_3O_7$ + 0.0835 mol dm^{-3} $NiSO_4$ + 0.0165 mol dm^{-3} $CoSO_4$ + 0.05 mol dm^{-3} Na_2MoO_4 solution at pH 6.6, $E = -870$ mV, $Q = -21.7$ C cm^{-2} and (b) 0.2 mol dm^{-3} Na_2MoO_4 solution at pH 1.0, $E = -275$ mV, $Q = -1.7$ C cm^{-2}. Si/Ti/Ni electrode. *Response of the deposited film.

The formation of not much reduced, blue-coloured oxides is favoured from solutions at low pH, whereas more reduced, yellow-brown oxides can be obtained increasing the pH.

According to the information gleaned from the electrochemical experiments, joined to UV–Vis and XPS analysis, alloy formation would only occur when sufficiently reduced molybdenum oxides can be formed on the electrode. The kind of oxide that satisfies this requirement corresponds to a Mo^{IV-V} oxidation state. It has been demonstrated that inclusion of cobalt and nickel in the oxide structure occurs during electrodeposition, so that doped molybdenum oxides are actually obtained. Moreover, the oxides obtained from solutions containing citrate at quasi-neutral pH were crystalline, whereas those prepared form citrate-free baths at acidic pH were amorphous. The citrate presence in the bath led to the formation of a more ordered oxide structure because it would induce a low deposition rate.

Reduced molybdenum oxides were formed at pH values from 2.0 to 6.6. The evolution of these oxides towards the metallic molybdenum requires the formation of an intermediate Mo_xO_y–M–citrate complex, M being cobalt or nickel [19]. Thus, Co–Mo or Co–Ni–Mo alloys will be only deposited under the experimental conditions that favour this interaction. The interaction between citrate and M in solution increases as the pH is raised [31]. Thus, the highest pH values in the studied range will be the most appropriate to further molybdenum oxide discharge.

Acknowledgements

The authors thank the Serveis Cientificotècnics (Universitat de Barcelona) for the use of their equipment. The authors also thank the CNM for supplying silicon-based substrates. This paper was supported by contract MAT 2003-09483-C02-01 from the *Comisión Interministerial de Ciencia y Tecnología (CICYT)* and by the *Comissionat* of the *Generalitat de Catalunya* under Research Project 2001 SGR 00046. E. Pellicer also thanks the DURSI of the *Generalitat de Catalunya* for a PhD grant.

References

[1] T. He, J. Yao, J. Photochem. Photobiol. C 4 (2003) 125.
[2] A. Guerfi, R.W. Paynter, L.H. Dao, J. Electrochem. Soc. 142 (1995) 3457.
[3] J. Scarminio, A. Lourenço, A. Gorenstein, Thin Solid Films 302 (1997) 66.
[4] Y.A. Yang, Y.W. Cao, B.H. Loo, J.N. Yao, J. Phys. Chem. B 102 (1998) 9392.
[5] A. Siokou, G. Leftheriotis, S. Papaefthimiou, P. Yianoulis, Surf. Sci. 482–485 (2001) 294.
[6] T. Ivanova, A. Szekeres, M. Gartner, D. Gogova, K.A. Gesheva, Electrochim. Acta 46 (2001) 2215.
[7] T. Ivanova, K.A. Gesheva, A. Szekeres, J. Solid State Electrochem. 7 (2002) 21.
[8] S.-H. Lee, M.J. Seong, E. Tracy, A. Mascarenhas, J.R. Pitts, S.K. Deb, Solid State Ionics 147 (2002) 129.
[9] J. Tang, Y. Lu, B. Liu, P. Yang, Y. Huang, J. Kong, J. Solid State Electrochem. 7 (2003) 244.
[10] S.-H. Baeck, T.F. Jaramillo, D.H. Jeong, E.W. McFarland, Chem. Commun. (2004) 390.
[11] O. Zelaya-Angel, C. Menezes, F. Sánchez-Sinencio, G.F.L. Ferreira, J. Appl. Phys. 51 (1980) 6022.
[12] T. Ivanova, M. Surtchev, K. Gesheva, Mater. Lett. 53 (2002) 250.
[13] K. Machida, M. Enyo, J. Electrochem. Soc. 137 (1990) 1169.
[14] S. Liu, Q. Zhang, E. Wang, S. Dong, Electrochem. Commun. 1 (1999) 365.
[15] T.M. McEvoy, K.J. Stevenson, Anal. Chim. Acta 496 (2003) 39.
[16] A. BrennerElectrodeposition of Alloys, vol. 1–2, Academic Press, New York, 1963.
[17] E.J. Podlaha, D. Landolt, J. Electrochem. Soc. 143 (1996) 885.
[18] E.J. Podlaha, D. Landolt, J. Electrochem. Soc. 143 (1996) 893.
[19] E.J. Podlaha, D. Landolt, J. Electrochem. Soc. 144 (1997) 1672.
[20] E. Gómez, E. Pellicer, E. Vallés, J. Electroanal. Chem. 556 (2003) 137.
[21] E. Gómez, E. Pellicer, E. Vallés, J. Electroanal. Chem. (in press).
[22] E. Gómez, E. Pellicer, E. Vallés, J. Appl. Electrochem. 33 (2003) 245.
[23] A. Davydov, Molecular Spectroscopy of Oxide Catalyst Surfaces, Wiley, Chichester, 2003.

[24] P.M.S. Monk, T. Ali, R. Partridge, Solid State Ionics 80 (1995) 75.
[25] G. Mestl, N.F.D. Verbruggen, H. Knözinger, Langmuir 11 (1995) 3035.
[26] V.R. Porter, W.B. White, R. Roy, J. Solid State Chem. 4 (1972) 250.
[27] J. Arris, J.A. Duffi, J. Chem. Soc. (1964) 1116.
[28] O. Krylov, Catalysis by Non-metals, Academic, New York, 1980.
[29] E. Gómez, E. Pellicer, E. Vallés, J. Electroanal. Chem. 568 (2004) 29.
[30] E. Gómez, E. Pellicer, E. Vallés, Electrochem. Commun. 7 (2005) 275.
[31] Douglas D. Perrin (Ed.), IUPAC Chemical Data Series, vol. 22, Pergamon Press, Exeter, 1983.

4.4.3 Resum de resultats

La deposició de Co-Ni en medi sulfat-citrat és anòmala. Els resultats electroquímics i les anàlisis químiques complementàries demostren que inicialment es forma una petita quantitat de níquel no hidrogenat sobre l'elèctrode, damunt del qual té lloc la deposició de l'aliatge. Aquest níquel no hidrogenat prové de la reducció de l'espècie Ni^{2+}, que és majoritària a pH=4.0. La deposició de níquel, però, no prossegueix perquè es produeix l'adsorció de Co(II) sobre aquest níquel inicial, de manera que n'inhibeix la deposició. Com a resultat d'aquesta adsorció, el cobalt es diposita preferentment i els dipòsits resultants són rics en cobalt.

El mecanisme d'electrodeposició Co-Ni-Mo és similar al proposat per explicar la deposició Co-Mo. A pH=4.0 i en condicions d'excés de [Co(II)]+[Ni(II)] respecte de citrat, el cobalt i el níquel existeixen majoritàriament com a Co^{2+} i Ni^{2+} respectivament. Per tant, la descàrrega d'ambdós metalls té lloc a partir dels cations lliures. La reducció del molibdat, en canvi, té lloc a partir d'un complex citrat-molibdat. S'ha comprovat també que la formació d'una petita quantitat inicial de níquel no hidrogenat s'esdevé durant el procés de deposició. La deposició de l'aliatge Co-Ni-Mo és induïda (Co i Ni actuen com a metalls inductors de la deposició de molibdè) i simultàniament anòmala entre els metalls Co i Ni. Les etapes proposades, anàlogues a les suggerides en el cas del sistema binari Co-Mo, són les següents:

$$Ni^{2+} + 2e^- \rightarrow Ni$$
$$Co^{2+} + 2e^- \rightarrow Co$$

$$MoO_4(H_3Cit)^{2-} + 2H^+ + 2e^- \rightarrow MoO_2 + 2H_2O + HCit^{2-}$$
$$NiCit^- + MoO_2 \rightarrow \left[MoO_2 - NiCit^-\right]_{ads}$$
$$\left[MoO_2 - NiCit^-\right]_{ads} + 2H_2O + 4e^- \rightarrow Mo + NiCit^- + 4OH^-$$

Mentre que en el cas del Co-Mo l'espècie $CoCit^-$ catalitza la reducció de l'òxid de molibdè a molibdè metàl·lic, ara és l'espècie $NiCit^-$ la que actuaria com a catalitzador, la qual cosa és raonable tenint en compte que és el complex metall-citrat més abundant en solució.

En mostres preparades a diferents potencials a partir d'un bany 0.2 mol dm^{-3} citrat + 0.0835 mol dm^{-3} $NiSO_4$ + 0.0165 mol dm^{-3} $CoSO_4$ + 0.012 mol dm^{-3} Na_2MoO_4 a pH=6.6 s'ha observat que els valors de rugositat són indicatius de l'obtenció d'òxids de molibdè o de dipòsits ternaris Co-Ni-Mo. Quan s'apliquen potencials més positius que el potencial llindar, és possible fer créixer exclusivament l'òxid de molibdè sobre l'elèctrode i el dipòsit resultant presenta una rugositat molt baixa. Si s'apliquen potencials lleugerament més negatius que el potencial llindar és factible visualitzar la formació d'illes de Co-Ni-Mo sobre una capa inicial d'òxids de molibdè. Quan l'aliatge és dipositat sobre l'elèctrode, aleshores els valors de rugositat són clarament superiors.

Els òxids de molibdè formats a partir d'un bany que només conté molibdat sòdic corresponen a un estat d'oxidació proper a Mo^{VI} i són amorfs. Per contra, els òxids de molibdè involucrats en el procés d'electrodeposició Co-Mo i Co-Ni-Mo corresponen a un estat d'oxidació mixt Mo^{IV-V} i presenten un cert grau de cristal·linitat. A més, durant el procés de deposició té lloc la inclusió de petites quantitats de Co o Co+Ni en la seva estructura. S'ha comprovat que el grau de reducció d'aquests òxids és funció del pH i que, per tant, aquest factor és clau a l'hora de possibilitar la formació d'òxids de molibdè suficientment reduïts capaços d'evolucionar fins a l'aliatge. A més, el pH de treball cal que garanteixi la interacció entre el citrat i els metalls inductors (Co i Ni), atès que el complex metall-citrat fa possible la reducció d'òxid de molibdè a molibdè metàl·lic. S'ha establert que la deposició de l'aliatge és reeixida a valors de $pH>2$.

4.5 Preparació i caracterització de capes Co-Ni-Mo

4.5.1 Finalitat

La preparació de dipòsits ternaris Co-Ni-Mo es va assajar a partir de banys que contenien concentracions fixes de citrat (0.2 mol dm^{-3}), $CoSO_4$ (0.05 mol dm^{-3}), $NiSO_4$ (0.25 mol dm^{-3}) i una concentració variable de Na_2MoO_4 (0.005-0.012 mol dm^{-3}) a pH=4.0. Es pretenia incorporar quantitats discretes de níquel a dipòsits Co-Mo amb un percentatge de Mo~10% que no comportessin una davallada significativa de la magnetització de saturació però que, en canvi, fossin suficients per millorar les propietats mecàniques i la resistència a la corrosió del material. Per això, es va escollir la mateixa relació [Ni(II)]:[Co(II)]=5:1 que s'havia testat per estudiar el mecanisme d'electrodeposició atesa la naturalesa anòmala de la deposició Co-Ni. Es va analitzar la composició dels dipòsits obtinguts a partir dels diferents banys i es va escollir el bany més adequat per obtenir capes ternàries Co-Ni-Mo tenint en compte criteris de composició dels dipòsits i d'estabilitat o control del bany.

Es van preparar capes Co-Ni-Mo sobre diferents tipus de substrat (grafit, coure, Si/capa llavor) a partir del bany seleccionat per estudiar-ne la seva morfologia, composició i estructura en funció del potencial aplicat, així com l'eficiència de corrent obtinguda. Així mateix es van enregistrar les corbes d'histèresi magnètica de capes ternàries Co-Ni-Mo gruixudes per tal de determinar l'efecte de la incorporació de níquel a les capes Co-Mo sobre les propietats magnètiques. També es va mesurar la rugositat dels dipòsits Co-Ni-Mo i es va estimar la seva velocitat de creixement sobre substrats Si/capa llavor.

Finalment es va dur a terme un estudi de corrosió comparatiu entre dipòsits de 2 μm de gruix de Co pur, Co-Ni, Co-Mo i Co-Ni-Mo. Es va determinar E_{corr} i j_{corr} en cada cas amb l'objectiu d'avaluar si la

incorporació de níquel als dipòsits Co-Mo era suficient per millorar la resistència a la corrosió del material.

Els resultats detallats d'aquest capítol s'inclouen en el següent article:

Structural, magnetic and corrosion properties of electrodeposited cobalt-nickel-molybdenum alloys
Electrochem. Commun. 7 (2005) 275

Structural, magnetic and corrosion properties of electrodeposited cobalt-nickel-molybdenum alloys

Available online at www.sciencedirect.com
SCIENCE DIRECT®
Electrochemistry Communications 7 (2005) 275–281
electrochemistry communications
www.elsevier.com/locate/elecom

Structural, magnetic and corrosion properties of electrodeposited cobalt–nickel–molybdenum alloys

Elvira Gómez, Eva Pellicer, Elisa Vallés *

Electrodep, Departament de Química Física, Universitat de Barcelona, Martí i Franquès 1, E-08028 Barcelona, Spain

Received 14 December 2004; received in revised form 4 January 2005; accepted 5 January 2005
Available online 26 January 2005

Abstract

Soft-magnetic ternary Co–Ni–Mo films were electrodeposited from a sulphate–citrate bath at pH 4.0 at a constant deposition rate of 2.5 μm h^{-1}. Both nickel and molybdenum incorporations in the ternary alloy were restrained in order to achieve low coercivity and maximum saturation magnetisation. 11–15 wt% Ni and 7–13 wt% Mo were considered the most appropriate percentage ranges for actuation applications in MEMS of the coatings. Deposits were silvery bright and showed low roughness. A nanometric grain size of ~8 nm was deduced from the X-ray diffractograms. A comparative corrosion study of Co, Co–Mo, Co–Ni and Co–Ni–Mo films was also carried out. Corrosion data demonstrated that small amounts of nickel in the deposits did not cause an E_{corr} shift towards more positive values but decreased the corrosion rate.

Keywords: Cobalt–nickel–molybdenum alloy; Electrodeposition; Corrosion

1. Introduction

In our laboratory, we undertook the preparation and characterisation of soft-magnetic Co–Mo electrodeposits compatible with silicon technology [1]. Molybdenum percentages lower than 15 wt% were needed to achieve coercivities clearly lower than that of pure cobalt with minimal decrease of the saturation magnetisation [2,3]. Further incorporation of nickel in the Co–Mo alloy would improve the corrosion resistance of the new material [4–6]. Nevertheless, it is desirable that the presence of nickel should not affect the magnetic behaviour of the Co–Mo alloy. Few studies concerning ternary Co–Ni–Mo alloys prepared by electrodeposition [7,8] or mechanically [9] have been reported, and those found are mainly based on their catalytic properties.

According to these premises, the first objective of this study was to test the electrodeposition capability for preparing ternary Co–Ni–Mo alloys controlling both molybdenum and nickel incorporation. On the one hand, molybdenum percentages in the ternary alloy might be similar to those achieved in the binary alloy if we want to maintain similar coercivity values. On the other hand, it is necessary to determine the nickel percentage that will improve corrosion resistance without decreasing excessively the saturation magnetisation.

Thus, an appropriate counterbalance between all of the electroactive species in the bath is necessary since electrodeposition of both the binary Co–Mo and Ni–Mo alloys is an induced process [10–13] and electrodeposition of the binary Co–Ni alloy is anomalous [14].

Once the desired composition of the ternary Co–Ni–Mo alloy is achieved, our second objective was to evaluate the morphological and structural properties as well as the magnetic behaviour and corrosion resistance of the deposits.

* Corresponding author. Tel.: +34 93 402 12 34; fax: +34 402 12 31.
E-mail address: e.valles@ub.edu (E. Vallés).

1388-2481/$ - see front matter © 2005 Elsevier B.V. All rights reserved.
doi:10.1016/j.elecom.2005.01.004

2. Experimental

The study of the electrodeposition process and deposit preparation was performed in a conventional three-electrode cell using a microcomputer-controlled potentiostat/galvanostat Autolab with PGSTAT30 equipment and GPES software. Solutions contained $CoSO_4$, $NiSO_4$, $Na_3C_6H_5O_7$ and Na_2MoO_4, all of analytical grade. H_2SO_4 was added to bring the pH to 4.0. All solutions were freshly prepared with water which was first doubly distilled and then treated with a Millipore Milli Q system. Solutions were de-aerated by argon bubbling before each experiment and maintained under argon atmosphere during it. The temperature was maintained at 25 °C.

For electrochemical study, a vitreous carbon (Metrohm) electrode of 0.0314 cm^2 was used as working electrode. It was polished to a mirror finish before each experiment using alumina of different grades (3.75 and 1.85 μm) and cleaned ultrasonically for 2 min in water. The reference electrode was an Ag/AgCl/1 mol dm^{-3} NaCl electrode mounted in a Luggin capillary containing 0.5 mol dm^{-3} Na_2SO_4 solution. All potentials are referred to this electrode. The counter electrode was a platinum spiral.

Voltammetric experiments were carried out under quiescent conditions at 50 mV s^{-1}, scanning initially from −500 mV towards negative potentials. Only one cycle was run in cyclic voltammetric experiments.

Various substrates were used for deposit preparation: vitreous carbon (Metrohm, 0.0314 cm^2), copper (Johnson Matthey 99.99%, 0.0314 cm^2), graphite (Alfa Aesar, 0.352 cm^2) and modified p-type 4–40 Ω cm ⟨1 0 0⟩ silicon samples with 0.3 cm^2 exposed area. The silicon surfaces were prepared for better adhesion and minimum mechanical stress by IMB-CNM.CSIC (Centro Nacional de Microelectrónica). A Ti(1000 Å)/Ni(500 Å) seed layer was sputtered on a previously grown phosphosilicate glass (PSG) layer 1 μm thick. This seed layer supplied an electrical connection for the electrodeposition process. The flat silicon-based substrates were cleaned with ethanol and then rinsed in water before each experiment.

Deposits were prepared under gentle stirring (60 rpm). Their morphology was examined with scanning electron microscopy, using a Hitachi S 2300. Deposit composition was determined by both electron probe micro-analyser (EPMA) with a CAMECA SX-50 microprobe and induced coupled plasma mass spectrometry (ICP-MS) with a Perkin–Elmer spectrometer Elan 6000. Data are reported in weight percentages (wt%). In the second case, films were dissolved in 1% nitric acid to perform the chemical analysis of the resulting solutions. ICP-MS analyses were also used to evaluate current efficiency involved in deposit preparation.

X-ray diffraction (XRD) phase analysis was performed on a Philips MRD diffractometer with low resolution parallel beam optics. Cu-Kα radiation (λ = 1.5418 Å) was selected by means of a diffracted beam flat graphite monochromator. $2\theta/\theta$ diffractograms were obtained in the 35–100° 2θ range with a step range of 0.05° and a measuring time of 5–65 s per step.

The roughness (rms) and thickness of the films were measured using a white-light interferometer from Zygo Corporation. Magnetic measurements were taken in a SQUID magnetometer at room temperature.

Corrosion experiments were performed at room temperature in 5% NaCl prepared with water which had been doubly distilled and treated with a Millipore Milli Q system, and with analytical grade reagents. The reference electrode was an Ag/AgCl/1 mol dm^{-3} NaCl mounted directly in a Luggin capillary. A platinum spiral served as a counter electrode. Flat specimens of 0.3 cm^2 exposed area were placed in the de-aerated NaCl solution for 3 h to determine the steady state potential (E_{ss}). Afterwards, a linear potentiodynamic sweep from E_{ss} − 300 to E_{ss} + 300 mV was carried out at 0.1 mV s^{-1} to determine E_{corr} and j_{corr}. Specimens were stationary during both polarisation and potentiodynamic scan. Average data from four replicates of each kind of specimen is reported.

3. Results

3.1. Bath design

The voltammetric response of baths containing fixed concentrations of complexing agent, cobalt (II) sulphate and nickel (II) sulphate but a variable concentration of sodium molybdate was analysed. An ion concentration ratio [Ni(II)]/[Co(II)] = 5 was chosen due to the anomalous nature of the Co–Ni deposition [14]. Molybdate concentration was kept low, between 0.005 and 0.012 mol dm^{-3} due to the great ability of molybdenum to incorporate into the deposit [2]. The onset of deposition was advanced as molybdate concentration in solution increased (Fig. 1). A reduction peak influenced by mass transport was recorded during the negative scan. In all cases, a low oxidation current was recorded during the positive scan from −600 mV. Q_{ox}/Q_{red} ratio was very low at any cathodic limit. This finding suggested that the species formed during the negative scan were hardly oxidised.

Chronoamperometric experiments were done from the baths previously studied by cyclic voltammetry. Our purpose was to determine molybdenum content in deposits formed potentiostatically on vitreous carbon in each case. Compositional data revealed that, for a given bath composition, molybdenum percentage decreased as the potential was made more negative

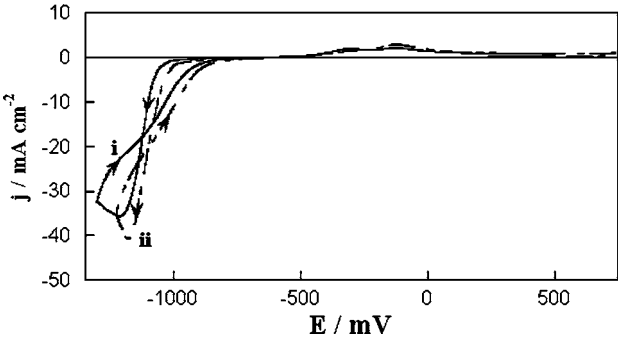

Fig. 1. Cyclic voltammetry of a 0.2 mol dm^{-3} $Na_3C_6H_5O_7$ + 0.05 mol dm^{-3} $CoSO_4$ + 0.25 mol dm^{-3} $NiSO_4$ + x mol dm^{-3} Na_2MoO_4 solution. (i) x = 0.005, (ii) x = 0.012.

(Table 1). Moreover, molybdenum percentage increased directly with molybdate concentration. High cobalt percentages were always obtained from the nickel (II)-rich solutions used. This corresponds to the anomalous Co–Ni deposition, even in the presence of the molybdate in the bath. Analogously, molybdenum codeposition took place by an induced codeposition mechanism even in the presence of two other metals.

According to the information gleaned from the tendencies observed, a 0.005 mol dm^{-3} molybdate concentration was chosen for subsequent assays, since molybdenum percentages <15 wt% were needed to obtain deposits showing low coercivity values. In this case, potentials/current densities needed to obtain the desired molybdenum percentages would be less negative than those used from higher molybdate concentrations, thereby minimising hydrogen evolution. Concentrations $[MoO_4^{2-}] < 0.005$ mol dm^{-3} were not considered of practical application since the faster depletion of the molybdate species would not assure the compositional stability of the plating bath. On the other hand, it was corroborated that a [Ni(II)]/[Co(II)] ratio in solution equal to five assured nickel percentages below 20 wt%.

3.2. Properties of the deposits

Several deposits were prepared potentiostatically from the selected bath (0.2 mol dm^{-3} $Na_3C_6H_5O_7$ + 0.05 mol dm^{-3} $CoSO_4$ + 0.25 mol dm^{-3} $NiSO_4$ + 0.005 mol dm^{-3} Na_2MoO_4) to examine their morphology, composition, structure, and magnetic properties. Graphite, copper and flat-silicon substrates were used as working electrodes since vitreous carbon favoured film detachment. Metal percentages were dependent on the applied potential, although the relative change was the smallest in the case of cobalt (Table 2). The molybdenum percentage fell and the nickel percentage increased as the potential was made more negative. The current efficiency (η) involved in deposit preparation was around 40%.

Co–Ni–Mo deposits were silvery bright. SEM images revealed that deposits with molybdenum percentages over ~6 wt% were cauliflower-like, showing incipient cracking as the thickness was increased (Fig. 2(a). In contrast, a non-homogeneous morphology tending to needle-like was observed for lower molybdenum percentages (Fig. 2(b)). Moreover, cracking was enhanced by increasing the deposition charge or by applying more negative potentials (Fig. 2(c)).

Structural analysis of the deposits was performed using X-ray diffraction. Copper substrates were used to improve deposit adherence. Co–Ni–Mo deposits with molybdenum percentages ranged between 4 and 12 wt% were analysed. Diffractograms showed a collection of main peaks assigned to the deposited film joined to two small peaks attributed to copper substrate (43.3 and 50.4° 2θ) (Fig. 3). Co–Ni–Mo deposits were crystalline and the main peaks corresponded to a single close-packed hexagonal structure (hcp). A certain 100 orientation was observed in the diffractogram. Peaks were broad, revealing a nanometric grain size. An average value of 8 nm grain size was estimated using Scherrer's equation. Peaks corresponding to intermetallic Co–Ni–Mo compounds were not detected, whereas other authors have reported the existence of Co_3Mo in deposits prepared by mechanical alloying [9].

The position of the coating peaks was similar to that of hcp cobalt, although the specific position was a function of the deposit composition. The lattice parameters of the hexagonal structure were calculated after fit profile and least square refinement (Table 3). Lattice parameters were similar to those of pure cobalt (a = 2.507 Å, c = 4.092 Å), although a slight increase was detected

Table 1
Composition of films obtained potentiostatically on vitreous carbon electrode under stirring. $[C_6H_5Na_3O_7]$ = 0.2 M, [Ni(II)] = 0.25 M and [Co(II)] = 0.05 M

$[MoO_4^{2-}]$ (mol dm^{-3})	$-E$ (mV)	%Co	%Ni	%Mo
0.005	900	72.9	12.2	14.9
0.007	850	71.0	10.8	18.2
0.012	850	66.1	12.7	21.2
	900	65.4	16.2	18.4

Table 2
Composition and current efficiency involved in deposit preparation from a 0.2 mol dm^{-3} $Na_3C_6H_5O_7$ + 0.05 mol dm^{-3} $CoSO_4$ + 0.25 mol dm^{-3} $NiSO_4$ + 0.005 mol dm^{-3} Na_2MoO_4 solution

Substrate	$-E$ (mV)	%Co	%Ni	%Mo	η (%)
Cu	890	72.6	13.7	13.7	26
Cu	900	74.5	15.1	10.4	40
Cu	950	76.5	18.0	5.5	41
Graphite	930	76.5	13.8	9.7	45
Graphite	935	75.0	17.6	7.4	38
Graphite	940	77.4	15.3	7.3	40

E is the applied potential.

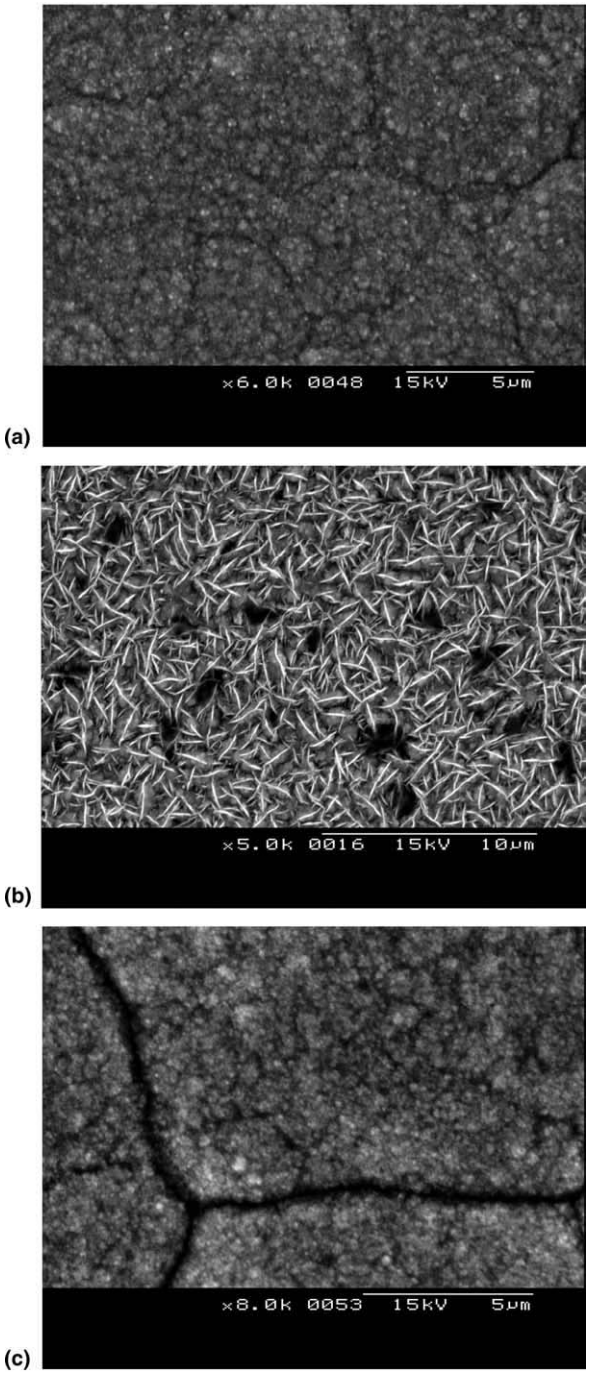

Fig. 2. SEM images of deposits obtained from a 0.2 mol dm^{-3} $Na_3C_6H_5O_7$ + 0.05 mol dm^{-3} $CoSO_4$ + 0.25 mol dm^{-3} $NiSO_4$ + 0.005 mol dm^{-3} Na_2MoO_4 solution. (a) At −930 mV over graphite, thickness 10 μm, 13.8 wt% Ni, 9.7 wt% Mo; (b) at −965 mV over copper, thickness 2 μm, 17.3 wt% Ni, 4.2 wt% Mo; (c) at −940 mV over graphite, thickness 42 μm, 15.3 wt% Ni, 7.3 wt% Mo.

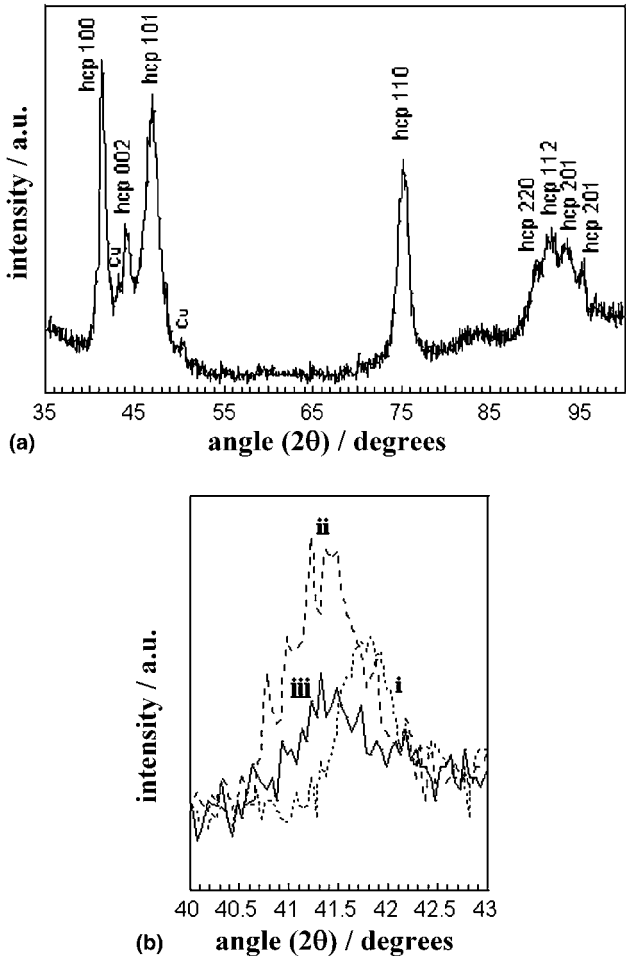

Fig. 3. (a) X-ray diffractogram of a Co–Ni–Mo deposit obtained from a 0.2 mol dm^{-3} $Na_3C_6H_5O_7$ + 0.05 mol dm^{-3} $CoSO_4$ + 0.25 mol dm^{-3} $NiSO_4$ + 0.005 mol dm^{-3} Na_2MoO_4 solution, 79 wt% Co, 17 wt% Ni, 4 wt% Mo, thickness 10 μm. (b) X-ray diffractogram in the range 40–43° 2θ of (i) 79 wt% Co, 17 wt% Ni, 4 wt% Mo, thickness 17 μm; (ii) 78 wt% Co, 13 wt% Ni, 9 wt% Mo, thickness 16 μm; (iii) 77 wt% Co, 11 wt% Ni, 12 wt% Mo, thickness 19 μm.

Table 3
Lattice parameters obtained from diffractograms corresponding to Co–Ni–Mo alloys of different composition

%Co	%Ni	%Mo	a (Å)	c (Å)
79	17	4	2.507	4.089
78	13	9	2.522	4.097
77	11	12	2.529	4.098

for parameter a as molybdenum percentage increased and as that of nickel decreased. Very low variation was detected for parameter c.

The increase of lattice parameter a of the ternary crystalline Co–Ni–Mo films is connected with the shift of peak positions to lower 2θ values with respect to those of pure-cobalt. From a structural point of view, Ni and Mo incorporate in the ε-Co phase. Since the atomic radius of Ni and Co is similar and the atomic radius of Mo is greater than that of Co, the lattice of the Co phase expanded as a consequence of the dissolved molybdenum.

The magnetic behaviour of Co–Ni–Mo films was analysed by taking hysteresis loops. A saturation magneti-

sation of 110 emu g^{-1} and a coercivity of 65 Oe were obtained (Fig. 4). In previous works the magnetic properties of Co–Mo deposits of similar thickness prepared in the same sulphate–citrate medium were measured, leading to similar coercivity values but a slightly higher saturation magnetisation (M_s = 120 emu g^{-1}) [3]. Therefore, the nickel amounts introduced in the film did not appreciably modify the magnetic properties of the material.

The roughness of Co–Ni–Mo films deposited on flat silicon-based substrates was also measured. Thin films showed very low rms values (~3 nm), which were of the same order of magnitude as that of the substrate (Table 4). However, thicker Co–Ni–Mo layers exhibited higher rms values due to incipient cracking.

Deposition rate was determined on flat silicon-based substrates, given that these films are of great interest due to their possible application in silicon technology devices. Growth rate was deduced after plotting the film thickness of deposits obtained at a given potential vs. the deposition time. Thickness was measured by white-light interferometry from the step height between the substrate and the coating. A constant growth rate of 2.5 μm h^{-1} was obtained.

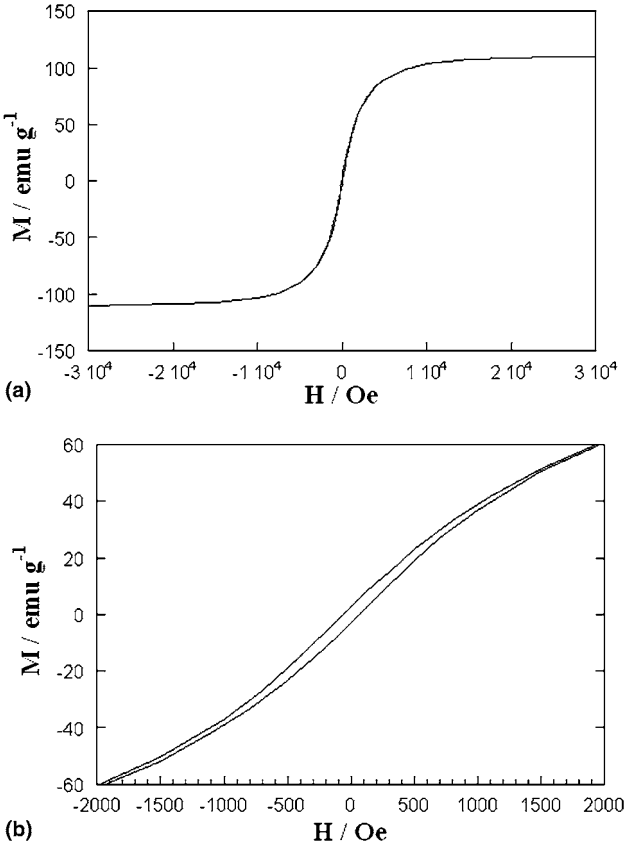

Fig. 4. (a) Parallel hysteresis loop and (b) zoomed detail for a deposit of 77 wt% Co, 16 wt% Ni, 7 wt% Mo, thickness 42 μm.

Table 4
Average roughness of Co–Ni–Mo coatings obtained on flat silicon-based substrates at fixed potential (−945 mV) but different deposition times

t (s)	rms (nm)
0	6
100	3
250	2
500	3
850	54
1250	97
2000	94

3.3. Corrosion experiments

A comparative study based on the corrosion behaviour of Co, Co–Ni, Co–Mo and Co–Ni–Mo films deposited on flat silicon-based substrates was performed. Film thickness was 2 μm. The corrosion phenomena occurring at the electrode/electrolyte interface was similar for all coatings. At immersion, the steady-state potential was reached rapidly and no further changes greater than 5 mV h^{-1} were observed. Fig. 5(a) shows a representative potentiodynamic curve of cobalt and cobalt-based alloys, in which an oxidation peak is followed by a passive range assigned to the formation of a barrier cobalt oxide film [15]. The dissolution of the barrier film depends on the pH of the solution. In neutral solutions,

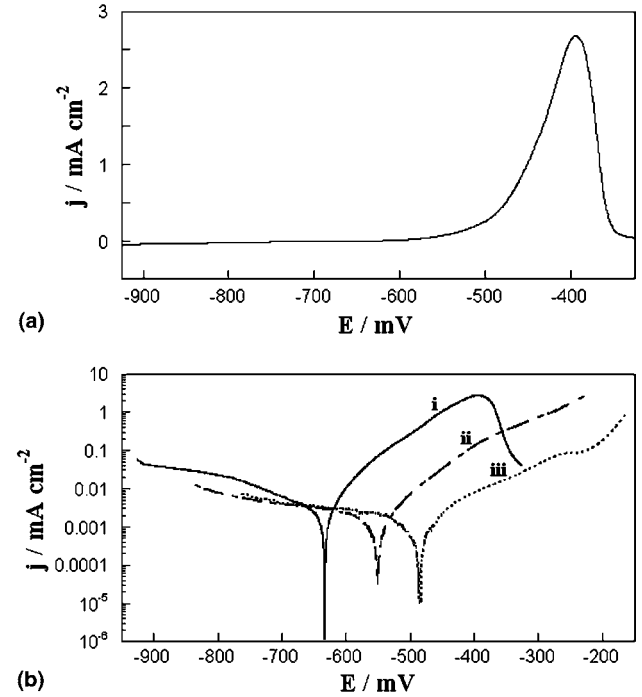

Fig. 5. (a) Potentiodynamic curve of a Co deposit prepared from a 0.2 mol dm^{-3} $Na_3C_6H_5O_7$ + 0.3 mol dm^{-3} $CoSO_4$ solution. (b) Potentiodynamic polarisation curves in logarithmic scale corresponding to Co–Ni deposits (i) 0 wt% Ni, (ii) 27 wt% Ni, (iii) 38 wt% Ni.

Table 5
Corrosion data of various cobalt-based coatings

Bath	Coating	$-E$ (mV)	$-E_{ss}$ (mV)	$-E_{corr}$ (mV)	j_{corr} (μA cm^{-2})
0.3 M $CoSO_4$	Co	935	625	633	7.7
0.3 M $CoSO_4$ + 0.012 M Na_2MoO_4	Co–11%Mo	930	630	668	3.2
0.05 M $CoSO_4$ + 0.25 M $NiSO_4$ + 0.005 M Na_2MoO_4	Co–12%Ni–13%Mo	945	620	636	1.5
0.05 M $CoSO_4$ + 0.25 M $NiSO_4$	Co–27%Ni	960	525	545	2.0
0.2 M $CoCl_2$ + 0.9 M $NiCl_2$	Co–38%Ni	800	462	470	2.1

E was the potential applied to prepare them.
$[Na_3C_6H_5O_7] = 0.2$ mol dm^{-3}.

the corrosion process would involve the electroformation of CoO [15]. In contrast, the passive film is unstable in acidic solutions, leading to higher corrosion rates [16].

The effect of nickel incorporation into cobalt deposits on the corrosion behaviour of the coatings was studied. The potentiodynamic polarisation curves of Co and Co–Ni deposits revealed that E_{corr} moved towards more positive potentials as nickel percentage in the deposit increased (Fig. 5(b)). E_{corr} was similar to E_{ss} in all cases. Indeed, j_{corr} decreased. According to these results, Co–Ni alloys had better anticorrosion properties than pure Co deposits.

However, E_{corr} did not appreciably vary when deposits contained low nickel percentages. E_{corr} values were similar for Co, Co–Mo and Co–Ni–Mo, although a lower j_{corr} was observed for the Co–Ni–Mo films (Table 5). The decrease of j_{corr} was understandable because voltammetric experiments showed a clearly lower oxidation current than that recorded from a nickel-free Co–Mo bath [2].

4. Conclusions

The preparation of a ternary Co–Ni–Mo alloy was successfully achieved in accordance with our initial goal: to obtain by electrodeposition homogeneous magnetic coatings of a specific composition under a reasonable current efficiency. The developed Co–Ni–Mo layers fit the magnetic requirements and the corrosion resistance properties needed in the fabrication of magnetic MEMS as magnetomechanic micropumps.

A low molybdate concentration in solution (0.005 mol dm^{-3}) is recommended to obtain <15 wt% molybdenum. Higher molybdenum percentages would significantly decrease the saturation magnetisation.

Data obtained from the selected plating bath revealed that cobalt percentage in the deposits was little dependent on the applied potential, whereas nickel and molybdenum percentages increased and decreased, respectively as the applied potential was made more negative. Molybdenum percentages can be achieved in the Co–Ni–Mo deposits similar to those obtained in the Co–Mo films because the induced behaviour of molybdenum discharge is maintained. The only prevention consists in working with high [Ni(II)]/[Co(II)] ratios in solution to obtain cobalt-rich deposits, since Co–Ni deposition is anomalous. According to these tendencies, it seems that the mechanism explaining binary Co–Mo deposition should not be significantly modified in spite of the introduction of nickel into the bath.

The Co–Ni–Mo deposits obtained were crystalline. However, other authors have reported the preparation of amorphous Co–Mo–Ni films using direct current electroplating from a sulphate–citrate bath at pH 10.5 [17,18]. Coatings were fine-grained and mirror-bright. The nanometric crystallite size and the low roughness measured from Co–Ni–Mo surfaces could explain the film brightness.

Co–Ni–Mo deposits prepared did not worsen the magnetic properties, but showed better anticorrosion properties than Co–Mo films. It is known that Ni–Mo alloys exhibit good corrosion resistance [6,11,19]. This study has demonstrated that important Ni amounts in cobalt electrodeposits clearly improved corrosion resistance. Moreover, corrosion resistance increased in the following order: Co < Co–Mo < Co–Ni–Mo, according to j_{corr} values. However, no clear variations of E_{corr} were observed, probably because both Mo and Ni percentages were discrete in the prepared coatings. In fact, these films are not so different from the pure-cobalt ones, even in terms of the crystalline structure. According to these results, nickel incorporation in Co–Mo layers would make them useful in MEMS applications for a longer period. Further work is in progress to reduce the stress in these coatings.

Acknowledgements

The authors thank the Serveis Cientificotècnics (Universitat de Barcelona) and the Servei de Magnetoquímica (Universitat de Barcelona) for the use of their equipment. The authors also thank the CNM for supplying silicon-based substrates. This paper was supported by contract MAT 2003-09483-C02-01 from the *Comisión Interministerial de Ciencia y Tecnología (CICYT)* and by the *Comissionat* of the *Generalitat de*

Catalunya under Research Project 2001 SGR 00046. E. Pellicer also thanks the DURSI of the *Generalitat de Catalunya* for a PhD grant.

References

[1] E. Gómez, E. Pellicer, E. Vallés, Electrochem. Commun. 6 (2004) 853.
[2] E. Gómez, E. Pellicer, E. Vallés, J. Electroanal. Chem. 568 (2004) 29.
[3] E. Gómez, E. Pellicer, E. Vallés, Surf. Coat. Technol. on line.
[4] H.H. Uhlig, P. Bond, H. Feller, J. Electrochem. Soc. 110 (1963) 650.
[5] W.Z. Friend, Corrosion of Nickel and Nickel Alloys, Wiley–Interscience, New York, 1980, pp. 95–135, 248.
[6] J. Crousier, M. Eyraud, J.-P. Crousier, J.-M. Roman, J. Appl. Electrochem. 22 (1992) 749.
[7] C. Fan, D.L. Piron, P. Paradis, Electrochim. Acta 39 (1994) 2715.
[8] I.A. Raj, K.I. Vasu, J. Appl. Electrochem. 22 (1992) 471.
[9] E.M. Arce-Estrada, V.M. Lopez-Hirata, L. Martinez-Lopez, H.J. Donantes-Rosales, M.L. Saucedo-Muñoz, F. Hernández-Santiago, J. Mat. Sci. 38 (2003) 275.
[10] A. Brenner, Electrodeposition of Alloys, vol. 2, Academic Press, New York, London, 1963, pp. 413–455.
[11] E. Chassaing, K.V. Quang, R. Wiart, J. Appl. Electrochem. 19 (1989) 839.
[12] E.J. Podlaha, D. Landolt, J. Electrochem. Soc. 144 (1997) 1672.
[13] E. Gómez, E. Pellicer, E. Vallés, J. Electroanal. Chem. 517 (2001) 109.
[14] E. Gómez, J. Ramirez, E. Vallés, J. Appl. Electrochem. 28 (1998) 71.
[15] W.A. Badawy, F.M. Al-Kharafi, J.R. Al-Ajmi, J. Appl. Electrochem. 30 (2000) 693.
[16] A. Aledresse, A. Alfantazi, J. Mat. Sci. 39 (2004) 1523.
[17] C.-F. Chu, S.-T. Wu, J. Electrochem. Soc. 147 (2000) 2190.
[18] C.-F. Chu, S.-T. Wu, J. Electrochem. Soc. 71 (2001) 248.
[19] E. Chassaing, M.P. Roumegas, M.F. Trichet, J. Appl. Electrochem. 25 (1995) 667.

4.5.3 Resum de resultats

A partir d'un bany sulfat-citrat a pH=4.0 és possible obtenir dipòsits ternaris Co-Ni-Mo coherents, de composició controlada i constant en profunditat i amb una eficiència de corrent ~40%. Una relació [Ni(II)]:[Co(II)]=5:1 en solució és apropiada per obtenir dipòsits base cobalt amb percentatges de níquel inferiors al 20%. Així mateix, una concentració 0.005 mol dm^{-3} de Na_2MoO_4 en solució assegura també incorporacions de molibdè de l'ordre del 4-13%.

Els dipòsits Co-Ni-Mo obtinguts són platejats i la seva composició depèn del potencial aplicat, de manera que el percentatge de molibdè disminueix i el de níquel augmenta a mesura que el potencial es fa més negatiu. Els dipòsits amb percentatges de molibdè superiors al 6% aprox. presenten una morfologia tipus col-i-flor, mentre que els dipòsits amb percentatges inferiors no són homogenis i tendeixen cap a una morfologia acicular típica del Co hcp amb orientació (hk0). Per bé que els dipòsits prims són compactes i coherents, s'observen esquerdes incipients a mesura que s'incrementa el gruix d'aquests dipòsits o s'apliquen potencials de deposició més negatius.

Els dipòsits Co-Ni-Mo són cristal·lins, amb una estructura hcp i un cert predomini de l'orientació (100). Els pics de difracció, però, presenten una amplada més gran que la instrumental, la qual cosa revela que la mida de gra és nanomètrica. La incorporació de níquel i molibdè a les capes de cobalt fa que s'expandeixi la xarxa cristal·lina de la fase ε-Co i que en resultin valors del paràmetre de xarxa *a* superiors, encara que el paràmetre *c* es manté pràcticament constant.

Incorporacions de níquel de l'ordre del 16% a capes Co-Mo amb 7-13% Mo no modifiquen apreciablement les propietats magnètiques del material. S'obtenen valors d'H_c similars als de l'aliatge Co-Mo (65 Oe) i valors de M_s lleugerament inferiors quan es comparen les corbes d'histèresi de dipòsits binaris i ternaris de gruix similar. Aquestes

capes ternàries preparades, doncs, també satisfan els requeriments necessaris perquè puguin ser implementades en MEMS.

Els dipòsits, a més, poden obtenir-se sobre substrats Si/capa llavor. Així, s'han preparat dipòsits Co-Ni-Mo coherents amb una rugositat molt baixa i a una velocitat, encara que inferior a la del Co-Mo, de 2.5 μm h^{-1}.

Els experiments de corrosió demostren que la incorporació de níquel a les capes binàries Co-Mo augmenta la resistència a la corrosió del material. Encara que no té lloc un desplaçament d'E_{corr} cap a potencials més positius, la qual cosa és raonable tenint en compte que s'incorporen percentatges baixos de níquel, la velocitat de corrosió sí que disminueix clarament.

La introducció de níquel a les capes Co-Mo no tan sols millora la resistència a la corrosió del material, sinó que també contribueix a augmentar la flexibilitat de les làmines, refinar-ne el gra i disminuir-ne la rugositat.

4.6 Implementació final dels electrodipòsits

4.6.1 Finalitat

Després de l'estudi electroquímic i de caracterització dels electrodipòsits Co-Mo i Co-Ni-Mo, es pretenia assajar la implementació d'aquests dipòsits en la tecnologia de MEMS.

En el cas del sistema binari es van testar capes amb baixos continguts de molibdè (~11%) obtingudes a partir del bany 0.2 mol dm^{-3} citrat + 0.3 mol dm^{-3} $CoSO_4$ + 0.012 mol dm^{-3} Na_2MoO_4 a pH=4.0, que havien estat optimitzades anteriorment.

En el cas del sistema ternari es van testar les capes desenvolupades en el capítol anterior, que contenien percentatges baixos tant de molibdè com de níquel. Abans de procedir a l'assaig tecnològic de les capes ternàries, però, es va estudiar l'ús d'un agent antiestressant com a mesura per reduir les tensions observades en aquests dipòsits a mesura que se n'augmentava el gruix. Es va estudiar l'efecte de l'agent antiestressant no tan sols sobre la coherència dels dipòsits sinó també sobre el procés de deposició, morfologia, composició, estructura i resistència a la corrosió de les làmines.

Una vegada es van optimitzar les capes Co-Ni-Mo, es va realitzar una anàlisi comparativa de les làmines binàries i ternàries pel que fa a propietats mecàniques i magnètiques. Aquest estudi comparatiu es va dur a terme en làmines primes de gruix controlat, apropiat per actuació magnètica, perquè fos immediat correlacionar els resultats obtinguts amb el comportament real que tindrien els electrodipòsits si s'incorporessin en MEMS.

Es va estudiar la selectivitat de la deposició Co-Mo i Co-Ni-Mo sobre substrats Si/capa llavor fotolitografiats i es van inspeccionar les

microestructures electrodipositades un cop eliminada la fotoresina, en particular la verticalitat de les parets laterals. També es va examinar la qualitat final de capes contínues després de sotmetre-les a un procés d'eliminació del substrat (silici) sobre del qual havien estat electrodipositades. L'eliminació del silici es va dur a terme en un medi d'hidròxid de tetrametilamoni (TMAH) al 25% i a 80ºC.

En darrer lloc es va provar la incorporació de làmines Co-Mo i Co-Ni-Mo de 2 μm en un prototipus de vàlvula consistent en un cos micromecanitzat de silici de 7-8 μm. Es va avaluar la deflexió de la vàlvula en cada cas sota l'acció d'un camp magnètic extern (M_s=1,2 T) i la seva resistència després de diversos cicles de *bending*.

Els resultats detallats d'aquest capítol s'inclouen en el següent article:

Molybdenum alloy electrodeposits for magnetic actuation
Enviat per a la seva publicació a la revista Electrochimica Acta

Molybdenum alloy electrodeposits for magnetic actuation

Assumpte: Your submission
Data: Wed, 07 Sep 2005
De: electrochim.acta@unimit.it
A: e.valles@ub.edu

Ms. Ref. No.: EAST05-444R1
Title: Molybdenum alloy electrodeposits for magnetic actuation
Electrochimica Acta

Dear Prof. Elisa Vallés,

I am pleased to inform you that the revised manuscript has been accepted for publication without further modifications. The manuscript will now go to the Production Department of Elsevier for technical editing. You will receive the proofs from the printers in due course.

Thank you for submitting your work to this journal.

With kind regards,

Sergio Trasatti
Editor-in-Chief
Electrochimica Acta

Molybdenum alloy electrodeposits for magnetic actuation

E. Gómez[1], E. Pellicer[1], M. Duch[2], J. Esteve[2], E. Vallés[1,*]

[1]Electrodep, Departament de Química Física, Universitat de Barcelona, Martí i Franquès 1, E-08028 Barcelona, Spain.

[2]Departament de Microsistemes, Centre Nacional de Microelectrònica (CNM-IMB), Campus Universitat Autònoma de Barcelona, E-08193 Bellaterra, Spain.

*Author to whom correspondence should be addressed
e-mail: e.valles@ub.edu
Phone: 34 93 403 92 38
Fax: 34 402 12 31

Abstract

This paper deals with the preparation and characterisation of alloys containing molybdenum applicable in MEMS. An electrodeposition process for achieving a homogeneous, low-stressed, soft-magnetic Co-Ni-Mo alloy is described. The electrochemical study allows setting bath composition and deposition conditions useful to perform the deposition process. Deposits with low nickel and molybdenum percentages (11-15 wt%) are virtually useful for magnetic actuation applications. Saccharine is an effective antistress agent and it also decreases grain size and surface roughness of the Co-Ni-Mo layers. The mechanical and magnetic properties of the ternary alloy have been compared with those shown by a binary Co-Mo alloy containing similar molybdenum percentages previously electrodeposited in our laboratory. Thin Co-Ni-Mo films exhibited higher microhardness values than Co-Mo films and better magnetic properties for magnetic actuation (H_c=50 Oe, M_r=90 emu g^{-1} and μ_r=670). Furthermore, film appearance (such as brightness) and corrosion resistance improved due to nickel presence. Electrodeposition has been tested on silicon/seed-layer substrates and the process selectivity has been investigated on photolithographed silicon. Both alloys are compatible with fabrication techniques involved in MEMS technology. No damage was observed when silicon was removed over alloy films to get stand-alone layers. The response of a microsized valve (silicon+seed-layer+electrodeposited Co-Mo or Co-Ni-Mo film) under an external magnetic field has been explored with good results.

Keywords: electrodeposition, cobalt-molybdenum, cobalt-nickel-molybdenum, MEMS, magnetic alloys

1. Introduction

Interest in electroplating alloys containing molybdenum developed mainly due to the resistance to corrosion and wear of the films [1-5]. In addition, some of them exhibit catalytic properties and usually have soft-magnetic characteristics [6-12]. Nowadays, the interest in applications of microelectromechanical systems (MEMS) has increased. The microelectromechanical technology is a broad area with many applications in e.g. biomedicine, microfluidics and integrated circuits. Electrochemical microfabrication presents competitive advantages over physical methods: high mass-production, low-cost and the ability of plating thin layers on non-flat substrates.

In many applications for magnetic actuators low coercivity, high saturation magnetisation and large permeability are required. Although electrodeposited Permalloy (80%Ni-20%Fe) has been the most widely used in magnetic microdevices, the interest in applications of MEMS has expanded to cobalt-based alloys [13-16]. It has been demonstrated in previous works that molybdenum incorporation in cobalt deposits causes a worthy decrease of the coercive force [17]. The magnetic properties of electrodeposited Co-Mo alloy were principally dictated by the composition of the deposits which, in turn, were determined by electrolyte composition and the applied potential during electrodeposition. Molybdenum can not be deposited alone in aqueous solutions, but it can be co-discharged with an iron-group metal in the presence of specific complexing agents [18]. An acid sulphate-citrate medium was capable of plating coherent Co-Mo films according to an induced process [19]. Best soft-magnetic results were obtained for deposits with molybdenum percentages ~11%.

In order to improve the properties of the developed Co-Mo electrodeposits, a third alloying element was added. With this aim, ternary Co-Ni-Mo layers were plated from a sulphate-citrate medium at pH 4.0 and characterised [20]. In addition to the induced discharge of

molybdenum, deposition of cobalt and nickel occurred according to an anomalous process [21]. It was demonstrated that the electrochemical technique was capable of plating Co-Ni-Mo deposits of a desired composition in spite of the complexity of the electrodeposition process. A nickel percentage between 11 and 15% was considered appropriate since it did not cause a large decrease of the saturation magnetisation, improved the appearance of the deposits and the corrosion resistance of the material. However, the developed ternary layers showed stress, which was enhanced as the applied potential was made more negative or the deposit thickness was increased.

Taking into account the promising magnetic properties of the ternary Co-Ni-Mo alloy and the chance for using it in MEMS applications, further investigation is required. In this work, the addition of an antistress agent to the bath is tested as a way of improving the layers quality. The effect of the antistress agent on the deposition process as well as on the morphological, structural and corrosion properties of the deposits has been investigated. Photolithographed silicon-based substrates have been used to explore the deposition selectivity and the profile of the patterned microstructures.

Although the magnetic response of thick (30-40 μm) Co-Mo and Co-Ni-Mo layers had been already studied [19, 20], the magnetic properties of thin layers were not investigated. Since few micrometers are required for magnetic actuation, a comparison between these two alloys has been carried out in terms of magnetic, mechanical and chemical properties of thin films. To this end, thin Co-Mo and Co-Ni-Mo coatings have been electrodeposited on silicon/seed-layer substrates. The magnetic layers have been released in order to determine their resistance to chemical treatment such as etching without damage. This condition is essential to assure that Co-Mo and Co-Ni-Mo alloys are truly compatible with MEMS technology. Finally, test devices have been developed to study the response of both alloys when an external magnetic field is applied.

2. Experimental

The study of the electrodeposition process and the deposit preparation were performed in a conventional three-electrode cell using a microcomputer-controlled potentiostat/galvanostat Autolab with PGSTAT30 equipment and GPES software. Reagents used were $CoSO_4$, $NiSO_4$, $Na_3C_6H_5O_7$, Na_2MoO_4 and saccharine, all of analytical grade. H_2SO_4 was added to bring the pH to 4.0. All solutions were freshly prepared with water which was first doubly distilled and then treated with a Millipore Milli Q system. Solutions were de-areated by argon bubbling before each experiment and maintained under argon atmosphere during it. The temperature was maintained at 25ºC.

For electrochemical study, a vitreous carbon (Metrohm) electrode of 0.0314 cm^2 was used as working electrode. It was polished to a mirror finish before each experiment using alumina of different grades (3.75 and 1.85 μm) and cleaned ultrasonically for 2 min in water. The reference electrode was an Ag/AgCl/1 mol dm^{-3} NaCl electrode mounted in a Luggin capillary containing 0.5 mol dm^{-3} Na_2SO_4 solution. All potentials are referred to this electrode. The counter electrode was a platinum spiral.

The electrochemical study was performed using cyclic voltammetry and linear sweep voltammetry (LSV) (combining negative and positive scans). Experiments were carried out under quiescent or stirring conditions at 50 mV s^{-1}. Cyclic Voltammetric experiments and negative LSV scans were performed from –500 mV towards negative potentials. LSV positive scans were carried out from –400 mV towards positive potentials. A single cycle was run in cyclic voltammetric experiments.

Deposits were prepared under gentle stirring (60 rpm) on modified p-type 4-40 Ω cm ⟨100⟩ silicon samples. The surfaces of 500 μm thick silicon were prepared for better adhesion and minimum mechanical stress. A Ti(1000Å)/Ni(500Å) seed-layer was sputtered on the silicon

to supply an electrical connection for the electrodeposition process. The silicon-based substrates were cleaned with ethanol and rinsed in water before depositing. Photolithographed Si/Ti/Ni substrates were used to plate alloy microstructures. Copper substrates (Johnson Matthey) of 0.63 cm^2 were used when electrodepositing thick films. Copper electrodes were polished using sandpaper (2400 and 4000) followed by damp alumina of 0.3 μm.

Corrosion experiments were performed at room temperature in 5% NaCl prepared with water which had been doubly distilled and treated with a Millipore Milli Q system, and with analytical grade reagents. The reference electrode was an Ag/AgCl/1 mol dm^{-3} NaCl mounted directly in a Luggin capillary. A platinum spiral served as a counter electrode. Flat specimens of 0.3 cm^2 exposed area were placed in the de-aerated NaCl solution for 3 hours to determine the steady state potential (E_{ss}). Afterwards, a linear potentiodynamic sweep from E_{ss}–300 mV to E_{ss}+300 mV was carried out at 0.1 mV s^{-1} to determine E_{corr} and j_{corr}. Specimens were stationary during both polarisation and potentiodynamic scan. Average data from 4 replicas of each kind of specimen is reported.

Morphology of deposits was examined with scanning electron microscopy using a Hitachi S 2300, and their composition was determined by both electron probe micro-analyser (EPMA) with a CAMECA SX-50 microprobe and inductively coupled plasma optical emission spectrometry (ICP-OES) with a Perkin Elmer Optima 3200 RL. In the second case, films were dissolved in 1% nitric acid to perform the chemical analysis of the resulting solutions. ICP-OES analyses were also used to evaluate current efficiency involved in deposit preparation.

X-ray diffraction (XRD) phase analysis was performed on a Siemens D-500 diffractometer. $2\theta/\theta$ diffractograms were obtained in the 5–120 º2θ range with a step range of 0.05 º and a measuring time of

5s per step. Magnetic measurements were taken in a SQUID magnetometer at room temperature.

Roughness (rms) of the coatings was measured using a white-light interferometer from Zygo Corporation. Step height analysis and surface profiling of alloy microstructures were performed by means of the same equipment.

Gloss measurements were made using a micro-glossmeter of BYK-Gardner at an angle of incidence light of 60º. The calibration was performed automatically by means of a highly polished black standard integrated in the glossmeter. Multiple measurements with each coating were made, so data was evaluated statistically.

The mechanical properties were measured using a Fischerscope HV 100 tester with Vickers indenter and a final test load of 15 mN stepwise applied. Hardness value and Young's modulus were calculated by means of the universal microhardness test, which is based on the measurement of a microindentation depth under dynamic local and for a controlled load-unload cycle.

The silicon layer was removed over the alloy films by an anisotropic wet etching in 25% tetramethyl ammonium hydroxide (TMAH) solution. The TMAH etching was carried out at 80ºC under nitrogen stirring, with a water-cooling system to reduce changes in concentration due to evaporation.

A confocal imaging profiler with PLμ software was used to evaluate the bending effect induced by a permanent magnet on test devices.

3. Results

3.1. Saccharine effect on the Co-Ni-Mo deposit properties

Saccharine is known as levelling, brightening and antistress agent. It has been claimed that stress of some binary and ternary cobalt-based alloys can be reduced by adding a low saccharine concentration to the plating bath [16, 23], although non-appreciable effects were observed for Co-Mo deposition [19, 20]. A 0.005 mol dm^{-3} of saccharine was selected for attempting to minimise the stress of Co-Ni-Mo deposits prepared from a bath developed earlier in our laboratory (0.2 mol dm^{-3} $Na_3C_6H_5O_7$ + 0.05 mol dm^{-3} $CoSO_4$ + 0.25 mol dm^{-3} $NiSO_4$ + 0.005 mol dm^{-3} Na_2MoO_4 at pH 4.0).

First of all, the effect of saccharine on the deposition process was analysed by means of the voltammetric technique. Saccharine presence in the bath caused a delay in the onset of deposition and enhanced enormously alloy oxidation (Fig. 1). These features suggested us that deposit properties would change somewhat due to saccharine presence in the bath. In contrast, this additive did not promote significant changes in the electrochemical response of baths previously used to plate Ni-free Co-Mo coatings [20]. As long as the electrochemical response did not vary, the Co-Mo properties remained the same. Thus, saccharine would not show the same effect for all cobalt-based systems.

Under quiescent conditions, the voltammetric response showed a reduction peak related to mass transport in the negative scan and a double oxidation peak in the positive scan (Fig. 1, curve ii). Under stirring conditions the depletion of electroactive species near the electrode was avoided (Fig. 2a). Moreover, the oxidation response evolved to a single peak. According to this, stirring of the solution would assure homogeneous bath composition around the electrode and the formation of deposits with uniform composition.

The electrochemical tools were also useful to ascertain the potential range more appropriate to deposit homogeneous Co-Ni-Mo coatings as Figure 2b illustrates. Combined linear sweep voltammetries (LSV), i.e. single negative scan followed by a positive scan, were used. The shape of the oxidation response depended on the cathodic limit reached during the negative scan. A single oxidation peak was recorded when scanning up to a short cathodic limit, whilst a double peak was recorded when a larger cathodic limit was reached. In the second case, the sharp current increase observed during the negative scan after the reduction peak would be related to a great hydrogen coevolution. This hydrogen coevolution would be responsible of the formation of a different type of Co-Ni-Mo deposit on the electrode from that deposited before the current increase. Thus, it is important to select deposition potentials for which hydrogen coevolution is low.

According to the electrochemical results, the use of saccharine, stirring conditions and moderate deposition potentials were chosen to perform Co-Ni-Mo deposition. Several Co-Ni-Mo deposits were prepared potentiostatically and their properties were compared with those previously reported for deposits obtained from the saccharine-free bath [21]. When the alloy composition was evaluated, it was found that the nickel percentage increased and that of molybdenum decreased as the potential was made more negative (Table 1). Potentials between –930 and –950 can be applied to obtain Co-Ni-Mo deposits under reasonably high current efficiency of the desired composition, i.e. with moderate nickel and molybdenum incorporations. Lower efficiency values were achieved at more positive potentials because molybdenum oxide deposition began to be enhanced [24]. It was also noticed that the addition of a low saccharine concentration to the plating bath did not change the elemental composition of Co-Ni-Mo alloy [21]. However, the EPMA analysis of Co-Ni-Mo coatings obtained in the potential range mentioned above revealed that a small sulphur amount (0.16%) was included in the deposits.

Co-Ni-Mo deposits of the required composition prepared in the presence of saccharine were imaged by SEM. Non-cracked, very fine-grained films were obtained. In contrast, films of similar composition and deposition charge obtained from saccharine-free baths showed cracks (Fig. 3). Moreover, very low surface roughnesses were measured (Table 2). Without additives, the deposition rate had been estimated in 2.5 μm h^{-1} [21]. The presence of saccharine in the plating bath decreased slightly the deposition rate to 2.3 μm h^{-1}.

The crystallographic structure of Co-Ni-Mo films prepared from solutions containing saccharine was analysed using X-ray diffraction experiments and compared with that shown by deposits obtained from saccharine-free solutions. 16 μm thick samples containing molybdenum percentages around 11% were analysed, using copper as substrate. The coatings were crystalline, showing a close-packed hexagonal structure (hcp) (Fig. 4) with similar lattice parameters as those of Co-Ni-Mo deposits having similar composition but prepared without saccharine. However, the presence of saccharine in the electrolytic bath caused the loss of preferred orientation and induced a slight grain size decrease. This grain size reduction was linked to an increase of the full width at half maximum (FWHM) of the adjusted peaks (Table 3).

Corrosion experiments were carried out to evaluate whether the corrosion resistance was sensitive to the additive content in the deposits. To this end, a comparison of the potentiodynamic polarisation curves corresponding to Co-Ni-Mo deposits prepared with or without saccharine was made. The response of a Co-Mo deposit containing a similar molybdenum percentage was chosen as a reference. An oxidation peak followed by a passive range corresponding to the electroformation of a barrier film was observed in all cases. E_{corr} values did not differ significantly as seen in Figure 5, although it can be noticed that E_{corr} tends to shift towards more positive values for the Co-Ni-Mo alloy. In contrast, the corrosion rate

did differ appreciably between the binary and the ternary alloy, so that the latter exhibited lower j_{corr} values. Although several studies point out that sulphur inclusion in the deposits commonly improves the corrosion resistance [23], non-relevant differences were observed here. However, a zoomed detail of the potentiodynamic polarisation curves shows that sulphur presence in Co-Ni-Mo deposits seems to advance the onset of alloy oxidation instead of delaying it. This feature was in agreement with voltammetric experiments, since saccharine presence in the bath enhanced alloy oxidation. In order to gain a better understanding of this behaviour, the voltammetric response of baths containing a different saccharine concentration in the range 0.001-0.005 mol dm^{-3} was recorded. The purpose of this study was to evaluate whether the oxidation current depended on saccharine concentration. Figure 6 shows that Q_{ox}/Q_{red} ratio for 0.001 mol dm^{-3} of saccharine is high, almost the same as that shown in Figure 1, curve ii. Compositional analysis of deposits prepared in the presence of 0.001 mol dm^{-3} saccharine revealed that sulphur inclusion in the deposits decreased until 0.04%. Thus, a minimum amount of additive is enough to promote alloy oxidation.

According to these results, saccharine was appropriate to decrease the stress of the developed Co-Ni-Mo coatings without varying meaningfully the deposition rate and the corrosion behaviour. Moreover, smoother surfaces were achieved with saccharine. Although a minimum saccharine amount in solution would be enough, concentrations below 0.005 mol dm^{-3} would not be of practical interest. Too low concentrations can not assure a constant bath composition. For these reasons, Co-Ni-Mo deposits were prepared in the presence of 0.005 mol dm^{-3} saccharine for further assays.

3.2. Comparative study of mechanical and magnetic properties and brightness of electrodeposited Co-Mo and Co-Ni-Mo alloys. Selectivity of the electrodeposition processes

In previous works it was seen that Co-11%Mo deposits were dark and slightly matte. In contrast, Co-Ni-Mo deposits prepared here were silvery-bright. From a qualitative point of view, the presence of nickel in the alloy improved the appearance of the material. In order to evaluate deposit appearance from more rigorous scientific criteria, gloss measurements of Co-Mo and Co-Ni-Mo layers were carried out. The ternary alloy exhibited high gloss values close to those of the substrate, whereas the binary alloy showed markedly lower gloss values (Table 4). Differences in brightness can be explained taking into account grain size and roughness. Co-Ni-Mo deposits are finer grained and have smoother surfaces than Co-Mo deposits [20], which enhance reflection of light from their surfaces.

The mechanical properties of both alloys were also analysed. Table 4 lists the hardness and Young's modulus of 2 μm thick Co-Mo and Co-Ni-Mo layers deposited on silicon-based substrates. The ternary alloy was harder than the binary. This feature was in accordance with the compact appearance and fine-grained (nanometric size) characteristics of the ternary deposit. Consequently, the ternary alloy was more resistant to localized plastic deformation. This result was in agreement with the general belief that nickel improves the wear resistance of a material. However, since hardness is not the only parameter that gives us an idea of the mechanical behaviour of a material, Young's modulus should be considered. Sometimes it is wrongly taken for granted that the hardest material is the best one. Elasticity has to be also measured since this property is relevant when the implementation of a material in MEMS technology is being evaluated. Regarding the Young's modulus, Co-Mo and Co-Ni-Mo alloys showed lower values than that of the substrate, although it was noted that the binary alloy was slightly more elastic than the ternary.

The magnetic properties of thin Co-Mo and Co-Ni-Mo layers were compared. Films of 2 μm thick were plated on silicon-based substrates and afterwards detached from the electrode to analyse their magnetic response. Figure 7 shows the hysteresis loops of both films recorded by applying a magnetic field parallel to the films. Parallel field was applied because an easier magnetization than in the perpendicular direction had been previously observed for Co-Mo coatings [20]. Ternary Co-Ni-Mo films showed 110 emu g^{-1} of saturation magnetization. This value was similar as that of Co-Ni-Mo coatings of greater thickness but prepared in the absence of saccharine [21]. Incorporation of low nickel percentages in the electrodeposited Co-Mo films caused a slight decrease of the saturation magnetization. Coercivity, remanence and maximum permeability were estimated from the zoomed detail of the magnetic response in the low field range (Table 5). Permeability was calculated from the maximum value of the M-H slope in each case. Coercivity decreased while remanence and permeability clearly increased when nickel was incorporated to Co-Mo electrodeposits. Thus, the ternary films showed higher magnetic performance.

Although the selectivity of Co-Mo electrodeposition had been already tested with good results [20], information about the selectivity of Co-Ni-Mo electrodeposition lacks. For this reason, photolithographed silicon-based substrates were used as working electrodes to assess the selectivity of the ternary deposition process. Appropriate deposition times were selected to avoid overplating across the UV-photoresist. Electrodeposited Co-Ni-Mo microstructures were characterised after removing the UV-photoresist with acetone. No damage was produced on Co-Ni-Mo surfaces during acetone removal. SEM images of released Co-Ni-Mo microstructures revealed that well-defined patterns were achieved. Moreover, these microstructures showed fine-grained and smooth surfaces as seen in continuous plated layers, whereas Co-Mo microstructures were rougher, with coarse grains (Fig. 8). This feature was in agreement with rms values listed in Table 2 for the Co-Ni-Mo

since those reported for the Co-Mo alloy were higher [20]. White-light interferometric images showed uniform filling of the conductive zones of the substrate (Fig. 9a), even when the vertical dimensions were larger than the lateral dimensions (Fig. 9b), and vertical-side walls (Fig. 9c).

3.3. Release of Co-Mo and Co-Ni-Mo layers. Development of a magnetically driven microvalve

The compatibility of Co-Mo and Co-Ni-Mo alloys with MEMS fabrication technologies was evaluated taking into account two aspects: damage produced on the surfaces during the removal of the silicon layers over the alloy films and the magnetic response induced by an external magnetic field on a test device such as a microvalve.

Since it may be important to get stand-alone pieces in some applications, the possibility of removing silicon from the Co-Mo and Co-Ni-Mo layers was investigated. For this purpose, 2-3 μm thick alloy films were electrodeposited on silicon-based substrates. This film thickness was considered suitable for actuation applications [14]. After the electrodeposition step, the silicon layer was removed by immersing the samples in 25% TMAH solution. The silicon was completely eliminated at an etch rate of 25 μm h^{-1}. The Ti/Ni seed-layer was not removed since its small thickness did not affect the magnetic or the mechanical properties of the alloy films. Although it took us a long period of time to remove the silicon, no damage was observed on Co-Mo and Co-Ni-Mo layers. An appreciable bending effect of almost 90º was observed when a permanent magnet was brought near to the stand-alone layers.

After verifying that alloy films were compatible with etching processes involved in MEMS fabrication, the magnetic response of Co-Mo and Co-Ni-Mo deposits plated on a silicon micromachined valve was

checked. Several wet and dry etching processes were combined to obtain the body of the valve that was formed of 7-8 μm of silicon. Once the silicon structures were patterned a 1500Å seed layer was sputtered and 2 μm of Co-Mo or Co-Ni-Mo films were electrodeposited on top (Fig. 10a). The external magnetic field was induced by a Nd-Fe-B magnet (M_s=1.2 T). A bending effect of 30 and 40 μm was achieved for Co-Mo and Co-Ni-Mo microvalves respectively (Fig. 10b). The bending effect was enlarged as the deposit thickness increased. In both cases high robustness and flexibility of the deposited layers were observed in spite of the displacement induced by the magnet.

4. Conclusions

The present study demonstrates the electrodeposition skill at plating binary Co-Mo and ternary Co-Ni-Mo deposits which fit the mechanical and magnetic characteristics required in actuation applications. Analyses have been focused on deposits containing low molybdenum and nickel percentages with a view to their virtual implementation.

The stress of Co-Ni-Mo coatings can be effectively reduced by adding saccharine to the plating bath without altering their elemental composition, although a little sulphur inclusion took place when electroplating. Crack-free deposits have been imaged by SEM. Furthermore, saccharine decreased grain size and surface roughness. Cyclic voltammetry and LSV experiments were useful as a preliminary electrochemical study since data obtained suggested that saccharine would affect Co-Ni-Mo deposit properties. Thus, the electrochemical study can be used as a primary test to determine whether a particular additive is suitable or not. Regarding the corrosion properties, no significant differences were observed associated to the use of saccharine. It has been demonstrated that Co-Ni-Mo electrodeposition process is also highly selective. Well-defined Co-Ni-Mo microstructures

with vertical-side walls can be obtained on photolithographed silicon-based substrates.

Roughness and grain size played an important role on film brightness. The ternary Co-Ni-Mo films showed lower roughness and smaller grain size than Co-Mo films, which would enhance light reflection. Both alloy films displayed an easier magnetisation in the parallel direction with similar saturation magnetisation values. Acceptable coercivity, remanence and permeability values were measured in both cases, although the ternary alloy showed better magnetic characteristics for actuation. Besides, no damage was produced on Co-Mo and Co-Ni-Mo films during silicon etching, which also proves that they are compatible with fabrication processes involved in MEMS technology. Indeed, similar mechanical properties have been observed.

Magnetically driven microvalves composed of 2 μm thick Co-Mo or Co-Ni-Mo films on Si/Ti/Ni have been successfully developed. The microvalves were sensitive to an external magnetic field and no breakage occurred during operation.

Acknowledgments

The authors wish to thank the Serveis Cientificotècnics (Universitat de Barcelona) and the Servei de Magnetoquímica (Universitat de Barcelona) for the use of their equipment. The authors sincerely thank Ana Ibáñez (Universitat Autónoma de Madrid), who spared no effort to measure the mechanical properties of the films. This paper was supported by contract MAT 2003-09483-C02-01 from the *Comisión Interministerial de Ciencia y Tecnología (CICYT)* and by the *Comissionat* of the *Generalitat de Catalunya* under Research Project 2001 SGR 00046. E. Pellicer also thanks the DURSI of the *Generalitat de Catalunya* for the research fellowship.

References

1. W. Z. Friend, 'Corrosion of Nickel and Nickel Alloys', Wiley-Interscience, New York, 1980, pp. 95-135, 248.

2. E. Chassaing, K. Vu Quang, R. Wiart, J. Appl. Electrochem. 19 (1989) 839.

3. J. Crousier, M. Eyraud, J.-P. Crousier, J.-M. Roman, J. Appl. Electrochem. 22 (1992) 749.

4. E. J. Podlaha, D. Landolt, J. Electrochem. Soc. 143 (1996) 885.

5. E. Beltowska-Lehman, P. Ozga, E. Chassaing, Surf. Coat. Technol. 78 (1996) 233.

6. E. Beltowska-Lehman, J. Appl. Electrochem. 20 (1990) 132.

7. C. Fan, D. L. Piron, A. Sleb, P. Paradis, J. Electrochem. Soc. 141 (1994) 382.

8. C. Fan, D. L. Piron, P. Paradis, Electrochim. Acta 39 (1994) 2715.

9. W. P. Taylor, M. Schneider, H. Baltes, M. G. Allen, Electrochem. Solid Stat. Lett. 2 (1999) 624.

10. C.-C. Hu, C.-Y. Weng, J. Appl. Electrochem. 30 (2000) 499.

11. T. Sato, H. Takahashi, E. Matsubara, A. Muramatsu, Mat. Trans. 43 (2002) 1525.

12. P. R. Zabinski, H. Nemoto, S. Meguro, K. Asami, K. Hashimoto, J. Electrochem. Soc. 150 (2003) C717.

13. F. E. Rasmussen, J. T. Ravnkilde, P. T. Tang, O. Hansen, S. Bouwstra, in: Eurosensors, XIV European Conference on Solid State Transducers 2000, Denmark, p. 915.

14. M. Duch, J. Esteve, E. Gómez, R. Pérez-Castillejos, E. Vallés, J. Micromech. Microeng. 12 (2002) 400.

15. D. Kim, D. Y. Park, B. Y. Yoo, P. T. A. Sumodjo, N. Myung, Electrochim. Acta 48 (2003) 819.

16. F. Lallemand, D. Comte, L. Ricq, P. Renaux, J. Pagetti, C. Dieppedale, P. Gaud, Appl. Surf. Science 225 (2004) 59.

17. E. Gómez, E. Pellicer, E. Vallés, J. Electroanal. Chem. 568 (2004) 29.

18. A. Brenner, 'Electrodeposition of Alloys', vols. 1 and 2, Academic Press, New York, 1963.

19. E. Gómez, E. Pellicer, E. Vallés, Surf. Coat. Technol. 197 (2005) 238.

20. E. Gómez, E. Pellicer, E. Vallés, Electrochem. Commun. 6 (2004) 853.

21. E. Gómez, E. Pellicer, E. Vallés, Electrochem. Commun. 7 (2005) 275.

22. E. Gómez, E. Pellicer, E. Vallés, J. Electroanal. Chem. 580 (2005) 222.

23. F. Lallemand, L. Ricq, P. Berçot, J. Pagetti, Electrochim. Acta 47 (2002) 4149.

24. E. Gómez, E. Pellicer, E. Vallés, J. Electroanal. Chem. 580 (2005) 238.

Table 1. Composition in weight per cent and current efficiency (η) involved in Co-Ni-Mo deposit preparation on Si/Ti/Ni substrates. *E* is the applied potential.

$-E$ / mV	% Co	% Ni	% Mo	η / %
920	71.4	13.2	15.4	37
930	72.7	13.4	13.8	45
940	72.0	12.6	15.4	68
945	72.4	13.8	13.8	66
950	72.3	13.3	14.3	70
980	74.5	21.9	3.6	69
1000	71.6	22.6	1.0	67

Table 2. Roughness values of Co-Ni-Mo deposits obtained at a fixed potential (–930 mV) on Si/Ti/Ni substrates by applying different deposition times.

t / s	rms / nm
850	3.3
2000	5.4
2240	5.0
2800	8.5
3600	5.9
4500	25.7

Table 3. FWHM values for the diffraction peaks corresponding to Co-Ni-Mo coatings obtained in the presence of saccharine and in its absence.

	FWHM / degrees	
peak	saccharine-free	with saccharine
100	0.74	0.93
101	1.67	2.19
110	1.14	1.28

Table 4. Universal microhardness (H_U), Young's modulus (E) and gloss of 2 μm thick electrodeposited Co-Mo and Co-Ni-Mo films. The values for the substrate (Si/Ti/Ni) are also reported.

Sample	H_U / GPa	E / GPa	Gloss /gloss units
substrate	7.1±0.3	192±7	584±8
Co-11%Mo	2.5±0.1	119±5	185±7
Co-14%Ni-13%Mo	4.4±0.1	157±5	458±9

Table 5. Coercivity (H_c), remanence (M_r) and permeability (μ_r) of 2 μm thick Co-Mo and Co-Ni-Mo films.

Sample	H_c / Oe	Mr / emu g^{-1}	μ_r
Co-11%Mo	70	60	130
Co-14%Ni-13%Mo	50	90	670

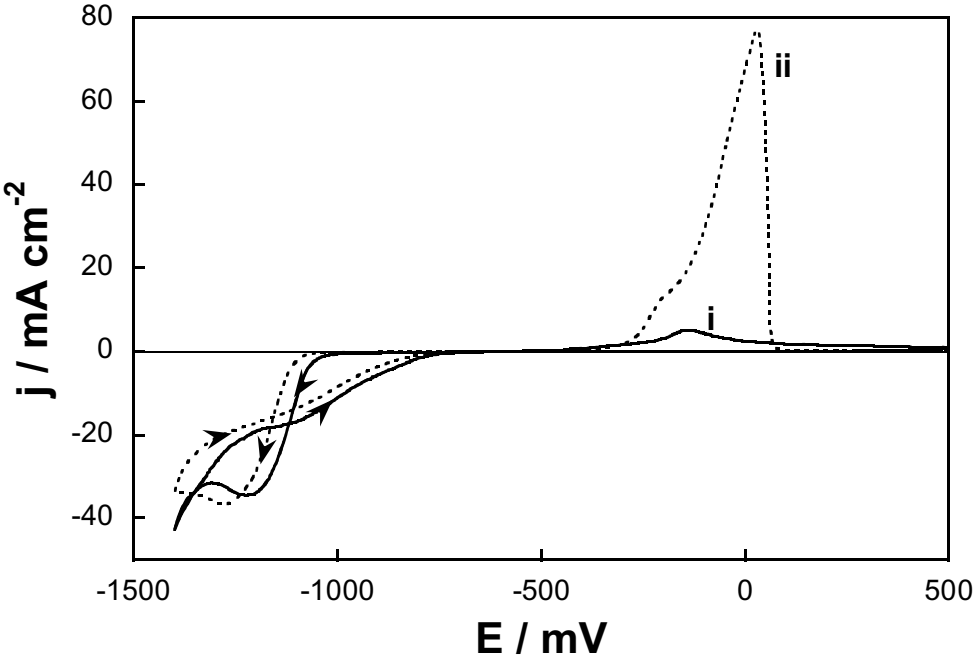

Figure 1. Cyclic voltammetry of a 0.2 mol dm^{-3} $Na_3C_6H_5O_7$ + 0.05 mol dm^{-3} $CoSO_4$ + 0.25 mol dm^{-3} $NiSO_4$ + 0.005 mol dm^{-3} Na_2MoO_4 solution (i) saccharine-free and (ii) with 0.005 mol dm^{-3} saccharine. Cathodic limit: −1400 mV. Quiescent conditions.

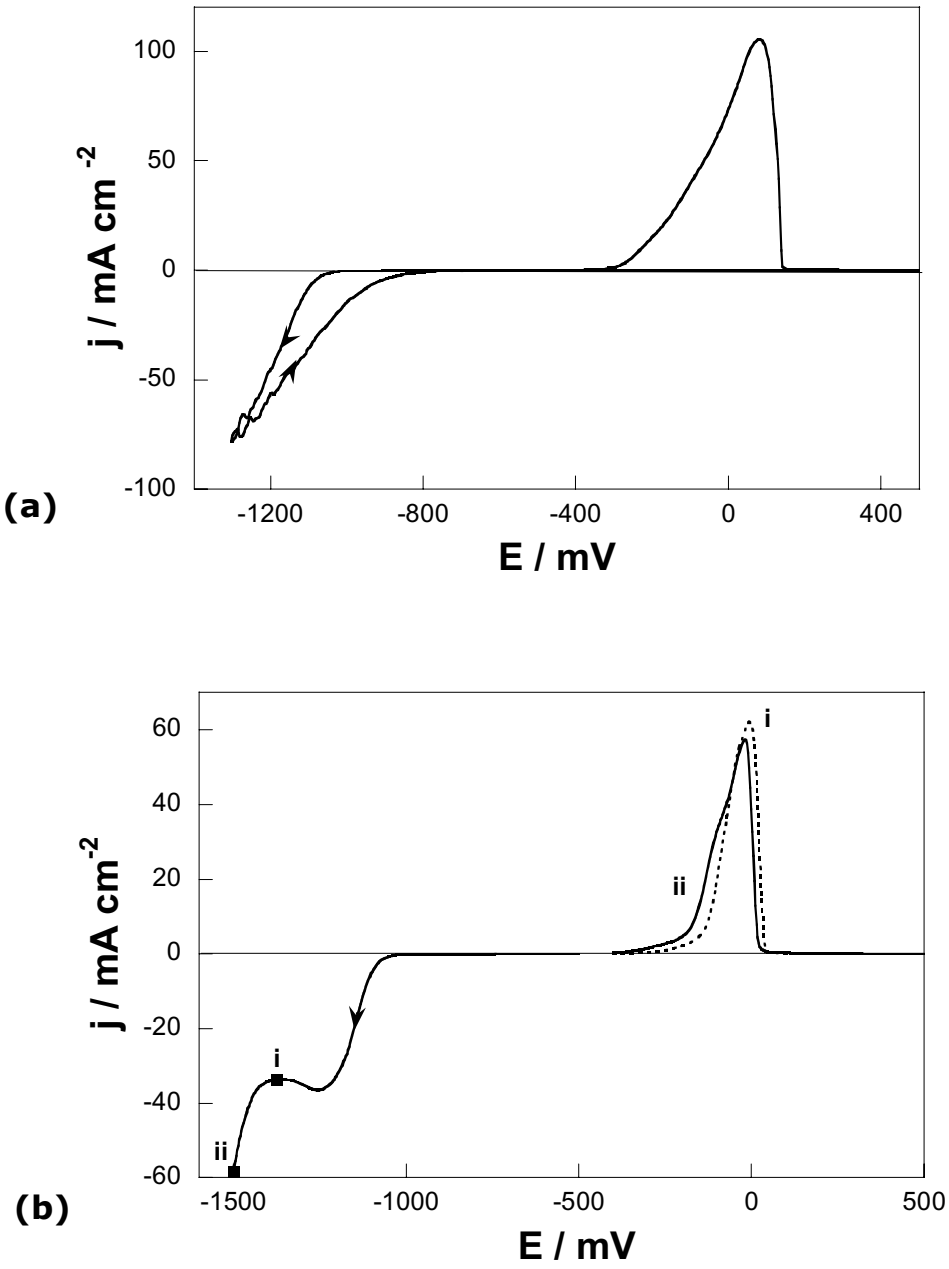

Figure 2. (a) Cyclic voltammetry under stirring conditions (ω=300 rpm) and (b) combined LSV scans under quiescent conditions, cathodic limit (i) –1400 mV and (ii) –1500 mV of a 0.2 mol dm^{-3} $Na_3C_6H_5O_7$ + 0.05 mol dm^{-3} $CoSO_4$ + 0.25 mol dm^{-3} $NiSO_4$ + 0.005 mol dm^{-3} Na_2MoO_4 solution + 0.005 mol dm^{-3} saccharine.

(a)

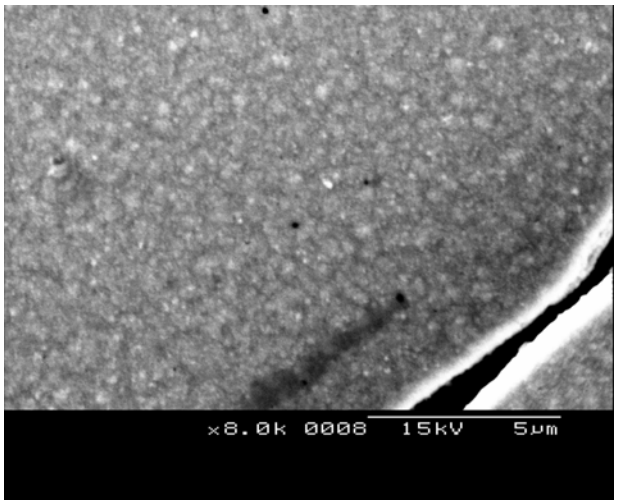

(b)

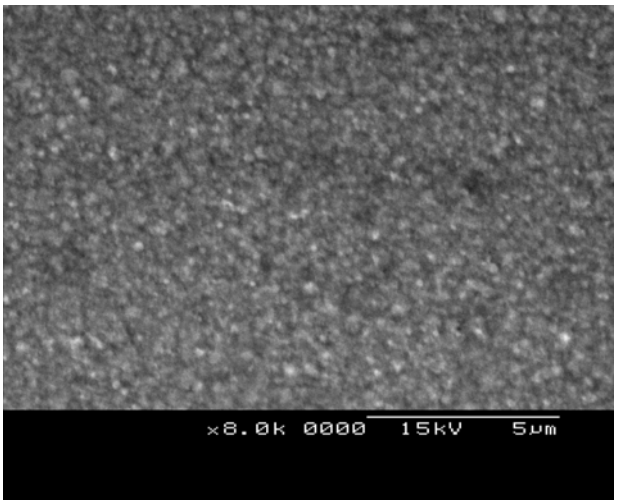

Figure 3. SEM images of 2 µm thick Co-Ni-Mo deposits obtained on Si/Ti/Ni substrates from (a) saccharine-free bath (composition: 12% Ni, 13% Mo) and (b) with 0.005 mol dm^{-3} saccharine (composition: 13% Ni, 15% Mo).

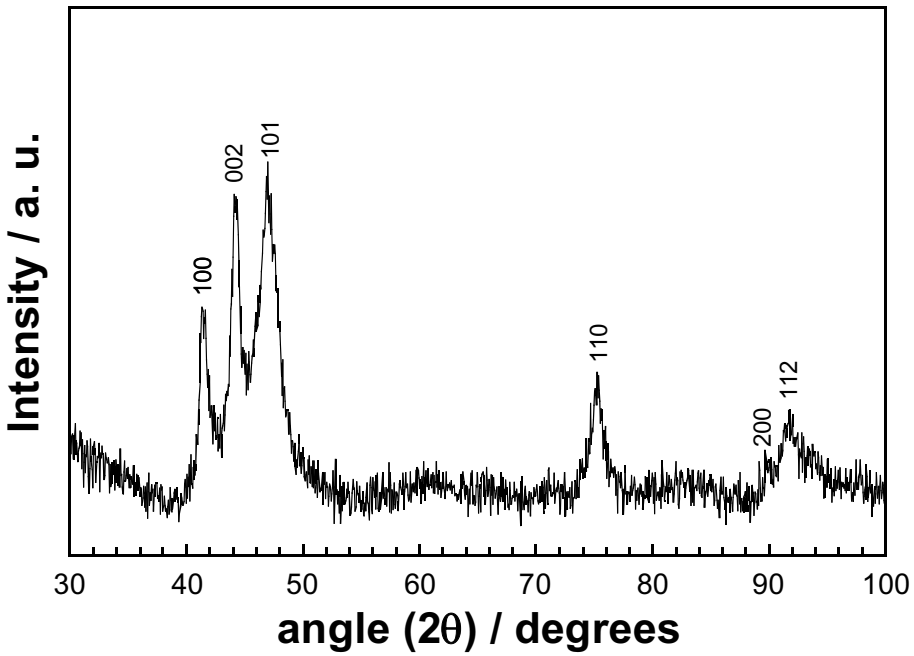

Figure 4. X-ray diffractogram of a Co-13%Ni-11%Mo deposit prepared on copper in the presence of 0.005 mol dm^{-3} saccharine.

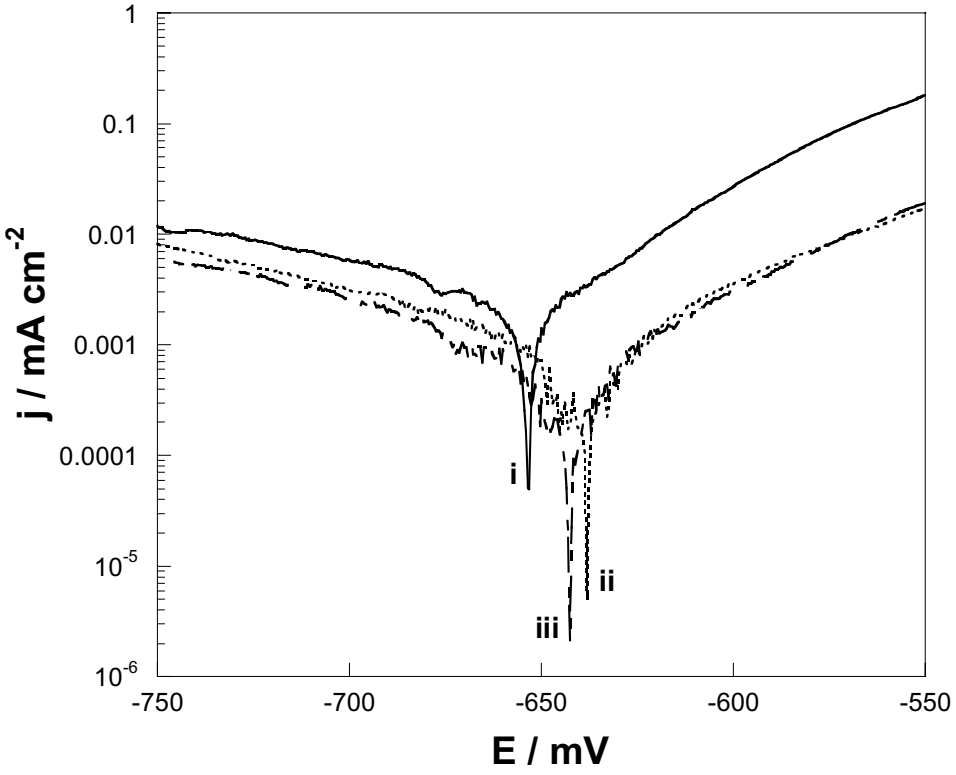

Figure 5. Potentiodynamic polarisation curves corresponding to (i) Co-11%Mo, (ii) Co-12%Ni-13%Mo (without saccharine) and (iii) Co-13%Ni-13%Mo (with saccharine) deposits.

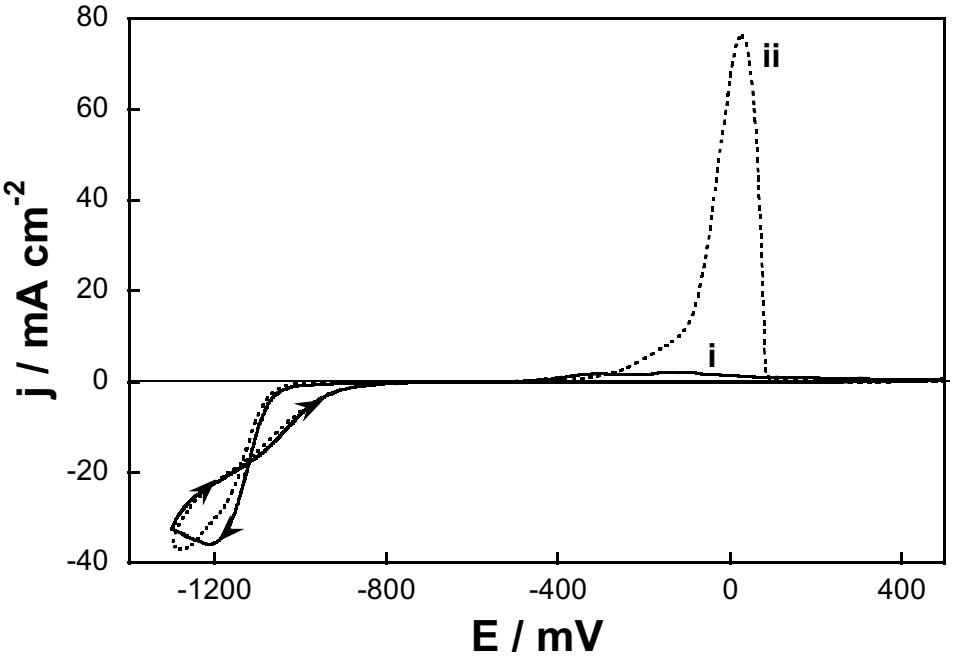

Figure 6. Cyclic voltammetry of a 0.2 mol dm^{-3} $Na_3C_6H_5O_7$ + 0.05 mol dm^{-3} $CoSO_4$ + 0.25 mol dm^{-3} $NiSO_4$ + 0.005 mol dm^{-3} Na_2MoO_4 + x mol dm^{-3} saccharine solution. (i) x=0, (ii) x=0.001. Cathodic limit: –1300 mV. Quiescent conditions.

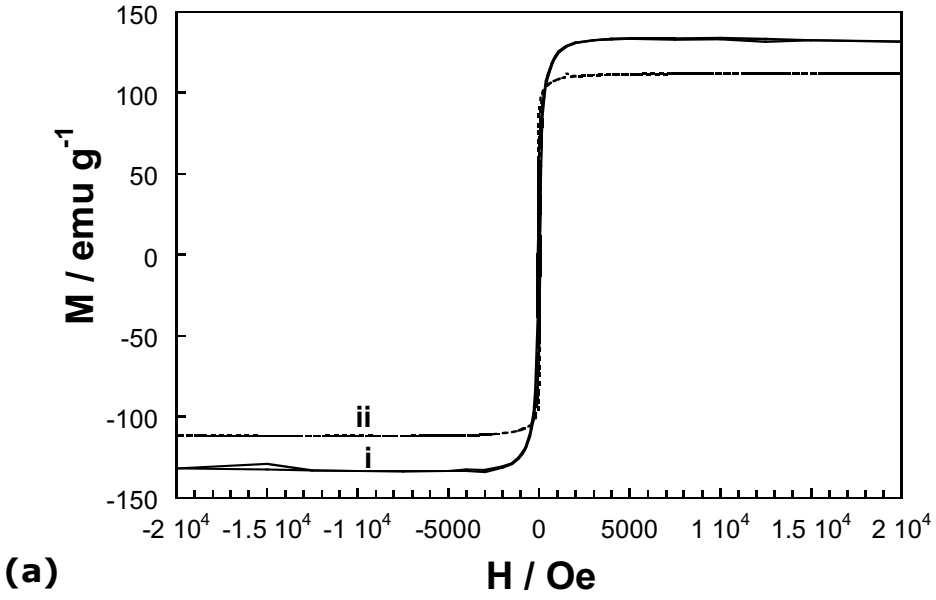

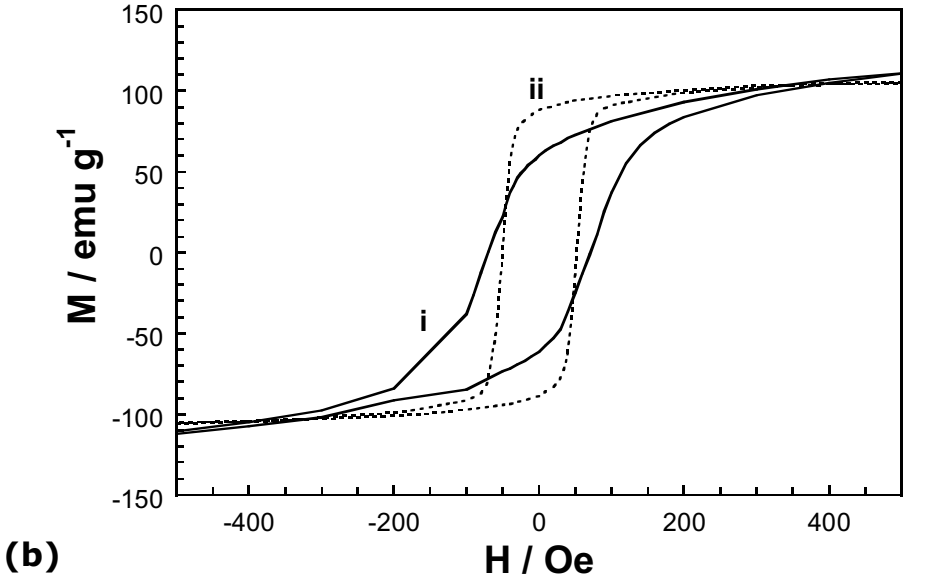

Figure 7. (a) Parallel hysteresis loops and (b) magnified detail of 2 μm thick (i) Co-11%Mo and (ii) Co-14%Ni-13%Mo films.

(a)

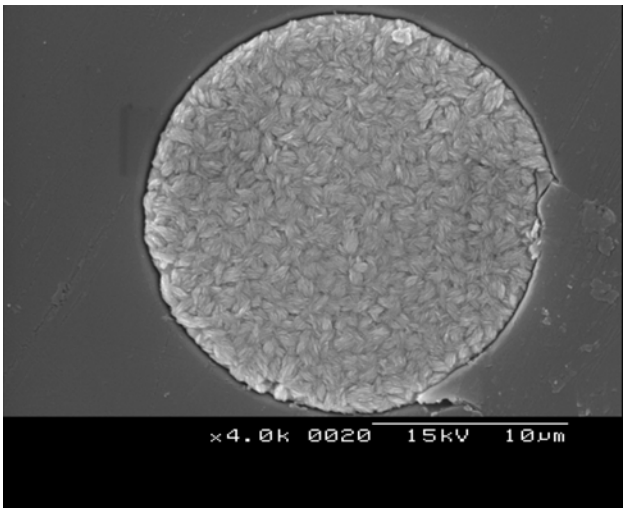

(b)

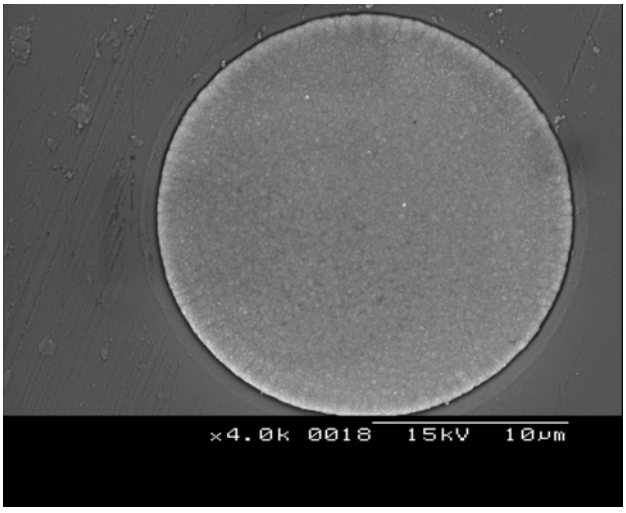

Figure 8. SEM images of (a) Co-Mo and (b) Co-Ni-Mo round-shaped microstructures.

(a)

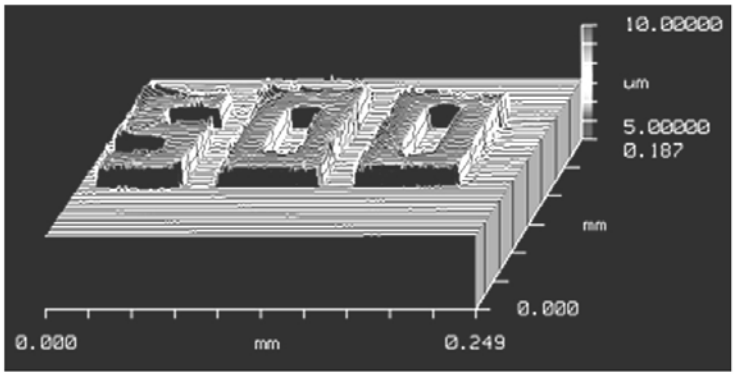

(b)

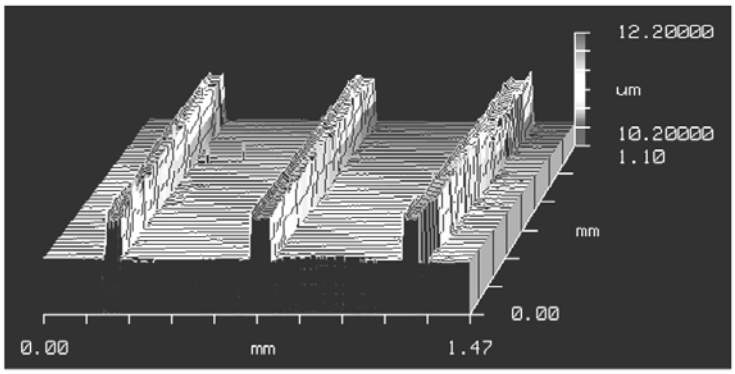

(c)

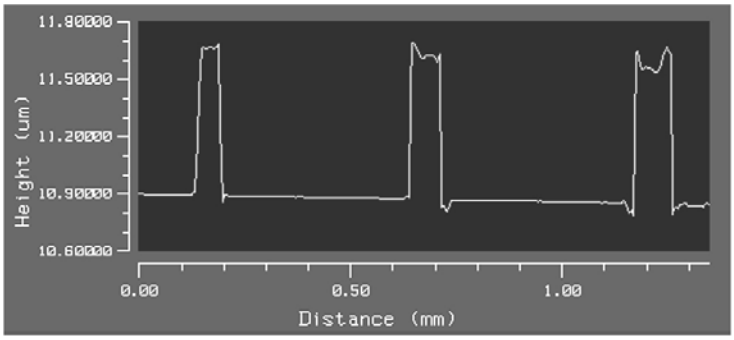

Figure 9. (a) and (b) 3D surface profile of Co-Ni-Mo microstructures outlined by white-light interferometry. (c) Step height analysis corresponding to microstructure (b).

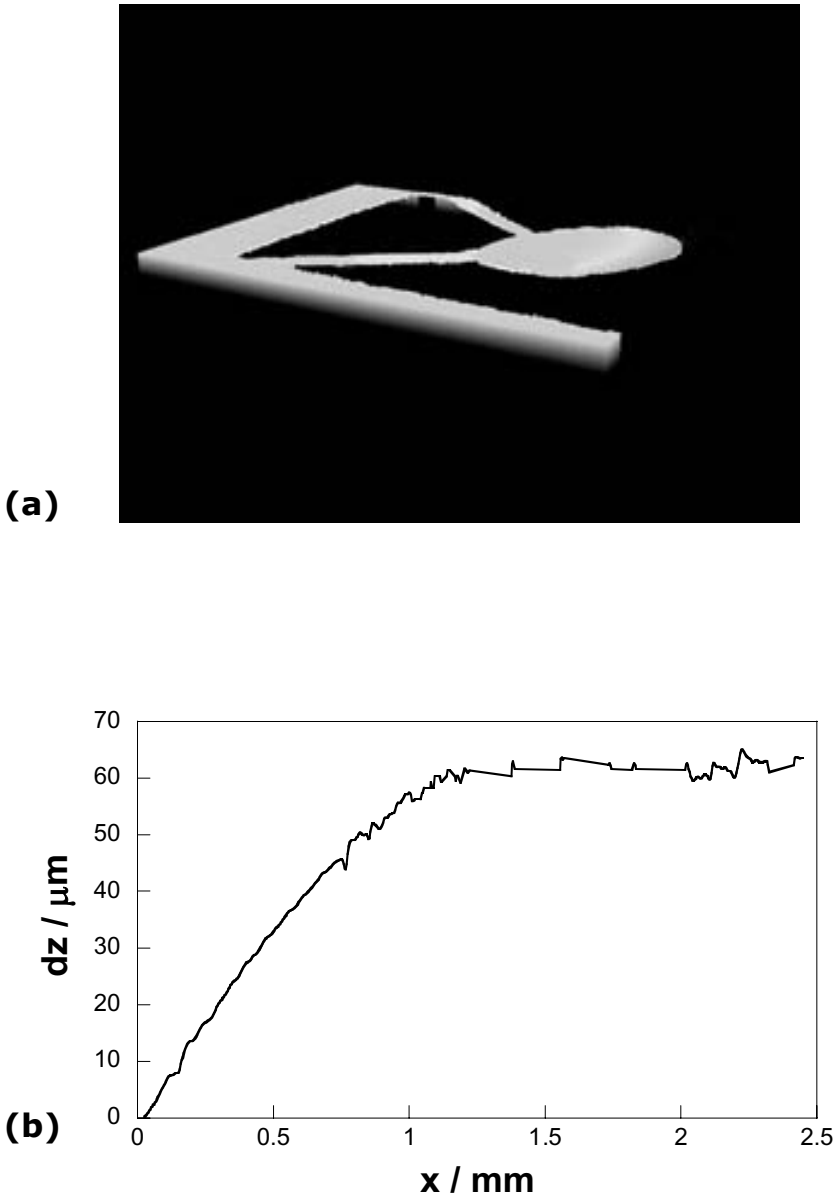

Figure 10. (a) View of the bending effect induced by a permanent magnet on a 2 µm Co-Mo film/1500Å Ti-Ni/ 8 µm silicon. (b) Displacement (dz) of the valve's body versus its length. The total displacement is the sum of that caused by the inherent deposit stress and that induced by the magnet.

4.6.3 Resum de resultats

L'addició de 0.005 mol dm^{-3} sacarina al bany 0.2 mol dm^{-3} citrat + 0.25 mol dm^{-3} $NiSO_4$ + 0.05 mol dm^{-3} $CoSO_4$ + 0.005 mol dm^{-3} Na_2MoO_4 a pH=4.0 permet reduir l'estrès dels dipòsits ternaris. La presència de sacarina en el bany retarda l'inici del procés de deposició i afavoreix l'oxidació de les espècies electrodipositades. D'altra banda, la sacarina no té efecte sobre la composició dels dipòsits, de manera que els percentatges de molibdè i níquel es mantenen al voltant del 10-15%. Tanmateix, s'incorpora una quantitat molt petita de sofre als dipòsits, per sota de l'1%.

La sacarina no tan sols evita l'aparició d'esquerdes als dipòsits Co-Ni-Mo sinó que també en refina el gra i provoca una pèrdua de l'orientació preferent de l'estructura hcp. Els experiments de voltametria cíclica demostren que una mínima concentració de sacarina en el bany (0.001 mol dm^{-3}) és suficient per promoure l'oxidació dels dipòsits. La resistència a la corrosió dels dipòsits, però, no varia significativament per bé que existeix un lleuger desplaçament del potencial de corrosió cap a valors més negatius.

A ull nu les capes ternàries són platejades i brillants, mentre que les capes binàries són fosques i menys lluents. La mesura de la brillantor permet quantificar aquesta diferència, de manera que s'obtenen valors de lluïssor clarament superiors en el cas de les capes Co-Ni-Mo. Aquesta major lluïssor metàl·lica està lligada a una menor rugositat i mida del gra (nanomètrica).

Tant les làmines binàries Co-Mo com les ternàries Co-Ni-Mo de 2 μm de gruix presenten propietats mecàniques i magnètiques adequades per a actuació magnètica. A partir dels valors de duresa es dedueix que, estrictament, les làmines ternàries són més resistents a la deformació plàstica localitzada, la qual cosa és atribuïble a la presència

de níquel als dipòsits. D'altra banda, però, les làmines binàries són lleugerament més elàstiques que les ternàries d'acord amb els valors del mòdul de Young. Pel que fa a les propietats magnètiques, en ambdós casos s'observa una magnetització més ràpida en la direcció del camp paral·lela a la làmina que en la direcció perpendicular. La incorporació de níquel a les capes Co-Mo provoca una disminució de la coercitivitat de 70 a 50 Oe i, simultàniament, un augment tant de la remanència com de la permeabilitat (μ_r passa de 130 a 670). Això fa que, en termes magnètics, les prestacions de les capes ternàries siguin superiors.

La selectivitat dels processos d'electrodeposició és alta, de manera que les microestructures Co-Mo i Co-Ni-Mo obtingudes respecten perfectament el relleu original, les parets laterals són verticals i no es malmeten després d'eliminar la fotoresina. Tampoc s'observen danys en làmines contínues electrodipositades sobre silici/capa llavor una vegada llevada la capa de silici amb TMAH, la qual cosa posa de manifest la compatibilitat dels aliatges desenvolupats amb les tècniques de fabricació habituals en MEMS. Aquestes làmines són capaces de deflexionar-se fins a un angle de pràcticament 90º per efecte d'un camp magnètic extern.

Les vàlvules formades per un cos de silici micromecanitzat + capa llavor + làmina electrodipositada són sensibles a un camp magnètic extern. En el cas de làmines de 2 μm de gruix, s'aconsegueix deflexionar la vàlvula unes 30 μm quan la làmina electrodipositada és Co-Mo i unes 40 μm quan la làmina electrodipositada és Co-Ni-Mo. A més, la deflexió s'incrementa en augmentar el gruix de l'electrodipòsit. En cap cas s'ha produït un trencament de les làmines electrodipositades durant els assaigs, la qual cosa posa de manifest la seva robustesa i flexibilitat.